



Faculteit Farmaceutische, Biomedische en Diergeneeskundige Wetenschappen

Departement Farmaceutische Wetenschappen

**Natural products as potential inhibitors of Advanced Glycation  
Endproducts (AGEs) and modulators of autophagy**

**Natuurproducten als potentiële remmers van Advanced Glycation  
Endproducts (AGEs) en modulatoren van autofagie**

Proefschrift voorgelegd tot het behalen van de graad van Doctor in de  
Farmaceutische Wetenschappen aan de Universiteit Antwerpen te verdedigen door

**Stefaniya Velichkova**

Promotoren:

Prof. Dr. Luc Pieters

Dr. Kenn Foubert

Antwerpen, 2020



To my parents,  
to Pieter and  
to baba (my grandmother)



*It is good to have an end to journey towards, but it is the journey that matters, in the end ...*



## TABLE OF CONTENTS

*A story to remember ... (Acknowledgements)*

*List of abbreviations*

### **CHAPTER 1: INTRODUCTION** **3**

---

#### **1. A TRIBUTE TO MEDICINAL PLANTS AND NATURAL PRODUCTS**

#### **2. ADVANCED GLYCATION ENDPRODUCTS (AGEs)**

##### 2.1 DEFINITION

##### 2.2 FORMATION PATHWAY

##### 2.3 CLASSIFICATION

##### 2.4 PATHOPHYSIOLOGICAL SIGNIFICANCE OF PROTEIN GLYCATION

##### 2.5 AGEs INHIBITORS/ BREAKERS: WHERE ARE WE NOW?

#### **3. THE MACHINERY OF AUTOPHAGY**

##### 3.1 DEFINITION

##### 3.2 TYPES OF AUTOPHAGY

##### 3.3 AUTOPHAGIC MACHINERY AND FLUX

##### 3.4 PHYSIOLOGICAL AND PATHOPHYSIOLOGICAL ROLE IN THE HUMAN BODY

##### 3.5 AUTOPHAGY MODULATORS

#### **4. CONCLUSION**

### **CHAPTER 2: AIM OF STUDY** **45**

---

### **CHAPTER 3: PHYTOCHEMICAL INVESTIGATION** **49**

---

#### **1. INTRODUCTION**

#### **2. GENERAL INSTRUMENTS AND REAGENTS**

##### 2.1 SOLVENTS AND REAGENTS

##### 2.2 INSTRUMENTS

##### 2.3 CHROMATOGRAPHIC AND ANALYTICAL TECHNIQUES

##### 2.3.1 THIN LAYER CHROMATOGRAPHY

##### 2.3.2 OPEN COLUMN CHROMATOGRAPHY

2.3.3 FLASH CHROMATOGRAPHY

2.3.4 HPLC (HIGH-PERFORMANCE LIQUID CHROMATOGRAPHY)

2.3.5 SEMI-PREPARATIVE HIGH-PERFORMANCE LIQUID CHROMATOGRAPHY

2.3.6 UPLC (ULTRA-PERFORMANCE LIQUID CHROMATOGRAPHY)

2.3.7 MASS SPECTROMETRY

2.3.8 NUCLEAR MAGNETIC RESONANCE (NMR) SPECTROMETRY

### **3. ISOLATION AND IDENTIFICATION OF POLYMETHOXYLATED FLAVONOIDS FROM *CITRUS SINENSIS* AND *CITRUS DEPRESSA***

3.1 INTRODUCTION

3.1.1 PLANT CHARACTERISTICS

3.1.2 TRADITIONAL MEDICINE

3.1.3 PHARMACOLOGICAL ACTIVITY

3.1.4 POLYMETHOXYLATED FLAVONOIDS

3.2 MATERIALS AND METHODS

3.2.1 PLANT MATERIAL

3.2.2 EXTRACTION, FRACTIONATION AND ISOLATION OF PMFS

3.3 RESULTS AND DISCUSSION

3.3.1 *CITRUS SINENSIS* PEELS

3.3.2 *CITRUS DEPRESSA* PEELS

### **4. ISOLATION AND IDENTIFICATION OF BIFLAVONOIDS FROM *GINKGO BILOBA***

4.1 INTRODUCTION

4.1.1 PLANT DESCRIPTION

4.1.2 TRADITIONAL MEDICINE

4.1.3 *GINKGO BILOBA* EXTRACT (EGb 761) – PHARMACOLOGICAL ACTIVITY

4.1.4 BIFLAVONOIDS

4.2 MATERIALS AND METHODS

4.2.1 PLANT MATERIAL

4.2.2 EXTRACTION, FRACTIONATION AND ISOLATION OF BIFLAVONOIDS

4.2.3 LC-MS ANALYSIS

4.4 RESULTS AND DISCUSSION

### **5. ISOLATION AND IDENTIFICATION OF QUINAZOLINE ALKALOIDS FROM *ADHATODA VASICA***

5.1 INTRODUCTION

5.1.1 PLANT DESCRIPTION



- 5.1.2 TRADITIONAL MEDICINE
- 5.1.3 PHARMACOLOGICAL ACTIVITY
- 5.1.4 QUINAZOLINE ALKALOIDS
- 5.2 MATERIALS AND METHODS
  - 5.2.1 PLANT MATERIAL
  - 5.2.2 EXTRACTION, FRACTIONATION AND ISOLATION OF QUINAZOLINE ALKALOIDS
  - 5.2.3 STRUCTURE ELUCIDATION
- 5.4 RESULTS AND DISCUSSION

**CHAPTER 4: METHOD VALIDATION *ADHATODA VASICA* AND  
QUANTIFICATION OF VASICINE IN COMERCIAL PRODUCTS 133**

---

- 1. OBJECTIVES**
- 2. MATERIALS AND METHODS**
  - 2.1 PLANT MATERIAL
  - 2.2 LOSS ON DRYING
  - 2.3 UNIFORMITY OF MASS OF SINGLE DOSE PREPARATIONS
  - 2.4 REAGENT AND EQUIPMENT
  - 2.5 INSTRUMENTATION AND CHROMATOGRAPHIC CONDITIONS
- 3. METHOD DEVELOPMENT**
  - 3.1 USP METHOD
  - 3.2 METHOD OPTIMIZATION
    - 3.2.1 CHROMATOGRAPHIC PARAMETERS
    - 3.2.2 EXTRACTION PROCEDURE
  - 3.3 FINAL METHOD
- 4. METHOD VALIDATION**
  - 4.1 MATERIALS AND METHODS
    - 4.1.1 CALIBRATION MODEL
    - 4.1.2 PRECISION
    - 4.1.3 ACCURACY
    - 4.1.4 SPECIFICITY
  - 4.2 RESULTS AND DISCUSSION
    - 4.2.1 LOSS ON DRYING
    - 4.2.2 CALIBRATION MODEL

- 4.2.3 PRECISION - INTERMEDIATE PRECISION
- 4.2.4 PRECISION - LINEARITY
- 4.2.5 ADDITIONAL TEST ON A NEW BATCH
- 4.2.6 ACCURACY OF THE METHOD
- 4.2.7 SPECIFICITY - SELECTIVITY
- 5. QUANTIFICATION OF VASICINE IN COMMERCIAL PRODUCTS**
- 5.1 MATERIALS AND METHODS
- 5.2 VALIDATION WITHIN FLEXIBLE SCOPE
- 5.3 RESULTS AND DISCUSSION
- 6. CONCLUSION**
- 7. ATTACHMENTS**

---

**CHAPTER 5: GENERAL ASSAYS FOR DETECTING AGES INHIBITION 173**

- 1. TO SET THE SCENE**
- 2. MATERIALS AND METHODS**
- 2.1 SOLVENTS AND REAGENTS
- 2.2 INSTRUMENTS
- 2.3 METHODS
- 2.3.1 BSA / GLUCOSE ASSAY
- 2.3.2 FRUCTOSAMINE ASSAY
- 2.3.3 DICARBONYL ENTRAPMENT MEASUREMENT
- 3. RESULTS AND DISCUSSION**
- 3.1 BSA / GLUCOSE ASSAY
- 3.2 FRUCTOSAMINE ASSAY
- 3.3 DICARBONYL ENTRAPMENT MEASUREMENT
- 4. CONCLUSION**

---

**CHAPTER 6: FROM VIAL TO FILE – A UPLC/MS METHOD DEVELOPMENT AND VALIDATION FOR QUANTIFYING AGES INHIBITION 213**

- 1. THE PIROUETTE OF IDEAS**
- 2. REAGENTS AND EQUIPMENT**
- 2.1 SOLVENTS AND REAGENTS

2.2 GENERAL APPARATUS

2.3 INSTRUMENTS

### **3. METHOD DEVELOPMENT**

3.1 THE STARTING POINT OF METHOD DEVELOPMENT

3.2 METHOD OPTIMIZATION

3.2.1 CHANGE OF CHROMATOGRAPHIC CONDITIONS

3.2.2 CONDITIONS FOR SAMPLE INCUBATION AND SAMPLE PREPARATION

3.2.3 A DEUTERATED INTERNAL STANDARD

### **4. METHOD VALIDATION**

4.1 MATERIALS AND METHODS

4.2 RESULTS AND DISCUSSION

4.2.1 BETWEEN-DAY PRECISION WITH D<sub>2</sub>-CML AS AN INTERNAL STANDARD

4.2.2 NEW INTERNAL STANDARD: D<sub>4</sub>-CML

**5. RESULTS FROM ISOLATED PURE COMPOUNDS AND COMMERCIAL STANDARDS TESTED IN THE METHOD**

**6. CONCLUSION**

---

## **CHAPTER 7: THE AUTOPHAGY EXPERIMENT**

**271**

**1. INTRODUCTION**

**2. MATERIALS AND METHODS**

2.1 MATERIALS

2.1.1 CELL CULTURE

2.1.2 WESTERN BLOT

2.1.3 CYTO-ID DETECTION KIT

2.2 METHODS

2.2.1 MAINTAINING CELL CULTURES

2.2.2. WESTERN BLOT

2.2.3 CYTO-ID DETECTION KIT

**3. RESULTS AND DISCUSSION**

**4. CONCLUSION**

---

## **CHAPTER 8: GENERAL DISCUSSION AND FUTURE PERSPECTIVES (QUO VADIS?)**

**297**

1. GENERAL DISCUSSION
2. FUTURE PERSPECTIVES

## **CHAPTER 9: BIBLIOGRAPHY**

---

**307**

*Summary (Dutch)*

*Scientific CV*

***A story to remember***  
**(ACKNOWLEDGEMENTS)**

The following pages would have never been possible without the many people – family, friends, colleagues who, in one or another way, had an impact on the realization of this long journey.

At first, I would like to express my gratitude to my promotors who advised and guided me through the frustrating steps of the project: To Professor Pieters, always available and responding to emails, no matter that it is weekend or not, within less than an hour! To Kenn, for her understanding, and the troubleshooting experience we shared with different analytical techniques and methods, and for her support during my first steps in guiding practical courses with pharmacy students. To Sandra, who believed in me a long time ago ...

I think this is the right place to say special thank you to some people who I met during my Erasmus stay in Antwerp but who played a crucial role in starting latter on as s PhD student. To Ines, my first supervisor ever who open the door (literally!) of the real job world and introduce me to the dynamic rhythm of the lab. Thank you for making me feel at ease in my first time alone in a foreign country, for the funny talks, for delegating me important tasks which I had always thought I can never do alone! To Hanna, this friendly face, it was a pleasure to talk to you and I knew I could always rely on you. To Vasiliki, that introduced me to the NMR world and with who we contemplated over the many future possibilities and perspectives.

And now, as Marry Poppins would say: “Just a spoon full of sugar helps the medicine goes down in the most delightful way!” My “spoon full of sugar”, which helped me to tackle the struggles through the research process, was my colleagues! To Emmy (Emilia), who introduced me to every equipment in the lab, who showed me all tests for AGEs (!), who sat with me to elucidate my first NMR spectra for isolated compounds, who guided me through the phone in the weekends how to fix another problem with equipment that failed! Thank you for doing all of this patiently, it set me on the track of my research path. Also, thank you for being a friend outside the lab, I do not think that there was an important moment during my stay here, that I did not share with you. To Tania (Taniakje), that I have been annoying since the very beginning with constant questions where I can find something, how can I order something, how to calibrate something. Hey, you would always just jump up and help

me, no complain always smiling - THANK YOU! The lab is not the same if you are not there. To Mart (Martinelli), an immense part of the AGEs-team! Thank you for your help, your understanding, your compassion in all analytical troubleshooting! We always have been “almost there”, right? (AGEs) To Laura (Laura Fabiani), for being a friend, listener, who can always see through me and question me in a way I can never hide something. Thank you that I could always ask you for advice, help, and for being understanding. To Anastasia (my lifestyle guru), thank you for the great pieces of advice, the guidance on any subject ranging from the best vacation spot to the best textbook about diabetes. I always have to take notes when I am talking with you! To Maxime (someone once said, mandarijntje), thank you for sharing the common struggles along the way, for your understanding, for the funny talks about cats and city trips, for the many adventurous moments outside the lab! To the most iconic duo Anneliese & Annelies, who despite their busy schedule would always find time to help me, to listen to me, to give any advice or just to have a funny talk about the most peculiar expressions in the Flemish language ... To Yunita (Unicorn), the most gentle and hard-working person, who would always respond and be there for me! Thank you for being a great friend, Unicorn! To Balde (the King), who ALWAYS has “a smile on (his) face for the whole human race” and who is always able to show me the simple through, which I always forget, the most important thing in life – SMILE! To Deborah, a support, a friend, a “partner in crime” during the practical courses, a guide in the career searching process! Thank you for all enlightening conversations and that I could always rely on you! To Andres (Andressito), thank you for being able to rely on you always, for the jokes and the hilarious pictures that could turn any dull moment into a story. With your dedication and passion for the work, you have always been a person that I looked up to! To Hien, thank you for your honest and precise judgments! It was fascinating to see your zest for open column chromatography and your dedication to the isolation of pure compounds (never lose this fire!).

I want to say special thank you to the Bulgarian trace in the lab - Yancho Zarev. Amai, Yancho, I owe you so much ... !! Thank you for explaining the logic behind natural products research, for revealing the mystery of open column chromatography, for exploring the small streets in Antwerpen, for the many funny and serious talks, for introducing me to special people ... I am glad I met you here!

To Nina and Tess, the team who keeps the projects running and who makes sure that new researchers are joining the team. To Harry, who is the biggest fan of Bulgarian criminal TV series in whole Belgium!

To Seijhan, mornings would never be the same without your energetic “Goede morgen!” and your bright smile. It is incredible that despite you could only speak Dutch and me only English (and few words in Turkish), we understood perfectly, my friend! Thank you for all! During this journey, I was also happy to meet some great Cuban friends, thank you for the joy, the music, and the stories you brought in the lab.

I also got to know some incredible people who made my stay in the beginning a great fun - the master students Nathalie and Karen (not students anymore)! I will never forget the sight of my desk on the 6<sup>th</sup> December when you two together with Maxime introduced me to the local tradition of Sinterklaas! To Marilena and Boriyana, who were always cheerful and smiling. To Rita and Woitjek, who gave me the taste of what it is like to be a teacher!

Last but not least, I am grateful for the collaboration with some other labs. To Dorien, for introducing me to the field of autophagy, for your patience in guiding me through the multistep procedures (!!!), and just for always finding time to help me. To the fantastic team from building T (the Physiopharmacology lab) – Isabelle, Farnaz, Besa, Paola, and Sofie, where I was always welcomed and could always ask questions. To Sofie (from upstairs, the Medicinal Chemistry lab), with who I developed my diplomatic skills while negotiating for the Prep system or the heating plates. I could always rely on you!

To Kris, who helped me with the realization of the thesis layout and the layout of my first poster ever! And although AGEs was a rather abstract definition for her (I can imagine!), she dived into the project and came up with some fantastic ideas! Thank you!

To Ali, for his time and for giving me guidance in the broad field of statistics.

There was life outside the lab, of course!

To my new friends in Belgium (but, originally from the Netherlands) Laura and Stijn, I cannot say enough how happy and thankful I am that I met you! Thank you for the short but intense trips, for the light conversations, for the serious conversations, for the ability to share everything! To the joyful ballet group, a great experience that I will never forget!

To family and friends, I am unable to list all of them here but who accepted me, who supported me, who were interested in me and my work, who cared for me and made me feel the most welcomed!

To my parents, thank you for being! Thank you that you have been by my side from the very beginning, thank you for everything you thought me, I am who I am because of you!!! Be blessed!

To Pieter, I would not be able to go through this journey without you. You made it happen, you gave me courage, you believed more in myself than me, you made it possible to be happy no matter how difficult it could get, you showed me that life can be beautiful! Thank you for being!



## LIST OF ABBREVIATIONS

3-DG	3-deoxyglucosone
AIIRIs	angiotensin II receptor inhibitors
ACE	angiotensin converting enzyme
AGE-R1, -R2, -R3	advanced glycation endproducts receptor 1, receptor 2, receptor 3
AGEs	advanced glycation endproducts
ALEs	advanced lipoxidation endproducts
ALT-711	4,5-dimethyl-3-phenacylthiazolium chloride
ANF	anti-nuclear antibodies
ANOVA	analysis of variances
ARPs	Amadori rearrangement products
ATG	autophagy-related proteins
AQC	6-aminoquinolyl- <i>N</i> -hydroxy-succinimidyl-carbamate
BSA	bovine serum albumin
CEL	carboxyethyllysine
CI	confidence interval
d <sub>2</sub> -CML	N- $\epsilon$ -carboxy[D <sub>2</sub> ]methyl-L-lysine
d <sub>4</sub> -CML	N- $\epsilon$ -carboxy[4,4,5,5-D <sub>4</sub> ]methyl-L-lysine
CML	N- $\epsilon$ -carboxymethyl-L-lysine
COSY	correlation spectroscopy
COX-2	cyclooxygenase -2
DAD	diode array detector
DEPT	distortionless enhancement by polarization transfer
DMSO	dimethyl sulfoxide
DOLD	deoxyglucosone-derived lysine dimer
EDQM	European Directorate for the Quality of Medicines
EGb 761	<i>Ginkgo biloba</i> extract
ELISA	enzyme-linked immunosorbent assay
ELSD	evaporative light scattering detector
ESI	electrospray ionization
FBS	fetal bovine serum

GC	gas chromatography
GEM	<i>Ginkgo</i> evaluation of memory study
GFP	green fluorescent protein
Glc	glucose
GO	glyoxal
GODIC	glyoxal derived imidazoline crosslink
GOLD	glyoxal-derived lysine dimer
GRx	glutathione peroxidase
GSH	glutathione
HbA <sub>1c</sub>	glycosylated hemoglobin A <sub>1c</sub>
HEK	human embryonic kidney cells
HILIC	hydrophilic interaction liquid chromatography
HPLC	high-performance liquid chromatography
HMBC	heteronuclear multiple bond correlation
HAS	human serum albumin
HSQC	heteronuclear single quantum coherence
HUVECs	human umbilical vein endothelial cells
IC <sub>50</sub>	half maximal inhibitory concentration
ICH	International Council for Harmonization
IgG	immunoglobulin G
IgM	immunoglobulin M
IL-1 $\alpha$ , - $\beta$ , -6	interleukins-1 $\alpha$ , - $\beta$ , -6
IR	infrared
IUCN	International Union for Conservation of Nature
LC	liquid chromatography
LC3	microtubule-associated protein light chain 3
LDL	low-density lipoproteins
LOD	loss on drying
LPO	lipid peroxidation
MCP-1	monocyte chemoattractant protein-1
MG-H <sub>1</sub>	N-(5-H-5-methyl-4-imidazolone-2-yl)-L-ornithine
MGO	methylglyoxal
MODIC	methylglyoxal derived imidazoline crosslink

MOLD	methylglyoxal-derived lysine dimer
MRM	multiple reaction monitoring
MS	mass spectrometry
mTOR	mammalian target of Rapamycin
MW	molecular weight
NADPH	reduced nicotinamide adenine dinucleotide phosphate
NF- $\kappa$ B	nuclear factor kappa light chain enhancer of activated B cells
NFPA	nonafluoropentanoic acid
NBT	nitro blue tetrazolium chloride
NMR	nuclear magnetic resonance
NO	nitric oxide
NOS	nitric oxide synthase
OH-PMFs	hydroxylated polymethoxylated flavonoids
OPA	<i>ortho</i> -phthalaldehyde
OTC	over the counter
PBS	phosphate buffered saline
PE	phosphatidylethanolamine
PEC	<i>S</i> - $\beta$ (4-pyridylethyl)-L-cysteine
PEG	polyethylene glycol
PGE <sub>2</sub>	prostaglandin E2
PMB	polymyxin B
PMFs	polymethoxylated flavonoids
PrSHs	protein thiol
P/S	penicillin/streptomycin
PVDF	polyvinylidene fluoride
QTOF	quadrupole time-of-flight
RAGE	receptor for advanced glycation end products
RCS	reactive carbonyl species
ROS	reactive oxygen species
RSD	relative standard deviation
SOD	superoxide dismutase
SDS-Page	sodium dodecyl sulphate polyacrylamide gel electrophoresis
STDEV	standard deviation

TCA	trichloroacetic acid
TGF- $\beta$	transforming growth factor- $\beta$
TLC	thin-layer chromatography
TNF- $\alpha$	tumour necrosis factor- $\alpha$
TOF	time-of-flight
TQD	triple quadrupole detector
UPLC	ultra-performance liquid chromatography
USE	ultrasound assisted extraction
USP	United States Pharmacopeia
UV	ultraviolet
VCAM-1	vascular cell adhesion molecule-1
WHO	World Health Organization

# Chapter 1

## Introduction



## *1. A tribute to medicinal plants and natural products*

For around 475 million years a vast array of chemicals have evolved in plant organisms to protect them from pathogens and an hostile environment.<sup>1</sup> Luckily, since then, those natural products provide plants with medicinal properties that human civilisation has relied on for many centuries.<sup>2</sup> Not surprisingly, nowadays natural sources are still considered as a starting point for drug discovery investigations.<sup>3</sup> The plant evolution of over million years resulted in a diverse arsenal of molecules, yet mostly unexploited. Traditional Chinese Medicine, Unani medicine and Ayurveda are ancient, yet, still alive medicinal systems widely used in Asia, which are based on complex herbal compositions, and have played an essential role in health maintenance and disease control.<sup>4</sup> The derived compounds and plant extracts attract wide attention for their potential application as novel therapeutic agents. In recent years, the enthusiasm in searching for treatment of current human diseases has yielded many positive hits from natural products.<sup>5</sup>

## *2. Advanced Glycation Endproducts (AGEs)*

Nowadays, age-related chronic inflammatory diseases like type 2 diabetes mellitus and cardiovascular diseases represent a major health problem.<sup>6</sup> The prevalence of those conditions is exponentially increasing since the population ages.<sup>7</sup> Therefore, prevention is of highest importance and clearly has a medical and economic impact. Not surprisingly, future strategies are focusing on the identification of individuals at risk for developing chronic complications by means of novel biomarkers for pathophysiological pathways; i.e. to improve risk prediction.<sup>8</sup> Various mechanisms have been proposed to explain the causes for initiation and progression of chronic diseases and on biochemical level, experimental and histological data suggest that protein glycation in biological systems (formation of advanced glycation endproducts (AGEs)) correlates with many pathological complications.<sup>9</sup>

## 2.1 Definition

Glycation is defined as the spontaneous, non-enzymatic reaction of glucose or other reducing sugars with an amino group of proteins, lipids and nucleic acids.<sup>10</sup> Protein glycation occurs predominantly on lysine, arginine and N-terminal residues of proteins, and it is considered as a post-translational modification of proteins found in biological systems.<sup>10,11</sup> Advanced Glycation Endproducts (AGEs) are complex, heterogeneous, sugar derived protein modifications that have been implicated in the pathogenesis of diabetic complications, Alzheimer's disease and in the process of normal aging.<sup>12,13</sup> They represent a core defect derived from abnormalities in glucose- and lipid-metabolism. In a physiological setting, one of the most important saccharides of mammalian metabolism, participating in glycation, is D-glucose.<sup>10</sup> Moreover, factors like 37 °C temperature, physiological pH, concentration and presence of oxygen and metal ions can influence the process.<sup>14</sup> Important physiological glycating agents apart from glucose are dicarbonyl metabolites, particularly glyoxal (GO), methylglyoxal (MG) and 3-deoxyglucosone (3-DG).<sup>15</sup>

## 2.2 Formation

### 2.2.1 In the beginning was ... La Réaction de Maillard

In the beginning of the 20<sup>th</sup> century, the French scientist Louis Camille Maillard (1878-1936) investigated the metabolism of urea and kidney function in order to gain better understanding of the genesis and treatment of kidney diseases. As a result, he started to study the interaction between amino acids and sugars, and in 1912 Maillard demonstrated that amino acids heated in the presence of a reducing sugar developed a characteristic yellow-brown colour. His research led to the discovery of a certain group of reactions which were named after him.<sup>16</sup> At that time Maillard presumed they were implicated in chemical modifications of food during preparation, and of protein modifications *in vivo* catalysed by hyperglycemia.<sup>17</sup> However, the first description of the chemical pathway of the Maillard reaction was done by John Hodge in 1953 regarding browning pigments in food samples treated at moderate temperatures.<sup>18</sup> The early recognition of AGEs *in vivo* can be traced back to the late 1960s when a non-enzymatic glycation process similar to the Maillard reaction was found in the



human body, namely, the glycation of hemoglobin (HbA<sub>1</sub>) in diabetic patients.<sup>19,20</sup> Further on, various types of AGEs have been described in different tissues, such as retinal blood vessel walls, arterial collagen, renal tissues, which were formed slowly and accumulated in time.<sup>21</sup> Moreover, AGEs were detected in different food matrixes after thermal processing of food (e.g. bakery and milk products) where heating increases the rate of glycation.<sup>14,22-23</sup> Moreover, the Maillard reaction was used to explain the variety of changes that occur during food preparation, such as flavors, aromas and colors.<sup>24</sup> Namely, it was studied for both its positive and negative effects on food quality and safety. Recently, the accumulation of AGEs *in vivo* has been implicated in the pathological conditions of diabetes and other health disorders such as atherosclerosis, Alzheimer's disease, and normal aging.<sup>17,25</sup> Thus, the Maillard reaction has been investigated in various fields for its chemical, physiological and toxicological aspects.<sup>26</sup>

### 2.2.2 Classical pathway for AGEs formation (Hodge pathway)

The reaction can be generally subdivided in three stages: initiation, propagation and an advanced stage (Figure 1.1). It usually takes several days to several weeks to complete, where the slow reaction rate can be explained by the lack of enzymatic catalysis during the process.<sup>26</sup> In the first step (**initiation**), reducing sugars (aldoses and ketoses) react with amino groups resulting in aldimines and ketoimines (Schiff bases). Subsequently, the unstable and reversible Schiff base undergoes Amadori or Heyns rearrangements, resulting in 1-amino-deoxyketosyl or 2-amino-deoxyaldos-2-yl adducts (relatively stable Amadori or Heyns products).<sup>12,27,28</sup> To summarize, the early stage glycation is characterized by the formation of Schiff bases and fructosamines, including structures such as N<sup>ε</sup>-fructosyl-lysine.<sup>29</sup>

During the **propagation** phase, the Amadori products can be transformed (within a period of weeks) to reactive dicarbonyl products. They initiate glycation by undergoing further non-oxidative dehydration and rearrangement reactions to dicarbonyl compounds, including 3-DG, GO and MGO. While 3-DG is formed by non-oxidative rearrangement and hydrolysis of Amadori product (Figure 1.1), MGO and GO can be produced in several additional pathways (see further). Alternatively, Amadori products can generate amines through a metal-ion-mediated catalysis and oxidation, while the glycosyl group is dehydrated to form deoxyglucosone (DG). Interestingly, AGEs

accumulate mainly in tissues containing proteins with long half-life, such as extracellular matrix collagen.

Further on, these early glycation products are highly prone to oxidative (glycooxidation) and non-oxidative degradation, cleavage and covalent binding, leading to a heterogeneous group of stable compounds and cross-linking of proteins, commonly called advanced glycation endproducts (AGEs). In particular, the **advanced stage** is characterized by a reaction between DG with lysine residues in the protein to produce pyrraline (Figure 1.1); or pentose with lysine and arginine to generate pentosidine and other products. As a result, intermolecular or intramolecular heterocyclic cross-linking and fragmentation occur in the protein molecules, leading to protein denaturation and irreversible damage. Interestingly, the Amadori products represent a challenging pharmacological target of the Maillard reaction. In contrast to AGEs, which accumulate exponentially with age in collagen and eye lenses, the Amadori products are in a steady state between formation, reversal and degradation.<sup>30</sup>

### 2.2.3 Additional pathways for AGEs formation

Meanwhile, AGEs can also be formed from Amadori products directly through rearrangement under both oxidative and non-oxidative conditions. If present, oxygen can accelerate advanced glycation of proteins, even though it is not always required. The oxidative Maillard reaction pathway was described firstly by Namiki (**Namiki pathway**), who indicated that the unstable initial products (Schiff bases) could be converted directly to oxoaldehydes (*glycooxidation*).<sup>31</sup> In this manner *N*<sup>ε</sup>-(carboxymethyl)-lysine (CML) and pentosidine can be formed.<sup>32</sup> Additionally, in 1987 the **Wolff pathway** was introduced, where metal-catalyzed *autoxidation* of reducing sugars could be involved in AGEs formation.<sup>33,34</sup> The products from both pathways are dicarbonyl intermediates, for example MGO, GO, 3-DG and free radicals. Moreover, the oxidation of polyunsaturated fatty acids (**lipoxidation pathway**) can also lead to GO or MGO formation, apart from the general advanced lipoxidation end products (ALEs). GO can react with free lysine groups to produce CML or GO-derived lysine dimer (GOLD). GO reacts with free arginine groups to form imidazolones. MGO can react with free lysine group to form *N*<sup>ε</sup>-(carboxyethyl)-lysine (CEL) and MGO-derived lysine dimer (MOLD). Additionally, the reaction between MGO and arginine residues may cause the formation of hydroimidazolones.<sup>35</sup> In conclusion, some AGEs like CML

and CEL could be end products of both glycooxidation and lipoxidation pathways, in contrast to pentosidine which can be formed only *via* glycooxidation.<sup>32</sup> Moreover, CML can be formed from fragmentation and subsequent glycation of ascorbic acid and dehydroascorbic acid.<sup>28</sup>

Inconsistency in the described AGEs formation pathways may arrive because glucose can degrade when it is unattached to protein, resulting in  $\alpha$ -oxoaldehydes. The latter are potent glycating agents, which react with proteins to directly form AGEs. The Schiff base adduct may also degrade *via* a non-Amadori rearrangement to  $\alpha$ -oxoaldehydes that are transformed to AGEs. As mentioned above glucose and other saccharides are important glycating agents but the most reactive glycating agents are  $\alpha$ -oxoaldehydes or dicarbonyl compounds such as GO, MGO and 3-DG.<sup>9</sup> Basically, AGEs can be formed by pre- and post-Amadori product reactions, and in such a way that the Amadori product is not a precursor. Therefore, AGEs are generated in both early and late stages of glycation processes. Nevertheless, the concept of early and advanced glycation adducts is rather simplifying the whole process but ensures a possibility of classifying the different glycation products.<sup>10</sup>

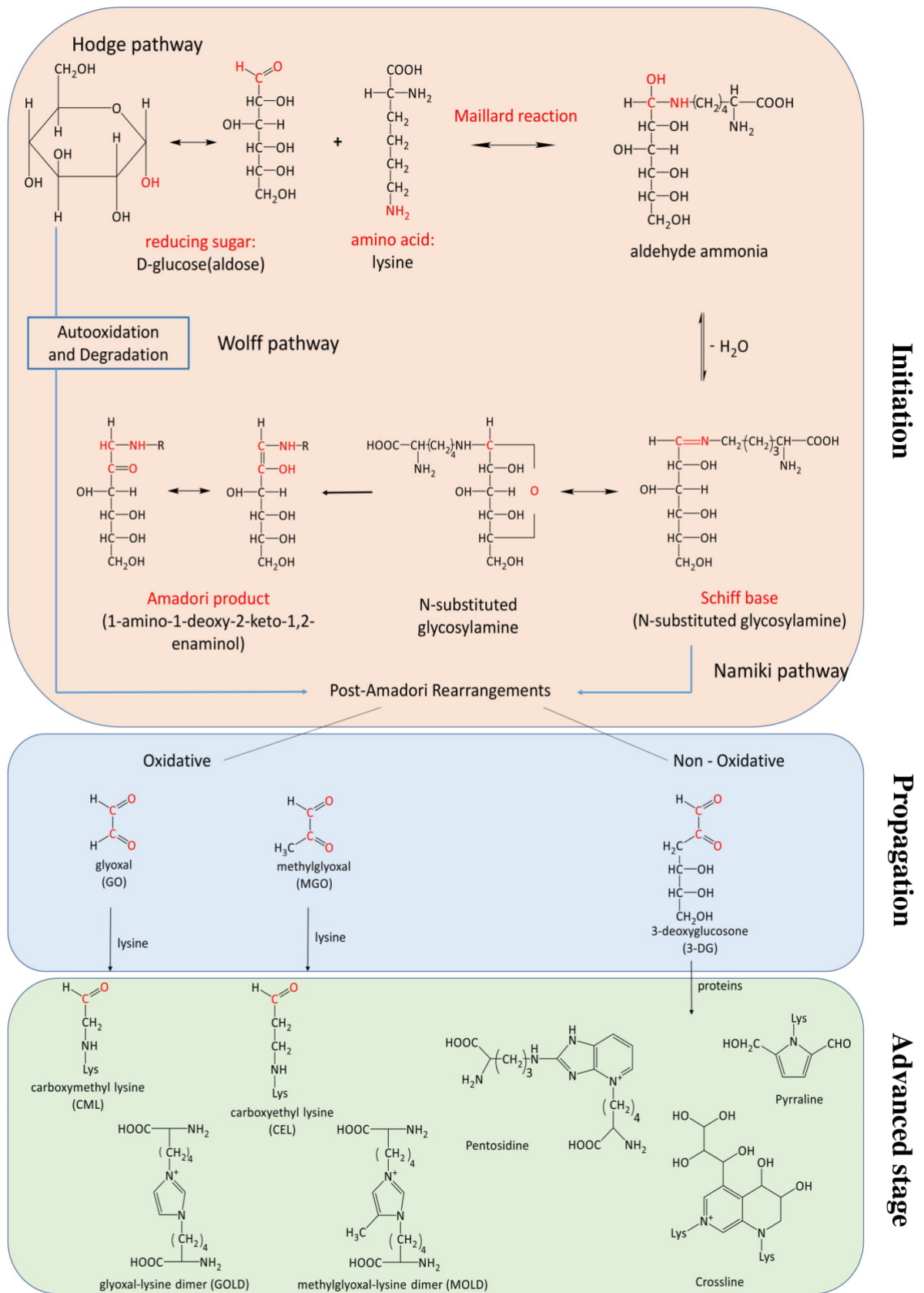


Figure 1.1. General scheme of advanced glycation end products (AGEs) formation.

## 2.3 Classification

Despite their complexity, the currently known AGEs produce the same chemical outcome. Namely, during the advance stage of the glycation process, intermolecular or intramolecular heterocyclic cross-linking and fragmentation occur in the protein molecule (e.g. collagen and elastin), leading to protein denaturation and irreversible damage.<sup>12,26</sup> Many attempts have been made to classify the diverse group of advanced glycation end products. For instance, one approach is based on their fluorescence properties and the presence of cross-linking in their structure.

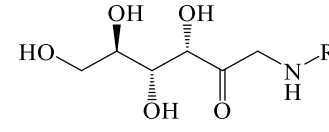
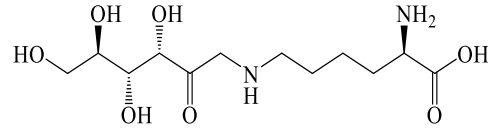
- Fluorescent cross-linked AGEs: pentosidine, crossline, vesperlysine A-C;
- Non-fluorescent cross-linked AGEs: glucosepane, MOLD, GOLD;
- Non-fluorescent non-cross-linked AGEs: CML, pyrraline, argpyrimidine.<sup>21</sup>

Another classification according to Rabbani and Thornalley is in terms of the molecular structure of glycation adducts, and on the mechanism of AGEs formation (Figure 1.2).<sup>10</sup>

### Fructosyl lysine

### Ketosamine (Amadori product)

#### Early glycation adduct residues

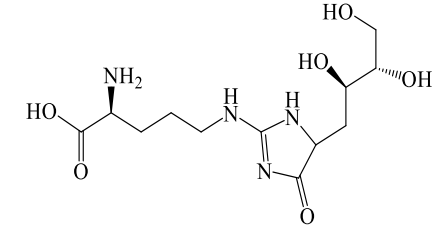
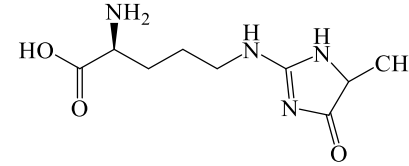
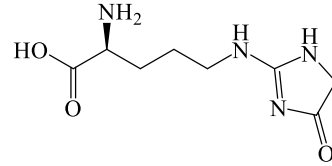


### G-H1

### MG-H1

### 3DG-H1

#### Hydroimidazolones

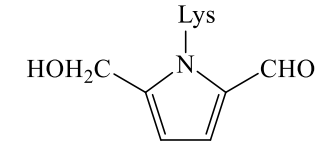
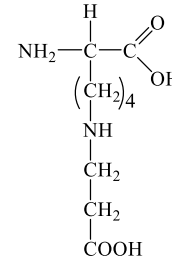
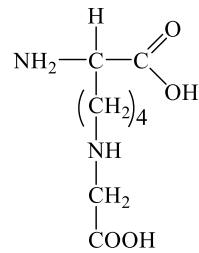


### CML

### CEL

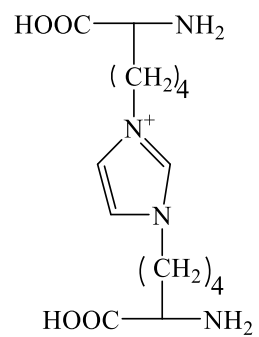
### Pyrraline

#### Monolysine adducts

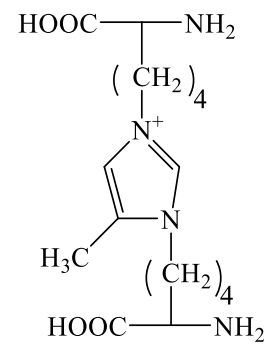


**Imidazolium and other cross-linked products**

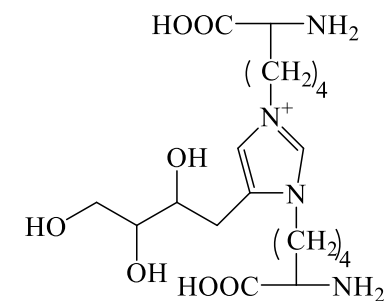
**GOLD**



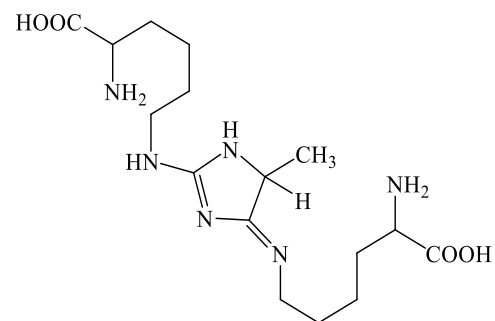
**MOLD**



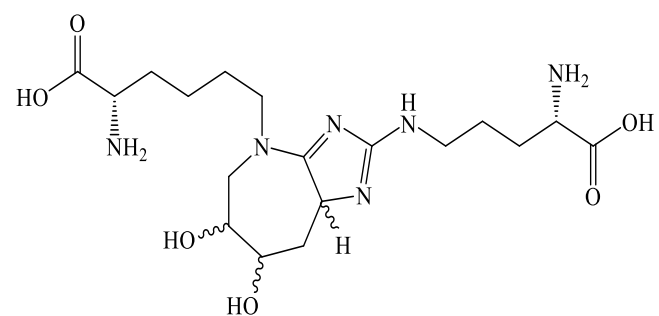
**DOLD**



**MODIC**



**Glucosepane**



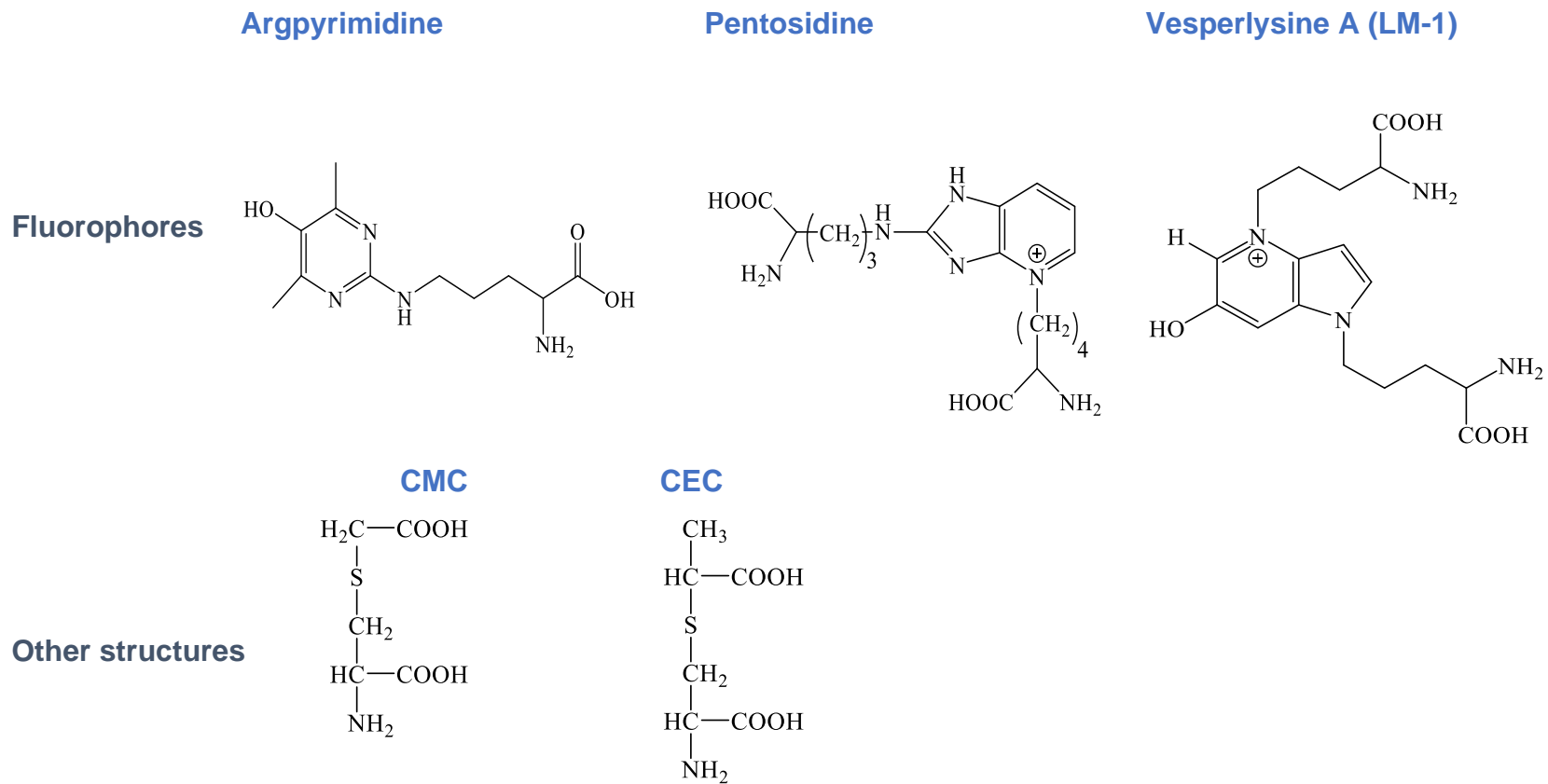


Figure 1.2. AGEs classification based on the molecular structure of glycation adducts and on the mechanism of AGEs formation.



**MGO** (methylglyoxal) has been identified as one of the most reactive glycation agents *in vivo* (approximately, 10.000 – 50.000 folds more reactive than glucose) and a major potent intracellular dicarbonyl intermediate.<sup>35,36</sup> MGO and its derivatives are formed in non-oxidative processes.<sup>37</sup> Recently, they have been reported as the most reactive dicarbonyls which generate reactive oxygen species (ROS).<sup>38</sup> They can interact with free lysine groups to form AGEs like CEL or MOLD. Moreover, reaction with free arginine groups leads to the formation of hydroimidazolones such as N-(5-H-5-methyl-4-imidazol-2-yl)-L-ornithine (MG-H1) or argpyrimidine.<sup>32</sup> These MGO derivatives were shown to cause progression of diabetic complications, such as nephropathy and atherosclerosis, and contribute to tissue injury and protein cross-linking.

**CML** (*N*<sup>ε</sup>-(carboxymethyl)-lysine) is an example of a monolysine non-fluorescent and non-cross-linked AGE which is generated by oxidative processes (glycooxidation product).<sup>37</sup> It is mainly formed through a reaction between lysine and dicarbonyls. Levels of CML in skin collagen and serum of diabetic patients were reported to have increased twofold compared to non-diabetic patients.<sup>39</sup> Additionally, CML could also be formed under food processing conditions, like milk production and baking.<sup>40</sup> As a result, it has become one of the most commonly utilized quality markers for heat-treated food. Its relative stability in acidic conditions facilitates its use as an indicator of the Maillard reaction in both biological and food systems.

**CEL** (*N*<sup>ε</sup>-(carboxyethyl)-lysine) is another monolysine AGE that arises from the reaction of MGO with lysine residues.<sup>12</sup>

**Pyrraline**, which forms non-fluorescent protein adducts, is a glucose-derived pyrrole compound that can be detected and quantified by reverse-phase HPLC in plasma proteins and in human skin collagen.<sup>12,41</sup>

**GOLD** - glyoxal-lysine dimer, **MOLD** - methylglyoxal-lysine dimer and **DOLD** - 3-deoxyglucosone-derived lysine dimer, are di-lysyl cross-linked structures.<sup>30</sup> Quantitative analysis indicated that MOLD is the major chemically characterized cross-link formed in

lens protein during the Maillard reaction.<sup>42</sup> DOLD, a product formed by reaction of 3-deoxyglucosone with protein, has not yet been detected in tissue proteins.<sup>42</sup>

**MODIC** (methylglyoxal derived imidazoline crosslink) and **GODIC** (glyoxal derived imidazoline crosslink) are cross-links of lysine and arginine with GO and MGO. In addition to glucose-derived AGE-protein cross-links, AGE cross-linking occurs between tissue proteins and AGE-containing peptide fragments. These reactive AGE-peptides are named “glycotoxins” because of their harmful properties to the body after a prolonged period of time.<sup>26</sup> Recently, tobacco smoke has been investigated as a potential source of MODIC and GODIC.<sup>9</sup>

**Glucosepane** is the single most important cross-linked AGE in old human collagen and human eye lenses, and it is, therefore, associated with increased stiffness of arteries, joints, and lenses in diabetes.<sup>30</sup>

**Argpyrimidine** is a protein modification of MGO and arginine-containing proteins. It has been detected in cataractous lenses by HPLC methods.<sup>12</sup>

**Pentosidine** is a fluorescent cross-linked AGE formed mainly in reactions with pentoses and lysine or arginine residues by oxidative processes.<sup>37</sup> It was determined in tissue proteins such as lens proteins and skin collagens, accumulating with age and diabetic conditions.<sup>43</sup>

**Vesperlysine A, B, C** are major fluorescent AGEs (acid stable) which are cross-linked products from two lysine sidechains in proteins, and are considered to be generated from lysine and the oxidative degradation of glucose.<sup>44</sup>

In conclusion, among the most studied and well characterized AGEs, which have been detected in a wide range of human tissues, are pentosidine, CML and MGO derivatives. They can be considered as biomarkers for AGEs formation.

## 2.4 Pathophysiological significance of protein glycation

Normally, two factors have significant impact on the glycation process in the human body, namely, the reactive sugar and the protein involved. Firstly, there has been particular interest in the type of monosaccharides, which could participate in protein glycation. Aside from aldohexoses (glucose and galactose), which play a vital nutritional role, aldopentoses (e.g. ribose) can be obtained from the diet or can be synthesized from glucose through the hexose monophosphate shunt. The rate of protein glycation varies depending on the reactivity of particular monosaccharides and their concentration and conformation. Ribose has been reported to be the most reactive sugar to trigger the glycation process and the formation of AGEs.<sup>45</sup> This can be explained by the chemistry of the molecule, since pentacyclic furan rings have a bit twisted conformation and are less stable than hexacyclic pyran rings, leading to a higher ratio of the open, reactive aldehyde, which easily reacts with the amino group of proteins.<sup>46</sup> Moreover, glycation of proteins can take place at the  $\epsilon$ -amino group of lysine residues in hemoglobin, human serum albumin,  $\alpha$ -crystallin, IgG and IgM; or in arginine residues and histidine, tryptophane and cysteine. The majority of the glycated proteins in plasma exist as Amadori products rather than the more labile Schiff bases; and only a small part is converted to AGEs.<sup>47</sup>

AGEs formation takes place under normal physiological conditions but the equilibrium can be shifted in a state of hyperglycemia.<sup>48</sup> Most AGEs accumulate with age in long-lived tissue proteins like lens crystallins and collagen.<sup>49</sup> Due to their slow formation, it was believed that AGEs accumulate only on long-lived extracellular proteins, although a rapid extracellular AGEs formation on short-lived proteins and intracellular AGEs formation by reactive dicarbonyl compounds has become a topic of research interest.<sup>50</sup> The damaging effects of AGEs could be related to several mechanisms of action:

- **production of free radicals;**
- **carbonyl stress;**
- **interaction with AGEs receptors (RAGE) on the cell surface;**
- fragmentation of proteins and lipids;
- altering enzyme activity;

- modifying immunogenicity;
- oxidation of nucleic acids and lipids.<sup>51</sup>

The most significant ones like production of free radicals, carbonyl stress and AGEs-RAGE interaction are discussed briefly: *Oxidative stress* is defined as a condition of serious imbalance between the production of free radicals (ROS) and antioxidant defence mechanisms, leading to potential tissue dysfunction and damage. ROS were reported as specific signaling molecules in both physiological and pathophysiological conditions. To a certain extent their generation is important to maintain homeostasis; however, a high oxidant level leads to damage of various cell components and to activation of specific signaling pathways like nuclear factor- $\kappa$ B (NF- $\kappa$ B) (Figure 1.3).

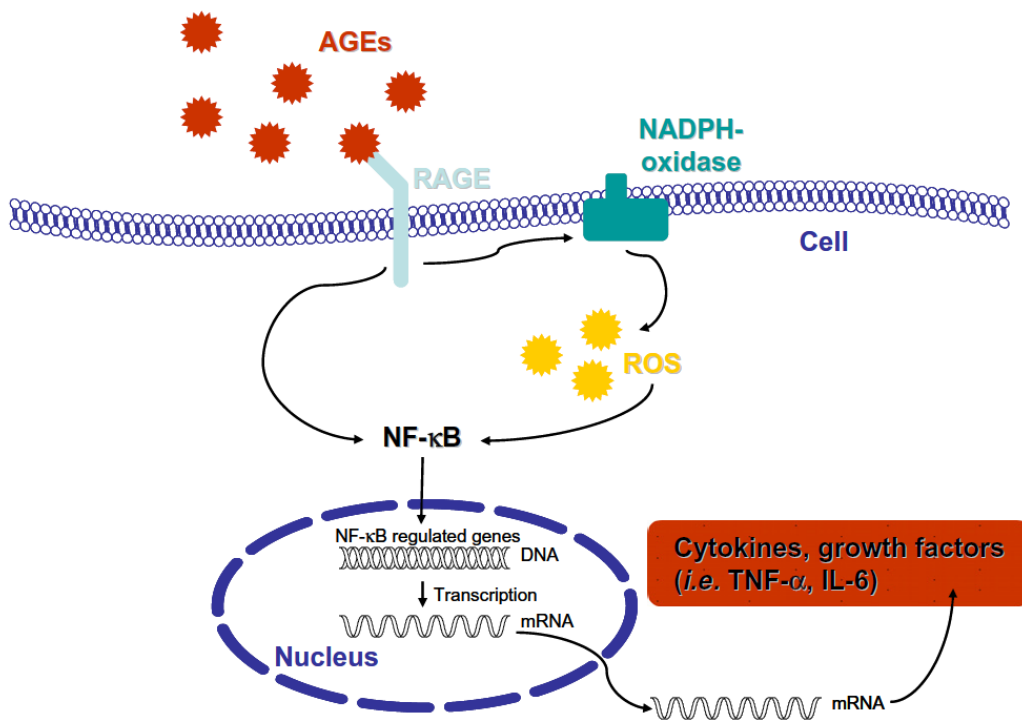


Figure 1.3. Interaction of AGEs with RAGE leading to oxidative stress and initiation of an inflammation cascade involving NF- $\kappa$ B, IL-6, TNF- $\alpha$ , leading to diabetic complications like atherosclerosis, nephropathy, neuropathy, retinopathy, wound healing.<sup>52</sup>

Inside cells, the impact of glycation is countered by high turnover and short half-life of many cellular proteins. Long-lived extracellular proteins, however, accumulate glycation

adducts with age. Extracellular degraded glycated proteins are recognized by specific receptors.<sup>29</sup> Multiple receptor independent and dependent pathways, linking AGEs to cellular and tissue dysfunction, have been proposed.<sup>53</sup> So far, it is well-understood that the interaction between AGE-modified proteins and AGE-specific receptors (RAGEs) on the cell surface induces the overproduction of ROS and inflammatory mediators, which lead to cellular disorder in biological systems. The receptors for AGEs (AGE-R1, AGE-R2, AGE-R3 and RAGE) have been identified as transmembrane multi-ligand receptors belonging to the immunoglobulin superfamily.<sup>46</sup> The receptors are widely expressed in vascular cells, smooth muscle cells, fibroblasts, and monocyte/macrophages. The link between RAGE and its ligands triggers a cascade of intracellular events, followed by the transcription of a range of genes involved in different biological systems, as well as other reactions such as the induction of oxidative stress. All of these reactions lead to series of functional changes that participate in neurological and vascular complications in diabetes, metabolic syndrome, etc.<sup>51,54</sup> In endothelial cells, for example, binding any of these ligands to RAGE activates NF- $\kappa$ B, subsequently leading to increased expression of pro-atherogenic mediators such as monocyte chemoattractant protein-1 (MCP-1) or vascular cell adhesion molecule-1 (VCAM-1).<sup>52</sup>

The hypothesis of cellular damage (to cardiac muscle and neuronal cells) associated with age-related diseases and explained by excessive oxidative stress, has been formulated a long time ago. However, recently new pharmaceutical targets have been characterized, opening new research challenges. A relatively new field of interest is the *carbonyl stress*, an imbalance of reactive carbonyl species (RCS) production and carbonyl scavenging mechanisms. Carbonyl stress may be both a cause and consequence of oxidative stress.<sup>55</sup> An important step in the glycation reaction is the generation of reactive intermediate products during all stages and pathways of glycation. For example, Schiff bases are highly prone to oxidation and free radical generation, which lead to the formation of RCS, such as GO, MGO and 3-DG. Compared to ROS, these aldehydes are more stable and diffuse within or even escape from the cell and attach to targets far away from their site of formation. MGO and GO can react with lysine residues to form CEL and CML, respectively, while the three oxoaldehydes can lead to the analogous di-lysyl cross-linked MOLD, GOLD and DOLD. The phenomenon accelerates in diabetes and in

glycemia. Through generation of ROS and RCS, AGEs contribute to tissue injury by alteration of extracellular matrix structures through formation of protein cross-links, and alteration of intracellular short-lived proteins like metabolic enzymes and mitochondrial protein complexes.<sup>53</sup>

In animals, there are number of enzymatic defence mechanisms against glycation, catalyzing the repair of early glycation adducts and preventing the formation of AGEs. For example, glyoxalase I/II and aldo-keto reductase prevent formation of AGEs by metabolism of dicarbonyl compounds.<sup>15</sup>

There is a considerable body of evidence that the formation and accumulation of AGEs is implicated as a major factor in the progression of various pathological conditions, such as:

### Atherosclerosis

It is well-known that diabetes is a risk factor for the progression of atherosclerosis. Hyperglycemia results in an accumulated amount of AGEs in the blood vessels, which induces proliferation of smooth muscle cells, thickening of the intima (plaque formation and sedimentation) and rigidity and stiffness of the vessels. Moreover, AGEs stimulate foam cell formation by lipid and protein glycosylation. The low-density lipoproteins (LDL) are not discarded in the normal way and then accumulate in the monocytes to form foam cells. The reason for this is that the LDL receptor does not recognize the glycated LDL. The AGE-RAGE complex induces atherosclerosis by enhanced expression of VCAM-1 on the endothelial cells. As a result, VCAM-1 promotes adhesion of the monocytes to the endothelial cells. Then, the monocytes differentiate to macrophages which transform to foam cells by lipid uptake. Generally, pathological glycation of collagen is the major cause of tissue dysfunction due to cross-linking that could cause decreased elasticity, increased thickness and rigidity of the vessel lumen. As a result, the vascular damage associated with diabetes is the key for microvascular complications like neuropathy, nephropathy and retinopathy.<sup>12,56</sup> The AGE-RAGE complex increases the production of cytokines and growth factors, which are responsible for the development of macrovascular complications like generalized atherosclerotic plaques.<sup>35</sup>

### Diabetic retinopathy

Retinopathy is the major cause of blindness in diabetic patients. The accumulation of AGEs leads to thickening of the capillary basement membrane, enhanced permeability of the capillaries, and apoptosis of pericytes. Hyperglycemia stimulates an excessive expression of RAGE on pericytes and endothelial cells, causing deterioration of the pericytes. The loss of pericytes is the clinical expression of retinopathy. Moreover, a high level of AGEs in retinal cells includes expression of vascular endothelial growth factor which causes destruction of the blood-retinal barrier and microvascular hyper-permeability, which finally leads to blindness or poor vision.<sup>51</sup>

### Diabetic nephropathy

Diabetic nephropathy, which is considered as the most life-threatening condition in diabetic patients, is associated with basal membrane thickening and decreased filtration.<sup>57</sup> The sedimentation of proteins in the glomerular space plays a significant role in the reduction of filtration. AGEs stimulate an extreme RAGE expression, which encourages cell inflammation signaling pathways, such as NF- $\kappa$ B activation, as well as generation of cytokines and growth factors. The transforming growth factor- $\beta$  (TGF- $\beta$ ) is increasing the synthesis of collagen matrix components, which leads to higher thickness of the basement membrane, increased vascular permeability and reduced barrier activity.<sup>58</sup> Further evidence for glomerular injuries comes from immunohistochemical studies that have identified a number of AGEs like CML, pyrraline and pentosidine in renal tissues of diabetic patients.<sup>12</sup>

### Diabetic neuropathy

In general, diabetes can affect the central, peripheral and autonomic systems. The manifestation of diabetic neuropathy can be characterized by functional abnormalities (reduced blood flow) and structural changes like axonal degeneration, fibre demyelination and neuronal apoptosis. Particularly, AGEs react with plasma proteins like IgM and IgG to activate the demyelination of the peripheral neurons. The complex AGE-RAGE induces ROS formation and several intercellular signaling pathways. ROS promotes both AGEs formation and AGEs quenching of nitric oxide (NO). Consequently, the NO level in the

cells is decreased, which results in nerve ischemia (lack of oxygen) and then nerve dysfunction.<sup>51</sup>

### Diabetic wound healing

Wound healing in diabetic patients is hindered by the AGE-RAGE complex which stimulates production of pro-inflammatory factors resulting in collagen degradation.<sup>51</sup>

### Alzheimer's disease (AD)

The increased number of AGEs can cause extensive cross-linking, oxidative stress and neuronal cell death representing the neuropathological and biochemical characteristics of Alzheimer's disease, hampering the function of proteins or tissues.<sup>59</sup>

## 2.5 AGEs inhibitors/ breakers: Where are we now?

Nowadays, there is an increased interest in agents with anti-glycation activity that could play a key role for prevention and amelioration of AGE-mediated health problems. Current studies attempt to search for effective phytochemical compounds from dietary plants, fruits, and herbal medicines to inhibit AGEs formation.<sup>46</sup> Considering the complexity of pathways and reactions involved in AGEs formation, not only the final products (AGEs and ALEs) but also the highly reactive intermediates (MGO) should be considered as a target group in the design of specific inhibitors or breakers. Secondly, glycoxylated proteins generate ROS and induce oxidative stress through the reaction with RAGE. Thus, antioxidants may also be considered to have a role in the inhibition of AGEs. Additionally, inhibitors of fructosamine and  $\alpha$ -dicarbonyl formation, as well as preventing further interaction with proteins could reduce AGEs formation.<sup>60</sup>

Glycation is a major source of ROS and RCS that are generated by both oxidative (glycoxidative) and non-oxidative pathways.<sup>61</sup> Therefore, potential AGE inhibitors are difficult to distinguish from general anti-oxidants, such as plant polyphenols. Contrary to the glycation of proteins by glucose, RCS such as MGO and GO exhibit both extracellular and intracellular glycating properties, and are involved in non-oxidative glycation reactions and the formation of AGEs *in vivo*. Glycation inhibitors, whose activity is based



on antioxidative properties, may not effectively inhibit non-oxidative protein glycation.<sup>60</sup> In addition, glucose itself can auto-oxidize to form hydrogen peroxide and keto aldehydes in the presence of transition metal ions, and subsequently accelerate the formation of AGEs. Knowing the link between glycation and oxidation, it could be hypothesized that antioxidants might possess antiglycoxidative activities.<sup>61</sup> Therefore, antioxidants have been tested for preventing protein glycation. The inhibition of free radicals generation derived from glycation processes and inhibition of protein modification is considered as one of the mechanisms of anti-glycation activity. Many data have shown that typical antioxidants / nutrients such as vitamin B1 (thiamine) and B6 (pyridoxamine) inhibited *in vitro* and *in vivo* AGEs formation.<sup>61</sup> Another preventive or therapeutic approach is to use nucleophilic anti-RCS molecules such as aminoguanidine, pyridoxamine or metformin. They could inhibit AGEs, remove RCS, and prevent the interaction of AGEs with RAGE. AGEs inhibitors can act through several mechanisms which have been discussed in more details below (Figure 1.4).



Figure 1.4. Possible mechanisms of action for AGEs inhibitors.<sup>32</sup>

AGEs inhibitors can be divided into two groups: synthetic compounds and natural products. The inhibitory mechanism is accomplished by blocking sugar attachment to proteins, attenuating glycoxidation and oxidative stress through trapping or scavenging some intermediates including reactive dicarbonyls, free radicals and nitrogen species produced in the process of glycation, and breaking down formed cross-links.<sup>35</sup> Example of specific AGEs inhibitors and AGE breakers are aminoguanidine, alagebrium; B-vitamins (thiamine and pyridoxamine) and synthetic derivatives of B-vitamins such as benfotiamine; and aldose reductase inhibitors (ARI) like epalrestat.<sup>50</sup> The investigation and discovery of “AGEs-inhibitors” and “AGEs-breakers” may represent a therapeutic approach for lowering the risk of diabetic or other pathogenic complications caused by AGEs formation.<sup>35</sup> So far, a large number of compounds have been reported as inhibitors of glycation and AGE-protein cross-link formation. Additionally, the term “AGEs-breakers” was suggested by Cerami and described compounds which may cleave glycation derived

cross-links and reverse the damaging effects of glycation associated with aging and diseases.<sup>62</sup>

### 2.5.1 Synthetic AGEs inhibitors

In general, the synthetic AGEs inhibitors are divided into three classes:

- Carbonyl trapping agents, which attenuate carbonyl stress;
- Metal ion chelators, which suppress glycooxidation;
- Cross-link breakers, which reverse AGEs cross-links.<sup>63</sup>

Few synthetic inhibitors affect the **early** stage of glycation. These are (Figure 1.5):

**Acetylsalicylic acid** – it is inhibiting the glycation process *via* acetylating free amino groups of proteins, thereby blocking the attachment of reducing sugars, and consequently, preventing late complications of diabetes such as sugar-induced cataract.<sup>35</sup> Historically, it was the first agent to reduce glycosuria in diabetic patients.<sup>12</sup>

**Diclofenac** – a non-steroidal anti-inflammatory agent (NSAIDs), is an Amadori product inhibitor *in vitro*.<sup>64</sup> It can protect proteins from sugar attachment due to its non-covalent interaction with proteins. It was reported that diclofenac blocked at least one of the major glycation sites of human serum albumin. In general, it is active at the early stage of glycation.<sup>30</sup>

**Metformin** – is an oral antidiabetic biguanide drug which possesses structural similarities to aminoguanidine and it is used in the treatment of type 2 diabetes. Beisswenger *et al.* described that type 2 diabetic patients have increased MGO concentration in blood, which was significantly reduced by high dose metformin treatment.<sup>65</sup> The mechanism of action is suggested to be trapping of MGO and other dicarbonyls. In contrast to aminoguanidine which is active on the Amadori stage, metformin shows greater effect on the post-Amadori

stages. It can be concluded that metformin is a multistage inhibitor of glycation, for both Amadori and, especially, post- Amadori pathways.

**Pioglitazone** – is a member of the thiazolidinedione compounds, sensitizing peripheral tissues to insulin. *In vitro* studies showed inhibition of glycation and AGEs formation due to direct interaction between the hydrazine nitrogen atom of pioglitazone and a carbonyl group.<sup>32,38</sup>

Most synthetic inhibitors (Figure 1.5), however, play a major role in preventing the formation of AGEs at the **latest** stage of glycation, which is related to their scavenging abilities on both reactive carbonyls and radicals formed during glycation, or blocking the formation of intermediate Amadori products. The activity of aminoguanidine and pyridoxamine can be related to their carbonyl scavenging activities.

**Aminoguanidine** – the nucleophilic hydrazine derivative, aminoguanidine (Pimagedine™), was the first compound reported to inhibit formation of AGEs and diabetes-induced protein cross-linking.<sup>66</sup> Due to its nucleophilic nature, aminoguanidine is highly reactive and can reduce AGEs formation by targeting  $\alpha$ -dicarbonyl intermediates such as GO, MGO and 3-DG to form 3-amino-1,2,4-triazine derivatives.<sup>6,67</sup> It is known to inhibit CML and CEL formation, cross-linking, and fluorescence in skin collagen of diabetic rats, and to significantly retard the development of diabetic nephropathy.<sup>12</sup> Moreover, aminoguanidine is a well-known inhibitor of NO formation.<sup>38</sup> The half-life of aminoguanidine in plasma is short (about 1 h), and as a result, it must be applied at a relatively high dose (1 g/L in drinking water) to produce a sufficiently active concentration.<sup>68</sup> Generally, the use of high concentration aminoguanidine is not recommended because of its reaction with vitamin B6, which can result in a deficiency.<sup>48</sup> In the period 1994-1998 Pimagedine™ was evaluated in clinical trials for the prevention of nephropathy in diabetic patients (ACTION I and ACTION II). The results suggested that aminoguanidine was beneficial in the prevention of short term glycation, in contrast to prevention of AGEs formation on long-lived proteins. In the end, the trails were eventually terminated due to the unfavorably perceived risk-to-benefit ratio and safety

concerns – elevation of liver enzymes and development of autoantibodies. In preliminary studies aminoguanidine retarded the development of nephropathy, retinopathy and vasculopathy; however, it had no effect on hyperglycemia. Among the side effects reported in patients were pernicious-like anemia, and the development of anti-nuclear antibodies (ANF) at high doses therapy.

**Pyridoxamine (vitamin B6)** – has been reported to inhibit the conversion of Amadori products to CML, to quench the  $\alpha$ -dicarbonyl precursors (MGO, GO) *in vitro*, and to block the oxidative degradation of glucose-derived Amadori intermediates.<sup>69-70</sup> Pyridoxamine does not directly interact with Amadori intermediates, but interferes with the post-Amadori oxidative reactions by binding catalytic redox metal ions. In 2014 the Phase III PIONEER program was started by NephroGenex Inc. to examine the efficacy of PYRIDORIN® (pyridoxamine dihydrochloride) in type 2 diabetic patients. The trial is still in progress.

**Thiamine (vitamin B<sub>1</sub>), benfotiamine (synthetic derivative)** – Vitamin B1 and vitamin B1 derivatives were reported for intracellular AGEs inhibition *in vitro*.<sup>71</sup> *In vivo* the activity is correlated with the bioavailability, which is higher for the lipid-soluble derivative benfotiamine.<sup>67</sup> So far, there is a lack of evidences for activity of those compounds on the concentration of  $\alpha$ -dicarbonyls or AGEs. The proposed mechanism of action of benfotiamine involves shunting of triose glycolytic intermediates towards the reductive pentose pathway.<sup>58</sup>

Series of other compounds like the calcium antagonist **amlodipine** show activity based on **radical scavenging properties**. They do not trap reactive dicarbonyl precursors of AGEs, but inhibit their production by chelating transition metals and blocking various oxidative steps including hydroxyl radicals at the pre-Amadori steps.

**Captopril, Ramipril** – Angiotensin Converting Enzyme (ACE) inhibitors have been reported to inhibit formation of fluorescent AGEs (e.g. pentosidine) and markers of the protein damage due to oxidative stress such as nitrotyrosine.<sup>30,72</sup>

**Olmesartan, Valsartan** – angiotensin II receptor inhibitors (AIIIRIs) inhibited the *in vitro* formation of pentosidine and CML.<sup>30</sup>

A few **cross-link breakers** have also been investigated.

**Alagebrium** – 4,5-dimethyl-3-phenacylthiazolium chloride (ALT-711<sup>®</sup>): Its mechanism of action against glycation is controversial. One of the suggested mechanisms is chemical cleavage of the carbon-carbon bond in  $\alpha$ -dicarbonyl-containing cross-linked structures (cross-link breaker). It directly targets the biochemical pathway leading to stiffness of the blood vessels, and as a result it was improving the ventricular and arterial compliance.<sup>50</sup> Interestingly, alagebrium is one of the most studied anti-AGE drugs in the clinical arena. Between 2001 and 2003 the SILVER, SAPPHIRE and DIAMOND studies were conducted with individuals with left ventricular hypertrophy; however no significant changes were observed. Four clinical trials were carried out in the 2004-2009 period, and one in 2013. Unfortunately, these trials were prematurely discontinued due to bankruptcy of the company and loss of patent protection during the global financial crisis. Two final randomized, double-blind, placebo-controlled studies used a combination of exercises with 200 mg daily intake of alagebrium for one year. Alagebrium was well tolerated and, whilst one study saw no independent effects on oxygen uptake, endothelial function and arterial stiffness, the other observed effects of alagebrium on left ventricle stiffness compared to the control. However, due to the lack of completed clinical studies the beneficial effects observed in diabetic rats were not proved for patients. To date, no further clinical trials have been carried out with alagebrium.<sup>67</sup>

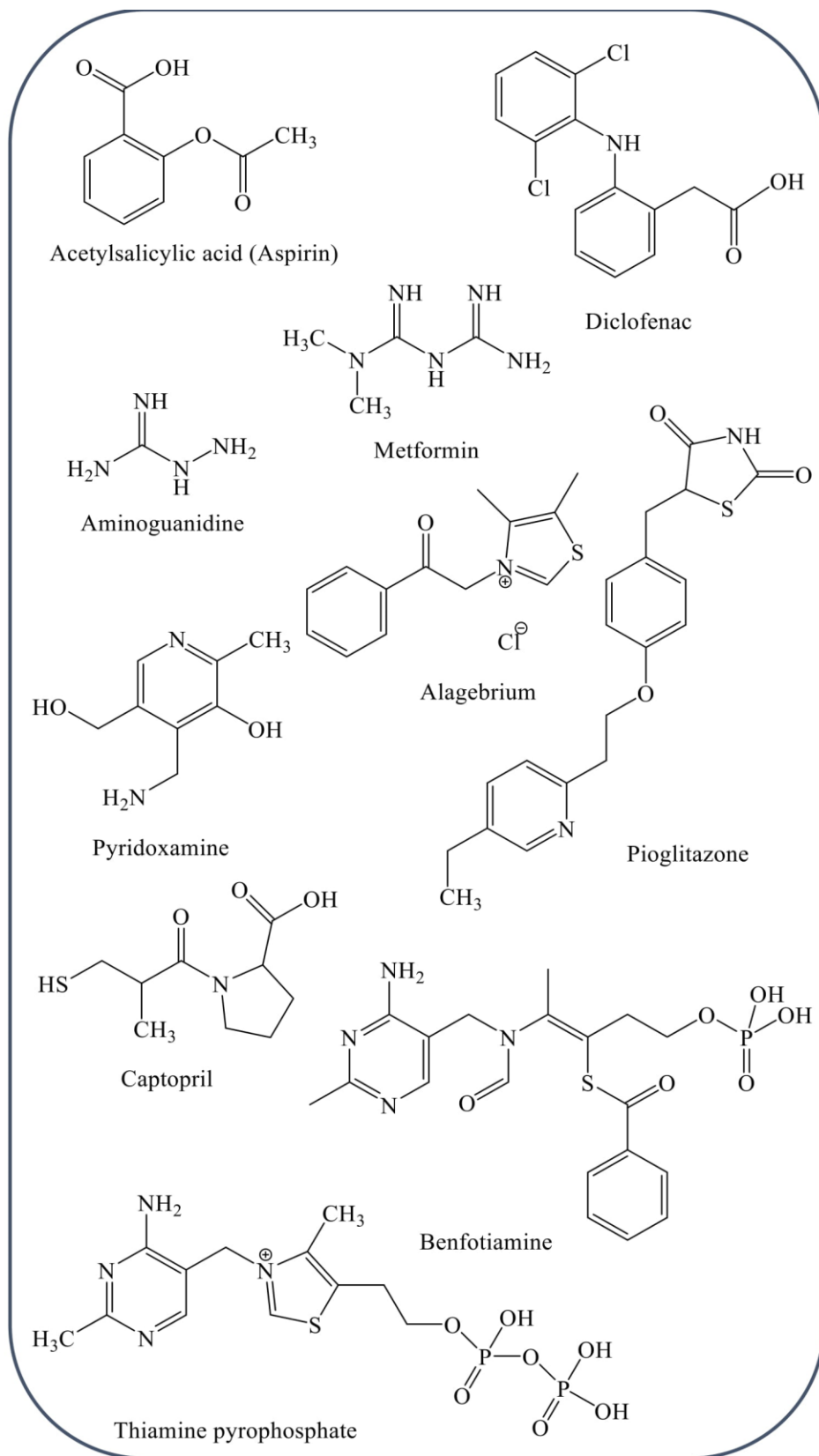


Figure 1.5. Chemical structures of several synthetic AGEs inhibitors.

## 2.5.2 Natural products as AGEs inhibitors

Considering the toxic or side effects of synthetic molecules in clinical trials, natural products can be more promising candidates as potent AGEs inhibitors. Phytochemicals exhibit several antiglycation mechanisms (see Figure 1.4), including effects on glucose metabolism, amelioration of oxidative stress, scavenging of dicarbonyl species, and up/down-regulation of gene expression.<sup>51</sup> So far, some plant extracts and their phenolic ingredients have been evaluated for activity against AGEs formation, and also for their antioxidant activity. Therefore, natural products with strong inhibitory properties on AGEs formation have great potential for further investigation as preventive drugs against AGE-associated diseases and disorders.<sup>35</sup> However, it remains unknown whether phytochemicals possess protective effects against glycotxin-induced damage. While the anti-AGEs activity of a wide variety of synthetic molecules has already been evaluated, the chemodiversity of natural products such as secondary metabolites of vegetal origin still needs to be thoroughly explored.<sup>52</sup> Many plant products and their active constituents have been reported for prevention and treatment of various pathological conditions in the human body. Particularly, various natural products, plant extracts, fractions or pure compounds have been excessively tested for AGEs inhibition.<sup>26,73</sup> In the group of plant extracts with anti-AGEs properties, as an example, the following species can be listed (Figure 1.6):

**Cinnamon:** due to the content of catechin, epicatechin and procyanidin B2 it inhibits CML and pentosidine formation. Additionally, the catechins were found to reduce MGO to the physiological level.<sup>26,51</sup>

**Garlic (*Allium sativa*):** S-ethylcysteine and S-propylcysteine are strong antioxidants and free-radical scavengers, inhibiting CML formation and the plasma HbA<sub>1c</sub> (glycated hemoglobin).<sup>26,35</sup> HbA<sub>1c</sub> is the most abundant of the hemoglobin derivatives in normal human red blood cells *in vivo*, accounting for approximately 5% of total hemoglobin. The measurement of HbA<sub>1c</sub> is used for the evaluation of long term glycemic control over the 6 - 8 weeks preceding analysis.<sup>9</sup>



***Ilex paraguariensis*** (maté): contains high level of antioxidants, which are proved in *in vitro* models to inhibit the second phase of the glycation reaction, namely, the free radical-mediated conversion of Amadori products to AGEs.<sup>26,35</sup>

***Rosmarinus officinalis***: carnosic acid and carnosol possess antioxidant activity and anti-glycation properties comparable to aminoguanidine.<sup>26</sup>

***Camellia sinensis***: (-)-epigallocatechin 3-O-gallate (EGCG) and (-)-epicatechin 3-O-gallate (ECG): strong antioxidant properties and inhibition of the accumulation of CML, CEL and the activation of RAGE.<sup>26</sup>

***Citrus reticulata x Citrus sinensis***, and ***Citrus reticulata x Citrus paradisis***: the exocarp extracts decreased AGEs formation by lowering the levels of carbonyl compounds in adipocyte cells *in vitro*.<sup>51</sup>

A standardized extract from ***Ginkgo biloba* (EGb 761)**, containing 24% flavonoids and 6% terpenoids, was proved to inhibit the RAGE activation in microvascular endothelial cells induced by hypoxic and hypoglycemic conditions.<sup>26</sup>

Of particular interest are some natural products with anti-AGEs properties (Figure 1.6):

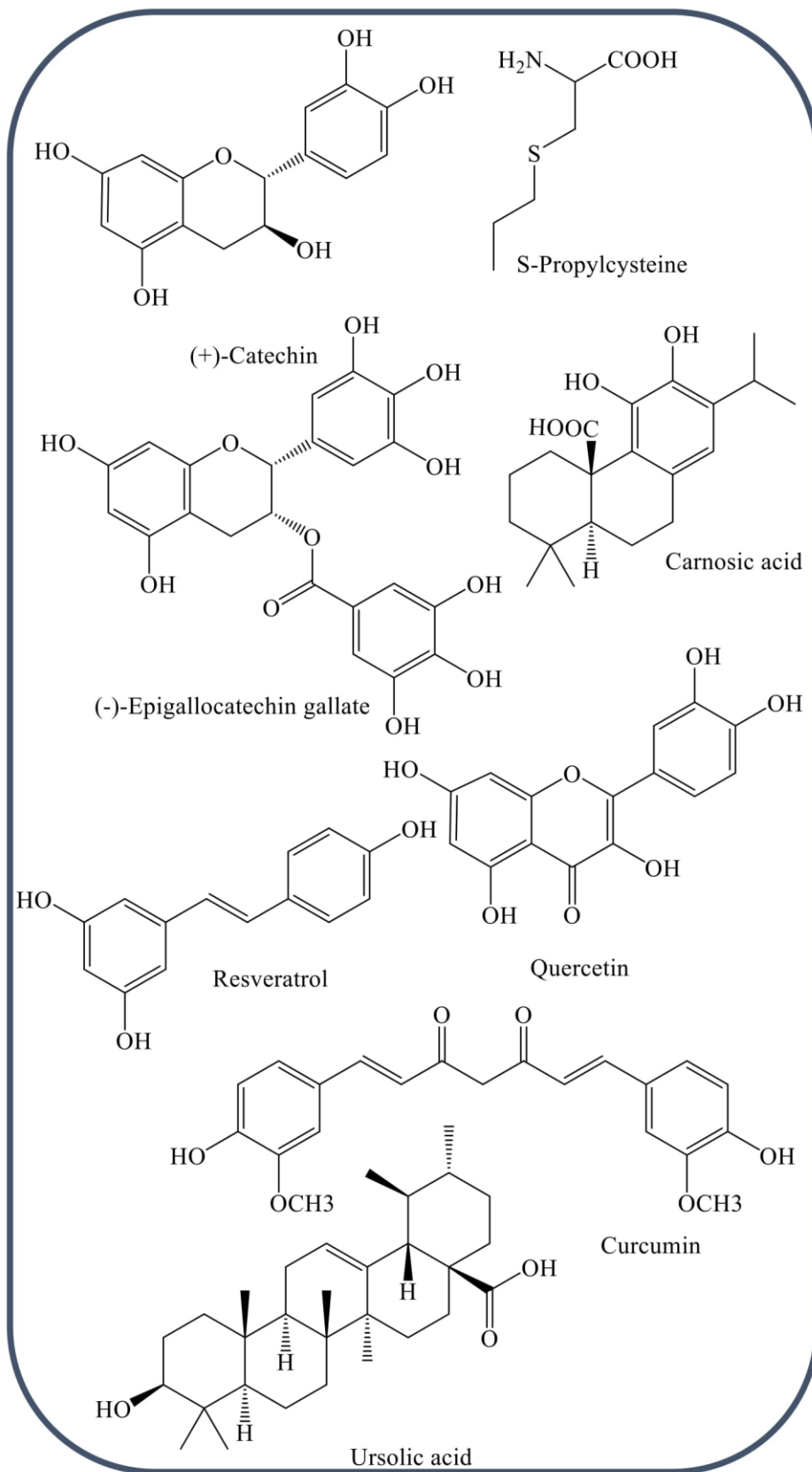


Figure 1.6. Chemical structures of several natural products with AGEs inhibiting properties.

**Flavonoids** have been extensively investigated as AGEs inhibitors. In general, it is difficult to draw a clear line between the structural characteristics of flavonoids for inhibition of protein glycation and radical scavenging activities. However, Matsuda *et al.* suggested the following requirements which should be present in the structures of potential AGEs inhibitors: (1) an increasing number of hydroxyl groups in position 3', 4', 5, 7 is associated with increased inhibitory activity; (2) flavones are more active than the corresponding flavonols, flavanones and isoflavones; (3) methylation or glycosylation of the 4'-hydroxyl group of flavones, flavonols and flavanones reduces activity; (4) methylation or glycosylation of the 3-hydroxyl group of flavonols tends to increase activity; (5) glycosylation of the 7-hydroxyl group of flavones and isoflavones reduces activity.<sup>74</sup> The most promising candidates for AGEs inhibitors have been the more polar compounds *sensu lato* such as hyperoside, (+)-catechin, apigenin, vitexin, quercetin, rutin, naringenin.<sup>75</sup>

**Resveratrol** – a natural antioxidant found in grapes has been described to inhibit AGEs-induced proliferation and collagen synthesis in vascular smooth muscle.<sup>76</sup>

**Curcumin** – additionally to its anti-oxidant and anti-inflammatory properties, curcumin was reported to be a potent inhibitor of AGEs formation and cross-linking of collagen in diabetic rats.<sup>77</sup> It prevented the accumulation of AGE-collagen in diabetic animals; also, Hu *et. al* reported trapping of MGO by curcumin in cell-free systems and in human umbilical vein endothelial cells (HUVECs). Thus, curcumin may prevent MGO-induced endothelial dysfunction by directly trapping MGO.<sup>26,78</sup>

**Silymarin** – a flavonolignan obtained from *Silybum marianum*: in addition to its free-radical scavenging properties, it has shown *in vitro* inhibitory effects on the late-stage glycation and subsequent cross-linking.<sup>26</sup>

Other groups of compounds include: anthraquinones (emodine), coumarins, **carotenoids**, especially lutein and  $\beta$ -carotene from the ethyl acetate fraction of the green microalgae *Chlorella zofingiensis*, contribute to the strong antiglycation activity of this

species; **unsaturated fatty acids** such as linoleic acid, arachidonic acid and eicosapentaenoic acid from *Nitzschia laevis* were reported as inhibitors of glycation; **triterpenes and saponins**: astragaloside V from the crude extract of Astragali Radix has shown inhibition of formation of CML and pentosidine in *in vitro* samples.<sup>26,63,75</sup> Moreover, **ursolic acid** was suggested to play a significant role in patients with diabetes in reducing hyperglycemia, hepatic glucose production, hyperlipidemia and the influx of glucose through the polyol pathway.

Considering that AGEs are major pathogenic propagators in many human diseases, and especially in diabetes and its complications, it is of great importance to identify anti-glycation substances and to examine their mode of action. It is important to note that one AGE inhibitor will not act on all pathways, therefore, it is difficult to accept the existence of a magic bullet. Nevertheless, the current project seeks to address the lacuna in contemporary research for new drugs or lead compounds with AGEs inhibiting properties.

### 3. *The machinery of autophagy*

Recently, it has been shown in cardiomyocytes that AGEs induced autophagy and that this process was blocked by RAGE inhibitors.<sup>79</sup> The autophagic process is classically considered to be a pathway contributing to cellular homeostasis and adaptation to stress by removing damaged or unwanted intracellular material. In this way, it may act as a pro-survival mechanism in an adverse and stressful environment. Therefore, induction of autophagy by RAGE may be considered as a protecting mechanism against oxidative stress caused by AGEs. Similar to AGEs, autophagy has been associated with a plethora of different pathological conditions including heart diseases, cancer, neurodegeneration, infectious diseases, diabetes and autoimmune diseases.<sup>80,81</sup> A considerable body of evidence indicates that autophagy is stimulated in atherosclerosis and in oxidative stress conditions.<sup>82,83</sup> Therefore, modulation of autophagy was chosen as a target to be investigated in the current project.

### 3.1 Definition

Derived from the Greek words meaning “to eat” (“phagy”) “oneself” (“auto”), the term autophagy refers to a lysosomal degradation pathway of self-digestion.<sup>80</sup> In other words, autophagy is a group of dynamic, multi-step, tightly regulated biological processes for the delivery of macromolecules and organelles into the lysosomes for degradation and recycling.<sup>84</sup> Like other cellular pathways, it can be modulated at several steps, both positively and negatively.<sup>85</sup> Autophagy targets excessive and defective organelles as well as aggregated and long-lived proteins for elimination. Based on hydrolysis steps, the major molecular components are recycled into the cytosol to serve as building blocks or as energy resources. Particularly, components of the cytoplasm are sequestered and moved into the lysosomes or the vacuole lumen, where they are broken into their basic components and returned to the cytosol for reuse. As a result, autophagy has a critical role in the cellular homeostatic mechanism, controlling the balance between available resources and energy consumption. A number of cellular stressors, such as starvation, hypoxia, immune and hormonal stimulation, may induce autophagy above the physiological level.

### 3.2 Types of autophagy

Three main types of autophagy exist in nature – macroautophagy, microautophagy and chaperone-mediated autophagy (Figure 1.7):<sup>86</sup>

Macroautophagy: the cytosolic components for degradation are included in a double-membrane vesicle (autophagosome). The autophagosome fuses with the lysosome, resulting in an autolysosome, where degradation of cytosolic components occurs.

Microautophagy: the lysosomes directly engulf the cytosolic components by membrane invagination.

Chaperone-mediated autophagy: the chaperone proteins interact with cytosolic components, which have to be degraded. The formed complex can be further recognized

by a lysosomal-associated membrane protein 2A receptor, resulting in the transition of the unfolded cytosolic proteins into the lysosome.<sup>81</sup>

Macroautophagy is thought to be the major type of autophagy, and it has been studied most extensively compared to microautophagy and chaperone-mediated autophagy.<sup>87</sup>

Therefore, in the current thesis, hereafter the process of macroautophagy is simply referred to as “autophagy”.

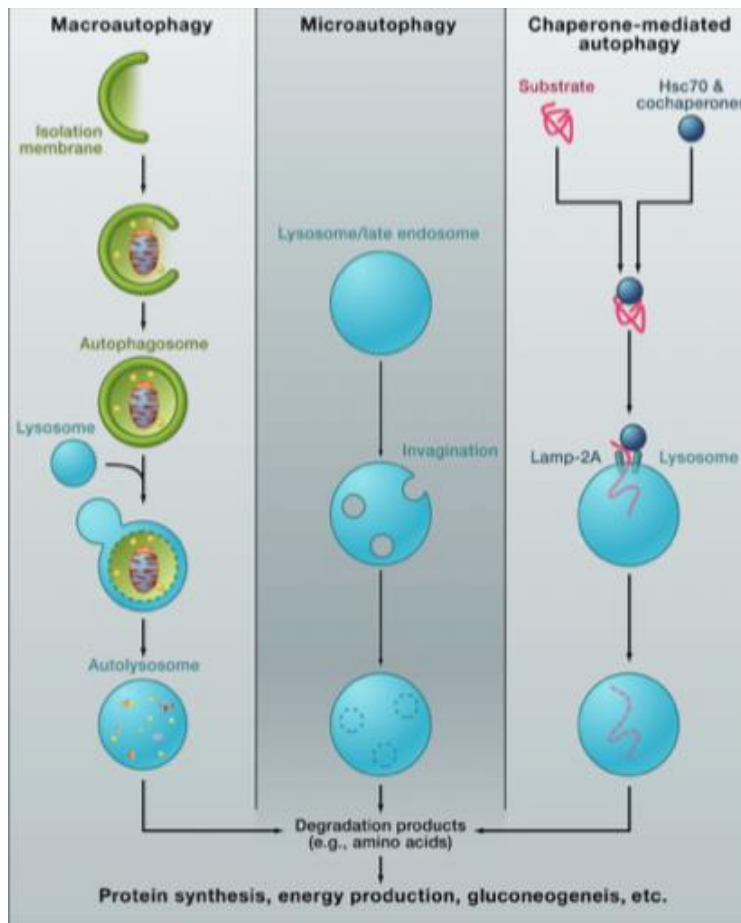


Figure 1.7. Different types of autophagy: macroautophagy – a portion of cytoplasm is enclosed by an isolation membrane (phagophore) to form an autophagosome. The membrane of the autophagosome fuses with the lysosome and the internal material is degraded in the autolysosome; microautophagy – small pieces of the cytoplasm are directly engulfed by inward invagination of the lysosomal membrane; and chaperone-mediated autophagy – the substrate proteins are first recognised by chaperons, then they are translocated into the lysosomal lumen after binding with Lamp-2A receptor.<sup>87</sup>

In general, cytosolic components can be degraded in bulk or *via* a selective mechanism. The selective autophagy pathways are named after the type of cargo for degradation (e.g. mitophagy – mitochondria, ribophagy – ribosomes, lipophagy – lipid droplets). Those pathways depend on the presence of two main factors: selective-autophagy receptors or lipidated proteins LC3 (microtubule-associated protein light chain 3), which ensure the specific degradation of various cellular components, among others. Selective autophagy receptors contain an LC3 interacting region for binding to LC3 family members, which can interact with cellular cargo – mitochondria, endoplasmic reticulum, aggregated proteins, ribosomes, *via* a second binding region (ubiquitin-dependent or ubiquitin-independent).

### 3.3 Autophagic machinery and flux

The autophagy process involves series of events including induction, vesicle nucleation, vesicle elongation, fusion and degradation (Figure 1.8).<sup>82</sup> In each step, autophagy-related proteins (ATG) catalyze specific reactions critical for the maintenance of the autophagic flux.<sup>81</sup>

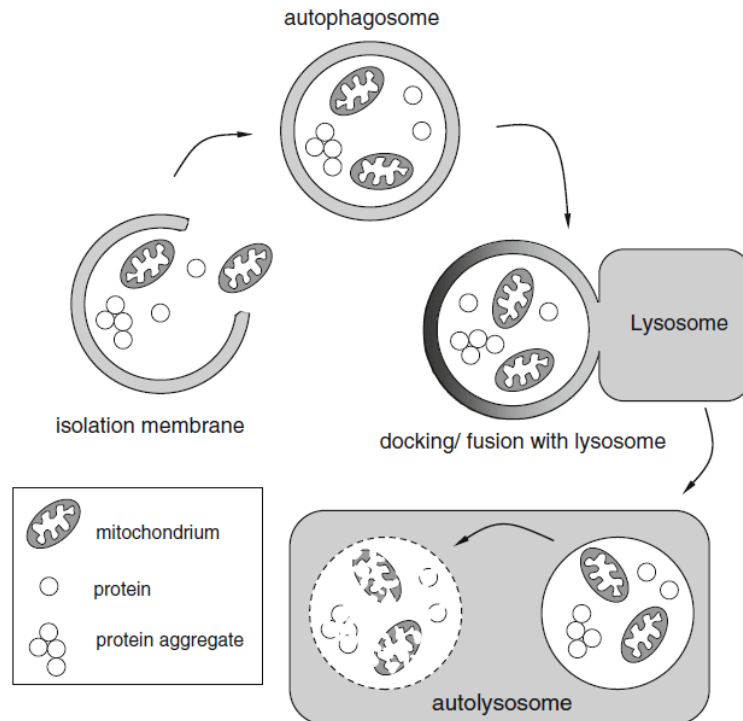


Figure 1.8. Schematic overview of macroautophagy. The process is initiated by formation of isolation membranes or phagophores, which sequester small portions of the cytoplasm and organelles for degradation. The enclosure of the cytoplasmic cargo leads to the formation of autophagosomes. These autophagic vacuoles fuse with the lysosome to form autolysosomes in which the cargo is degraded.<sup>82</sup>

**Induction:** autophagy is induced by many stimuli, including starvation (reduced nutrients availability like amino acids, glucose), withdrawal of growth factors (e.g. insulin and insulin-like growth factors), reduced cellular energy levels (e.g. ATP), extra- or intracellular stress (such as oxidative stress, hypoxia), and pathogenic infections.<sup>88</sup>

**Nucleation and phagophore formation:** the membrane involved in the phagophore formation can originate from the Golgi apparatus, endoplasmic reticulum, mitochondria or endosomes.

**Elongation, autophagosome formation:** the process of vesicle elongation is directed by the activation of two ubiquitin-like conjugation complexes. In the second complex, the critical moment is the processing of the hydrophilic LC3-I to its lipophilic conjugated form - LC3-II. Together, the two complexes take part in the formation of the autophagosome. The moment when the phagophore membrane is entirely closed, completing the



sequestration of the cytosolic content, all ATG proteins dissociate from the autophagosome except LC3, which is the only one associated with the membrane.

Fusion and degradation: the fusion of the autophagosome with lysosomes leads to the formation of a mature hydrolytic organelle – autolysosome that can enable cargo acidification and hydrolysis.

### 3.4 Physiological and pathophysiological role in the human body

Originally characterized as a hormonal and starvation response, autophagy has a much broader role in biology, including organelle remodelling, protein and organelle quality control, prevention of genotoxic stress, tumor suppression, pathogen elimination, regulation of immunity and inflammation, metabolism and cellular survival.<sup>8</sup> Under stress conditions, autophagy mostly plays a protective role by removing damaged or unwanted intracellular material in order to keep the homeostasis e.g. protein and organelle turnover.<sup>8</sup> Additionally, nutrient starvation induces autophagy to recycle the intracellular components, generating the essential metabolites required for the maintenance of the cell viability.<sup>89</sup> However, autophagy is not only involved in physiological conditions but also implicated in a wide range of pathophysiological conditions.<sup>5</sup> Due to the vital role of autophagy in cellular and tissue homeostasis, disruption of autophagy can lead to various disease. For example, loss of autophagy has been proved to result in accumulation of misfolded proteins, which are insoluble aggregates toxic to the cells, and as a result, cause neurodegenerative diseases (Alzheimer, Parkinson, Huntington, tauopathies), and cardiovascular and cerebrovascular diseases (stroke, hypertension, atherosclerosis, cardiomyopathy).<sup>5,84,8,90</sup> Additionally, autophagy plays paradoxical roles in promoting cell survival and cell death during tumor development and in cancer therapy. It functions as a tumor suppression mechanism by removing damaged organelles and proteins, preventing genomic instability that drives tumorigenesis, and inhibiting inflammation. On the other hand, autophagy has been demonstrated to promote the survival of tumor cells under nutrient or chemical stress. As a result, therapeutic modulation of autophagy may serve as an important and challenging endeavour in cancer treatment.<sup>91,92</sup> Similarly, malfunction of autophagy induces the accumulation of ROS and concomitant increase of

DNA damages, such as double-strand breaks, which are closely related to cancer initiation and development.<sup>89</sup> Moreover, in their research paper, Kang *et. al* described a correlation between RAGE expression with elevated levels of autophagy in pancreatic cancer *in vivo* and *in vitro*.<sup>93</sup> In type 2 diabetes, for instance, autophagy is not only providing nutrients to maintain cellular energy during fasting but is also removing damaged organelles, lipids and miss-folded proteins. In addition, autophagy plays an important role in regulating the function of pancreatic  $\beta$ -cells and insulin-target tissues. However, in pathological conditions the process can lead to pancreatic  $\beta$ -cell dysfunction and insulin resistance. Moreover, upon insulin resistance, pancreatic cells enhance their insulin secretion (hyperinsulinemia) to compensate for hyperglycemia, while the number of pancreatic cells is progressively diminished through apoptotic cell death.<sup>94</sup>

### 3.5 Autophagy modulators

Development of autophagy-targeting therapies will depend on a deeper understanding of the benefits, and potential consequences, of altering autophagic activity.<sup>80</sup> Due to the previously described relationship between AGEs formation and autophagy modulation, it is not a surprise that many AGEs inhibitors will have an effect on the autophagy process as well. For example, curcumin and resveratrol (Figure 1.6), apart from their antiglycation, anti-inflammatory, chemo preventive and/or antitumor properties, have been investigated as **autophagy activators** or enhancers.<sup>92</sup> Activation of autophagy plays an important role to ameliorate neurodegenerative disease by removing the aggregate-prone proteins. A series of patents disclosed several alkaloids as novel autophagy enhancers with potential therapeutic application in cancer or neurodegenerative disorders. Recent scientific findings demonstrated that berberine (Figure 1.9), an isoquinoline alkaloid, can induce autophagic cell death and apoptosis by the activation of Beclin-1 and inhibition of the m-TOR signaling pathway.<sup>89</sup> Also, onjisaponin B isolated from Radix Polygalae was claimed as a novel autophagy enhancer, which is useful for treating neurodegenerative diseases.<sup>95</sup> One of the greatest risk factors for neurodegenerative diseases is aging, and the level of autophagy has been shown to diminish with age.<sup>96</sup> A series of compounds related to urolithins (A, B, C, D) and ellagic acid induced autophagy in mammalian cells

across species, and improved motor activity and muscle strength in aged mice.<sup>89</sup> Quercetin (Figure 1.6), an anti-oxidant and antiglycation flavonoid widely distributed in fruits and vegetables, has been reported to inhibit tumor growth through the induction of cancer cell cycle arrest and promotion of apoptotic cell death. Quercetin induces autophagy through the modulation of a signaling pathway (Akt-m-TOR), which plays a protective role in gastric cells. **Autophagy inhibitors** may represent other anti-cancer therapeutic agents, as suggested by evidence that autophagy promotes survival of cancer cells in a stressful cancer microenvironment (e.g. hypoxia, nutrient-limitation). Oblongifolin C, one of the polyprenylated benzoylphloroglucinols isolated from *Garcinia yunnanensis*, was discovered to be a potent anti-tumor agent.<sup>97</sup> It was claimed to be an autophagy flux inhibitor and effective for treating cancer metastasis. The oral administration of butylidenphthalide, a bioactive phthalide compound isolated from *Angelica sinensis*, delays the spinal motor neuronal death in transgenic mice by inhibiting autophagy in those neurons. Plumbagin, a quinonoid isolated from the root of *Plumbago zeylanica* has been reported to inhibit the proliferation of cancer cells *in vivo* and *in vitro* through inhibiting autophagy.<sup>5</sup> The diterpenoid lactone, andrographolide (Figure 1.9) isolated from the plant *Andrographis paniculata*, was proved to possess anti-inflammatory and anticancer activity.<sup>98</sup> The plant was traditionally used for the treatment of respiratory infection, bacterial dysentery, diarrhea and fever, however, its active constituent andrographolide was investigated as autophagy inhibitor. The mechanism of action was related to inhibition of autophagosome-lysosome fusion, resulting in autophagic cell death.<sup>5</sup>

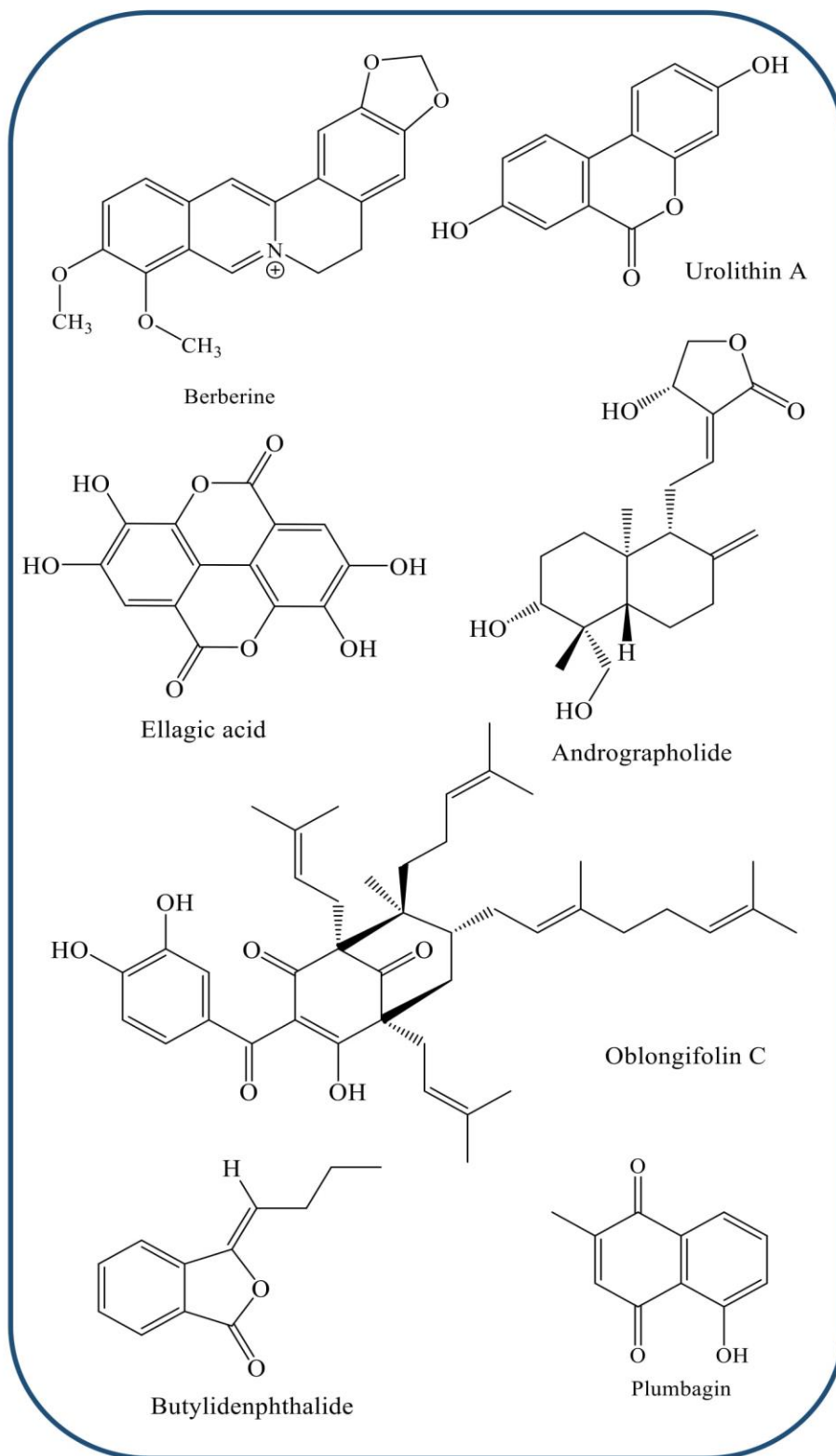


Figure 1.9. Natural products as modulators of autophagy.

#### *4. Conclusion*

In conclusion, the tight regulation of both AGEs formation and the autophagy process is necessary to maintain physiological cellular homeostasis and to avoid diseases. While the anti-AGEs activity and autophagy modulation of a wide range of synthetic molecules has already been evaluated, the chemodiversity of natural products, such as secondary metabolites of natural origin, still needs to be thoroughly explored.



# Chapter 2

*Aim of study*





Due to the important role of advanced glycation end products (AGEs) and autophagy in many pathological conditions such as diabetes, atherosclerosis, neurodegenerative diseases and the normal aging process, discussed in **Chapter 1**, this work aimed to contribute to the discovery of novel AGEs inhibitors and autophagy modulators derived from natural sources (**Chapter 2**).<sup>12</sup> The main focus of the current dissertation was to develop and to validate reliable *in vitro* methods for quantification of the AGEs inhibiting properties of selected classes natural products, which were isolated and identified in the host laboratory. Additionally, similar to AGEs, the autophagy modulatory properties of the same compounds were tested as well.

In **Chapter 3** the phytochemical investigations, regarding the isolation and identification of pure compounds by various chromatographic and spectroscopic techniques, are discussed. In the current project, four different plant species were selected based on literature search and previous investigations on their phytochemical constituents and pharmacological activity in the host laboratory.<sup>99</sup> These plants included: *Citrus sinensis* (Rutaceae), *Citrus depressa* (Rutaceae), *Ginkgo biloba* (Ginkgoaceae) and *Adhatoda vasica* (Acanthaceae). Three specific classes of compounds, i.e. polymethoxylated flavonoids (PMFs) from the *Citrus* species, biflavonoids from *Ginkgo* and quinazoline alkaloids from *Adhatoda*, were tested for AGEs inhibiting properties and autophagy modulation through established methods.

*Adhatoda vasica* Nees is a herb widely used in Ayurvedic and Unani medicine for the treatment of respiratory disorders (cough, bronchitis, and asthma) in a number of proprietaries, over the counter (ODC) and polyherbal products.<sup>100</sup> Therefore, it was of utmost importance to find a valuable and convincing method for the characterization of the quinazoline alkaloids from *Adhatoda* species, which are thought to be responsible for the main therapeutic effects. Additionally, they can be used for the quality control of the herbal products. For this reason, the development and the validation of a method for quantifying vasicine in *Adhatoda vasica* plant material is outlined in **Chapter 4**. Moreover, vasicine was also determined in commercially available products applying the validated procedure.

Chapter 5 and Chapter 6 challenge the question on how to evaluate in a reliable way the AGEs inhibiting properties of natural products using existing and novel methods. Particularly, **Chapter 5** focuses on the results from the general AGEs experiments like BSA – glucose assay, fructosamine assay and dicarbonyl entrapment method. Moreover, in this chapter the drawbacks of the discussed methods are addressed, revealing the need for improvement of the existing procedures. Consequently, **Chapter 6** focuses on the development and validation of a new experimental procedure that can circumvent the problems with the aforementioned techniques. The aim of the project was to develop and to validate a specific, sensitive and reliable method for evaluating the AGEs inhibiting properties of test compounds by means of HILIC Ultra-Performance Liquid Chromatography coupled to a Xevo G2-XS QToF MS system for the quantification of N<sup>ε</sup>-(carboxymethyl)-lysine (CML) in *in vitro* samples. Finally, the isolated compounds from the four plant species and a selection of other natural products were tested in the new method for estimating their anti-AGEs properties.

**Chapter 7** explores the theoretical background and the complexity of the techniques used to study the autophagy flux. Then, in the second part of the chapter the autophagy modulation properties of the previously isolated compounds and selected standards were investigated.

The last chapter (**Chapter 8**) represents a general discussion and with concluding remarks on the results, followed by the perspectives for future investigation.

# Chapter 3

## Phytochemical investigation



## 1. Introduction

The subject of phytochemistry contains an enormous variety of organic substances that are elaborated and accumulated by plants, and deals with the chemical structures of these substances, their biosynthesis, metabolism, their natural distribution and biological function.<sup>101</sup> The term “natural product” is reserved for secondary metabolites, small molecules produced by the organism but not absolutely necessary for the survival of the organism, unlike the more prevalent macromolecules (proteins, nucleic acids, polysaccharides). Secondary metabolites are often unique to a particular species or group of organisms and, while some act as antifeedants, sex attractants, or antibiotic agents, many have no apparent biological role. Isolation of natural products differs from that of the more prevalent biological macromolecules because natural products are smaller and chemically more diverse.<sup>102</sup> Keeping this in mind, the isolation approach - separation, purification and identification of many different constituents in plants, should be individually investigated for each plant material or class of natural compounds. The current chapter presents the phytochemical work on four medicinal plants included in this thesis, i.e. *Citrus sinensis*, *Citrus depressa*, *Adhatoda vasica* and *Ginkgo biloba*, and particularly, the isolation of three selected classes natural products - polymethoxylated flavonoids, biflavonoids, and quinazoline alkaloids.

## 2. General materials and techniques

### 2.1 Solvents and reagents

The solvents acetonitrile, methanol, dichloromethane, absolute ethanol, acetone, isopropanol, *n*-butanol (99%), dimethyl sulfoxide (DMSO) and ethyl acetate were analytical grade and were purchased from Fisher Scientific (Hampton, NH, USA) or from Acros Organics (Geel, Belgium). The reagents acetic acid (99.8%), formic acid (99+%), sulphuric acid (p.a. 85%) and trifluoroacetic acid (p.a. 99%) were obtained from Acros Organics. Sodium hydroxide was from Merck (Darmstadt, Germany). Water was obtained by a Milli-Q system from Millipore (Bedford, USA) and was filtered through a 0.22 µM membrane filter.

## 2.2 Instruments

Ultrasonication was performed with a Branson 3510 ultrasound bath. Also, a small centrifuge Sigma 1-15 PK (Fisher Bioblock Scientific, Merelbeke, Belgium), a vacuum centrifuge Savant equipped with Refrigerator Vapor Trap (RVT) 400 and SpeedVac Concentrator (SPD) 121P (Thermo Scientific, Massachusetts, USA) and a freeze dryer Lyovapor L-200 (Buchi, Ambacht, the Netherlands) were used. Measurements of the pH were achieved with SensION (Hach, Mechelen, Belgium). Concentration under reduced pressure was done using a Rotavapor from IKA (VWR, Oud-Heverlee, Belgium) with a pump PC 3001 and CVC 3000 Vacuubrand. Round bottom flasks were heated using an Isopad Labmasters heating mantle (VWR).

## 2.3 Chromatographic and analytical techniques

### 2.3.1 Thin layer chromatography

Normal phase TLC plates (20 x 20 cm, silica gel 60 F<sub>254</sub>, Merck) were used. Samples were spotted manually by using a micropipette (Blaubrand®, intraMARK, Hinckley, UK), the plates were developed using a glass developing tank and were heated on a TLC Plate Heater III (Camag, Muttenz, Switzerland). The preparation of several spraying reagents used during the practical work was as follows: The **Dragendorff reagent** contains solution A: 0.85 g bismuth (III) subnitrate, 40 ml water and 10 ml glacial acetic acid, and solution B: 8 g potassium iodide and 20 ml water, which are mixed after being individually prepared in advance. The **iodoplatinate reagent** consists of solution A: 10% potassium hexaiodoplatinate (IV) in water, and solution B: 6% potassium iodide in water, that are mixed after preparation. The **ninhydrin spraying solution** is prepared by dissolving 30 mg ninhydrin in 10 ml *n*-butanol and adding 300 µl of 98% acetic acid. After spraying, the TLC plate is heated and observed in visual light. The **anisaldehyde reagent** is prepared by mixing 0.5 ml anisaldehyde with 10 ml glacial acetic acid, followed by 85 ml methanol and 5 ml concentrated sulfuric acid, in that order. Other spraying solutions were: 10% sulphuric acid (*v/v*) in methanol and ferric chloride (FeCl<sub>3</sub>) 2% ethanol solution.<sup>103</sup>

### 2.3.2 Open column chromatography

Open column chromatography with different stationary phases was applied according to the polarity of the natural products and extracts, including: Polyamide CC6 (Macherey-Nagel, Duren, Germany), Diaion HP-20 (Supelco, Bellefonte, USA), Sephadex LH-20 (Pharmacia Fine Chemicals, Uppsala, Sweden), MCI gel CHP 20 P 75-150  $\mu\text{m}$  particle size (Supelco, USA).

### 2.3.3 Flash chromatography

A Reveleris<sup>®</sup> iES Flash Chromatography System Grace (Columbia, USA) was used to perform a medium pressure fractionation of plant extracts. The system is equipped with a sample injection compartment which allows dry or liquid loading, a binary pump and four solvent reservoirs, a UV detector (operating simultaneously at two wavelengths (between 200-400 nm) and an Evaporative Light Scattering Detector (ELSD) which were used for detection dependent collection, and a fraction collector with two collection trays. A pre-packed Flash Grace Reveleris<sup>®</sup> silica column (40 g, 40  $\mu\text{m}$ ) was used.

### 2.3.4 HPLC (High-Performance Liquid Chromatography)

For the routine screening of extracts and fractions, and gradient optimization for pure compound isolation, an Agilent 1200 Series instrument was used. It is equipped with a degasser, quaternary pump, automated liquid sampler, thermostatic column compartment, diode array detection (DAD) and the data was interpreted by ChemStation software (Agilent Technologies, Eindhoven, The Netherlands). Different analytical columns were used, namely, Luna C18 (250 x 4.6 mm, 5  $\mu\text{m}$ ) (Phenomenex, Utrecht, Netherlands), Kinetex EVO C18 (250 x 4.6 mm, 5  $\mu\text{m}$ ) (Phenomenex), X-Bridge BEH C18 (250 x 4.6 mm, 5  $\mu\text{m}$ ) (Waters, Milford, USA), Grace Smart C18 column (250 x 4.6 mm, 5  $\mu\text{m}$ ) (Grace, Duren, Germany) and Purosphere STAR RP-18 Endcapped (250 x 4.6 mm, 5  $\mu\text{m}$ ) (Merck, Darmstadt, Germany).

### 2.3.5 Semi-preparative high-performance liquid chromatography

Pure compounds were obtained through an AutoPurification™ semi-preparative HPLC system from Waters (Milford, USA), which contains a binary sample manager, injector and fraction collector, a quaternary gradient module, an HPLC pump, a 515 HPLC make-up pump, a system fluidics organizer, a column compartment, a flow splitter which allowed simultaneous detection and collection, DAD and a Micromass Quattro mass spectrometer. The software for processing the data was MassLynx version 4.1. Several columns were used: Luna C18 (250 x 10 mm, 5µm) (Phenomenex, Torrance, CA, USA) and Kinetex C18 (250 mm x 10.0 mm, 5 µm) (Phenomenex).

### 2.3.6 UPLC (Ultra-Performance Liquid Chromatography)

Ultra-Performance Liquid Chromatography (UPLC) was performed using a Waters Acquity® system (Waters Assoc., Milford, MA) that comprised a binary solvent manager, sample manager, column manager and UV detector. MassLynx version 4.1 software was used. The chromatographic conditions were optimized using Acquity UPLC BEH C18 column (100 mm x 2.1 mm, 1.7 µm) (Waters).

### 2.3.7 Mass spectrometry

Ultra-Performance Liquid Chromatography (UPLC) offers significant theoretical advantages in resolution, speed, and sensitivity for analytical determinations, particularly when coupled with mass spectrometers capable of high-speed acquisitions.<sup>104</sup> UPLC/MS is a hyphenated technique, which combines the separating power of the UPLC, with the detection power of mass spectrometry. An Acquity Ultra-Performance Liquid Chromatography system (Waters) with a sample manager, binary solvent manager, DAD and a triple quadrupole detector were used. MassLynx version 4.1 software was used.

### 2.3.8 Nuclear Magnetic Resonance (NMR) spectrometry

1D and 2D NMR spectra were recorded on a Bruker DRX-400 instrument (Rheinstetten, Germany), equipped with a 3 mm broadband inverse (BBI) probe or a



5 mm dual  $^1\text{H}/^{13}\text{C}$  probe, both with a z-gradient 5 mm dual probe, using standard Bruker pulse sequences and operating at 400 MHz for proton spectra and at 100 MHz for carbon-13 spectra. The data was processed with Topspin software version 1.3. The spectral assignments were confirmed by comparison with MODGRAPH NMRPredict version 4.8.61. The chemical shifts ( $\delta$ ) are presented in ppm and the coupling constants ( $J$ ) in Hz.

The performed 1D experiments included  $^1\text{H}$ -NMR,  $^{13}\text{C}$ -NMR, distortionless enhancement by polarization transfer (DEPT-135, DEPT-90); and the 2D experiments were  $^1\text{H}$ - $^1\text{H}$  correlation spectroscopy (COSY),  $^1\text{H}$ - $^{13}\text{C}$  heteronuclear single quantum coherence (HSQC) and  $^1\text{H}$ - $^{13}\text{C}$  heteronuclear multiple bond correlation (HMBC).

Chloroform- $d_6$  99.9% D, methanol- $d_4$  99.8% D, acetone- $d_6$  99.9% D, dimethyl sulfoxide- $d_6$  99.9% D were purchased from Sigma-Aldrich.

### *3. Isolation and identification of polymethoxylated flavonoids (PMFs) from Citrus sinensis and Citrus depressa*

#### 3.1 Introduction

##### 3.1.1 Plant characteristics



Figure 3.1. *Citrus sinensis* flower and fruit.<sup>264</sup>

*Citrus sinensis* L. Osbeck (sweet orange) is native to Asia and is now widespread throughout the Pacific and warm areas of the world. It is an evergreen flowering tree with an average height of 9-10 m, with large spines on the branches. Leaves are alternate, with narrowly winged-petioles (3-5 mm wide, 6.5-15 cm long); the shape of the leaves ranges from elliptical, oblong to oval, bluntly toothed and they emit a strong characteristic citrus odour due to the

presence of volatile oil. The fruit may be globose to oval (6.5 to 9.5 cm wide) and ripens to orange or yellow (Figure 3.1). Anatomically, the fruit consists of two distinct regions, the pericarp (also called the peel or the skin) and the endocarp or pulp with juice sac glands.<sup>105</sup>

*Citrus depressa* Hayata (Shiikuwasha) is an indigenous mandarin species on the Ryukyu Islands, which include Okinawa, located in the subtropical region of Japan (Figure 3.2).<sup>106</sup>

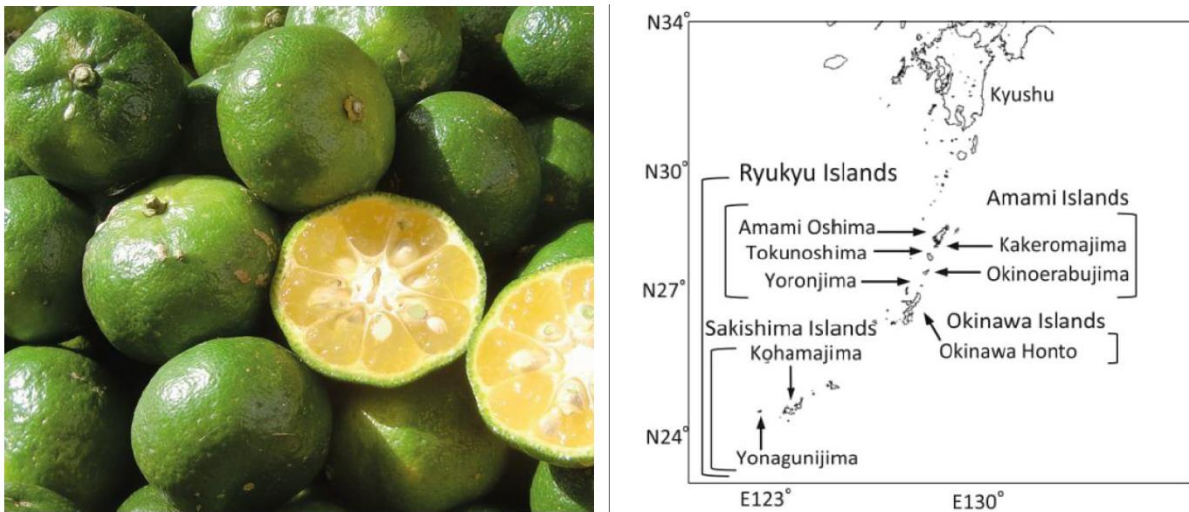


Figure 3.2. *Citrus depressa* and a map of the Ryukyu Islands.<sup>107</sup>

*Citrus depressa* is a small-sized evergreen broadleaf tree that naturally grows in mountain regions and limestone regions, and reaches till 16 feet height. Its yellowish-green fruits ripen between November and February with a diameter of 0.8 – 1.2 inches.<sup>108</sup> The fruit has a very sour taste and strong characteristic aroma.<sup>109</sup>

### 3.1.2 Traditional medicine

The genus *Citrus*, which belongs to the family Rutaceae, is the most important fruit tree crop in the world nowadays.<sup>110</sup> Moreover, many species of this genus are known for their potent biological activity which can be traced back in the traditional medicine of different regions. *Citrus sinensis* is highly consumed as an excellent source of vitamin C, which is a powerful natural antioxidant that strengthens the body's immune system. Traditionally, *C. sinensis* has been used in the treatment of constipation, cramps, colic's, diarrhoea, bronchitis, tuberculosis, cough, cold, obesity, menstrual

disorder, angina, hypertension, and stress.<sup>105</sup> The inhabitants of Okinawa use plants as medicinal herbs or in the preparation of typical Okinawan food. Moreover, researchers have indicated that the intake of Okinawan medicinal and edible plants contributes to the longevity of the local people since these plants are rich in phytochemicals with a broad range of bioactivities.<sup>99</sup> Such an example is *Citrus depressa* which is a very popular food in the Okinawa district.

### 3.1.3 Pharmacological activity

*C. sinensis* and *C. depressa* are rich sources of secondary metabolites, and the latter contribute to the various pharmacological activities of these species. So far, it is widely accepted that *Citrus* fruits and juices are health-promoting foods and they exert beneficial effects against many degenerative diseases like cardiovascular diseases and several types of cancer.<sup>111</sup> More specifically, polymethoxylated flavonoids (PMFs), which exist almost exclusively in the *Citrus* family, have been known for their wide range of nutraceutical functions. This may be related to their higher uptake compared to other compounds since the methoxylation of the phenolic groups decreases the hydrophilicity of the flavonoids, and therefore, increases their bioavailability *in vivo*.<sup>112</sup>

PMFs seem to possess stronger **anti-inflammatory** activities than other *Citrus* flavonoids.<sup>113</sup> For nobiletin, one of the most abundant PMFs, has been reported that it effectively suppressed production and gene expression of prostaglandin E2 (PGE2) by selective down-regulation of cyclooxygenase-2 (COX-2) genes. Moreover, it has been shown that PMFs can down-regulate gene expression of some pro-inflammatory cytokines such as interleukins (IL-1 $\alpha$ , IL-1 $\beta$ , and IL-6) and tumour necrosis factor- $\alpha$  (TNF- $\alpha$ ) in mouse macrophages.<sup>114,115</sup>

Proofs for the **anticancer** properties of PMFs have been provided by numerous *in vitro* and *in vivo* studies. For example, they have been shown to selectively inhibit the growth of human HL-60 cell lines *in vitro*, to reduce the invasion of tumours in animal models, to induce the differentiation of myeloid leukemic cells, and to suppress proliferation while promoting apoptosis.<sup>116</sup> It is reported that nobiletin by its significant anti-proliferative and pro-apoptotic effects can inhibit the development of human prostate, skin, breast, and colon carcinoma cell lines.<sup>113,107,117</sup> Other studies focused on the activity of nobiletin and sinensetin as novel antiangiogenesis agents.<sup>118,119</sup>

Meanwhile, hydroxylated polymethoxylated flavonoids (OH-PMFs), which are less abundant than permethoxylated PMFs, have drawn more and more attention recently, because accumulating evidence has suggested that OH-PMFs have much stronger health-promoting biological activities compared to their permethoxylated counterparts. The anti-proliferative effects could be related to higher permeability due to their non-polar nature in combination with the present hydroxy group(s) which are responsible for the free radical scavenging properties. Since numerous reports indicate that inflammation and infection are closely associated with cancer initiation and proliferation, in this context, it is not a surprise that 5-hydroxy polymethoxyflavones have been proved to exhibit greater potency when it comes to anticancerogenic and anti-inflammatory effects.<sup>120,121</sup>

Varieties of *Citrus* are reported to **reduce** the risk of adverse **cardiovascular events** by decreasing the total cholesterol concentration in plasma through inhibiting its hepatic production.<sup>105</sup> Another mechanism for the cardioprotective effects of PMFs is in terms of affecting the NO production and the expression of endothelial nitric oxide synthase (eNOS).<sup>113</sup> As a result, they improve the endothelial function, leading to vasodilatation, hypotensive and vasoprotective effects. PMFs have the capacity to inhibit the proliferation of vascular smooth muscle cells and suppress low-density lipoproteins (LDL) oxidation, which plays a crucial role in atherosclerosis.<sup>113</sup>

Other activities include **antioxidant** properties by scavenging free radicals, **antihyperglycemic** and antirheumatism properties.<sup>105,122</sup> The two major PMFs in *Citrus* peels, namely, nobiletin and tangeretin, have been reported for **anti-obesity effects**. In other studies, Shiikuwasha juice has demonstrated hepatoprotective effects against liver injury.<sup>109</sup>

#### 3.1.4 Polymethoxylated flavonoids

*Citrus* flavonoids are classified into three principal types: flavanones, flavones, and flavonols. PMFs are sometimes considered as an individual type of flavonoids because of their rather special structure and high biological activity. By definition, PMFs are flavones bearing two or more methoxy groups on their benzo- $\gamma$ -pyrone (15-carbon, C<sub>6</sub>-C<sub>3</sub>-C<sub>6</sub>) skeleton with a carbonyl group at the C<sub>4</sub> position.<sup>123</sup> The content of the main PMFs in *Citrus sinensis* and *Citrus depressa* has been reported by Kawaii *et al.* (Table 3.1).<sup>124</sup> This data is based on one of the most widely utilized taxonomical

systems in *Citrus* scientists community established by Tyozaburo Tanaka, a Japanese botanist from University of Osaka.<sup>125</sup> The Tanaka taxonomy recognizes up to 162 species, however, his overall scheme is not supported by the modern genetic research.

Tanaka's no.	Scientific name	Conventional name	sinensetin <sup>a</sup>	nobiletin <sup>a</sup>	tangeretin <sup>a</sup>
V-16-100	<i>C. sinensis</i>	Valencia	4.0	1.3	0.3
VII-27-153	<i>C. depressa</i>	Shiikuwasha	6.0	21.0	8.8

<sup>a</sup>All values are given in µg/100 mg of dried peels.

Table 3.1. Amount of main PMFs in *C. sinensis* and *C. depressa*.

The goal of the present phytochemical work was to build a library of PMFs (see Figure 3.29, page 90) from *Citrus depressa* and the commercially available *Citrus sinensis*, in order to evaluate their biological activities.

## 3.2 Materials and Methods

### 3.2.1 Plant material

In September 2015 around 40 kg fresh *Citrus sinensis* fruits, the commercially available orange, were purchased from Carrefour® (Antwerpen, Belgium) and further on hand-pressed as the juice, the pulp and the peels were collected separately. The cleaned peels were dried in an oven (Memmert UF 55) at 60 °C until constant weight.<sup>126</sup> Then the dry peels were cut to smaller pieces, grounded in a mill (IKA MF 10) and sieved to obtain particles with size of 1 mm in a total amount of 2.8 kg dry peels powder.

About 10 kg of *Citrus depressa* fruits were bought from and identified by Dr. Srijan Shrestha (Makise Lifeup Laboratory) in Okinawa, Japan in September 2015. The peels were removed, dried and powdered, and an amount of about 400 g powdered peel was shipped to Belgium.

### 3.2.2 Extraction, fractionation and isolation of PMFs

An amount of 300 g and 250 g of dry peel powder of *Citrus sinensis* and *Citrus depressa*, respectively, were exhaustively **extracted**, using ultrasound assisted solid-liquid extraction (USE) by sequential use of solvents with increasing polarity (Figure 3.3).<sup>127,128</sup> These included: dichloromethane, ethyl acetate, pure ethanol, 80% ethanol. In particular, the extraction was performed in 1 liter glass bottles, where 100 g of powder and one liter of solvent were mixed (drug extract ratio 1:10) and then transferred into an ultrasound bath (Branson 3510) for 1 h. The duration of the extraction was optimized based on the method used by M.K. Khan *et al.*<sup>111</sup> The latter was focused on monitoring the effect of the temperature and the polarity of the extracting solvents on the ultrasound extraction process.

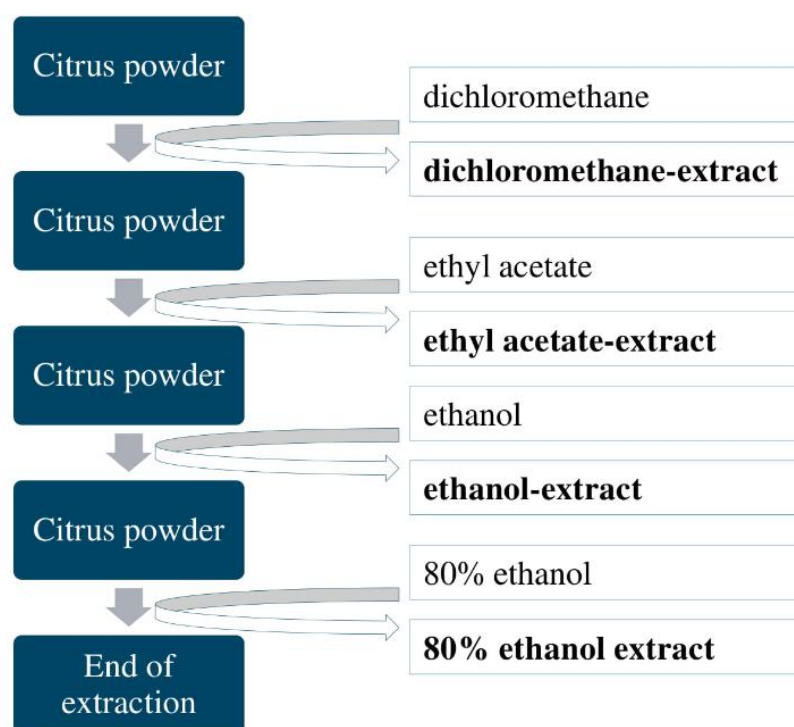


Figure 3.3. General scheme of Citrus ultrasound assisted solid-liquid extraction (USE).

All different extracts obtained by USE were further vacuum filtered using filter paper (Whatman 40) and then the solvent was removed in a rotary evaporator at 40 °C under vacuum.

The TLC analysis was performed on Merck TLC plates (silica gel 60 F<sub>254</sub>, 20 x 20 cm). Each solution was applied with a capillary tube. The mobile phase for the non-polar fractions (dichloromethane and ethyl acetate fractions) consisted of chloroform : methanol : 1% (v/v) phosphoric acid (65:35:5, v/v/v). The developed plate was dried and visualized by spraying 10% sulphuric acid in methanol (v/v) and then heated to 100 °C.<sup>129</sup> The mobile phase for the more polar fractions (ethanol and 80% ethanol fractions) consisted of ethyl acetate : methyl-ethyl-ketone : formic acid : water (5:3:1:1), and anisaldehyde was used for further visualization.<sup>130</sup> All developed TLC plates were observed at 254 nm before spraying, and at 366 nm after spraying where the PMFs gave a characteristic blue fluorescence.

The composition of PMFs in the different fractions was studied using an HPLC system (Agilent 1200 Series) with gradient elution based on the one suggested by C. Rojas-Garbanzo *et al.*<sup>131</sup> Several columns have been explored to achieve the best separation of the PMFs in the individual fractions: Luna C18, Kinetex EVO C18 and X-Bridge BEH C18. The mobile phase (v/v) consisted of water and 0.1% formic acid (eluent A), and acetonitrile and 0.1% formic acid (eluent B). The following gradient (v/v) system was used for the non-polar fractions: starting with 40% B at 0 min till 5 min; from 5 min to 35 min increasing to 60% B; then at 40 min reaching 100% B and keeping it for five minutes; at the end the initial conditions were restored for 10 min. The samples were prepared in acetonitrile 80%. For the polar fractions, the gradient was: starting point 10% B for 5 min, then increasing to 15% B in 5 min, at the 15<sup>th</sup> minute 18% B was reached, which rose to 20% at the 20<sup>th</sup> minute; then for the next 20 min B reached 40% and in the next five min 100% B was maintained; at the end the initial conditions were restored for 10 min. The samples were dissolved in acetonitrile 30%. The flow was maintained at 1 ml/min and the injection volume was 20 µl. The UV-absorbance was monitored at 210 nm, 265 nm, 330 nm and 360 nm. However, based on reports from previous investigations, 330 nm was chosen as the primary wavelength for further analysis of the PMFs.<sup>132</sup>

The total extracts from the *Citrus* species were **fractionated** by open column chromatography and/or Reveleris Flash Chromatography equipped with a normal phase silica column. Several sorbents were applied for open column separation: Polyamide CC 6, MCI gel CHP 20 P, Diaion HP 20, Sephadex LH-20. The promising PMF-containing fractions were further separated by repeated semi-preparative HPLC equipped with DAD and TQD mass analyser. The fractions were separated on a Luna

C18 column (250 x 10 mm, 5 $\mu$ m). The gradient started with 45% B at 0 min till 5 min; from 5 min to 35 min increase to 60% B; then at 40 min reaching 100% B, kept for 5 min; at the end, the initial conditions were restored for 10 min. The flow rate was 4.75 ml/min. The detection was performed at 330 nm and 360 nm, and by mass spectrometric analysis. A full scan in positive ionization mode ranging from  $m/z$  200 to 800 was applied and fraction collection was done for peaks with  $m/z$  373, 403, 343 and 433. These peaks seemed to be the major constituents in the UV chromatogram and were also showing an UV spectrum typical for PMFs. The injection volume was 400  $\mu$ l and the concentration of the fractions was 10 mg/ml.

### 3.3 Results and discussion

Based on previous research, the highest content of PMFs was expected to be present in the dichloromethane and ethyl acetate fractions, where nonpolar or medium-polar compounds can be collected.<sup>99</sup> However, no reports were found on the phytochemical composition of the more polar fractions, which provoked an interest for investigating those fractions in a search for previously unreported compounds, e.g. hydroxylated polymethoxylated (non-permethoxylated) flavonoids. Therefore, the ethanol (e.g. 14 g from *C. depressa*) and the 80% ethanol (e.g. 6 g from *C. depressa*), as well as the ethyl acetate fraction (e.g. 683 mg from *C. depressa*), were further separated on MCI gel (20 g), Diaion HP 20 (90 g) and Polyamide CC6 (68 g) open column, respectively. Consequently, their subfractions were continuously fractionated on a Sephadex open column or by Reveleris Flash Chromatography. Despite the considerable amount of time spent on trying to obtain PMFs from the more polar fractions, especially from *Citrus depressa*, a positive result was not achieved; therefore, the data regarding this part of the research project is not included in the thesis.

#### 3.3.1 *Citrus sinensis* peels

The total amount of the dichloromethane fraction from *Citrus sinensis* was 12 g. It was further fractionated by flash chromatography, using a Grace<sup>®</sup> Flash Cartridge 80 g silica column (Figure 3.4) and as eluting solvents, dichloromethane and ethyl acetate with 0.1% trifluoroacetic acid. Based on TLC and HPLC analyses the fractions with



similar profile were combined. In the end, five subfractions were collected from the dichloromethane fraction:

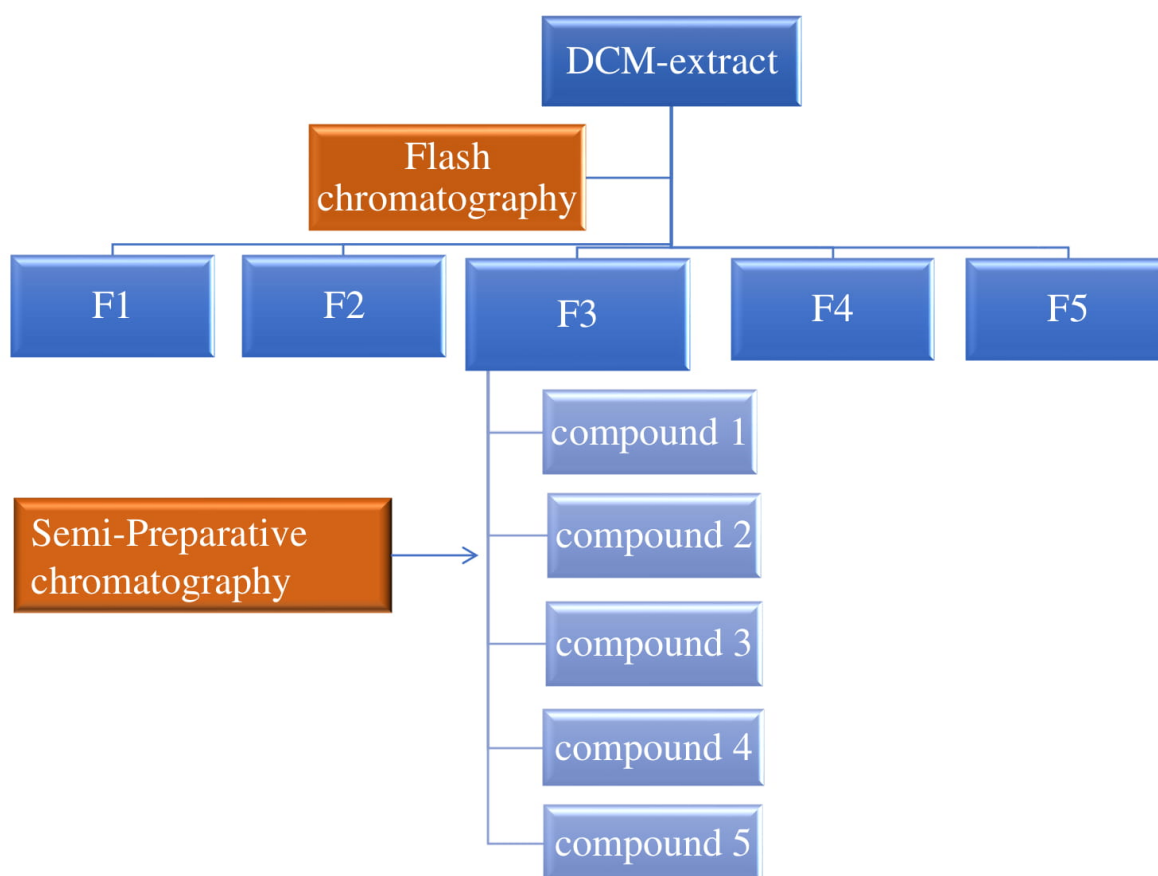


*Figure 3.4. Fractionation steps of Citrus sinensis dichloromethane extract and isolation of five pure compounds.*

The most prominent amount was obtained with fraction F2 and F3, 79 mg and 545 mg, respectively. Fraction 3 was further separated by semi-preparative chromatography (Figure 3.5).

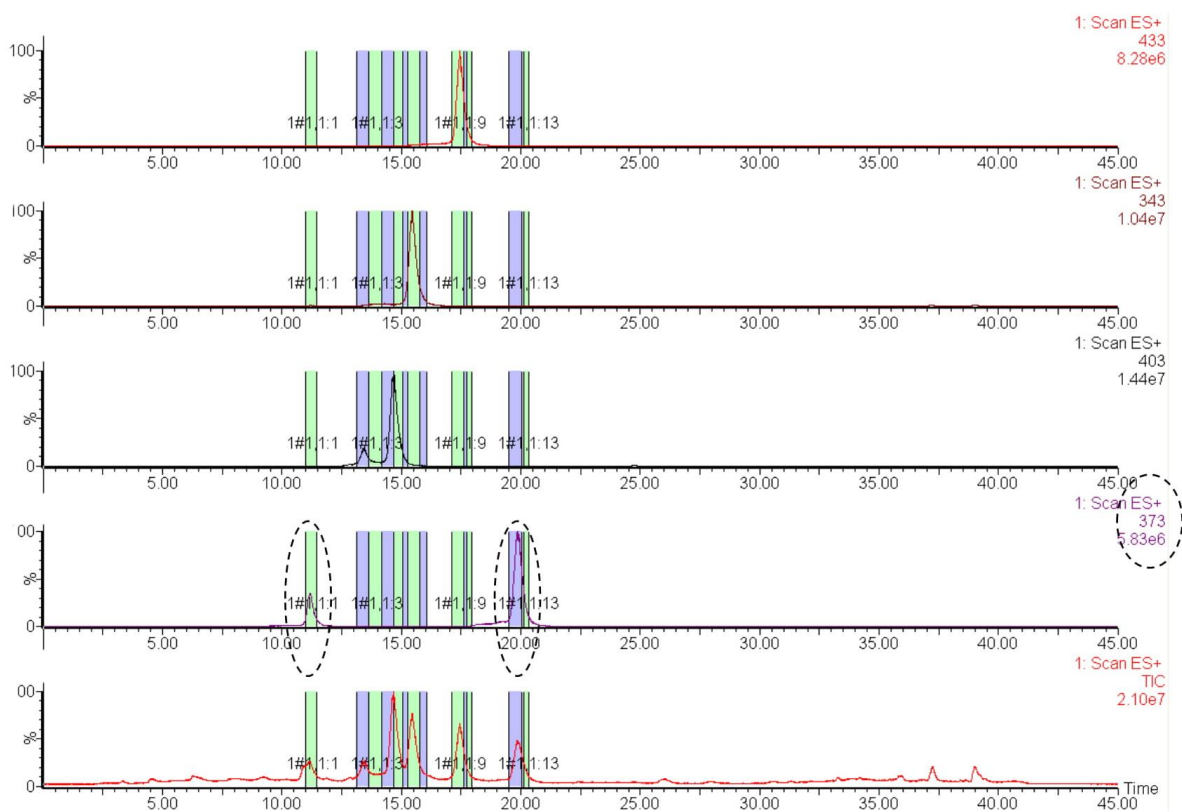


Figure 3.5. Semi-preparative HPLC chromatogram and molecular ions of the collected pure compounds:  $m/z$  403  $[M+H]^+$ ,  $m/z$  433  $[M+H]^+$ ,  $m/z$  343  $[M+H]^+$  and two compounds with  $m/z$  373  $[M+H]^+$ .

As a result, five PMFs were successfully isolated. Their structure was elucidated by means of 1D- ( $^1\text{H-NMR}$ ,  $^{13}\text{C-NMR}$ , DEPT-135, DEPT-90) and 2D- (HMBC, HSQC) NMR techniques. In addition, their molecular mass was confirmed by UPLC triple quadrupole MS detection system.

The  $^1\text{H-NMR}$  (Table 3.2) and  $^{13}\text{C-NMR}$  (Table 3.3) spectra for **compound 1, 2, 3, 4** and **5** were consistent with those reported in the literature.<sup>123,133,134</sup>  $^1\text{H-NMR}$  signals between  $\delta$  3.5 – 4.4 (methoxy groups) and 6.5 – 8.0 (aromatic protons) indicated that all the compounds possessed a structure typical for PMFs. Moreover, the spectra of **compounds 3, 4** and **5** had no A-ring aromatic proton resonances, suggesting substitution at C-5, -6, -7 and -8. The  $^1\text{H-NMR}$  spectra of **compounds 1, 3**, and **4** revealed that they have an ABX system (H-2', H-5' and H-6'), which was confirmed by the coupling constants of the signals at  $\delta$  7.5 – 7.7 (dd,  $J=8.4$ ,  $J=2.2$ , H-6'),  $\delta$  7.3 -7.5 (d,  $J=2.2$ , H-2') and  $\delta$  6.9 -7.1 (d,  $J=8.4$ , H-5') in the B-ring. The size of the coupling constant ( $J=2$  and  $J=8$  Hz) was characteristic for *meta* and *para* coupling, respectively,

typical for 3', 4'- methoxylated flavonoids. Additionally, for those compounds two methoxy groups in position 3' and 4' were confirmed by HMBC analysis. The spectra of **compounds 2 and 5** had a pair of two-proton, *ortho*-coupled doublets arising from two pairs of protons (H-2',6' and H-3',5'), revealing the presence of an A<sub>2</sub>B<sub>2</sub> system in the B-ring, which is typical for a *para*-substituted benzene ring. This was confirmed by the coupling constant of the signals at  $\delta$  8.7 - 8.9 (H-2',-6') and  $\delta$  8.7 - 9.0 (H-3',-5') ( $J$  = 8.9 Hz). In general, the aromatic proton signals were different for the various compounds, depending on the number and location of the functional groups (methoxy, hydroxy). The <sup>13</sup>C-NMR spectral assignments were made on the basis of DEPT -90, DEPT-135, HMBC and HSQC spectra (Table 3.3).

For **compound 1** the aromatic proton singlets at  $\delta_{\text{H}}$  6.61 and 7.10 were assigned to H-3 and H-8, respectively (Figure 3.7). The five methoxy signals at  $\delta_{\text{C}}$  62.4, 61.5, 56.8, 56.4 and 56.3 (Figure 3.8) were at position C-5, C-6, C-7, C-3' and C-4'. The ESI-MS spectrum showed a pseudo-molecular ion at  $m/z$  373 [M+H]<sup>+</sup>. Compound 1 was isolated as colourless needles and was identified as **sinensetin** (C<sub>20</sub>H<sub>20</sub>O<sub>7</sub>).

**Compound 2**, which was isolated as pale yellow needles, showed aromatic proton singlets at  $\delta$  6.57 and 7.13 that were corresponding to H-3 and H-8 (Figure 3.9). Four methoxy signals at the C-5, C-6, C-7 and C-4' position were observed at  $\delta_{\text{C}}$  62.3, 61.5, 56.8 and 56.2, respectively (Figure 3.10). The pseudo-molecular ion was found at  $m/z$  343 [M+H]<sup>+</sup> and the compound was identified as **5,6,7,4'-tetramethoxyflavone** (C<sub>19</sub>H<sub>18</sub>O<sub>6</sub>).

**Compound 3** exhibited an aromatic proton singlet at  $\delta$  6.66 for H-3 (Figure 3.11). The six signals at  $\delta_{\text{C}}$  62.4, 62.3, 61.9, 61.92, 56.2 and 56.2 (Figure 3.12) were assigned to the methoxy groups at C-5, C-6, C-7, C-8, C-3' and C-4', respectively, by the HMBC experiment (Figure 3.13). The ESI-MS spectrum showed a pseudo-molecular ion at  $m/z$  403 [M+H]<sup>+</sup>. Compound 3 (C<sub>21</sub>H<sub>22</sub>O<sub>8</sub>) was obtained as colourless needles and was identified as **nobiletin**.

**Compound 4** showed no aromatic proton singlets (Figure 3.14). The seven methoxy group signals at  $\delta_{\text{C}}$  62.4, 62.2, 61.99, 61.92, 59.8, 56.1 and 56.0 (Figure 3.15) were assigned to the methoxy groups at C-3, C-5, C-6, C-7, C-8, C-3' and C-4', respectively. The ESI-MS pseudo-molecular ion was found at  $m/z$  433 [M+H]<sup>+</sup>. Compound 4 (C<sub>22</sub>H<sub>24</sub>O<sub>9</sub>) was confirmed to be **heptamethoxyflavone** and it was obtained in the form of yellow needles.

**Compound 5** – isolated as colourless needles, showed an aromatic proton singlet at  $\delta$  6.56 assigned to H-3 (Figure 3.16). The five signals at  $\delta_c$  62.3, 62.1, 61.8, 61.7 and 55.5 were assigned to the methoxy groups at C-5, C-6, C-7-, C-8- and C-4' (Figure 3.17). A pseudo-molecular ion was observed at  $m/z$  373  $[M+H]^+$ . The compound was identified as **tangeretin** with the formula  $C_{20}H_{20}O_7$  in the form of light yellow needles. In conclusion, the isolated PMFs from *C. sinensis* were identified as sinensetin (**compound 1**); 5,6,7,4'-tetramethoxyflavone (**compound 2**); nobiletin (**compound 3**); 3,5,6,7,8,3',4'- heptamethoxyflavone (**compound 4**) and tangeretin (**compound 5**). Their elution order during HPLC analysis, which is in line with literature reports, is presented in Figure 3.6.<sup>123,133,135</sup> The peak around 40 min was reported to be an unidentified structural isomer of nobiletin, having the same UV spectrum and molecular ion, but it was not possible to obtain this compound during the semi-preparative chromatography.<sup>136</sup>

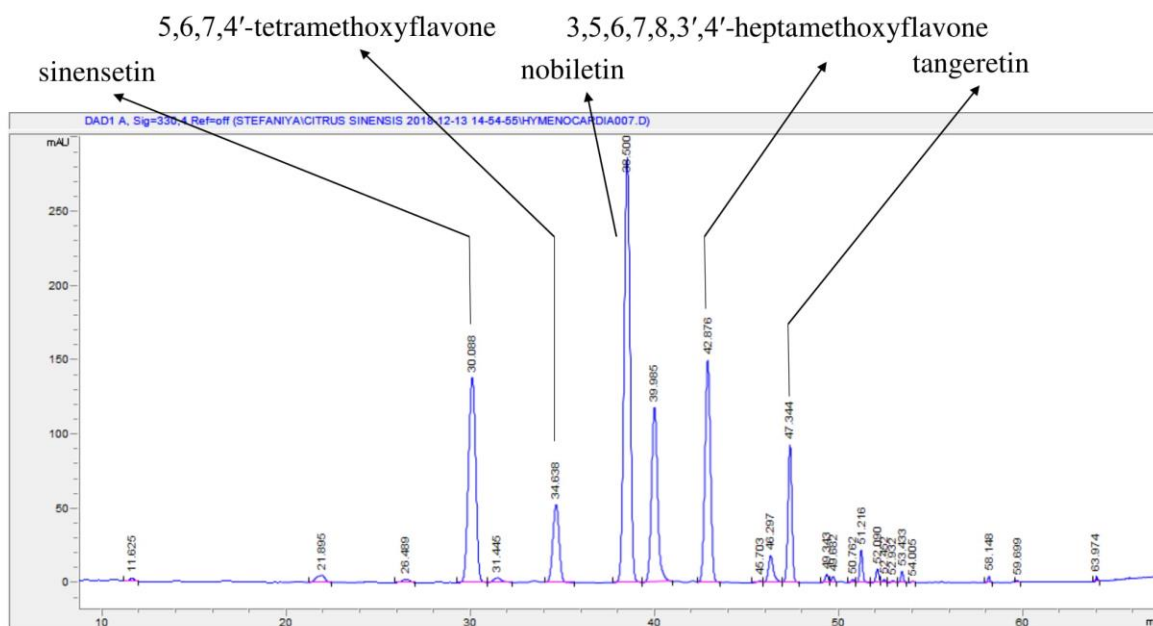


Figure 3.6. HPLC chromatogram (UV 330 nm) of *C. sinensis* total dichloromethane extract.

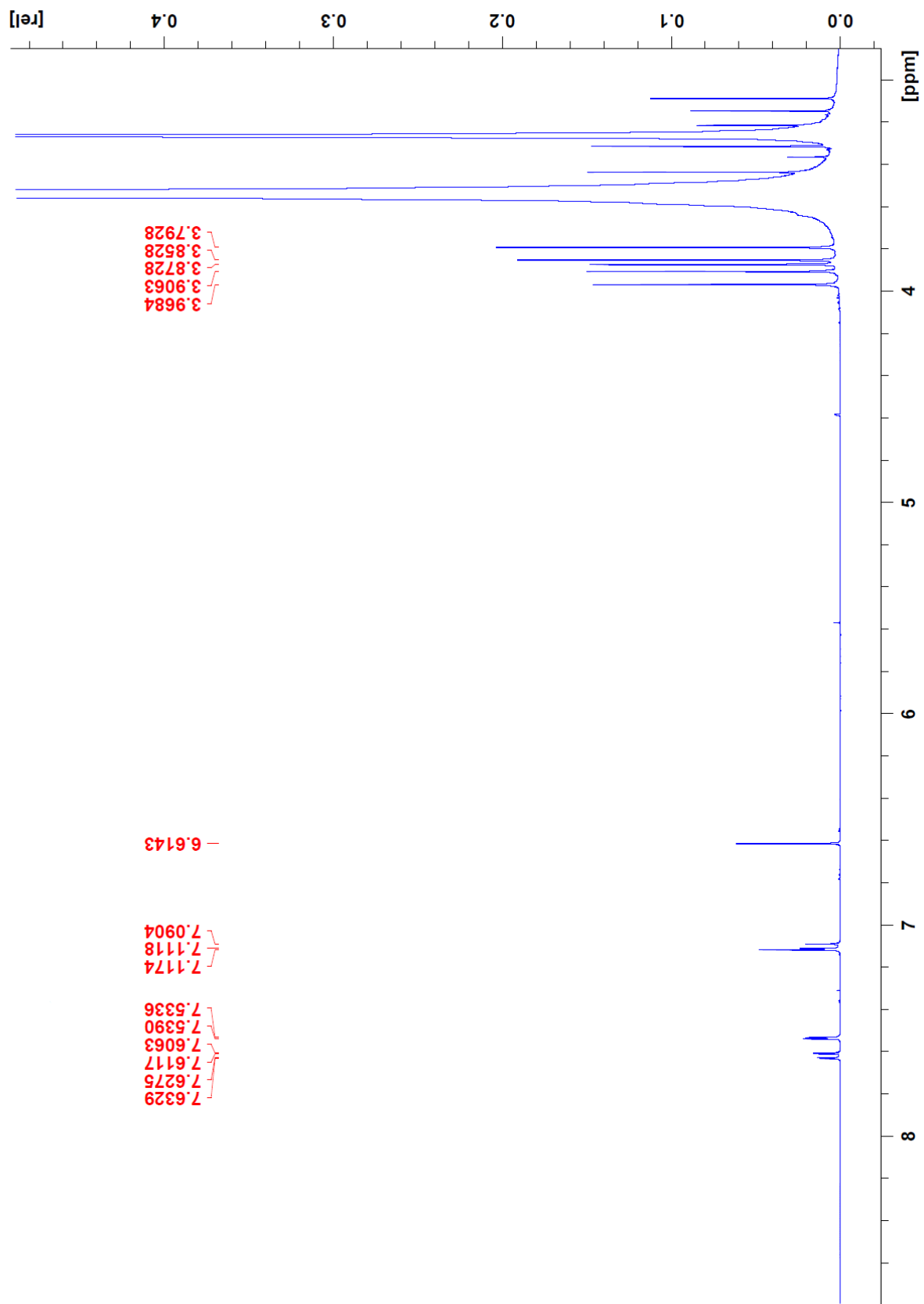


Figure 3.7.  $^1\text{H}$ -NMR spectrum (400 MHz, acetone- $d_6$ ) of **compound 1** (sinensetin).

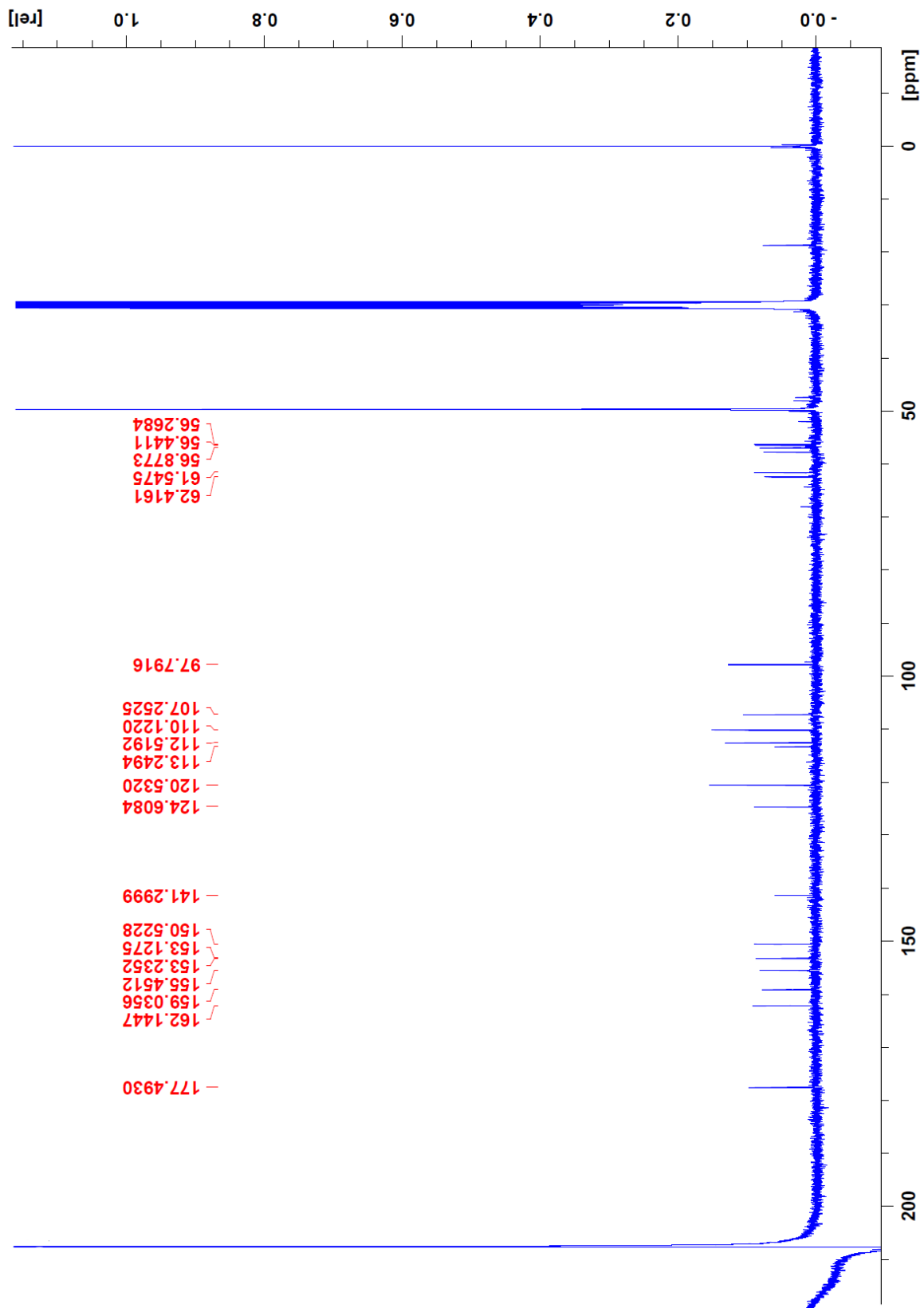


Figure 3.8.  $^{13}\text{C}$ -NMR spectrum (100 MHz, acetone- $d_6$ ) of **compound 1** (sinensetin).

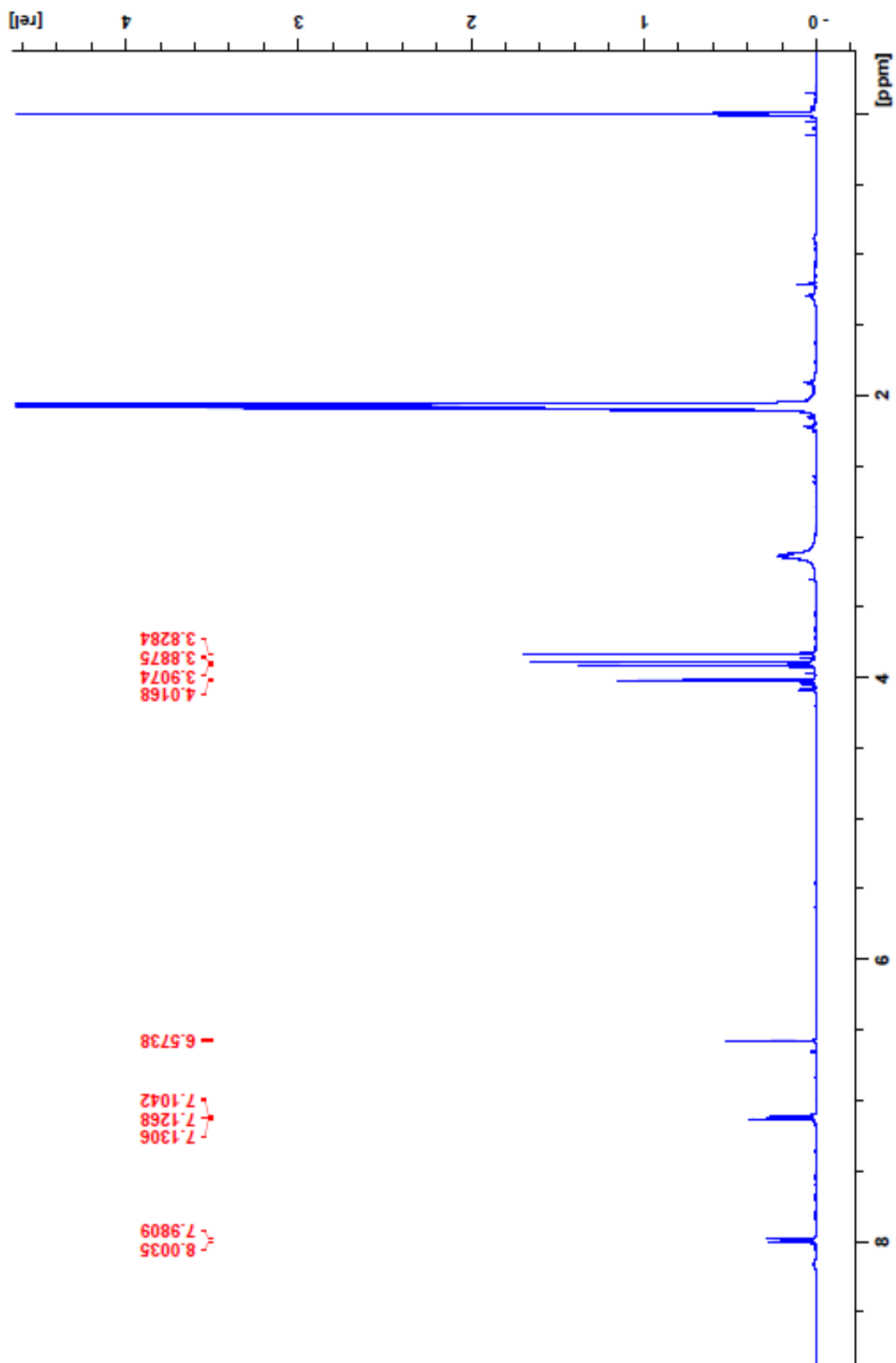


Figure 3.9.  $^1\text{H-NMR}$  spectrum(400 MHz, acetone- $d_6$ ) of **compound 2** (5,6,7,4'-tetramethoxyflavone).

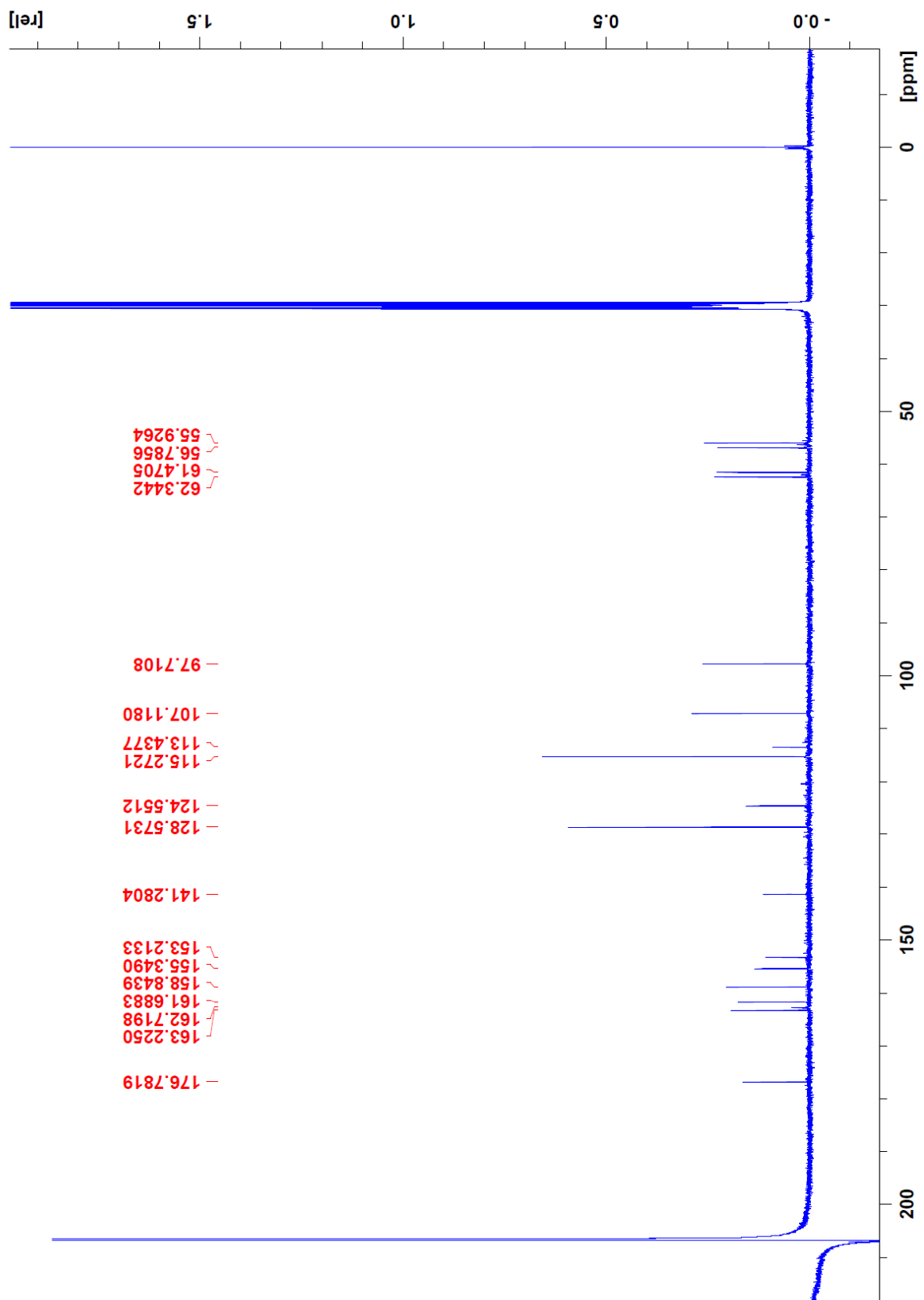


Figure 3.10.  $^{13}\text{C}$ -NMR spectrum (100 MHz, acetone- $d_6$ ) of **compound 2** (5,6,7,4'-tetramethoxyflavone).



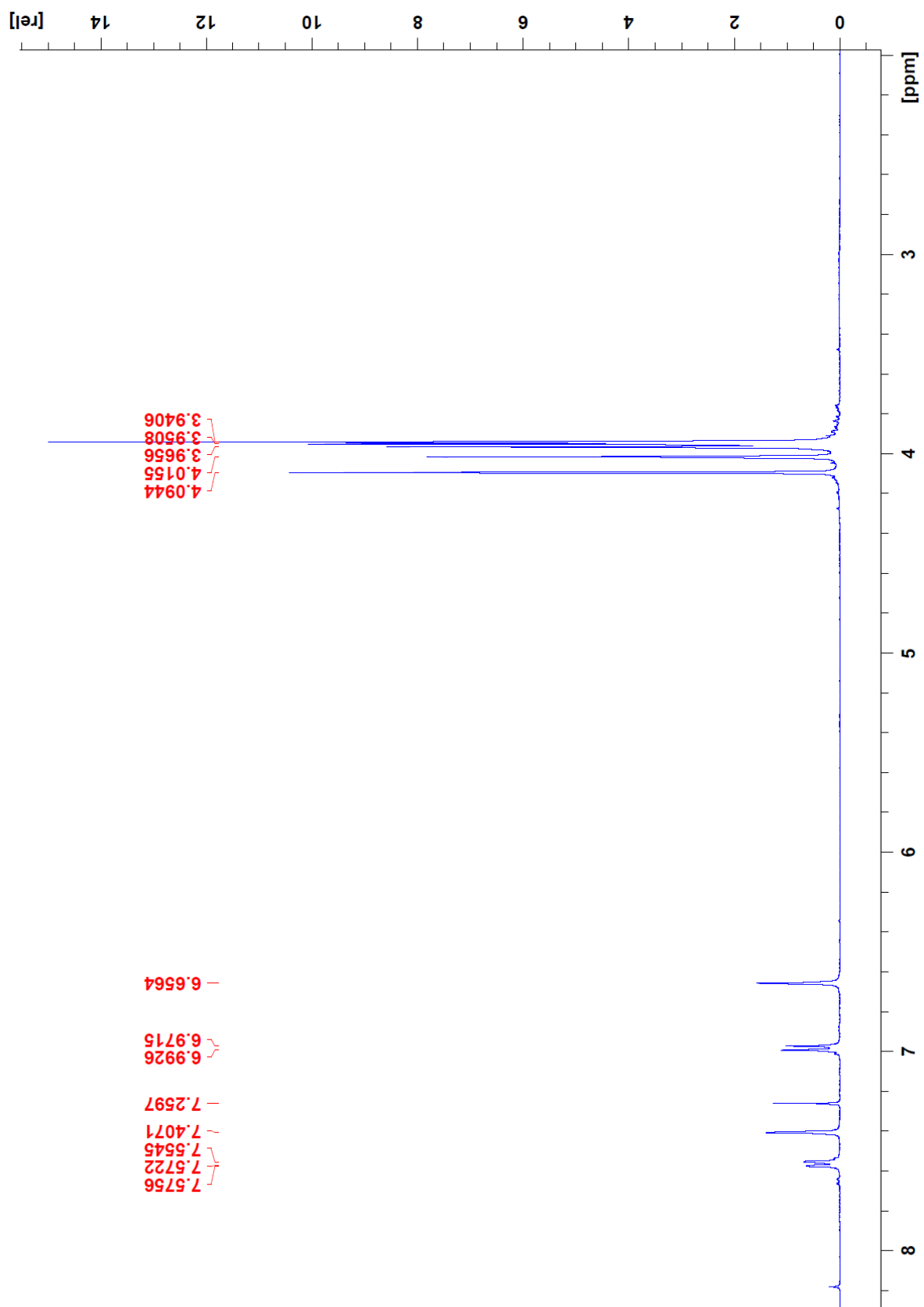


Figure 3.11.  $^1\text{H-NMR}$  spectrum (400 MHz,  $\text{CDCl}_3$ ) of **compound 3** (nobiletin).

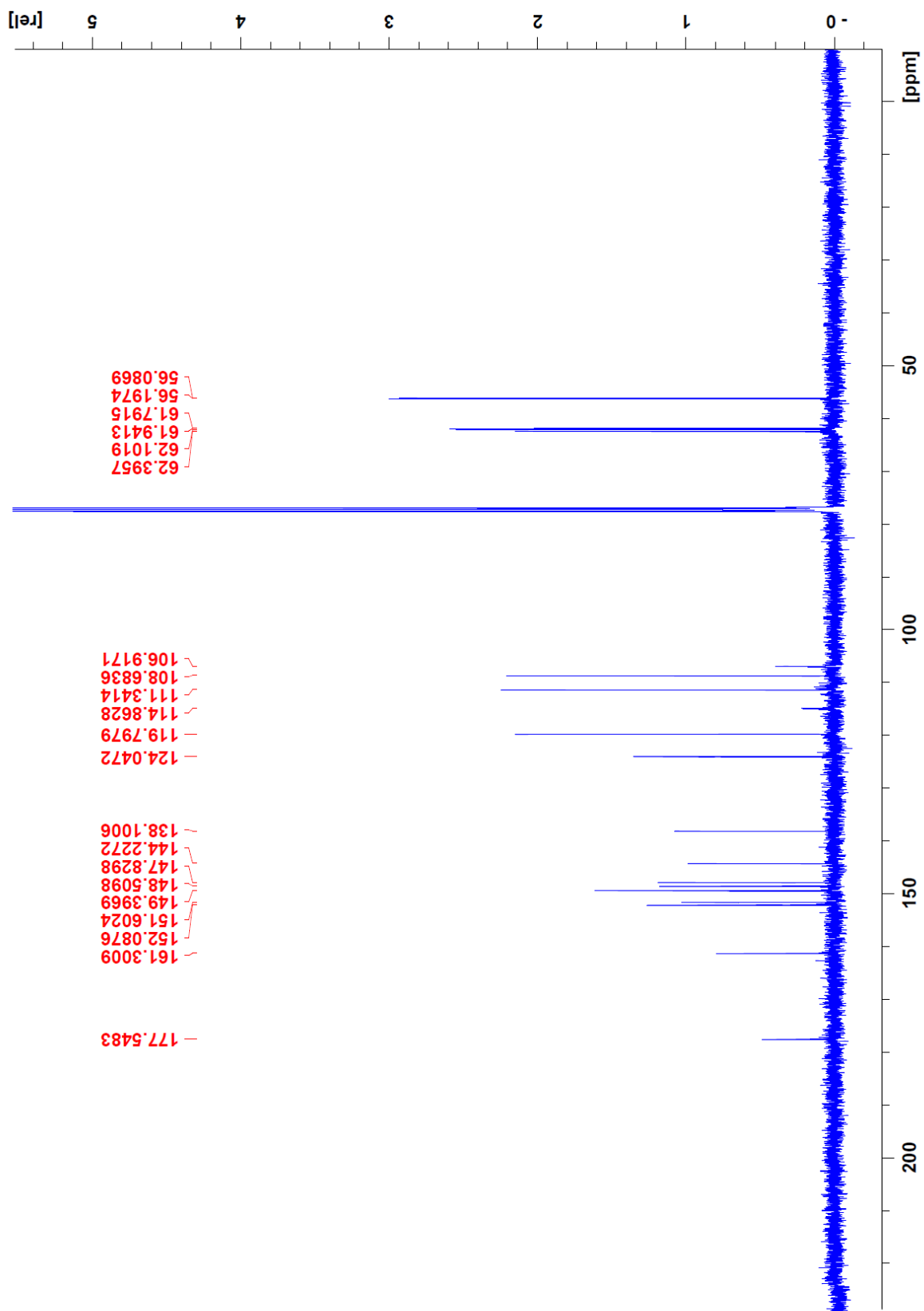


Figure 3.12.  $^{13}\text{C}$ -NMR spectrum (100 MHz, chloroform- $d$ ) of **compound 3** (nobiletin).

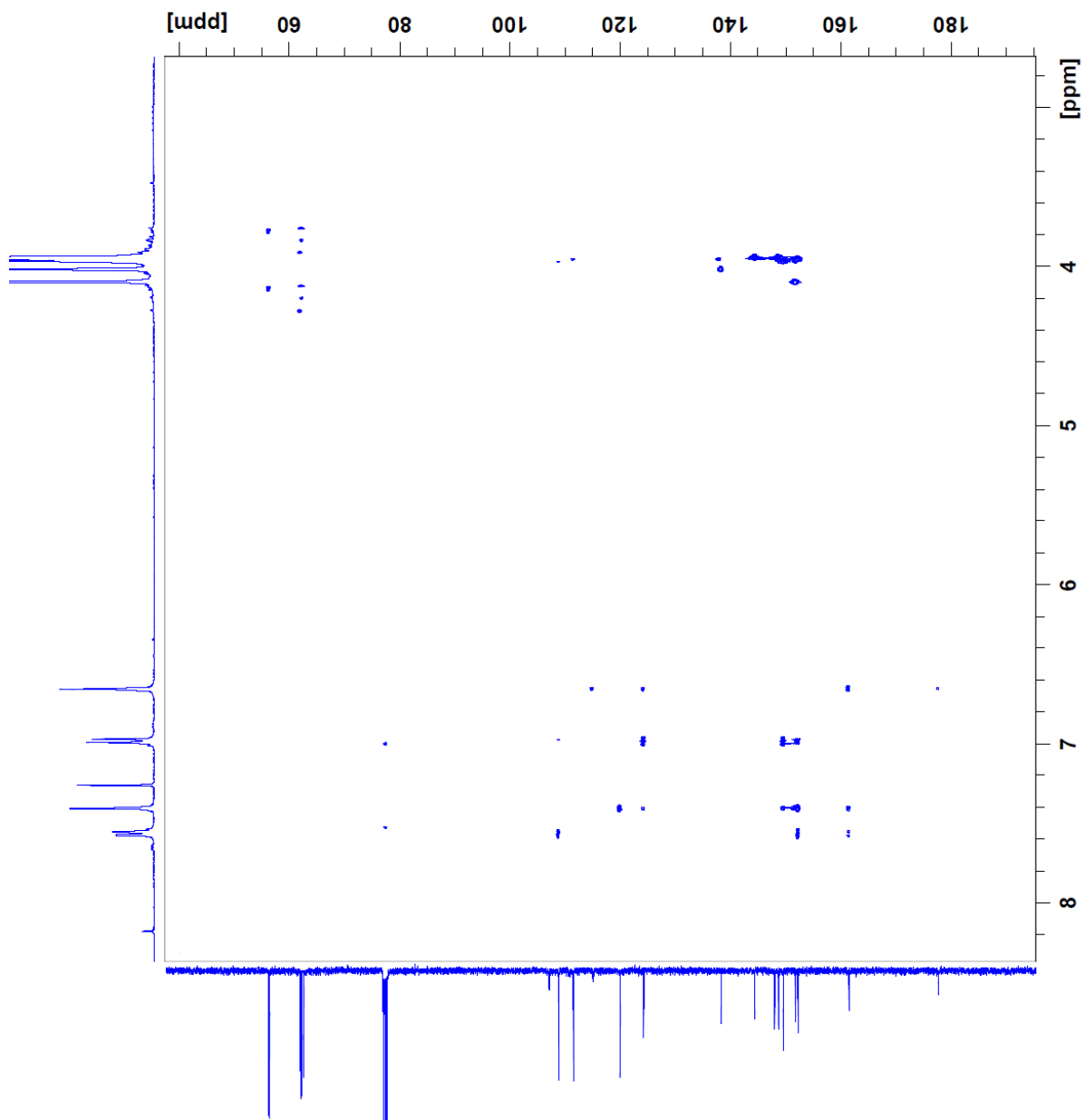


Figure 3.13. HMBC spectrum (400 MHz, chloroform-d) of **compound 3** (nobiletin).

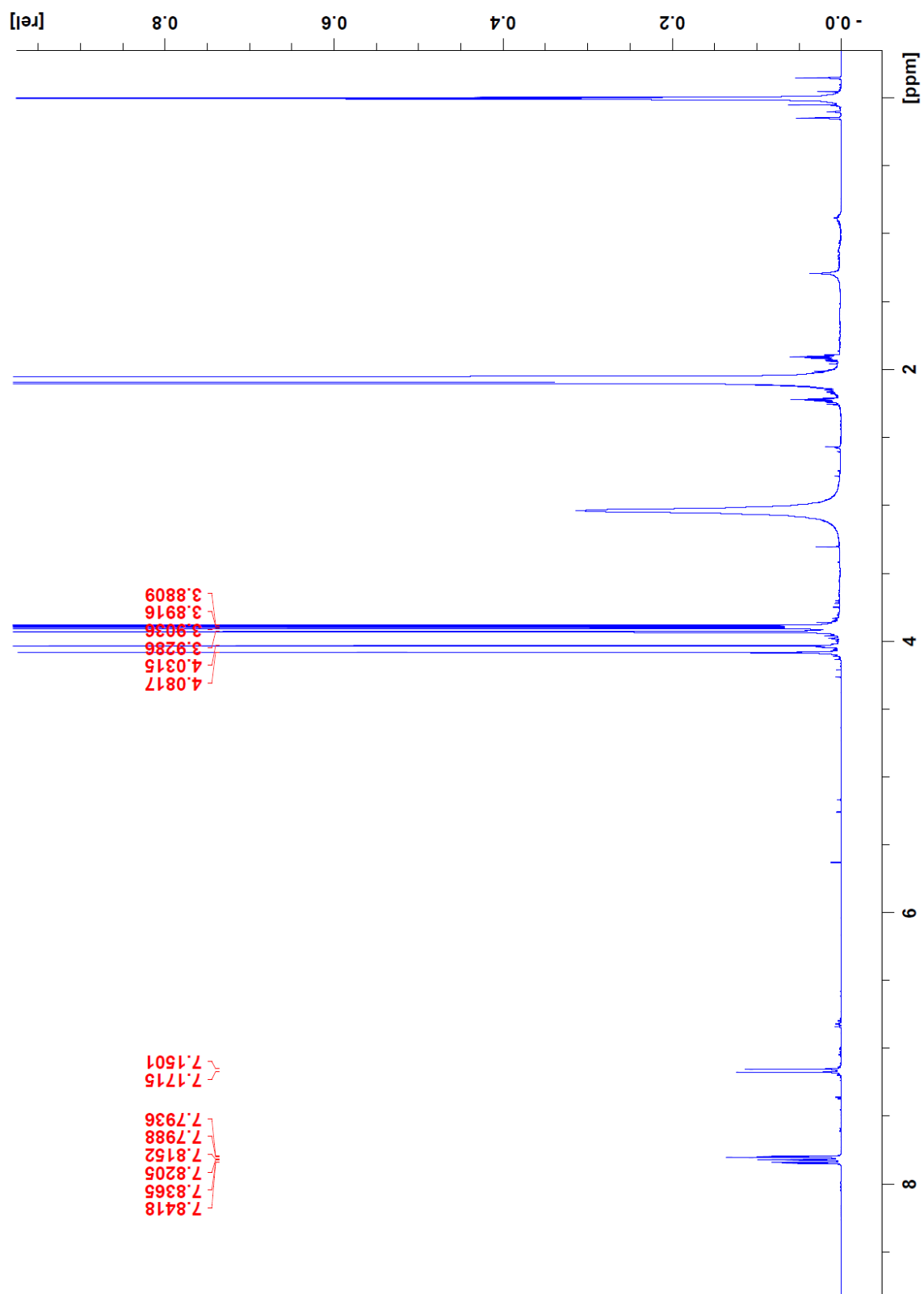


Figure 3.14.  $^1\text{H-NMR}$  spectrum (400 MHz, acetone- $d_6$ ) of **compound 4** (heptamethoxyflavone).

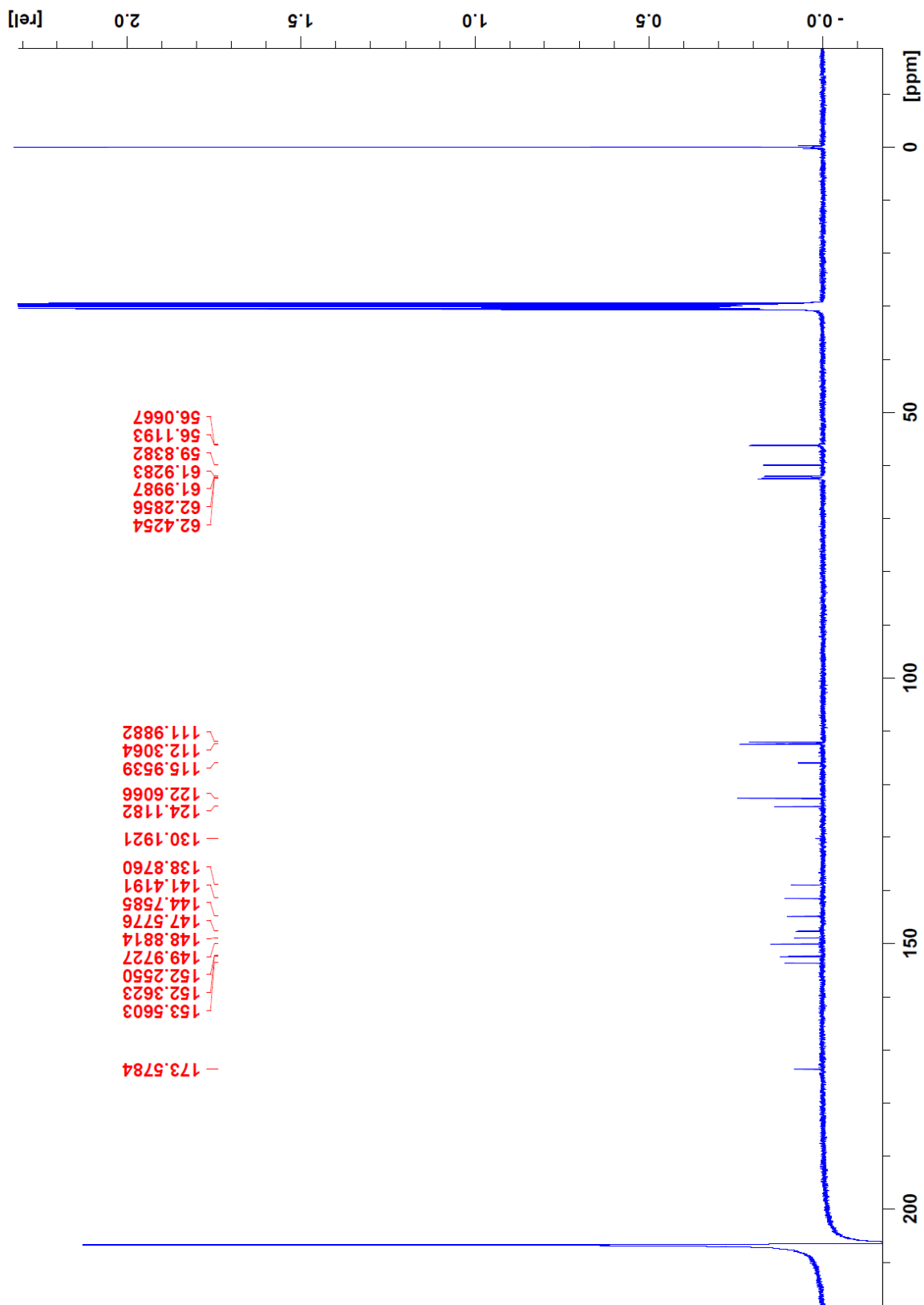


Figure 3.15.  $^{13}\text{C}$ -NMR spectrum (100 MHz, acetone- $d_6$ ) of **compound 4** (heptamethoxyflavone).

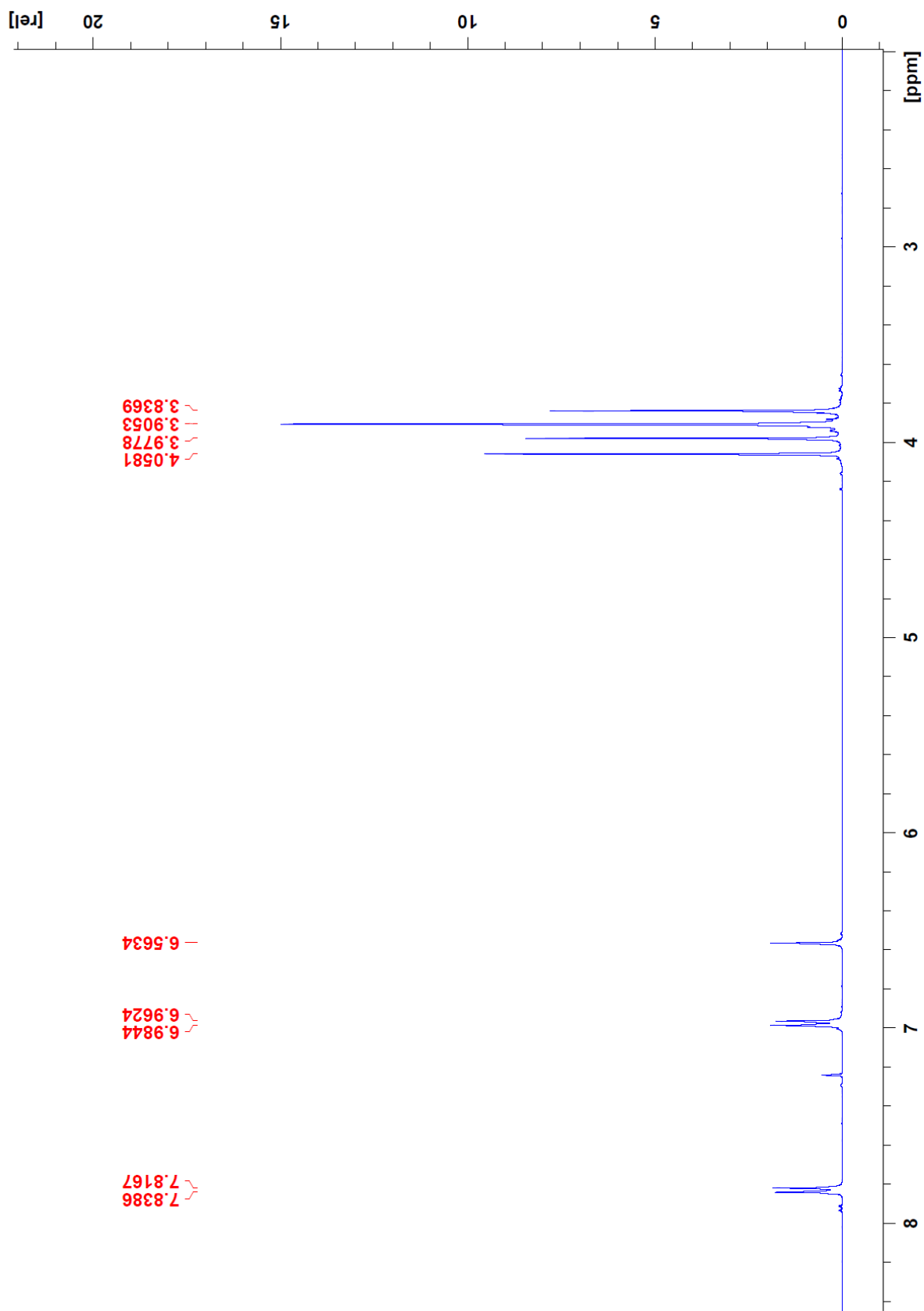


Figure 3.16. <sup>1</sup>H-NMR spectrum (400 MHz, chloroform-d) of **compound 5** (tangeretin).

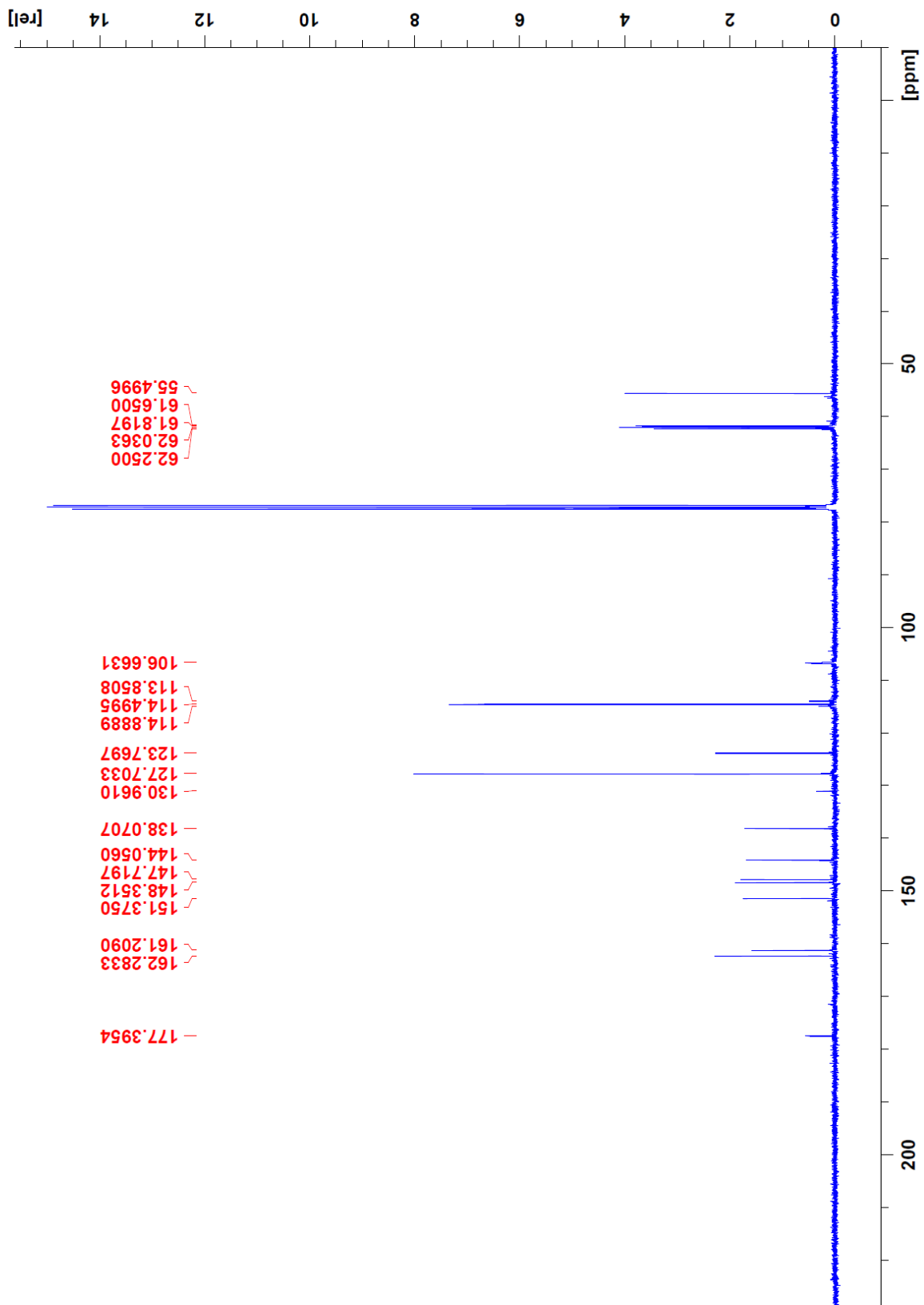


Figure 3.17.  $^{13}\text{C}$ -NMR spectrum (100 MHz, chloroform- $d$ ) of **compound 5** (tangeretin).

### 3.3.2 *Citrus depressa* peels

The amount of the obtained total extracts from *Citrus depressa* was as follows: 10 g dichloromethane extract, 683 mg ethyl acetate extract, 14 g ethanol extract and 6 g 80% ethanol extract. An amount of 5 g of the dichloromethane fraction from *Citrus depressa* was first fractionated using Polyamide CC6 (500 g) open column. In the beginning, a mixture of *n*-hexane and dichloromethane (95:5) was used as eluting solvent; further on, the percentage of *n*-hexane gradually decreased until pure dichloromethane was applied. The final elution was executed with dichloromethane in ethanol (50:50) and pure ethanol (Figure 3.18).

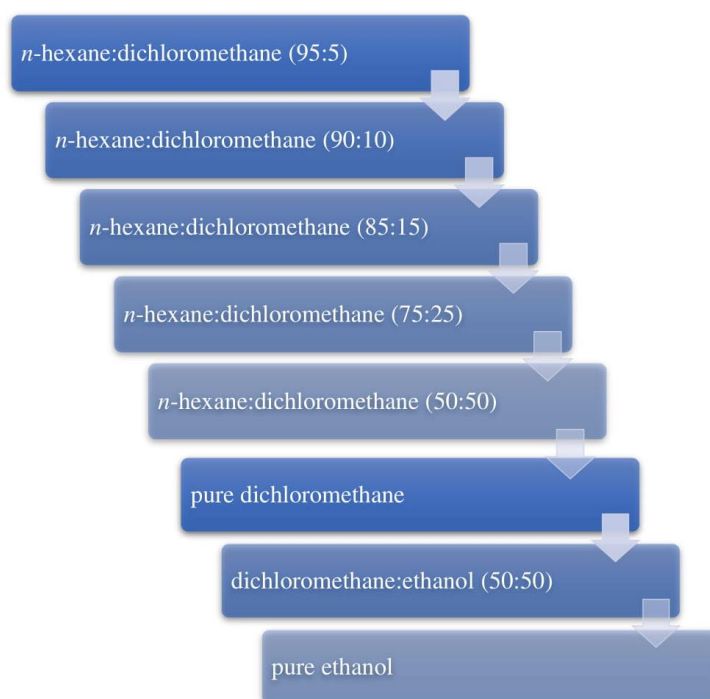


Figure 3.18. Eluting solvents for Polyamide CC6 open column chromatography of the dichloromethane fraction of *C. depressa*.

While working with the first five solvent mixtures, fractions of 20 ml were collected; for the last solvents the amount of the fractions increased to approximately 100 ml. All the fractions from the dichloromethane extract of *C. depressa* were analysed by TLC and combined as shown in Figure 3.19. Finally, after the Polyamide open column, nine subfractions were obtained from the dichloromethane extract: A1 – 612 mg; A2 – 248



mg; A3 – 317 mg; A4 – 228 mg; A5 – 817 mg; A6 – 857 mg; A7 – 535 mg; A8 – 212 mg; A9 – 798 mg.

Further on, based on HPLC analysis, A6 and A7 were fractionated by flash chromatography with a Grace® Flash Cartridge 80 g silica column and gradient elution. The mobile phase was dichloromethane with 0.1% trifluoroacetic acid (eluent A), 70% dichloromethane in ethyl acetate with 0.1% trifluoroacetic acid (eluent B), 50% dichloromethane in ethyl acetate with 0.1% trifluoroacetic acid (eluent C) and 70% ethyl acetate in ethanol with 30% dichloromethane and 0.1% trifluoroacetic acid (eluent D). The fractions collected following flash chromatography were combined after a TLC analysis. The separation of fraction A6 resulted in five subfractions: A6\_1, A6\_2 – 174 mg, A6\_3, A6\_4 – 515 mg, A6\_5 – 185 mg. The promising ones were submitted for purification and isolation by semi-preparative HPLC. As it is shown in Figure 3.19, three PMFs were successfully obtained from A6\_2 and A6\_4 subfractions, and two PMFs were isolated from fraction A6\_5. The phytochemical analysis of fraction A7 resulted in seven subfractions from which the A7\_6 (68 mg) was submitted to semi-preparative HPLC for isolation and purification. Two pure compounds, not isolated previously in the investigation, were acquired.

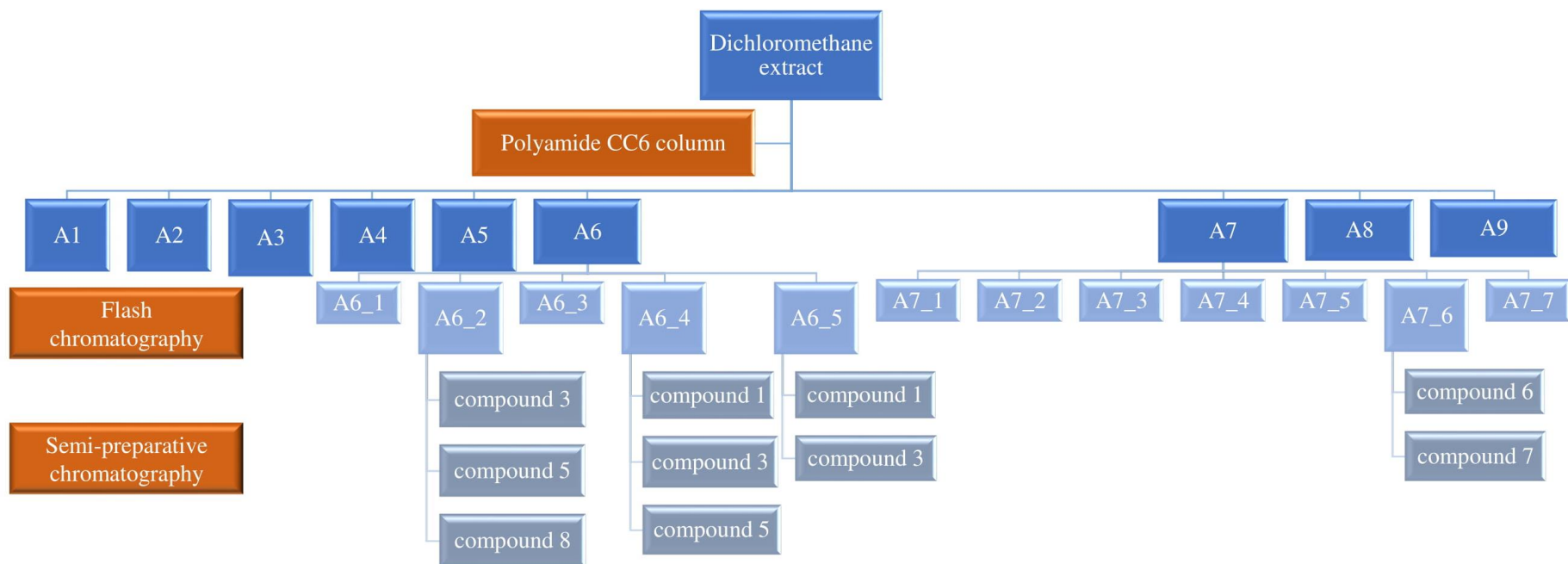


Figure 3.19. Different steps performed during the purification of *Citrus depressa* dichloromethane extract resulting in the isolation of six pure compounds.

The structure of these compounds was further elucidated and confirmed, by applying the same techniques as described in the phytochemical investigation for *C. sinensis*, namely, 1D- and 2D-NMR, and mass spectrometry for conformation of the chemical structure. Similar to the previously characterized compounds, the  $^1\text{H-NMR}$  signals between  $\delta$  3.5 – 4.4 and 6.5 – 8.0 were typical for PMFs. The  $^1\text{H-NMR}$  spectra for compounds 6 and 8 revealed that they have an ABX system (H-2', H-5' and H-6'), which was confirmed by the coupling constants at  $\delta$  7.5 – 7.7 (dd,  $J=8.4$ ,  $J=2.1$ , H-6'),  $\delta$  7.3 -7.5 (d,  $J=2.1$ , H-2') and  $\delta$  6.9 -7.1 (d,  $J=8.4$ , H-5') in the B-ring. The coupling constant ( $J=2$  and  $J=8$  Hz) was characteristic for *meta*- and *para*- couplings, typical for 3', 4'- methoxylated flavonoids. Additionally, by HMBC analysis two methoxy groups in position 3' and 4' were confirmed for those compounds. The  $^1\text{H-NMR}$  spectrum of compound 7 had a pair of two-proton, *ortho*-coupled doublets arising from two pairs of protons (H-2',6' and H-3',5'), revealing the presence of an  $A_2B_2$  system in the B-ring, which is typical for a *para*-substituted benzene structure. Another proof is given by the coupling constant, namely:  $\delta$  8.9 (H-2',-6') and  $\delta$  9.0 (H-3',-5') ( $J = 8.9$  Hz). In general, the chemical shift of the aromatic proton signals were different for the various compounds, depending on the number and location of the functional groups (methoxy, hydroxy). The  $^{13}\text{C-NMR}$  spectral assignments were done based on DEPT -90, DEPT-135, HMBC and HSQC spectra.

**Compound 6** showed aromatic proton singlets at  $\delta$  6.59 and 6.40 (Figure 3.20). Their position was deduced from COSY (Figure 3.22) and HMBC (Figure 3.23) analyses. The characteristic correlations from HMBC analysis that helped to elucidate the structure were: strong correlation between C-2, C-1', C-10 and the singlet at  $\delta$  6.59 (H-3), strong correlation between C-7, C-8, C-10 and the singlet at  $\delta$  6.40 (H-6). In the COSY experiment an interaction between the signal at  $\delta$  6.40 and the signals of the two methoxy groups at C-5 and C-7 ( $\delta$  3.95 and  $\delta$  3.97) was observed, which can be explained by a very long-range 1H-1H coupling. The HMBC correlations between C-10 and the two proton singlets, as well as the data from the COSY experiment, confirmed that the first aromatic proton ( $\delta$  6.59) was at the 3-position and the second ( $\delta$  6.40) at the 6-position. The signals at  $\delta_{\text{H}}$  3.97, 3.95, 3.92, 3.93 and 3.92 were assigned to the five methoxy group at C-5, C-7, C-8, C-3' and C-4' (Figure 3.21), as shown by HMBC analysis. The ESI-MS spectrum revealed a pseudo-molecular ion at  $m/z$  373  $[\text{M}+\text{H}]^+$ . This compound was identified as **5,7,8,3',4'-pentamethoxyflavone** ( $\text{C}_{20}\text{C}_{20}\text{O}_7$ ) and was isolated as colourless needles.

**Compound 7** possessed two aromatic proton singlets at  $\delta$  6.70 and  $\delta$  6.40 (Figure 3.24). Their position was elucidated by HMBC analysis, which revealed characteristic correlations between: C-4, C-2, C-1' and  $\delta$  6.70; C-4, C-7, C-8 and  $\delta$  6.40; and C-10 and the two aromatic singlets (Figure 3.26). In the end, the signal at  $\delta$  6.70 was assigned to C-3 and the signal at  $\delta$  6.40 at C-6. The signals at  $\delta_c$  56.2, 56.4, 61.5 and 55.4 were assigned to the four methoxy groups at C-5, C-7, C-8 and C-4', respectively (Figure 3.25), as confirmed by the HMBC analysis. The pseudo-molecular ion was found at  $m/z$  343  $[M+H]^+$  and the compound was identified as **5,7,8,4'-tetramethoxyflavone** (C<sub>19</sub>H<sub>18</sub>O<sub>6</sub>). It was obtained as colourless needles.

For **compound 8** an aromatic proton singlet was observed at  $\delta$  6.58 and a signal at  $\delta$  12.5, the latter indicating the presence of a hydroxyl group in the structure (Figure 3.27). The five methoxy group signals at  $\delta_H$  4.08, 3.95, 3.95, 3.94 and 3.92, assigned to the methoxy groups at C-6, C-7, C-8, C-3' and C-4' were correlating with the signals at  $\delta_c$  62.1, 61.7, 61.1, 56.1 and 56.0 (Figure 3.28), as confirmed by literature data and NMRPredict.<sup>133</sup> The product was obtained as yellow needles and its pseudo-molecular ion was observed as  $m/z$  389  $[M+H]^+$ . It was identified as **5-hydroxy-6,7,8,3',4'-pentamethoxyflavone** (C<sub>20</sub>H<sub>20</sub>O<sub>8</sub>).

The <sup>1</sup>H- and <sup>13</sup>C-NMR assignments for 5,7,8,3',4'-pentamethoxyflavone (**compound 6**), 5,7,8,4'-tetramethoxyflavone (**compound 7**) and 5-O-demethylnobiletin (**compound 8**) are presented in Table 3.2 and Table 3.3, respectively. The data was consistent with those reported in literature.<sup>123,133,134</sup>

In summary, from the dichloromethane fraction of *C. depressa* the most abundant PMFs sinensetin (**compound 1**), nobiletin (**compound 3**) and tangeretin (**compound 5**), as well as 5,7,8,3',4'-pentamethoxyflavone (**compound 6**), 5,7,8,4'-tetramethoxyflavone (**compound 7**) and 5-O-demethylnobiletin (**compound 8**) were successfully isolated.

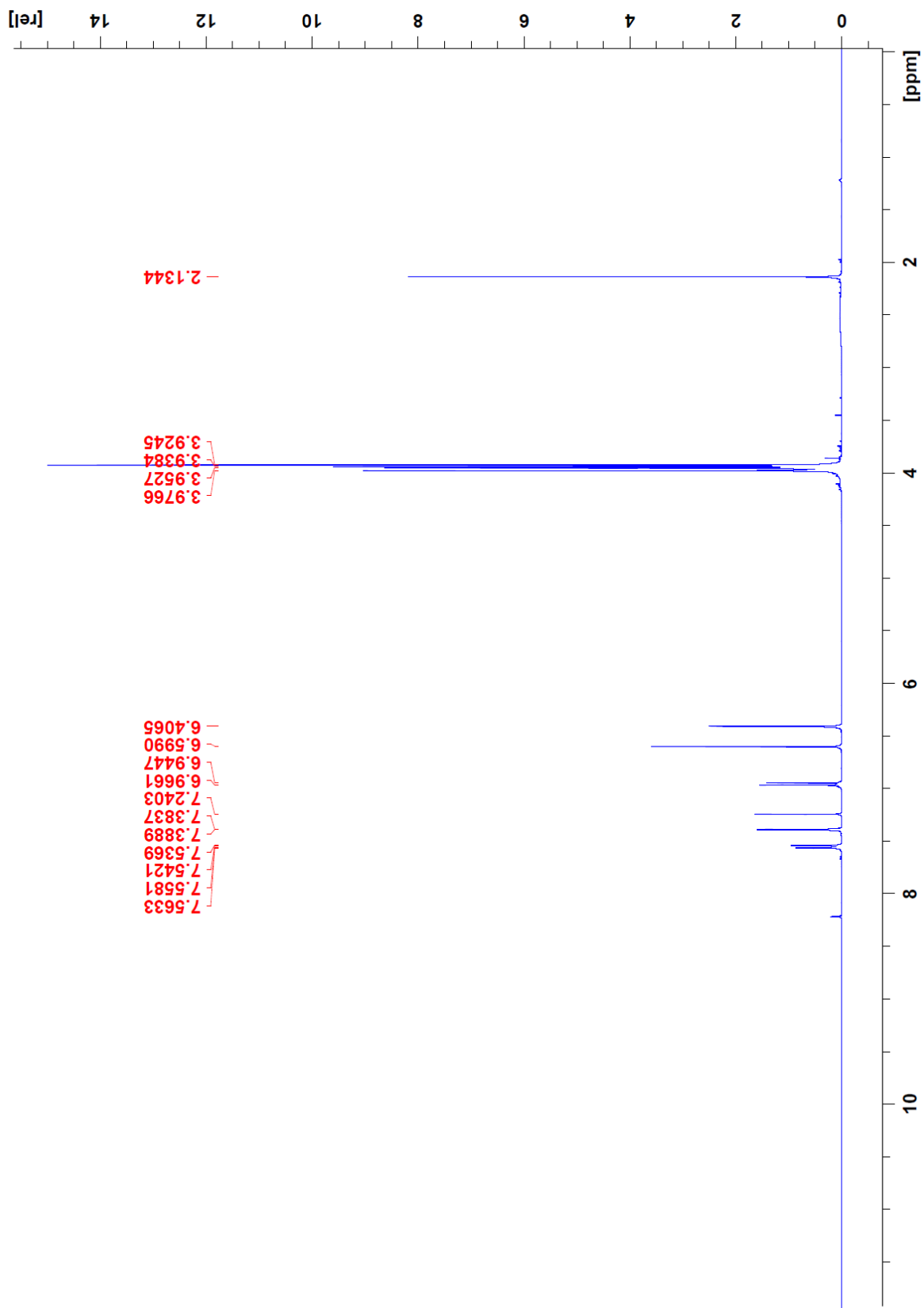


Figure 3.20. <sup>1</sup>H-NMR spectrum (400 MHz, chloroform-d) of **compound 6** (5,7,8,3',4'-pentamethoxyflavone).

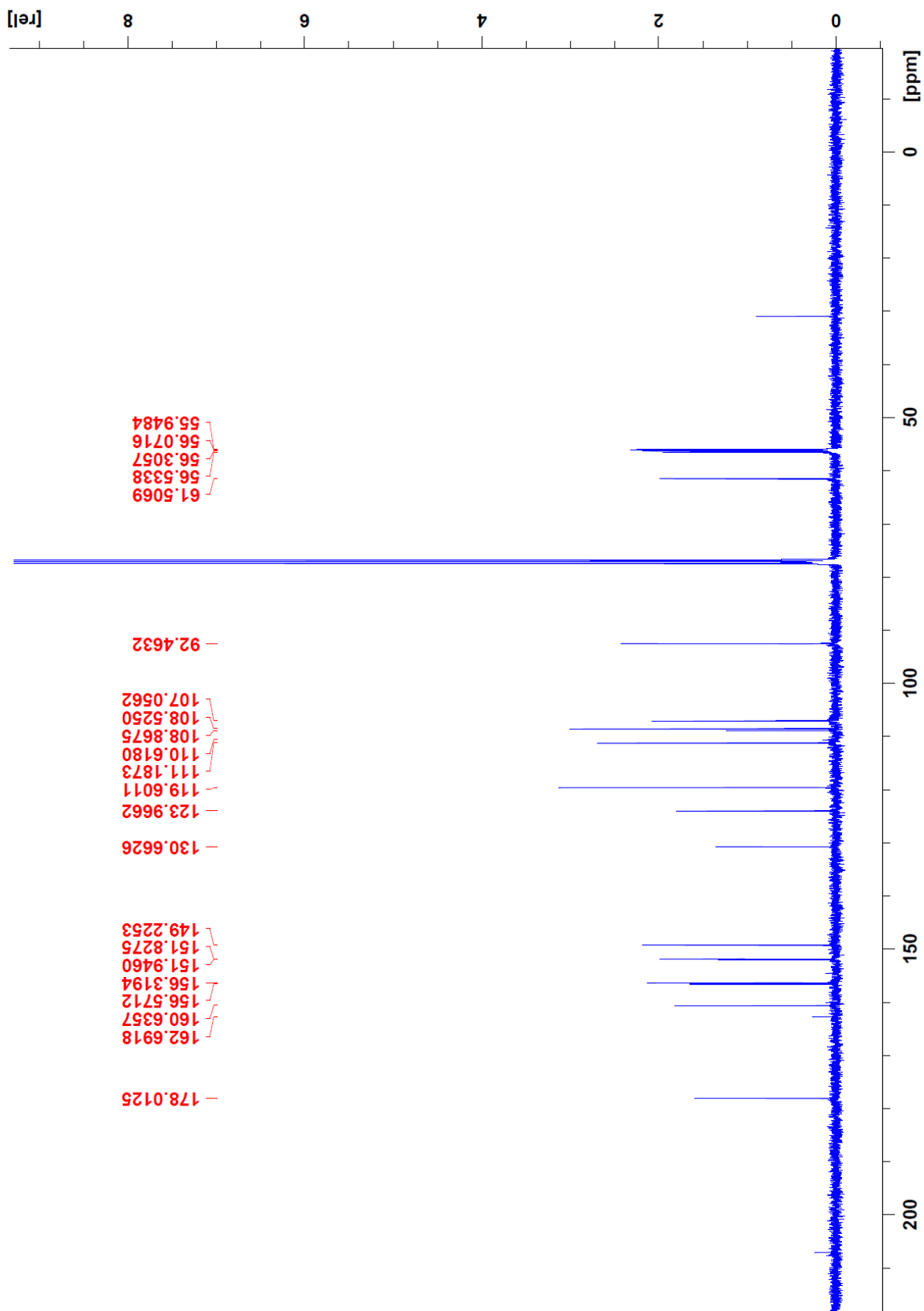


Figure 3.31.  $^{13}\text{C}$ -NMR spectrum (100 MHz, chloroform-d) of **compound 6** (5,7,8,3',4'-pentamethoxyflavone).

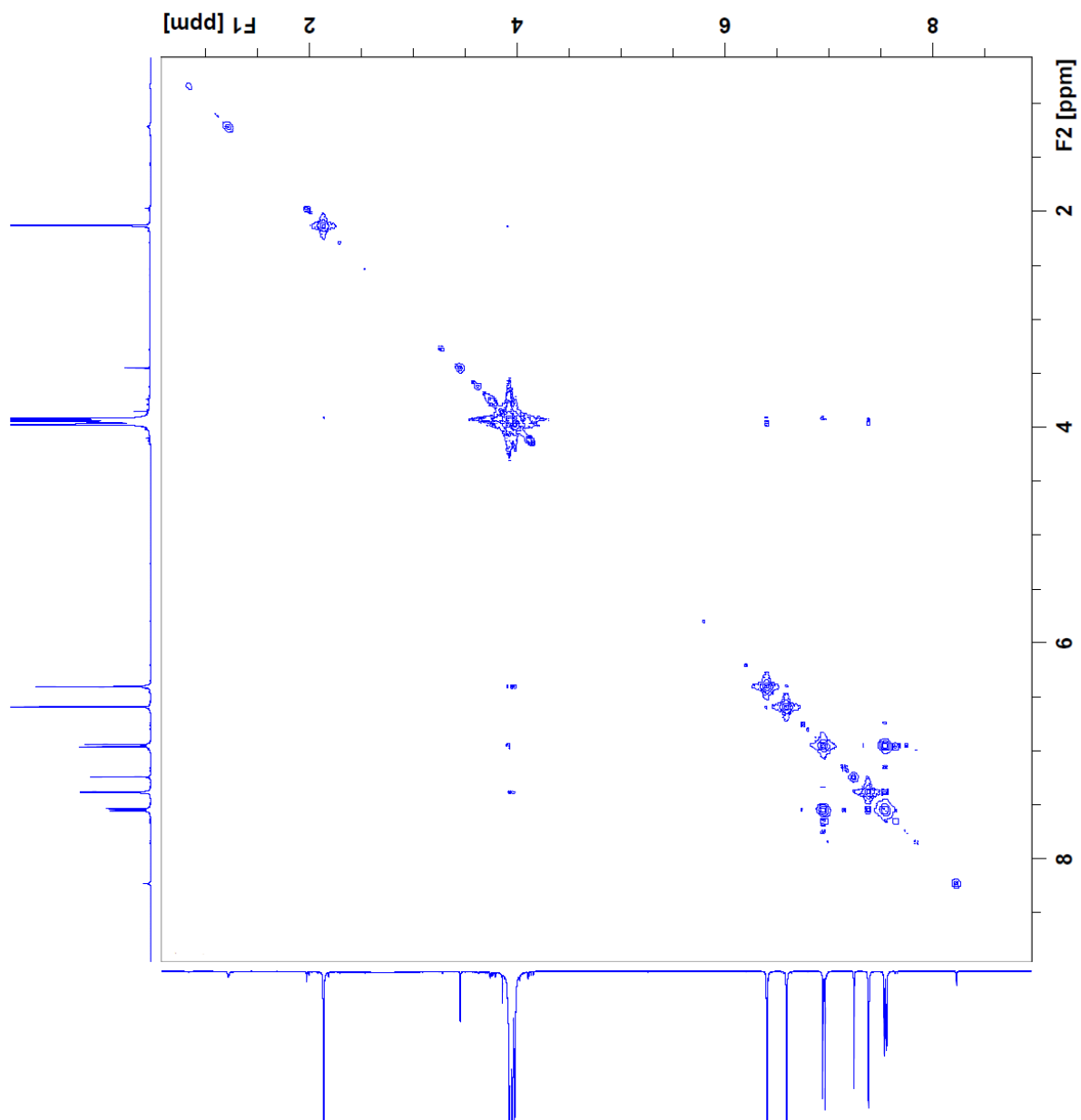


Figure 3.22. COSY spectrum (100 MHz, chloroform-d) of **compound 6** (5,7,8,3',4'-pentamethoxyflavone).

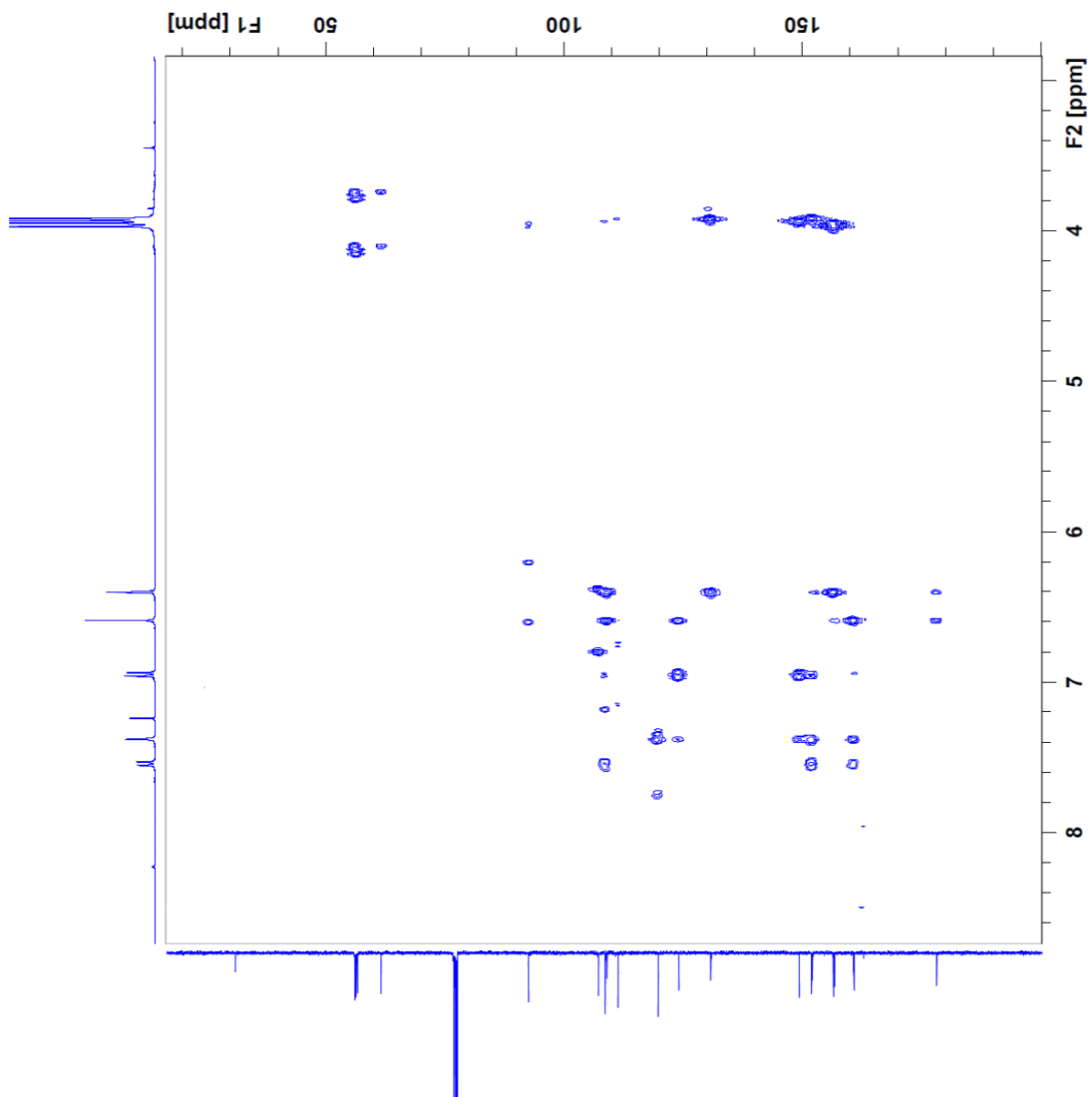


Figure 3.23. HMBC spectrum (400 MHz, chloroform-d) of **compound 6** (5,7,8,3',4'-pentamethoxyflavone).



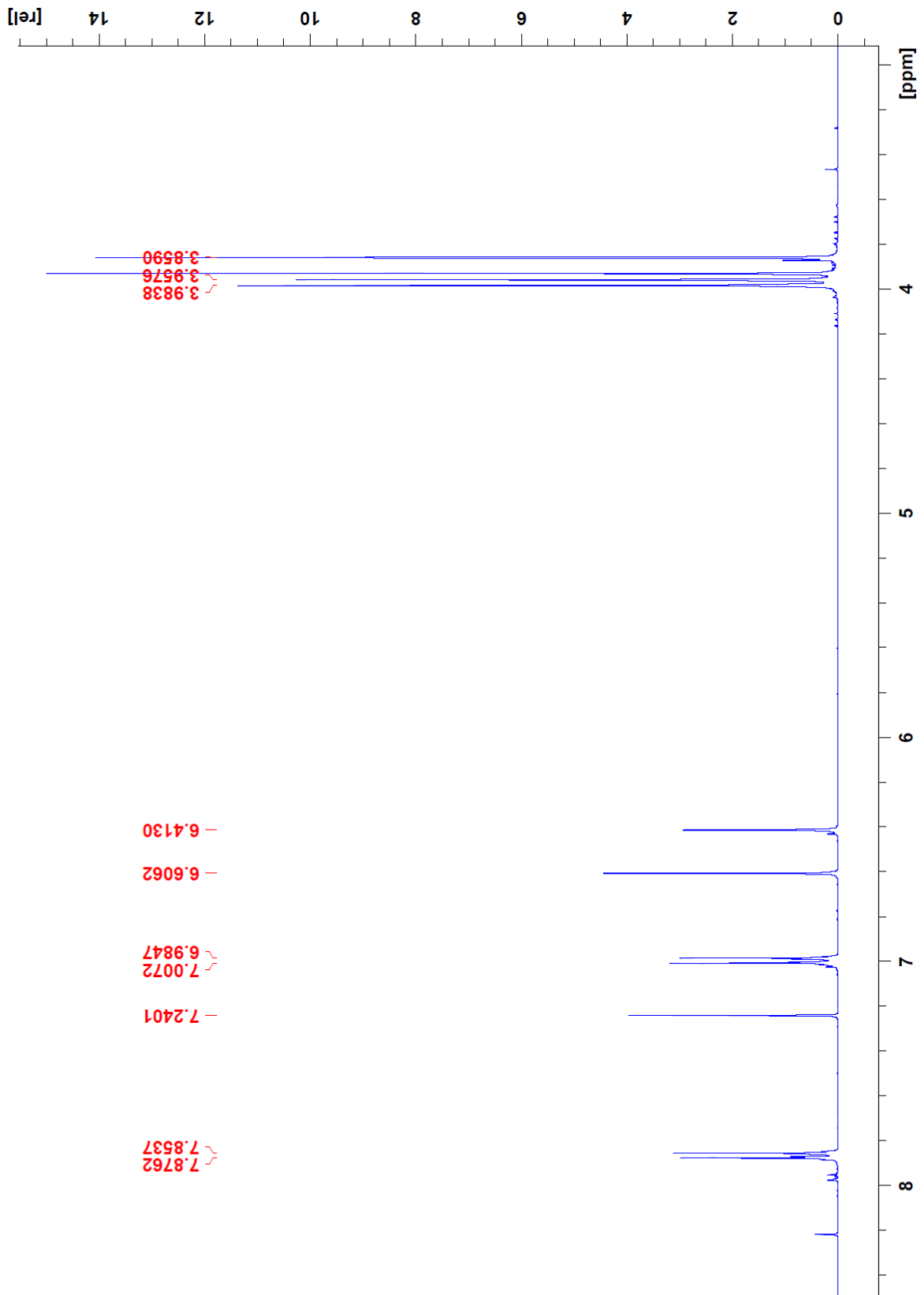


Figure 3.24.  $^1\text{H-NMR}$  spectrum (400 MHz, chloroform- $d$ ) of **compound 7** (5,7,8,4'-tetramethoxyflavone).

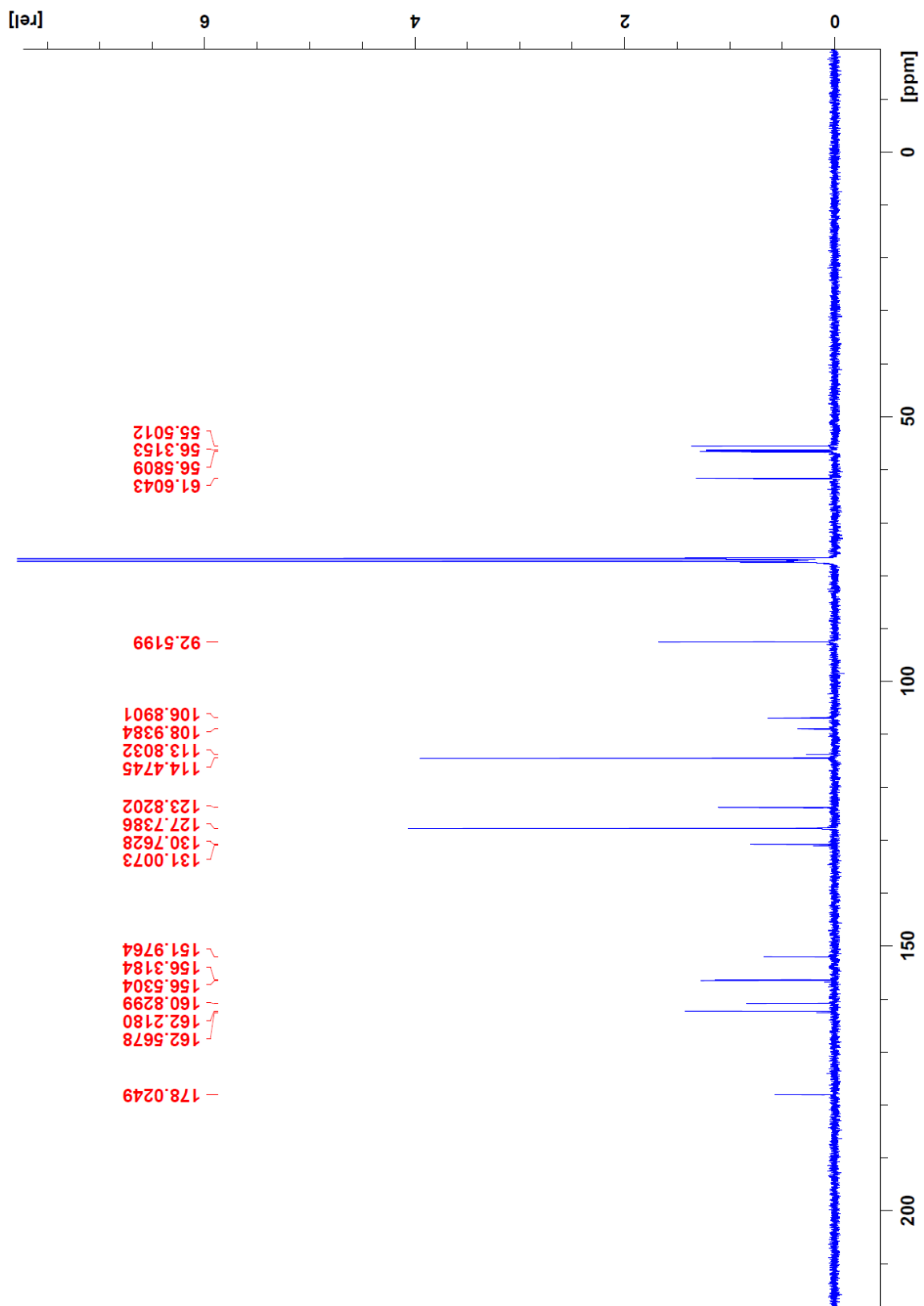


Figure 3.25.  $^{13}\text{C}$ -NMR spectrum (100 MHz, chloroform- $d$ ) of **compound 7** (5,7,8,4'-tetramethoxyflavone).

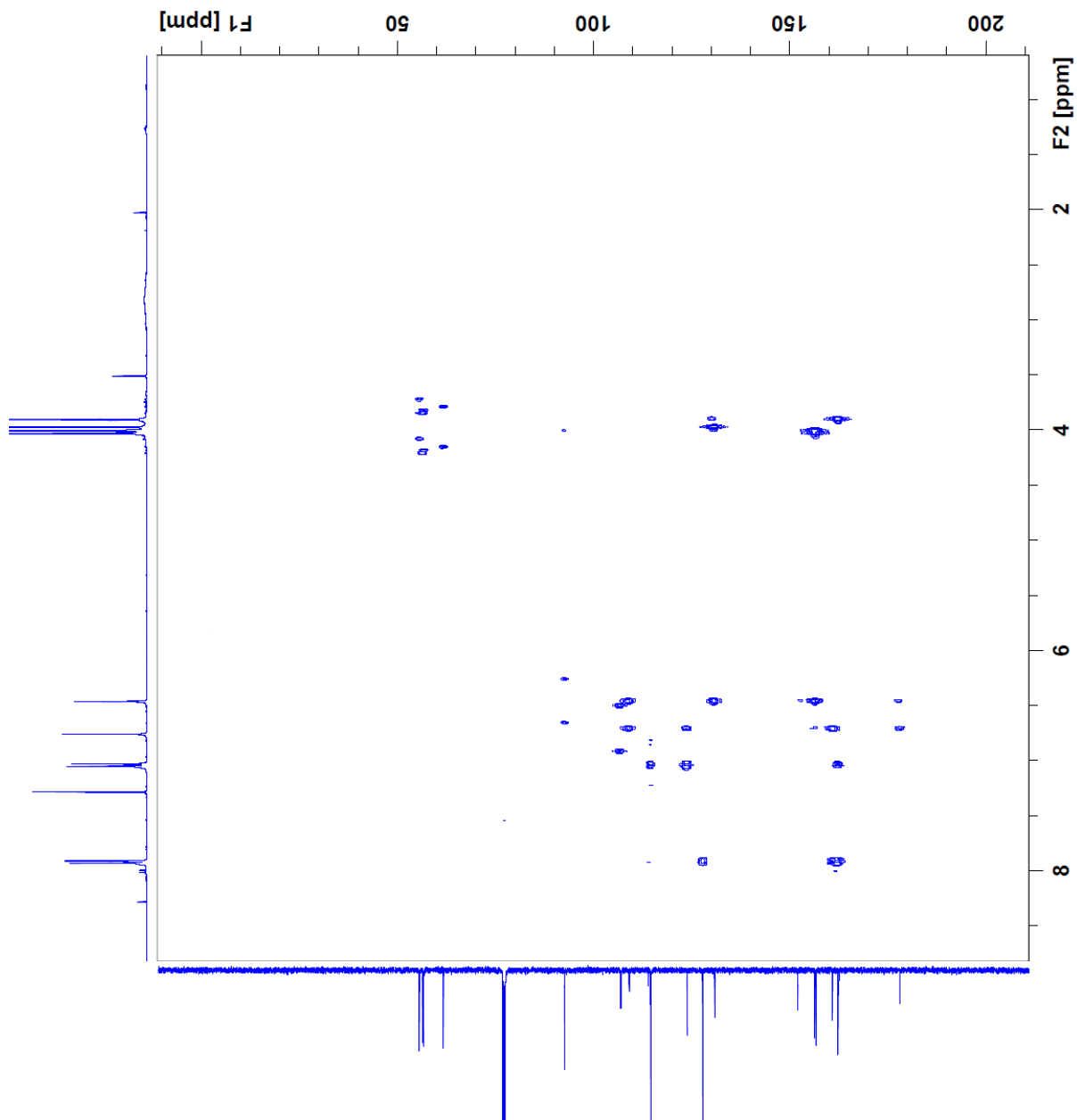


Figure 3.26. HMBC spectrum (400 MHz, chloroform-*d*) of **compound 7** (5,7,8,4'-tetramethoxyflavone).

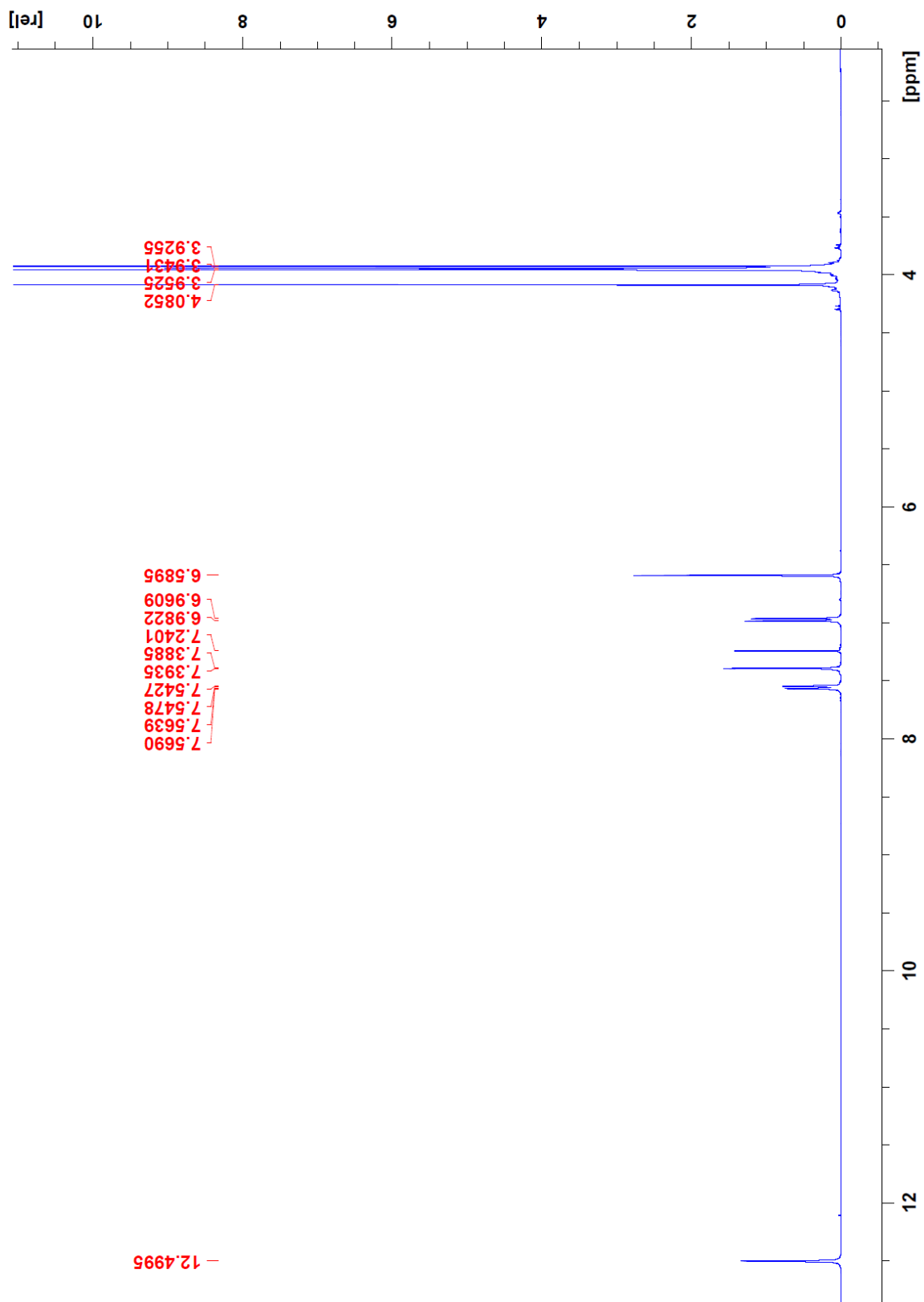


Figure 3.27.  $^1\text{H-NMR}$  spectrum (400 MHz, chloroform- $d$ ) of **compound 8** (5-O-demethylnobiletin).

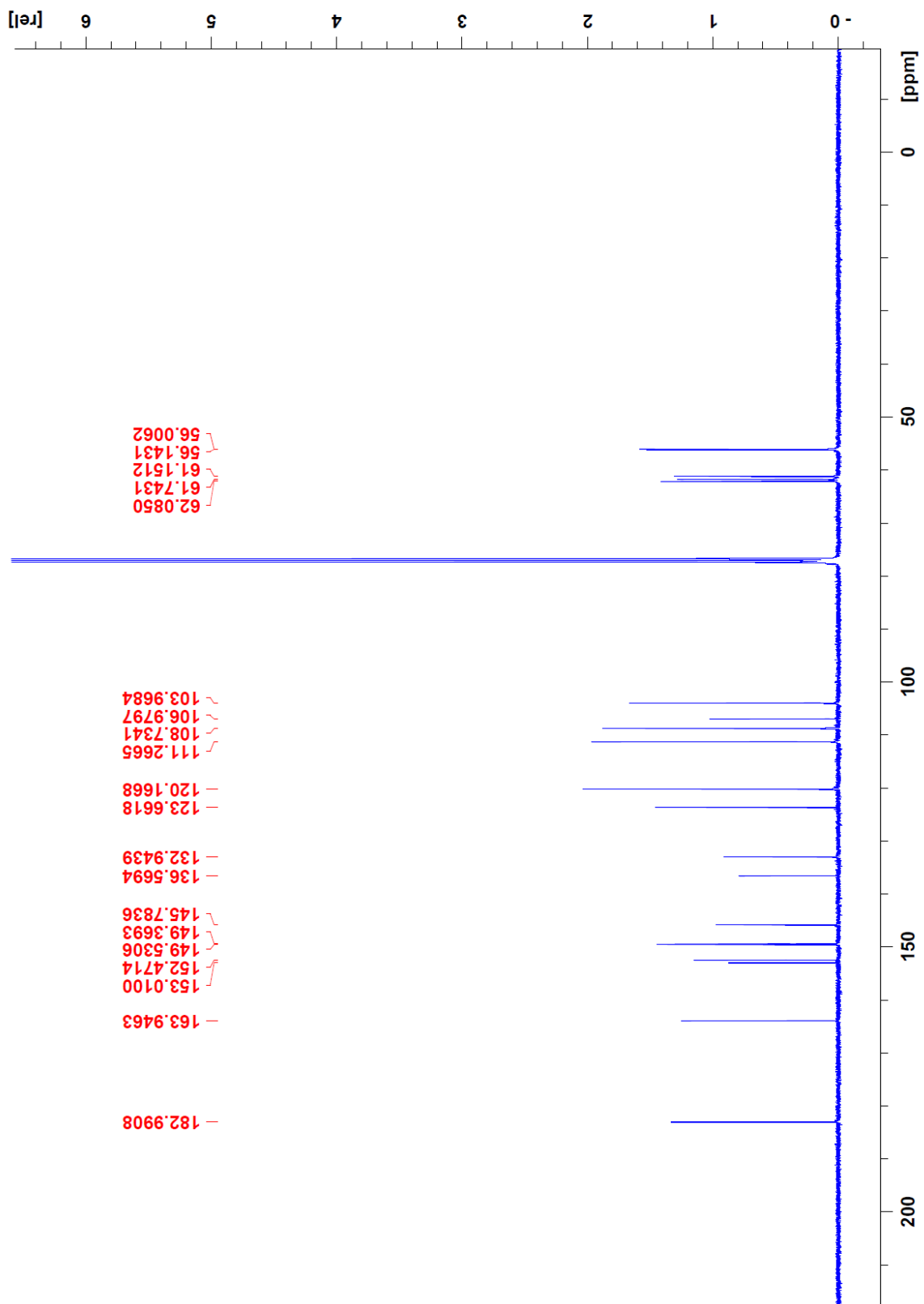
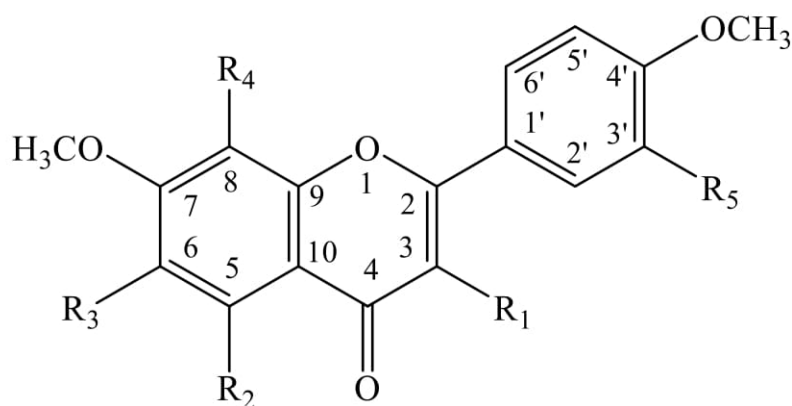


Figure 3.28.  $^{13}\text{C}$ -NMR spectrum (100 MHz, chloroform- $d$ ) of **compound 8** (5-O-demethylnobiletin).

The chemical structures of the isolated pure compounds for *C. sinensis* and *C. depressa* are summarised in Figure 3.29.



<b>Compound</b>	<b>R1</b>	<b>R2</b>	<b>R3</b>	<b>R4</b>	<b>R5</b>	<b>Plant sp.</b>
<b>sinensetin (1)</b>	H	OCH <sub>3</sub>	OCH <sub>3</sub>	H	OCH <sub>3</sub>	<i>C. sinensis</i>
<b>5,6,7,4'- tetramethoxyflavone (2)</b>	H	OCH <sub>3</sub>	OCH <sub>3</sub>	H	H	<i>C. sinensis</i>
<b>nobiletin (3)</b>	H	OCH <sub>3</sub>	OCH <sub>3</sub>	OCH <sub>3</sub>	OCH <sub>3</sub>	<i>C. sinensis</i> , <i>C. depressa</i>
<b>3,5,6,7,8,3',4'- heptamethoxyflavone (4)</b>	OCH <sub>3</sub>	OCH <sub>3</sub>	OCH <sub>3</sub>	OCH <sub>3</sub>	OCH <sub>3</sub>	<i>C. sinensis</i>
<b>tangeretin (5)</b>	H	OCH <sub>3</sub>	OCH <sub>3</sub>	OCH <sub>3</sub>	H	<i>C. sinensis</i> , <i>C. depressa</i>
<b>5,7,8,3',4'- pentamethoxyflavone (6)</b>	H	OCH <sub>3</sub>	H	OCH <sub>3</sub>	OCH <sub>3</sub>	<i>C. depressa</i>
<b>5,7,8,4'- tetramethoxyflavone (7)</b>	H	OCH <sub>3</sub>	H	OCH <sub>3</sub>	H	<i>C. depressa</i>
<b>5-demethylnobiletin (8)</b>	H	OH	OCH <sub>3</sub>	OCH <sub>3</sub>	OCH <sub>3</sub>	<i>C. sinensis</i> , <i>C. depressa</i>

Figure 3.29. Isolated PMFs from *C. sinensis* and *C. depressa*.

Compound	H-3	H-5	H-6	H-7	H-8	H-2'	H-3'	H-4'	H-5'	H-6'	OCH <sub>3</sub>	solvent
<b>sinensetin</b> <b>(1)</b>	6.61 s				7.10 s	7.54 d (J=2.2)			7.11 d (J=8.4)	7.63 dd (J=8.4 J=2.2)	3.86 3.8 3.98 3.91 3.88	acetone-d <sub>6</sub>
<b>5,6,7,4'-</b> <b>tetramethoxyflavone</b> <b>(2)</b>	6.57 s				7.13 s	7.99 d (J=9.0)	7.11 d (J=1.8)		7.11 d (J=1.8)	7.99 d (J=9.0)	3.82 3.88 3.90 4.01	acetone-d <sub>6</sub>
<b>nobiletin</b> <b>(3)</b>	6.66 s					7.41 d (J=2.2)			6.99 d (J=8.4)	7.57 dd (J=8.4 J=2.2)	3.94 4.01 3.93 4.09 3.95 3.97	chloroform-d
<b>3,5,6,7,8,3',4'-</b> <b>heptamethoxyflavone</b> <b>(4)</b>						7.7 d (J=2.2)			7.1 d (J=8.4)	7.8 dd (J=8.4 J=2.2)	3.88 3.89 3.90 3.92 4.03 4.08	acetone-d <sub>6</sub>
<b>tangeretin</b> <b>(5)</b>	6.56 s					7.83 d (J=8.9)	6.97 d (J=9.0)		6.97 d (J=9.0)	7.83 d (J=8.9)	3.85 3.91 3.98 4.06	chloroform-d
<b>5,7,8,3',4'-</b> <b>pentamethoxyflavone</b> <b>(6)</b>	6.59 s		6.40 s			7.38 d (J=2.2)			6.95 d (J=8.4)	7.54 dd (J=8.4 J=2.2)	3.97 3.95 3.92 3.93 3.92	chloroform-d
<b>5,7,8,4'-</b> <b>tetramethoxyflavone (7)</b>	6.70 s		6.41 s			7.0 d (J=9.0)	7.9 d (J=8.9)		7.9 d (J=8.9)	7.0 d (J=9.0)	4.0 4.0 3.97 3.9	chloroform-d
<b>5-demethylnobiletin</b> <b>(8)</b>	6.58 s	12.5 s				7.39 d (J=2.2)			6.97 d (J=8.4)	7.55 dd (J=8.4 J=2.2)	3.92 3.94 3.95 3.95 4.08	chloroform-d

Table 3.2. <sup>1</sup>H-NMR assignments of the isolated compounds from *C. sinensis* and *C. depressa* (where J is in Hz).

Compound	C														OCH <sub>3</sub>							
	2	3	4	5	6	7	8	9	10	1'	2'	3'	4'	5'	6'	6	7	8	5	3	3'	4'
<b>sinensetin** (1)</b>	162.1 (s)	107.2 (d)	177.5 (s)	153.1 (s)	141.3 (s)	159.0 (s)	97.8 (d)	155.4 (s)	113.2 (s)	124.6 (s)	110.1 (d)	150.5 (s)	153.2 (s)	112.5 (d)	120. 5 (d)	61.5 (q)	56.8 (q)		62.4 (q)		56.4 (q)	56.3 (q)
<b>5,6,7,4'- tetra- methoxy- flavone** (2)</b>	163.2 (s)	107.1 (d)	176.8 (s)	153.2 (s)	141.2 (s)	158.8 (s)	97.7 (d)	153.2 (s)	113.4 (s)	124.5 (s)	128.6 (d)	115.3 (d)	161.7 (s)	115.3 (d)	128. 6 (d)	61.5 (q)	56.8 (q)		62.3 (q)			56.2 (q)
<b>nobiletin* (3)</b>	161.3 (s)	106.9 (d)	177.5 (s)	144.2 (s)	138.1 (s)	151.6 (s)	148. 5 (s)	147.8 (s)	114.9 (s)	124.0 (s)	108.6 (d)	149.4 (s)	152.1 (s)	111.3 (d)	119. 8 (d)	61.9 (q)	61.8 (q)	62.4 (q)	62.1 (q)		56.2 (q)	56.1 (q)
<b>3,5,6,7,8,3', 4'hepta- methoxy- flavone** (4)</b>	152.2 (s)	141.4 (s)	173.6 (s)	149.9 (s)	144.7 (s)	152.3 (s)	138. 8 (s)	147.6 (s)	115.9 (s)	124.1 (s)	111.9 (d)	148.8 (s)	153.6 (s)	112.3 (d)	122. 6 (d)	62.0 (q)	61.9 (q)	59.8 (q)	62.2 (q)	62.4 (q)	56.1 (q)	56.0 (q)
<b>tangeretin* (5)</b>	161.2 (s)	106.7 (d)	177.4 (s)	144.1 (s)	138.1 (s)	151.4 (s)	148. 4 (s)	147.7 (s)	114.8 (s)	123.7 (s)	114.5 (d)	127.7 (d)	162.2 (s)	127.7 (d)	114. 5 (d)	62.0 (q)	61.8 (q)	61.7 (q)	62.3 (q)			55.5 (q)
<b>5,7,8,3',4'- penta- methoxy- flavone* (6)</b>	160.6 (s)	107.1 (d)	178.0 (s)	151.9 (s)	92.4 (d)	156.3 (s)	130. 6 (s)	156.6 (s)	108.8 (s)	123.9 (s)	108.5 (d)	149.2 (s)	154.8 (s)	111.1 (d)	119. 6 (d)		56.5 (q)	61.5 (q)	56.3 (q)		55.9 (q)	56.1 (q)
<b>5,7,8,4'- tetra- methoxy- flavone* (7)</b>	160.8 (s)	106.9 (d)	178.0 (s)	151.9 (s)	92.5 (d)	156.5 (s)	130. 7 (s)	156.3 (s)	108.9 (s)	123.8 (s)	114.5 (d)	127.7 (d)	162.2 (s)	127.7 (d)	114. 5 (d)		56.6 (q)	61.6 (q)	56.3 (q)			55.5 (q)
<b>5-demethyl- nobiletin* (8)</b>	163.9 (s)	103.9 (d)	182.9 (s)	149.4 (s)	136.5 (s)	152.4 (s)	132. 9 (s)	145.7 (s)	106.9 (s)	123.6 (s)	108.7 (d)	149.5 (s)	153.0 (s)	111.2 (d)	120. 1 (d)	62.1 (q)	61.7 (q)	61.1 (q)			56.1 (q)	56.0 (q)

Table 3.3. <sup>13</sup>C-NMR assignments of the isolated compounds from *C. sinensis* and *C. depressa*. Solvents: chloroform-d (\*) and acetone-d<sub>6</sub> (\*\*)



## 4. Isolation and identification of biflavonoids from *Ginkgo biloba* sludge

### 4.1 Introduction

#### 4.1.1 Plant description

*Ginkgo biloba* L. (Ginkgoaceae), also called maidenhair tree, is native to China and is now valued in many parts of the world as a fungus- and insect-resistant ornamental tree. Although widely cultivated, the plant is listed as an endangered species by the IUCN (International Union for Conservation of Nature) Red List and it is threatened in



Figure 3.30. Image of *Ginkgo biloba* leaves.<sup>265</sup>

the wild. A ginkgo tree is pyramidal in shape, with branched trunk up to 30 meters tall and 2.5 meters in diameter. The bark is greyish and has a corky texture. Fan-shaped ginkgo leaves (Figure 3.30) are borne on short, spurlike but greatly thickened shoots. The leathery leaves are up to 8 cm long and are sometimes twice as broad. Two parallel veins enter each blade from the point of attachment of the long leafstalk and fork repeatedly toward the leaf edge. Most leaves are divided into two lobes by a central notch. Dull grey-green to yellow-green in summer, they turn golden yellow in autumn, remaining on the tree until late in the season, and then fall rapidly.<sup>137</sup>

the wild. A ginkgo tree is pyramidal in shape, with branched trunk up to 30 meters tall and 2.5 meters in diameter. The bark is greyish and has a corky texture. Fan-shaped ginkgo leaves (Figure 3.30) are borne on short, spurlike but greatly thickened shoots. The leathery leaves are up to 8 cm long and are sometimes twice as broad. Two parallel veins enter each blade from the point of attachment of the long leafstalk and fork repeatedly toward the leaf edge. Most

#### 4.1.2 Traditional medicine

*Ginkgo biloba* is one of the most ancient living trees, which is the only surviving member of its family. Therefore, it has been named a living fossil, and its therapeutic effects are already known for 5000 years in traditional Chinese medicine.<sup>138</sup> Important constituents in *Ginkgo biloba* leaves include terpene trilactones (ginkgolides A, B, C, J and bilobalide), many flavonol glycosides, biflavones, proanthocyanidins, ginkgolic

acids and related alkylphenols, simple phenolic acids and polyphenols, of which the flavonol glycosides, terpene trilactones, and proanthocyanidins are considered to be the main components for their beneficial effects.<sup>139</sup>

#### 4.1.3 *Ginkgo biloba* extract (EGb 761) – pharmacological activity

*Ginkgo biloba* extract EGb 761 is a well-defined and complex product prepared from green leaves of the plant. The mode of culturing, harvesting and extraction are perfectly standardized and controlled, therefore, the amount of undesired substances has been reduced and the content of active principles enriched.<sup>140</sup> Nowadays, the extract from the leaves is one of the most popular herbal medicines for treatment of peripheral vascular diseases and dementia in Europe.<sup>141</sup>

According to the European Pharmacopoeia 10.0 the refined and quantified dry extract (standardized) produced from *Ginkgo* leaves should contain:

- flavonoids, expressed as flavone glycosides: 22% to 27% (dried extract);
- bilobalide: 2.6% to 3.2% (dried extract);
- ginkgolides A, B and C: 2.8% to 3.4% (dried extract);
- ginkgolic acids: maximum 5 ppm (dried extract).<sup>142</sup>

Ginkgolide B and bilobalide account for about 0.8% and 3% of the total extract, respectively. However, ginkgolic acids are considered as potentially hazardous contents in *Ginkgo* leaves because they possess possibly mutagenic and carcinogenic activity, and they provoke allergic reactions and contact dermatitis.<sup>143</sup> The EGb 761 extract (*Ginkgo biloba* extract EGb 761, Tanakan<sup>®</sup>, Tebonin<sup>®</sup>) is a standardized extract from *Ginkgo biloba* leaves and has antioxidant properties as a radical scavenger (flavonol glycosides, proanthocyanidins). The product promotes vasodilatation and improves the blood flow through arteries, veins and capillaries. It inhibits platelet aggregation and prolongs bleeding time (terpene trilactones-ginkgolides A, B, C, J, bilobalide). EGb 761, which was developed by Dr. Willmar Schwabe Pharmaceuticals, is available in Europe as a herbal extract since the early 1990s.<sup>144</sup> The psychological and physiological effects of *Ginkgo* are explained by its primary action on regulating neurotransmitters and exerting neuroprotective effects on the brain, preventing or retarding nerve cell degeneration. In 2002, the Cochrane Collaboration, one of the most prominent scientific reviews of clinical trials in medicine, confirmed that the

published literature so far strongly supports the safety and potential benefits of *Ginkgo* in treating memory loss and cognitive disorders associated with age-related dementia.<sup>145</sup>

Because of its beneficial effect on the brain it has been used extensively for the treatment of diseases related to the central nervous system including Alzheimer's disease and cognition disorders, thromboses and vascular disorders.<sup>144</sup> Moreover, the standardized extract has shown activity against arrhythmias, diabetes and ischaemic heart disease.<sup>146</sup> The data suggests that EGb 761 protects neuronal cell membranes from the free radical damage *in vitro*. This characteristic mediates the beneficial effect on cognitive function, since the presence of free radicals may reduce the normal fluidity, consequently, resulting in age-related functional decline.<sup>144</sup> On the other hand, a recent large (3069 people), double blind clinical trial of long duration (6.1 years) – the GEM (The *Ginkgo* Evaluation of Memory) study, showed no effect of a standardized EGb 761 extract in preventing dementia of any type.<sup>147</sup>

On a phytochemical level, flavonoids and terpenes are considered to contribute to the main pharmacological effects of the plant species and the EGb 761 extract. Although the biological activity of the major constituents is well studied, the biflavonoids, which are partly removed during the extraction procedure of the EGb 761 extract (see below), have only poorly been investigated. Since *Ginkgo biloba* is well known for the presence of biflavonoids and because of their promising biological activities, these compounds have been selected as one of the classes of target compounds in the present project. Crude *G. biloba* plant material was used as a source for isolating some representatives of this class, in order to evaluate their biological activities.<sup>148</sup>

#### 4.1.4 Biflavonoids

Biflavonoids have appeared to be natural fungal toxins and insect feeding deterrents, which are involved in warding off insects and microbial attack. For example, amentoflavone was found to inhibit the growth of *Aspergillus fumigatus* and *Trichoderma glaucum*. In leaf tissues biflavonoids may also have a role, together with other flavonoids, as UV filters.<sup>149</sup>

A number of pharmacological effects of biflavonoids have been reported, including the ability to inhibit the adhesion of blood platelets, the release of histamine, blocking the inflammatory effects of hepatotoxins, and actions as a heart stimulant.<sup>149</sup> More

specifically, studies have been carried out to prove the variety of pharmacological activities of amentoflavone, including analgesic, anti-inflammatory and antiviral activity,  $\alpha$ -glucosidase and  $\alpha$ -amylase inhibitory activity, non-enzymatic lipid peroxidation inhibitory activity, superoxide scavenging activity, and anti-ulcerogenic activity.<sup>150,151</sup> Other recent investigations revealed an inhibition of the formation of advanced glycation end-products (AGEs) by the dichloromethane and methanol extracts from *Calophyllum flavoramulum*, both of them containing amentoflavone as a main constituent. The anti-glycation activity could be explained through various mechanisms such as radical scavenging, chelation of divalent metal ions, as well as catching dicarbonyl species.<sup>52</sup> Moreover, a study by Zhang *et al.* reported that amentoflavone stimulated apoptosis in hypertrophic scar fibroblasts (HSFBs) and inhibited angiogenesis by endothelial cells.<sup>152</sup> Also 7,7'-dimethoxyagastiflavone isolated from *Taxus x media* cv. Hicksii has displayed several important activities, namely, antiproliferative and antineoplastic effect in three human cancer cell lines: HT-29 human colon cancer cells, A549 human lung cancer cells, and HepG2 human hepatoma cells.<sup>153</sup>

Within the group of the flavonoids, biflavones are characteristic constituents of some species from the Gymnospermae (to which *G. biloba* belongs), while flavones, catechins and procyanidins are present also in other medicinal plants.<sup>141</sup> The main biflavonoids in *Ginkgo biloba* are bilobetin, ginkgetin, isoginkgetin and sciadopitysin. Other minor constituents are amentoflavone and 7-O-methylamentoflavone (sequoiaflavone) (Figure 3.35, page 104).<sup>151</sup>

The majority of naturally occurring biflavonoids are dimers of flavone and flavanone, linked by a C-O-C bond (e.g. hinokiflavone) or C-C bond (e.g. amentoflavone).<sup>149,154</sup> The constituent monomers may be of the same or of different types, i.e. flavone-flavone, flavone-flavanone or flavanone-flavanone. For instance, amentoflavone is a biapigenin derivative linked in positions C-3'/C-8". Also, one or more of the hydroxyl groups present may be methylated. Biflavonoids can be classified based on their interflavonoid linkage and basic flavone structure.

## 4.2 Materials and Methods

### 4.2.1 Plant material

In October 2017, *Ginkgo biloba* decanter sludge (PSC0148/501396080/B/EXCh.116-2) was provided by Dr. Willmar Schwabe GmbH & Co.KG, Karlsruhe Germany. During the production process of EGb 761, water-insoluble compounds are eliminated from the 60% primary acetone extract and the remaining so-called sludge, normally, contains at least a large portion of the biflavonoids.<sup>155</sup>

### 4.2.2 Extraction, fractionation and isolation of biflavonoids

The solubility of any individual biflavonoid depends very much on its structure, especially the degree of methylation. Therefore, the more highly hydroxylated compounds (e.g. amentoflavone) are more completely extracted with acetone, absolute or aqueous methanol or ethanol. Crystallization is the most common method for isolation of biflavonoids.<sup>156</sup> Figure 3.31 shows the extraction process for the production of EGb 761. According to the scientific and patent literature, the dry leaves of *Ginkgo biloba* are exhaustively extracted by maceration with an acetone : water mixture (60:40) for 24 h at 50 °C with stirring. The proportion between the leaves and the solvent mixture is 1:10. The final extract is further concentrated by means of rotary evaporation. The remaining aqueous / acetone extract is submitted to liquid-liquid partition with *n*-hexane in order to remove the inactive lipophilic substances such as chlorophyll, hazardous ginkgolic acids, polyprenols, aliphatic alcohols, free and esterified sterols. However, the ginkgolides and bilobalides, whose presence is desired in the end product, are not extracted with *n*-hexane, despite that they are also relatively lipophilic substances. The defatted aqueous / acetone solution is concentrated, kept in a refrigerator for 24 h at a temperature of about 2 °C, and then centrifuged. The precipitate or sludge, which is separated by centrifugation, comprises a mixture of biflavonoids, and it is used in the present investigation.

The remaining water phase is extracted with a toluene : *n*-butanol mixture (1:4) in order to obtain all the active principles but also the tannins. The water phase is concentrated under vacuum at a temperature not higher than 40 °C. The residue then is dissolved

in 70% aqueous ethanol, in order to remove the tannins, filtrated, concentrated and dried.<sup>157</sup>

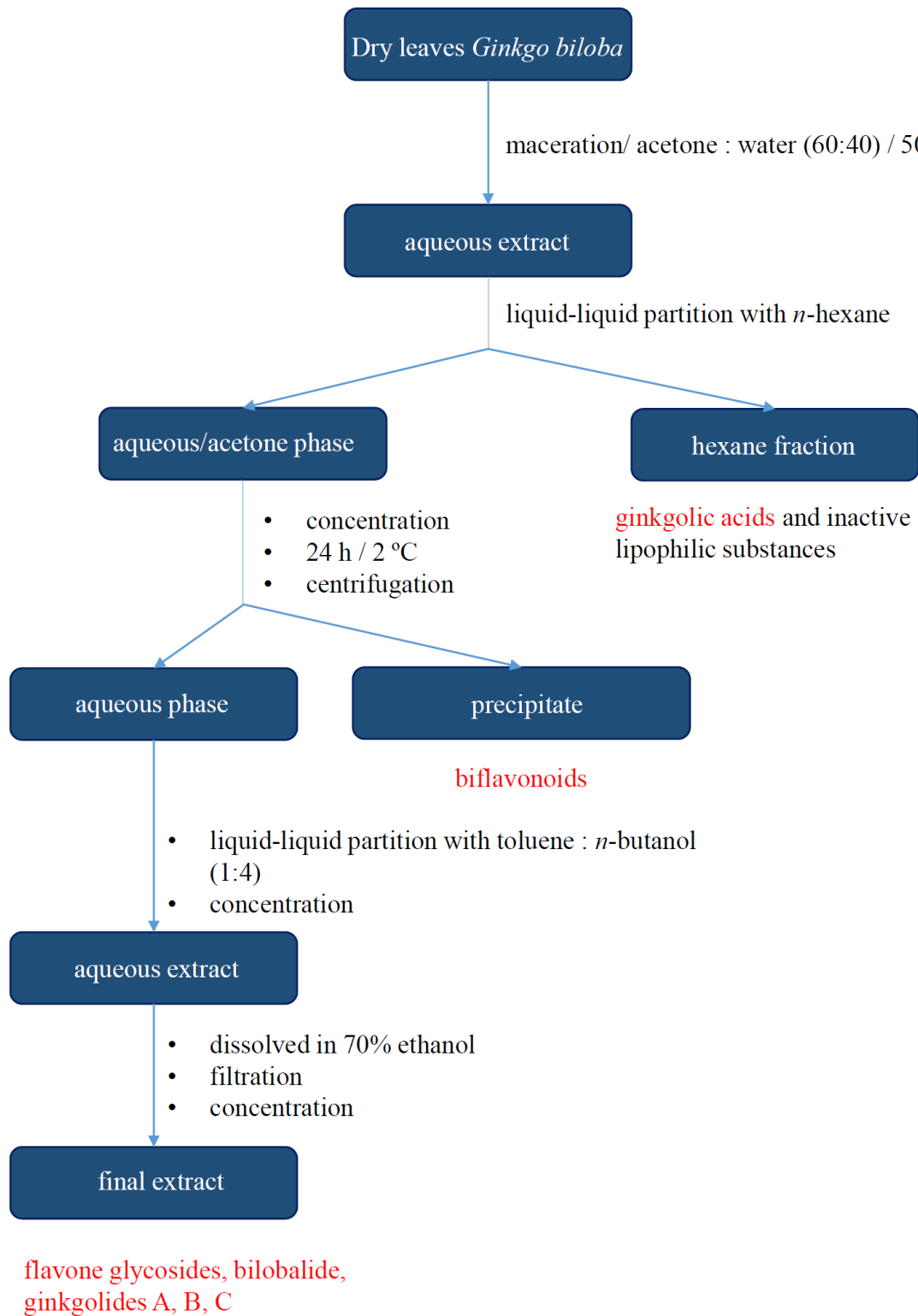


Figure 3.31. General extraction scheme for obtaining *Ginkgo biloba* extract (EGb 761).

The *Ginkgo biloba* sludge was fractionated on a Diaion HP-20 column after dry loading of the sample (firstly, 40 g dissolved in methanol and then absorbed on a small portion Diaion). The ratio between sample and amount of sorbent was approximately 1:15. The chromatographic elution was performed with solvents of decreasing polarity: starting with pure water; 40%, 50%, 60%, 70%, 80%, 90% and 95% aqueous methanol, pure methanol; 10%, 20%, 30%, 40%, 50% and 70% ethyl acetate in methanol and pure ethyl acetate. One liter of each solvent was used, except 95% aqueous methanol, pure methanol and 50% ethyl acetate in methanol, where two liters of each were applied. Fractions of 100 ml were collected. In the end, the eluates were evaporated under reduced pressure. After TLC and HPLC analysis they were combined to a total of twenty fractions.

The mobile phase for TLC analysis consisted of toluene : ethyl formate : formic acid (5:4:1) and as a spraying reagent ferric chloride ( $\text{FeCl}_3$ ) 2% ethanol solution was used.<sup>150,156</sup> The fully methylated compounds give characteristic blue, blue-green, yellow-green fluorescence under UV light.

In order to establish the optimal HPLC conditions, different columns were tested: Kinetex EVO C18, GraceSmart RP 18 and Luna C18. The mobile phase included as eluent A water with 0.1% trifluoroacetic acid, and as eluent B acetonitrile. Then, a gradient elution was performed: the starting conditions till 5 minutes were 38% eluent B; in 40 min solvent B increased from 38% to 100%; then, the percentage was kept constant for 5 min; at the end, the initial conditions were restored in 5 min. Equilibration time between the injections was 5 min.<sup>151</sup> The test samples (extracts or pure compounds) were prepared in methanol.<sup>158</sup> A flow rate of 1 ml/min was applied and the injection volume was 20  $\mu\text{l}$ . Detection was carried out at 330 nm.<sup>151</sup> In the end, the optimal separation was achieved by the Kinetex column and it was used for further analyses.

Based on the HPLC analysis, three fractions collected after the Diaion open column were directly submitted to semi-preparative HPLC (Waters) for the isolation of pure compounds on a Kinetex C18 column (250 mm x 10.0 mm, 5  $\mu\text{m}$ ). Regarding the mobile phase, eluent A was water with 0.1% formic acid, and eluent B – acetonitrile with 0.1% formic acid.<sup>159</sup> The optimal gradient for the different fractions was optimized at first on analytical scale.

Other fractions (three in total) were firstly submitted to flash chromatography where the conditions for the extracts were based on the method proposed by D'Arc Felicio *et*

*al.*<sup>160</sup> A gradient elution on a Grace Reveleris C<sub>18</sub> cartridge (40 g, particle size of 40 µm) was performed by applying as eluting solvents toluene, ethyl acetate and methanol.

#### 4.2.3 LC-MS analysis

The molecular weight of the isolated compounds after semi-preparative HPLC was confirmed by MS data from a triple quadrupole detector (TQD) operating in full scan mode. For the analysis, 5 µl of pure compounds were injected on an Acquity UPLC BEH C18 column (100 mm x 2.1 mm, 1.7 µm) (Waters) and gradient elution was applied (min/%B): 0.0/30, 0.68/30, 5.44/100, 6.12/100, 6.80/30, 7.48/30. The mobile phase solvents consisted of 0.1% formic acid in water and acetonitrile. The flow rate was 0.4 ml/min and the column temperature was 40 °C. Additionally, other parameters were optimized by using commercially available amentoflavone (≥ 99%, Extrasynthese, Genay, France) as a standard: capillary voltage 3.5 kV, cone voltage 40 V, source temperature 120 °C, desolvation temperature 550 °C; the cone gas flow was 50 L/h and the desolvation gas flow was 1000 L/h.

#### 4.4 Results and discussion

From the twenty fractions collected after open column (Diaion) separation of the sludge (Figure 3.32), three were further fractionated on semi-preparative HPLC (fractions G – 231 mg, H – 189 mg and J – 1.12 g); and three (K – 1.81 g, L – 7 g, N – 983 mg) were firstly submitted on automated flash chromatography, which was followed by semi-preparative HPLC isolation and purification.



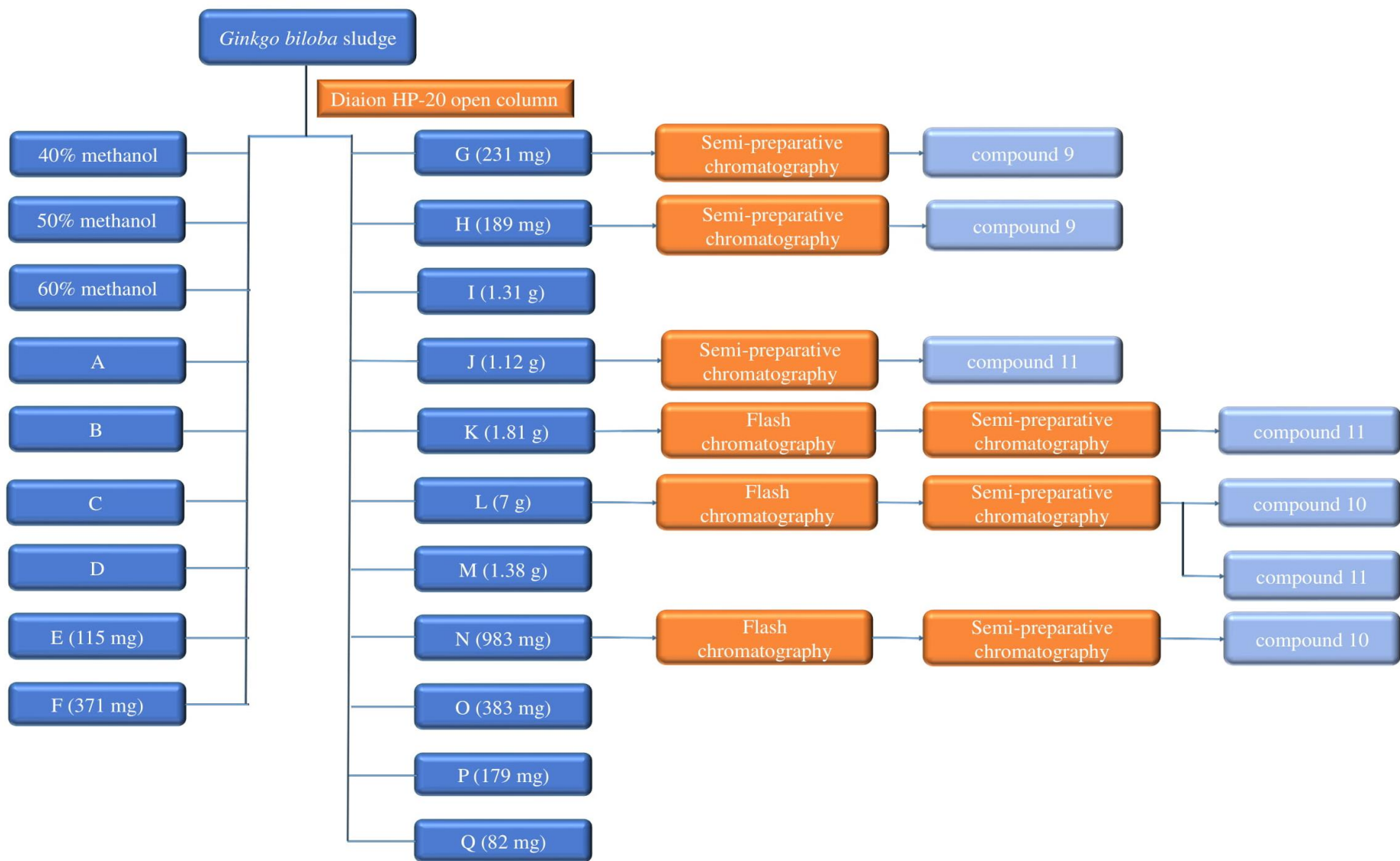


Figure 3.32. Fractionation scheme and isolated compounds from *Ginkgo biloba* sludge.

Finally, two biflavonoids and a mixture of two isomers were isolated. The compounds were identified through comparison of their mass spectrometric and  $^1\text{H-NMR}$  data in the literature (Figure 3.33). Due to their relatively low amount, other 1D- and 2D-spectra were not obtained.

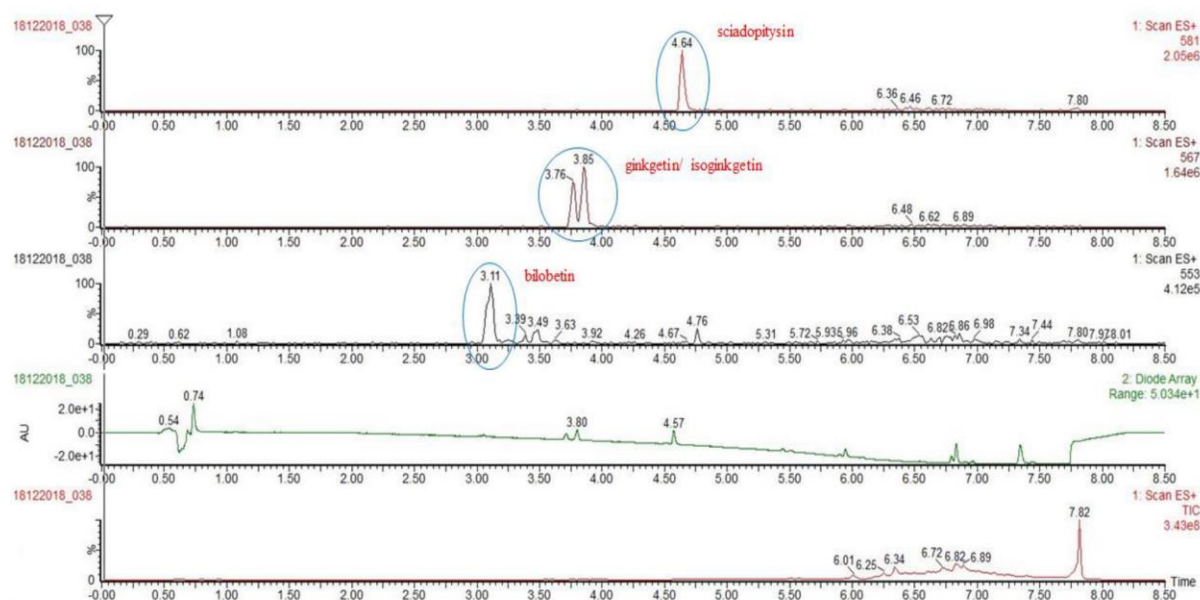


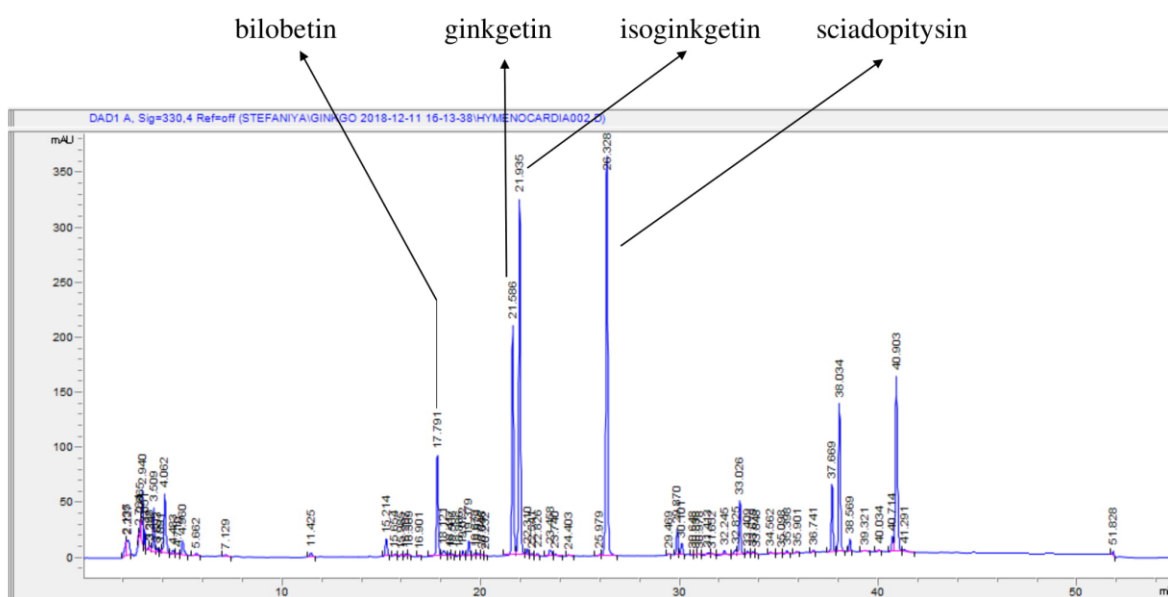
Figure 3.33. Chromatographic elution and MS data of isolated compounds from the *Ginkgo biloba* sludge.

For all compounds a flavone skeleton was identified by the characteristic MS data and the aromatic signals from the  $^1\text{H-NMR}$  spectra. The  $^1\text{H-NMR}$  spectrum (Figure 3.36) of **compound 9** revealed an AMX coupling system with signals at  $\delta$  7.97 (d,  $J = 2.3$  Hz),  $\delta$  8.11 (dd,  $J = 8.9, 2.3$  Hz), and  $\delta$  7.35 (d,  $J = 8.9$  Hz), which is in agreement with 3'-C as a linkage site. The two *meta*-coupled protons at  $\delta$  6.41 and  $\delta$  6.17 (each d,  $J = 2.1$  Hz), and the AA'XX' system with signals at  $\delta$  7.47 and  $\delta$  6.72 (each d,  $J = 8.9$  Hz) excluded the possibility of a linkage between the two flavone moieties at C-6, C-8, C-3'', C-5'', C-2'' and C-6''. Moreover, from the  $^1\text{H-NMR}$  multiplicities of the signals at  $\delta$  7.47 and  $\delta$  6.72 (both d,  $J = 8.9$  Hz), which were part of the AA'XX' system, a 1,4-*para*-disubstituted B'-ring was deduced for the second moiety. One substituent was identified as a hydroxyl group by the singlet signal at  $\delta$  8.54. The ESI-MS spectrum of **compound 9** revealed a pseudo-molecular ion at  $m/z$  553  $[\text{M}+\text{H}]^+$ . Based on the MS data and the signals from the  $^1\text{H-NMR}$  experiment, the structure of **compound 9** was elucidated by comparison with literature data (Table 3.4) and identified as **bilobetin**.<sup>161</sup>

The general structure of **compound 10** was similar to the previously described biflavonoid ( $^1\text{H-NMR}$  spectrum, Figure 3.37). In particular, a doublet of doublets at  $\delta$  8.30 ( $J = 8.8, 2.5$  Hz), a doublet at  $\delta$  8.10 ( $J = 2.5$  Hz) and a doublet at  $\delta$  7.40 ( $J = 8.8$  Hz) were assigned as part of an AMX system in ring B. Moreover, the doublets at  $\delta$  7.60 ( $J = 9.0$  Hz) and 7.0 ( $J = 9.0$  Hz) were characteristic for an AA'XX' spin system of a *para*-substituted B'-ring. Three singlets at  $\delta$  13.12,  $\delta$  12.98 and  $\delta$  10.95 were assigned as hydroxyl groups and three singlets at  $\delta$  3.89,  $\delta$  3.86 and  $\delta$  3.81 had integration 3, confirming the presence of three methoxy groups in the structure. The ESI-MS spectrum of compound 10 revealed a pseudo-molecular ion at  $m/z$  581  $[\text{M}+\text{H}]^+$ . Based on the MS data and the signals from the  $^1\text{H-NMR}$  experiment, the structure of compound 10 was elucidated by comparison with literature data as **sciadopitysin** (Table 3.4).<sup>143</sup>

The distinctive  $^1\text{H-NMR}$  signals of **compound 11** confirmed the structure of a biflavonoid (Figure 3.38). The presence of an AMX system was deduced from the signals at  $\delta$  8.08 (dd,  $J = 8.7, 2.3$  Hz),  $\delta$  7.95 (d,  $J = 2.3$  Hz) and  $\delta$  7.31 (d,  $J = 8.7$  Hz); and the AA'XX' system was shown by the signals at  $\delta$  7.50 and  $\delta$  6.80 (both d,  $J = 8.9$ ). Two singlets at  $\delta$  3.81 and  $\delta$  3.77 had an integration value of 3, which revealed the existence of two methoxy groups in the structure. The ESI-MS spectrum of compound 11 showed a pseudo-molecular ion at  $m/z$  567  $[\text{M}+\text{H}]^+$ , which based on literature data, could be either **ginkgetin** or **isoginkgetin**.<sup>143</sup> The amount of the isolated compound was not sufficient to carry out further experiments for the complete elucidation of the structure. Additionally, a larger amount of a compound with a pseudo-molecular ion at  $m/z$  567 was isolated through semi-preparative HPLC. However, it was found to be a mixture of ginkgetin and isoginkgetin that could not be separated.

In conclusion, the isolated compounds from *Ginkgo biloba* sludge were identified as bilobetin (**compound 9**) and sciadopitysin (**compound 10**); and the mixture contained the two isomers ginkgetin and isoginkgetin (**compound 11**). An overview of the isolated compounds from the *Ginkgo biloba* sludge is presented in the HPLC chromatogram (UV 330 nm) in Figure 3.34.



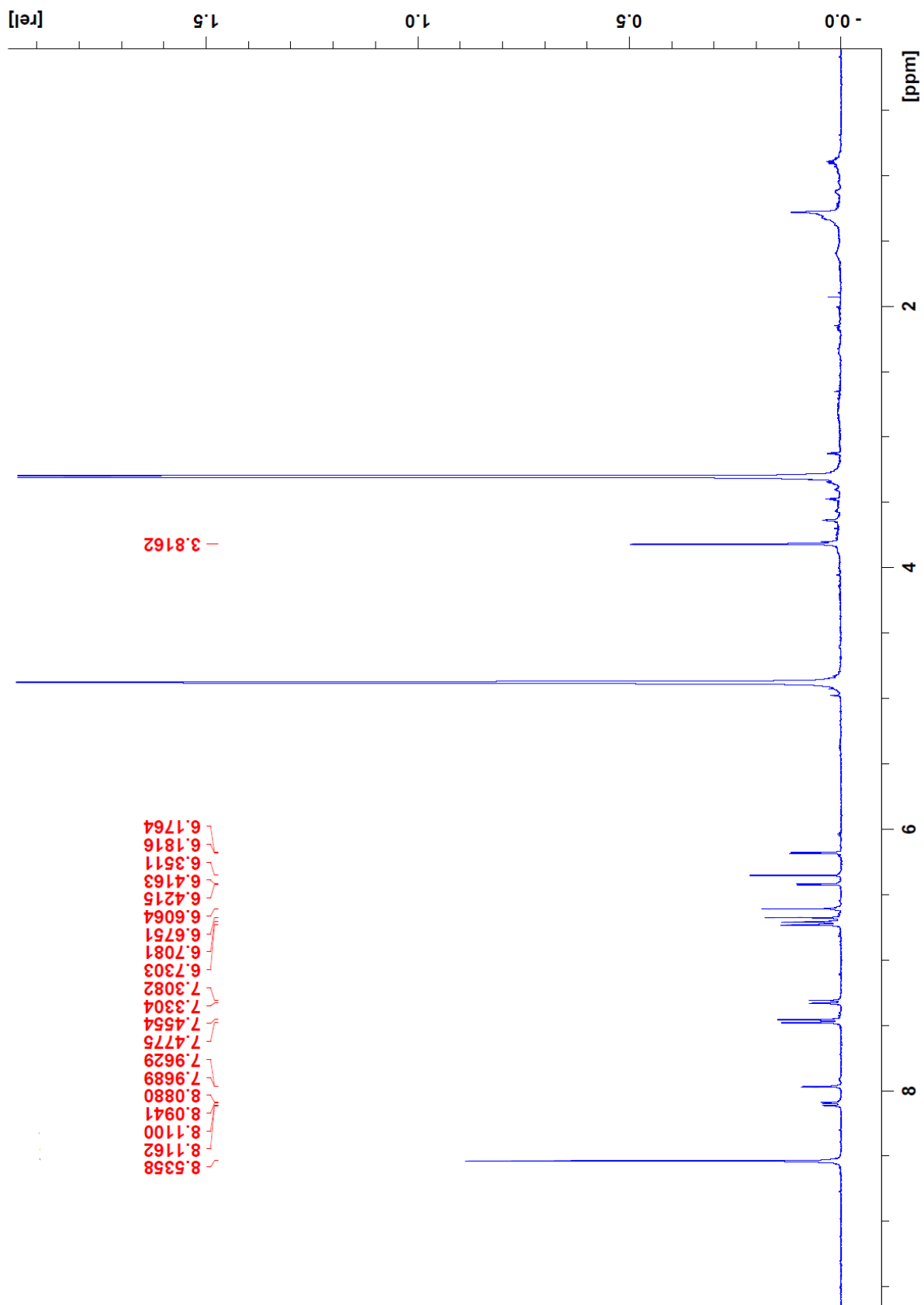


Figure 3.36.  $^1\text{H-NMR}$  spectrum (400 MHz,  $\text{methanol-d}_4$ ) of **compound 9** (bilobetin).

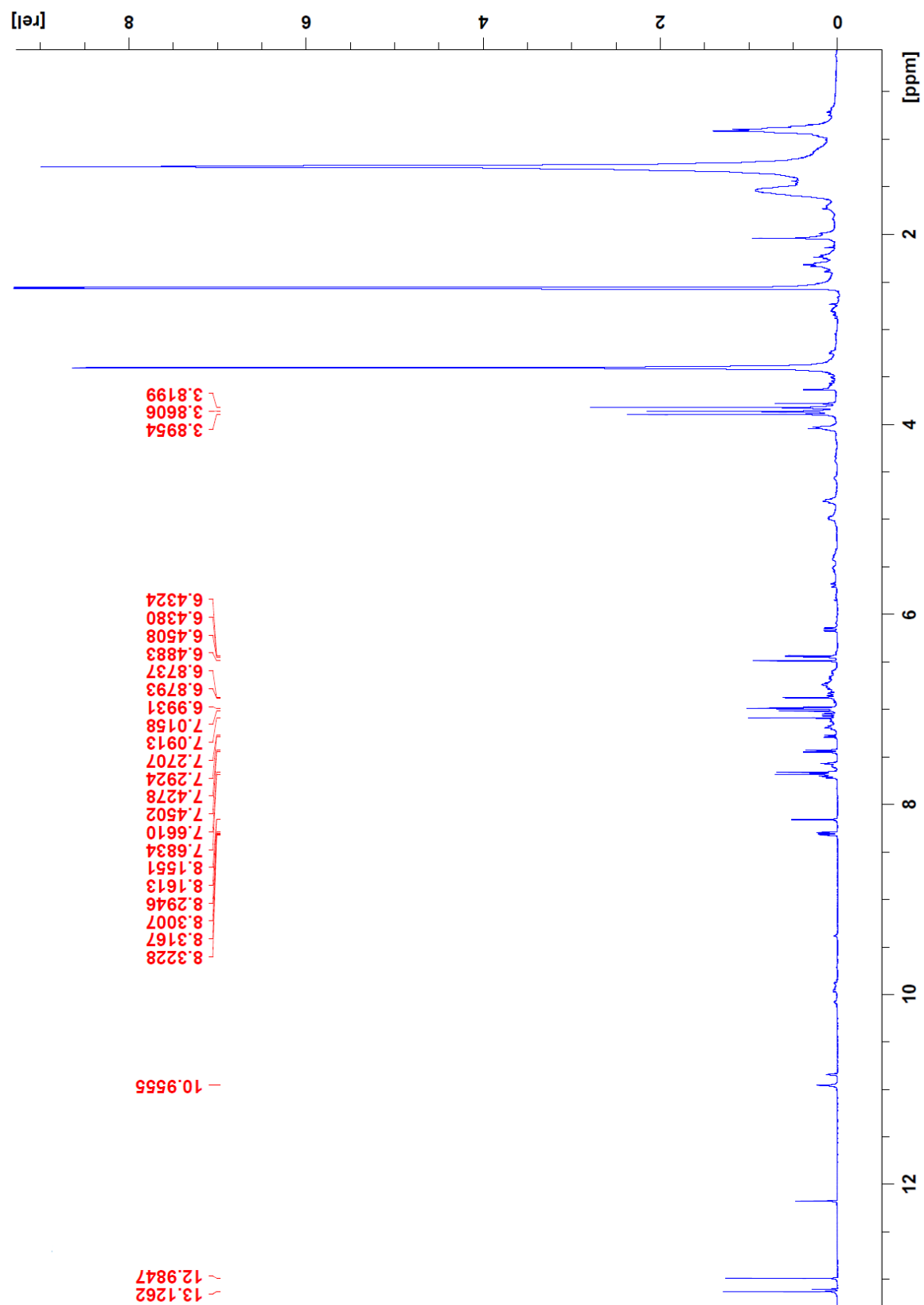


Figure 3.37.  $^1\text{H-NMR}$  spectrum (400 MHz, dimethyl sulfoxide- $d_6$ ) **compound 10** (sciadopitysin).

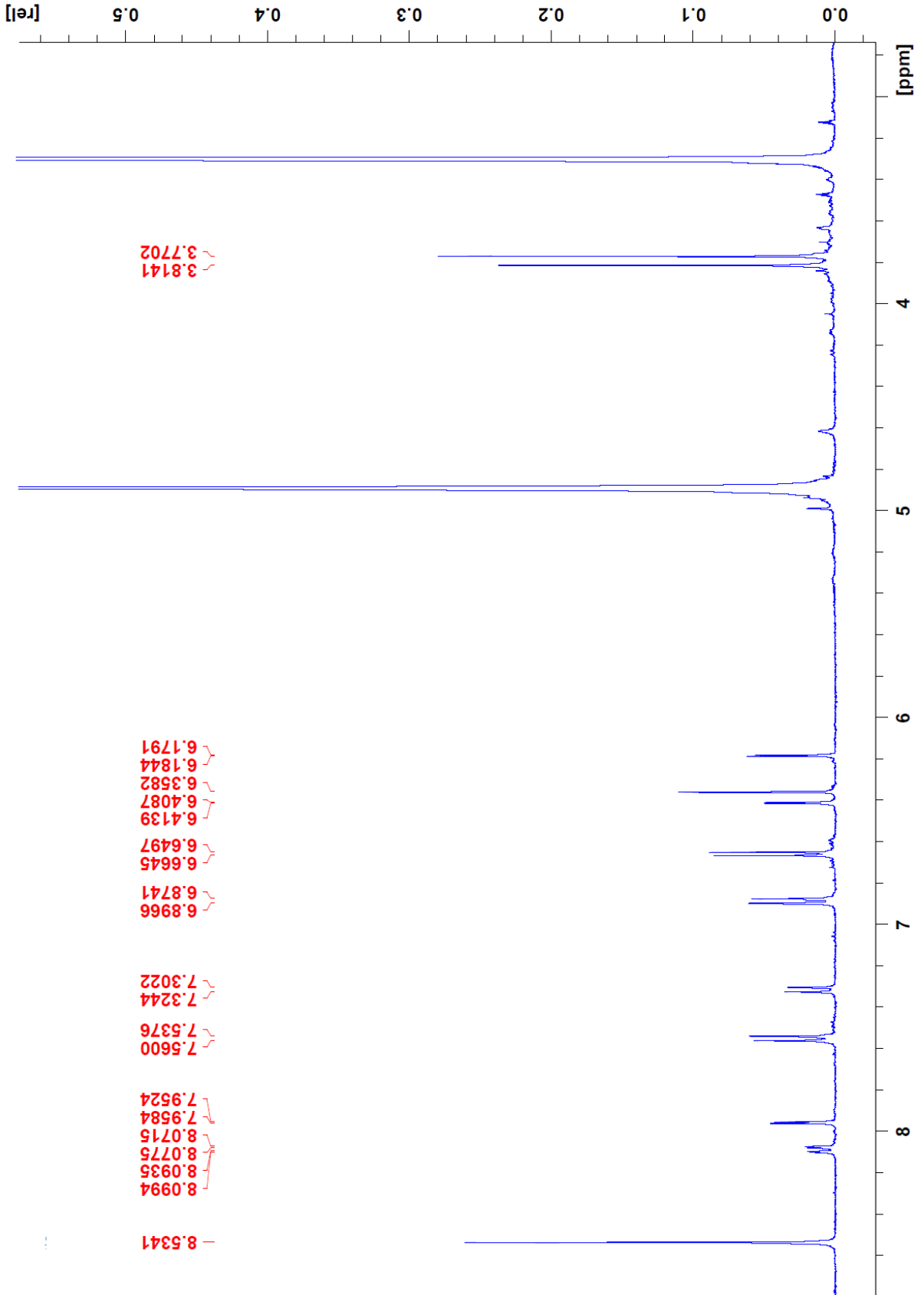


Figure 3.38.  $^1\text{H}$ -NMR spectrum (400 MHz, methanol- $d_4$ ) of **compound 11** (ginkgetin/ isoginkgetin).

	<b>Compound 9</b>	<b>Compound 10</b>	<b>Compound 11</b>
<b>H-3</b>	6.6 s	7.97 s	6.40 s
<b>H-6</b>	6.41 (d, $J = 2.1$ )	7.87 (d, $J = 2.2$ )	6.40 (d, $J = 2.1$ )
<b>H-8</b>	6.17 (d, $J = 2.1$ )	6.43 (d, $J = 2.2$ )	6.17 (d, $J = 2.1$ )
<b>H-2'</b>	7.97 (d, $J = 2.3$ )	8.10 (d, $J = 2.5$ )	7.95 (d, $J = 2.3$ )
<b>H-5'</b>	7.35 (d, $J = 8.9$ )	7.40 (d, $J = 8.8$ )	7.31 (d, $J = 8.7$ )
<b>H-6'</b>	8.11 (dd, $J = 8.9, 2.3$ )	8.30 (dd, $J = 8.8, 2.5$ )	8.08 (dd, $J = 8.7, 2.3$ )
<b>H-3''</b>	6.67 s	6.98 s	6.66 s
<b>H-6''</b>	6.35 s	6.48 s	6.30 s
<b>H-2'''</b>	7.47 (d, $J = 8.9$ )	7.60 (d, $J = 9.0$ )	7.50 (d, $J = 8.9$ )
<b>H-3'''</b>	6.72 (d, $J = 8.9$ )	7.0 (d, $J = 9.0$ )	6.88 (d, $J = 8.9$ )
<b>H-5'''</b>	6.72 (d, $J = 8.9$ )	7.0 (d, $J = 9.0$ )	6.88 (d, $J = 8.9$ )
<b>H-6'''</b>	7.47 (d, $J = 8.9$ )	7.60 (d, $J = 9.0$ )	7.50 (d, $J = 8.9$ )
<b>OCH<sub>3</sub></b>	3.81	3.89 3.86 3.81	3.81 3.77

Table 3.4. <sup>1</sup>H-NMR assignments of the isolated compounds from *Ginkgo biloba* (where  $J$  is in Hz).



## 5. Isolation and identification of pyrroquinazoline alkaloids from *Adhatoda vasica*

### 5.1 Introduction

#### 5.1.1 Plant description

*Adhatoda vasica* Nees./ *Justicia adhatoda* L. (Acanthaceae) is an evergreen dense



Figure 3.39. *Adhatoda vasica* plant.<sup>266</sup>

bush distributed all over the plains of India and in the lower Himalayan ranges, reaching a height of 1-2.5 m high with opposite ascending branches. It grows throughout the Indian peninsula up to an altitude of 1300 m. The leaves (Figure 3.39) are simple, opposite, 7-19 cm long and 4-7 cm wide. The flowers are white, pink or purple. It has capsular four seeded fruits. In Ayurveda, the mature leaves, flowers, roots and the bark of the plant are used.<sup>162</sup>

#### 5.1.2 Traditional medicine

*Adhatoda vasica* Nees. / *Justicia adhatoda* L., also known as Asuro in Nepalese and Malabar nut in English, is found in the tropical regions of Southeast Asia. Since centuries, it has been widely used in Ayurveda (a Hindu traditional health theory from India) and Unani (the Arabian medicine) for the treatment of respiratory diseases, such as asthma, allergen-induced bronchial obstruction, diseases related to the female reproductive system, and tuberculosis.<sup>163,164</sup> Moreover, it is considered as a natural source of vitamin C.

### 5.1.3 Pharmacological activity

So far, it has been reported that vasicine (Figure 3.41, page 112), the major quinazoline alkaloid in *Adhatoda vasica*, is responsible for the most prominent pharmacological properties of the plant, namely, its antioxidant, anti-inflammatory and bronchodilatory activities.<sup>163</sup> The **antioxidant** and **anti-inflammatory** activities can be explained by its effects on superoxide dismutase, catalase, glutathione peroxidase (GPs) and GSH, and also on lipid peroxidation (LPO). More specifically, the level of GSH was found to be increased and LPO to be decreased.<sup>163,165,166</sup> In addition, **antidiabetic** and **antibacterial** activity of various extracts of *Adhatoda vasica* has also been investigated.<sup>163</sup> Moreover, the **hepatoprotective** effect reported for *Adhatoda* extracts is based on its antioxidant properties.<sup>163</sup> The traditional application of *Adhatoda* in respiratory disorders has been the base for researchers to synthesize molecules similar to or derivatives of vasicine, which have been investigated for their **bronchodilatory** and **antitussive effects**. An example of such a molecule is bromhexine (Figure 3.40) which has been reported for its mucus liquifying and expectorant activities. The observed effects in clinical trials were fewer bronchial aspirations, less fluid secretion, and a reduced increase in total mucus. Ambroxol (Figure 3.40), a widely used secretolytic agent developed from vasicine, was found to inhibit the IgE-dependent mediator secretion from human mast cells and basophils, which are the main effector cells of allergic inflammation.<sup>167</sup> Also, significant attenuation of basophil IL-4 and IL-13 secretions was observed.<sup>163</sup>

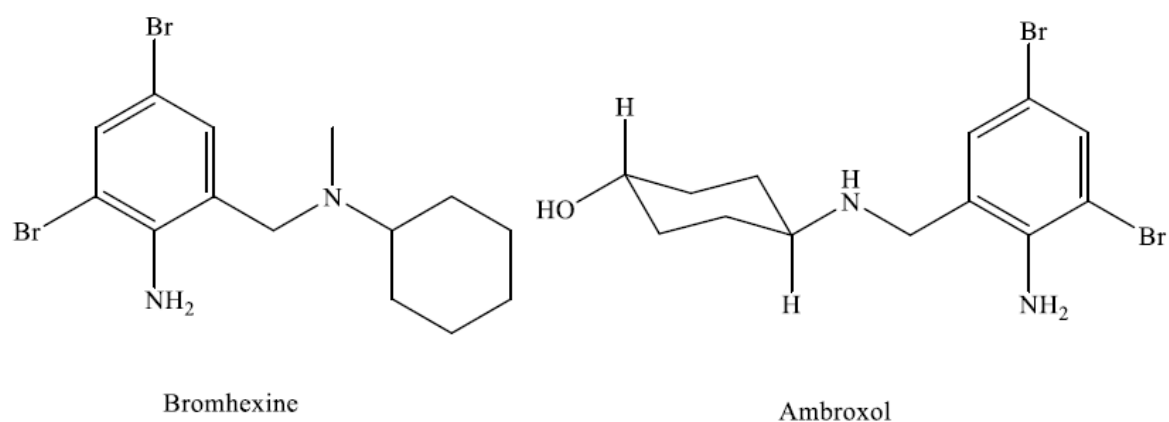


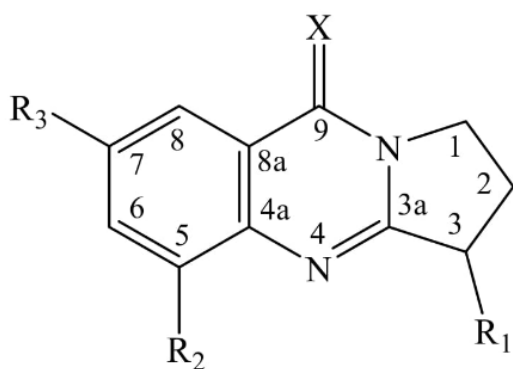
Figure 3.40. Chemical structure of bromhexine and ambroxol.<sup>167</sup>

Moreover, the **uterotonic activity** of vasicine was proven to be similar to methergine and oxytocin, and the mechanism of action was based on the release of prostaglandins. In animal models and human beings, vasicine has been reported for its abortive and oxytocin potentiating effects, to inhibit implantation of the foetus, and for effectively controlling post-partum haemorrhage.<sup>162,163</sup> After these discoveries and due to the fact that there is a great need for new drugs for fertility regulation, World Health Organization (WHO) has included the herb in a research program for human reproduction.<sup>162</sup> Gao *et al.* highlighted the role of vasicine as irreversible inhibitor of sucrose metabolism, which can **reduce glucose levels** by inhibiting the conversion of sucrose to glucose and fructose in the intestinal track.<sup>168</sup>

Interestingly, vasicinone, an autoxidation product of vasicine, can possess opposite pharmacological effects than vasicine. For example, although it has been confirmed that vasicine may cause bronchodilation and vasicinone bronchoconstriction *in vitro*, the two alkaloids in combination showed a bronchodilatory activity both *in vitro* and *in vivo*. The mechanism of action is explained by the similarity in their structures, as a result, acting through the same receptors and also being metabolized by the same enzymes. However, studies have suggested that low concentrations of vasicine induced bronchodilation and relaxation of the tracheal muscles *in vitro* and *in vivo*; and higher concentrations of vasicine offered significant protection against histamine-induced bronchospasms in guinea pigs.<sup>162,164</sup>

#### 5.1.4 Quinazoline alkaloids

Quinazoline alkaloids are rather abundant in nature and *Adhatoda vasica* is the richest source.<sup>169</sup> Das *et al.* have estimated the content of the main quinazoline alkaloids present in *Adhatoda* leaves (Table 3.5), namely, vasicine and vasicinone, to be 0.65 % dry weight and 0.047 % dry weight, respectively.<sup>100</sup> Pyrroquinazoline alkaloids, such as vasicine, deoxyvasicine and vasicinone, are a small group of secondary natural compounds that have a quinazolinone ring fused with a pyrrole ring system (Figure 3.41).



<b>Compound</b>	<b>X</b>	<b>R1</b>	<b>R2</b>	<b>R3</b>
<b>vasicine</b>	H <sub>2</sub>	OH	H	H
<b>vasicinol</b>	H <sub>2</sub>	OH	H	OH
<b>5-hydroxy vasicine</b>	H <sub>2</sub>	OH	OH	H
<b>5-methoxyvasicinol</b>	H <sub>2</sub>	OH	OCH <sub>3</sub>	OH
<b>deoxyvasicine</b>	H <sub>2</sub>	H	H	H
<b>vasicine acetate</b>	H <sub>2</sub>	OCOCH <sub>3</sub>	H	H
<b>5-methoxyvasicine</b>	H <sub>2</sub>	OH	OCH <sub>3</sub>	H
<b>vasicinolone</b>	O	OH	H	OH
<b>vasicinone</b>	O	OH	H	H

Figure 3.41. Chemical structures of known and isolated pyroquinazoline quinazoline alkaloids from *Adhatoda* species.

Vasicine (1,2,3,9-tetrahydropyrrole-[2,1-b] quinoxalin-3-ol) is a pyroquinazoline type alkaloid mainly obtained from the leaves of *Adhatoda vasica*. The compound is present in leaves, roots and flowers, and in physiological conditions it can be converted to vasicinone by oxidation. Other chemical constituents of this plant are vasicinone (leaves, stem, roots), vasicinol (stem and roots) and deoxyvasicinone (leaves). Vasicine is an optically active molecule in its natural condition but experiences racemization during the extraction process.<sup>163</sup>

## 5.2 Materials and Methods

### 5.2.1 Plant material

For the purpose of the phytochemical investigation, the mature leaves were collected in the mountain region of Eastern Nepal and identified by dr. D. Subba (Tribhuvan

University, Nepal). Subsequently, the leaves were air dried and transferred to the University of Antwerp.

### 5.2.2 Extraction, fractionation and isolation of quinazoline alkaloids

The choice for the extraction procedure tightly depends on the chemical characteristics of the molecules of interest. Namely, vasicine possesses a secondary amine group which makes the molecule alkaline. This facilitated the isolation and purification, since water-soluble salts can be formed in the presence of acids. It is worth to mention that the whole extraction procedure was carried out in dark due to the sensitivity of the alkaloids when exposed to light.<sup>170</sup> The dried leaves of *Adhatoda vasica* were ground with an IKA MF 10 mill which was equipped with a sieve of 1 mm. In the end, 700 g of powder was obtained. Subsequently, 500 g of the powder was extracted with 2 liters absolute ethanol by maceration at room temperature for 24 h, using a magnetic stirrer.<sup>169</sup> The extraction was repeated six times. Afterwards, the extract was further vacuum filtered, using filter paper Whatman 40 and the solvent was removed by a rotary evaporator at 40 °C under reduced pressure. The final amount of total extract was around 30 g. Further on, the ethanol extract was dissolved in one liter of water and the pH was adjusted with 0.2 M hydrochloric acid until it was less than 3. Litmus paper was used to monitor the changes in pH. The acidified water extract was transferred into a separation funnel where liquid-liquid extraction was performed by adding an equal amount of dichloromethane to the water phase. The extraction was repeated four times till the colour of the dichloromethane layer faded. The latter was expected to contain all the neutral compounds, while the alkaloids remained in the water phase. Afterwards, the acidified water solution was brought up to pH higher than 9 by the mean of 0.1 M sodium hydroxide solution. Then, a liquid-liquid extraction with dichloromethane was performed in order to collect the alkaloid fraction. The extract obtained after the entire extraction process (Figure 3.42) was dried under vacuum at 40 °C.

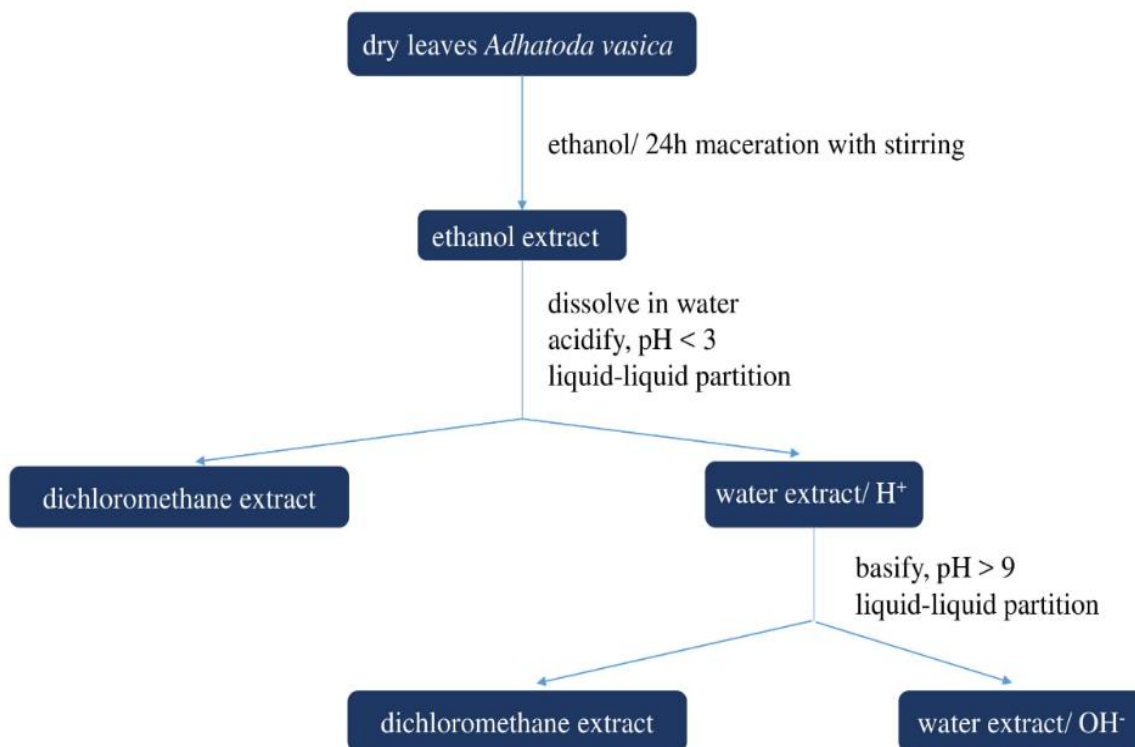


Figure 3.42. General extraction scheme of *Adhatoda vasica*.

TLC was performed on Merck TLC plates (silica gel 60 F<sub>254</sub>, 20 x 20 cm). Each solution was applied with a capillary tube and the solvent system chloroform : methanol : ethyl acetate (75:15:10 v/v/v) was used. The developed plates were dried and sprayed with several visualizing reagents, such as Dragendorff, iodoplatinate and ninhydrin solutions. However, the most clear result was achieved with the iodoplatinate reagent. The developed TLC plates were observed in visible light after heating.

The HPLC conditions were optimized on a Luna C18 column (250 x 4.6 mm, 5 µm) and a Kinetex EVO C18 (250 x 4.6 mm, 5 µm) column. Different buffers with various pH were tested (between 2.5 and 6.8). Consequently, a mobile phase - water with 0.1% formic acid (eluent A, pH around 2.7) and acetonitrile (eluent B) in gradient elution (min /%B): 0.0/ 10, 12.0/ 10, 17.0/ 50, 22.0/ 50, 25.0/ 10, was used.<sup>169</sup> The flow was kept at 0.7 ml/min and the injection volume was 20 µl. The detection was performed at 285 nm.

After preliminary observations, the conditions for isolating pyrroquinazoline alkaloids through semi-preparative HPLC included: a Kinetex C18 column (250 mm x 10.0 mm, 5 µm), gradient elution and a mobile phase water with 0.1% formic acid (A), and

acetonitrile (min/ %B): 0.0/ 5, 11.0/ 5, 16.0/ 50, 20.00/ 50, 23.0/ 5. The flow rate was 3 ml/min and the injection volume was 200  $\mu$ l. The UV detection was set at 285 nm. The samples were prepared at a concentration of 10 mg/ml in acetonitrile 50%. A full scan in positive ionization mode ranging from  $m/z$  200 to 800 was applied and fraction collection was done for peaks with  $m/z$  171  $[M+H]^+$  (**compound 12**) and  $m/z$  201  $[M+H]^+$  (**compound 13**).

### 5.2.3 Structure elucidation

The isolated pure compounds were dissolved in methanol- $d_4$  for NMR analysis because it has been reported that in chloroform- $d$ , due to their instability, a mixture of L- and D-isomers could be formed.<sup>171</sup> Studies have been carried out to investigate the degradation of vasicine in various solvents under normal laboratory light conditions. It has been observed that in non-polar solvents not only vasicine but also its benzene-substituted analogues were oxidized by direct sunlight to the corresponding vasicinone analogues.<sup>172</sup>

## 5.4 Results and discussion

The HPLC chromatogram of the alkaloid fraction from the leaves extract of *Adhatoda vasica* is presented in Figure 3.43:

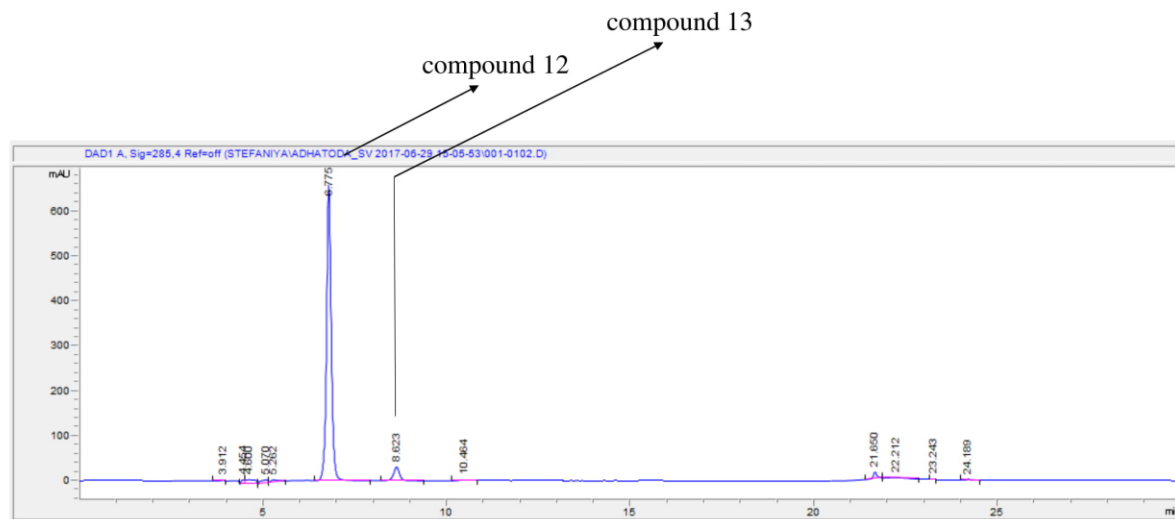


Figure 3.43. HPLC chromatogram (UV 285 nm) of the alkaloid fraction in *Adhatoda vasica* leaves extract.

After successive fractionation, two pyrroquinazoline alkaloids were isolated from the *Adhatoda vasica* leaves extract and their structure was elucidated by 1D- ( $^1\text{H-NMR}$ ,  $^{13}\text{C-NMR}$ , DEPT-135, DEPT-90) and 2D- (COSY) NMR experiments. Also, the structure of the compounds was confirmed by MODGRAPH NMRPredict. Table 3.5 gives the  $^1\text{H}$ - and  $^{13}\text{C}$ -NMR chemical shift assignments of **compounds 12** and **13**.

The  $^1\text{H-NMR}$  spectrum of **compound 12** revealed signals for four aromatic protons between  $\delta$  7.10 – 7.40; a one-proton triplet at  $\delta$  5.10; two proton multiplets at  $\delta$  3.75 and 3.70, and at  $\delta$  2.51 and 2.60; a two-proton singlet at  $\delta$  4.80; and finally, a singlet at  $\delta$  8.54 (Figure 3.45). Comparison of the  $^{13}\text{C-NMR}$  spectrum (Figure 3.46), DEPT-135 and DEPT-90 analysis (Figure 3.47) with literature data, suggested the structure of vasicine.<sup>171</sup> Due to correlations in the COSY experiment (Figure 3.48), the signals at  $\delta$  3.75 and 3.67 were assigned to H-1 $\alpha$  – and H-1 $\beta$ , respectively. Also, the multiplets at  $\delta$  2.12 and  $\delta$  2.64 were assigned to H-2 $\alpha$  – and H-2 $\beta$ , respectively. Correlations between the triplet at  $\delta$  5.10 and H-2 $\beta$  (COSY), as well as with the carbon at  $\delta$  72.4 (HSQC, Figure 3.49) and at  $\delta$  164.8 (HMBC, Figure 3.50), confirmed its assignment as H-3. The signals of the four aromatic protons ( $\delta$  7.14, 7.34, 7.24 and 7.19) was assigned to be H-5, H-6, H-7 and H-8, respectively, confirmed through correlations in the HSQC experiment and the characteristic correlations between C-7 and H-5, H-7 and C-8a. The position of the two-proton singlets at  $\delta$  4.83 and  $\delta$  4.78 was unambiguously established through correlations between C-9 and H-9 $\beta$  (HSQC), C-



8a and H-9 $\alpha$  (HMBC), and H-9 $\alpha$  and H-8 (COSY). The ESI-MS spectrum revealed a pseudo-molecular ion at  $m/z$  171 [M+H]<sup>+</sup>, and **compound 12** was assigned as **vasicine**. The reported optical rotation in literature for L-vasicine was:  $[\alpha]_D - 61.5^\circ$  (obtained in ethanol).<sup>171</sup>

The <sup>1</sup>H-NMR spectrum on Figure 3.51 shows a mixture of vasicine and **compound 13**. The four aromatic proton signals between  $\delta$  7.10 – 7.40 can be assigned to vasicine, which was also evident by overlaying the two spectra (Figure 3.52). However, the proton signals at  $\delta$  7.09 (d,  $J = 8.8$  Hz),  $\delta$  6.90 (dd,  $J = 8.8$  Hz,  $J = 2.7$  Hz) and at  $\delta$  6.77 (d,  $J = 2.7$  Hz), together with the size of their coupling constant, were characteristic for the presence of an ABX system in the aromatic region. In contrast to the spectrum of vasicine, a singlet was detected at  $\delta$  3.80, which had an integration of 3, suggesting the presence of a methoxy group. The <sup>1</sup>H-NMR spectrum (Figure 3.51) also showed a one-proton triplet at  $\delta$  5.05 and two one-proton multiplets around  $\delta$  3.70 and  $\delta$  2.50, a two-proton singlet at  $\delta$  4.80, a singlet at  $\delta$  8.54, similarly to the previously described spectrum of vasicine. Therefore, it could be deduced that the structure of **compound 13** was similar to vasicine, except for the presence of an additional methoxy group. The following correlations in an HSQC experiment (Figure 3.53) were used for verification:  $\delta_C$  120.1 and  $\delta_H$  7.09,  $\delta_C$  115.6 and  $\delta_H$  6.9,  $\delta_C$  113.1 and  $\delta_H$  6.7,  $\delta_C$  72.2 and  $\delta_H$  5.05 (5-position),  $\delta_C$  47.4 and  $\delta_H$  4.7 (9-position),  $\delta_C$  56.0 and  $\delta_H$  3.8 (methoxy group),  $\delta_C$  51.3 and  $\delta_H$  3.70/  $\delta$  3.6 (H-1 $\alpha$ /1 $\beta$ ) and  $\delta_C$  30.7 and  $\delta_H$  2.6/ 2.1 (H-2 $\alpha$ /2 $\beta$ ). In the HMBC experiment (Figure 3.54) strong correlations were observed between carbon signals at  $\delta$  126.2,  $\delta$  115.6,  $\delta$  160.0 and a doublet at  $\delta$  7.09; also, the <sup>1</sup>H-NMR signal from the methoxy group at  $\delta$  3.80 was correlating with the carbon at  $\delta$  160.0, indicating it is an aromatic methoxy group; and the <sup>13</sup>C-NMR signal at  $\delta_C$  113.1 was correlating with  $\delta_H$  4.76, as well as  $\delta_C$  119.7 with  $\delta_H$  4.76 and  $\delta_H$  4.72 (see Figure 3.44). The latter correlations and comparison with the vasicine spectrum suggested the assignment of the  $\delta_C$  113.1 signal to C-8 and the signal at  $\delta_C$  119.7 to C-8a. The position of the methoxy group, however, was yet to be investigated. Due to the presence of an ABX system in the aromatic region, the doublet of doublets (dd,  $J = 8.8$  Hz,  $J = 2.7$  Hz) should be in an *ortho*-position to the doublet with  $J = 8.8$  Hz, and in *meta*-position to the doublet with  $J = 2.7$  Hz. Another confirmation was the correlation between the doublet at  $\delta$  7.09 and the doublet of doublets at  $\delta$  6.9 (Figure 3.55). If the methoxy group was in position 5 or 8, this coupling pattern would not be possible; if it was located in position 6, the signal at  $\delta_C$  113.1 should be assigned to C-

5, which would then be the isolated C-H, but then an HMBC correlation with H-9 would be unlikely since this is a 4-bond correlation. Finally, the ESI-MS spectrum revealed a pseudo-molecular ion at  $m/z$  201  $[M+H]^+$  and **compound 13** was identified as **7-methoxyvasicine** or 7-O-methyl-vasicinol. Interestingly, 7-methoxy-vasicine has been previously synthesized. However, it has not yet been isolated from *Adhatoda vasica* or any other natural source.<sup>173</sup> Since ethanol has been used for extraction, and no methanol, 7-methoxy-vasicine cannot be an artefact.

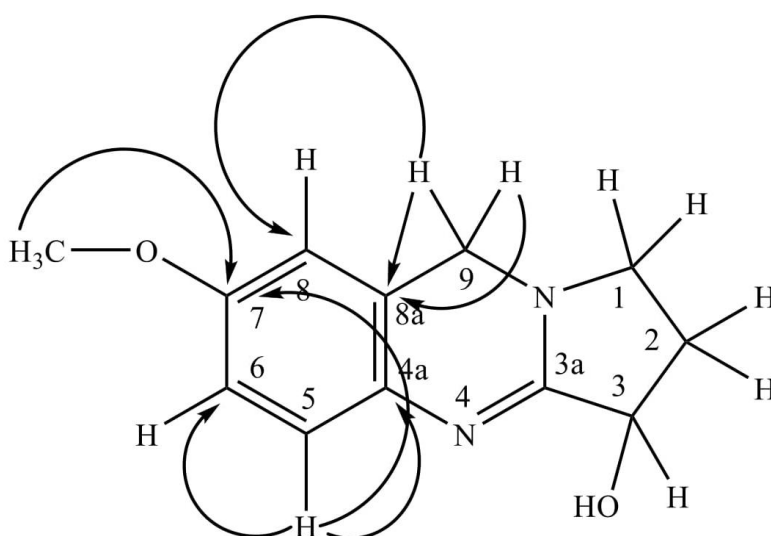


Figure 3.44. HMBC correlation in the structure of 7-methoxyvasicine.

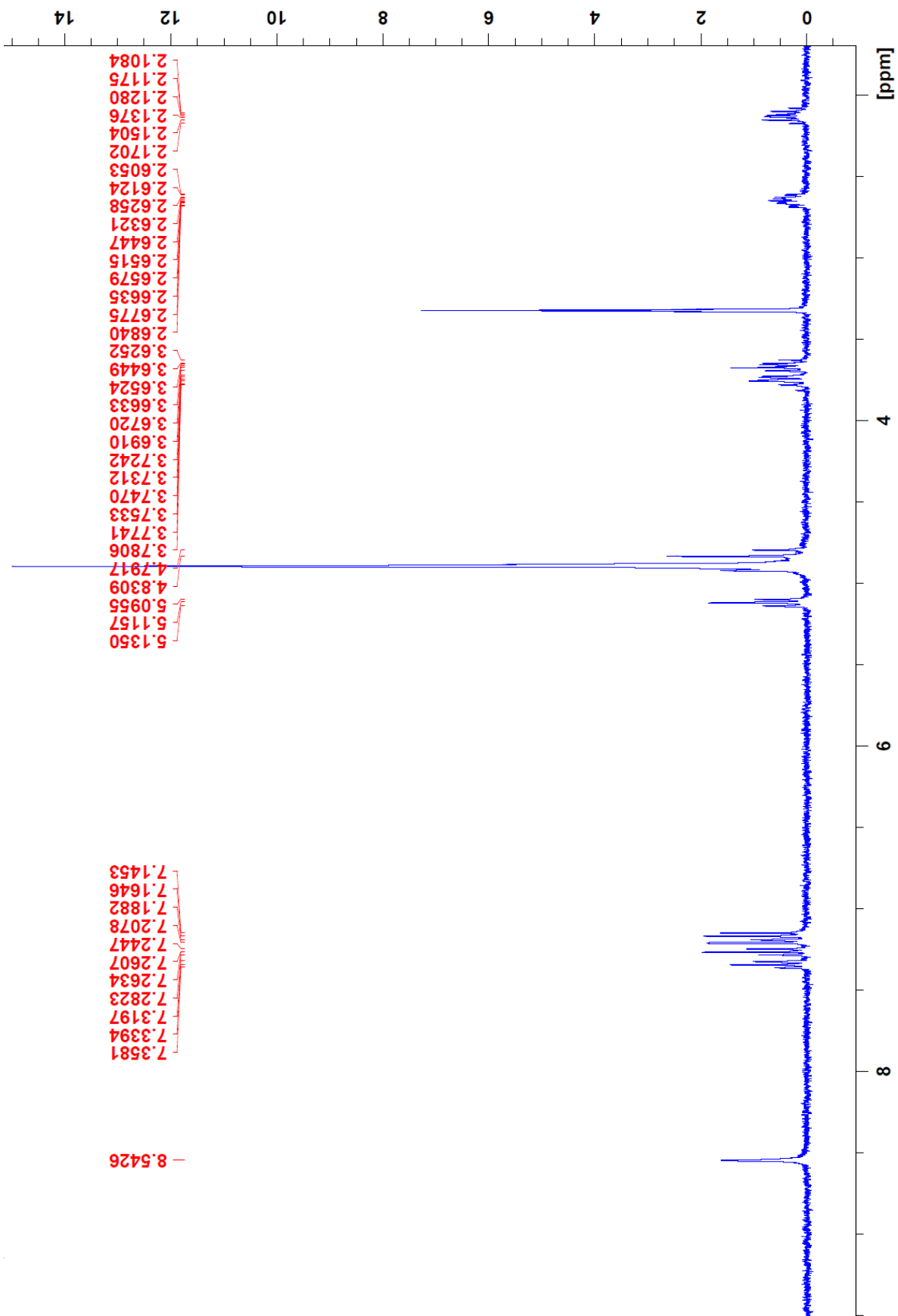


Figure 3.45.  $^1\text{H}$ -NMR spectrum (400 MHz, methanol- $d_4$ ) of **compound 12** (vasicine).

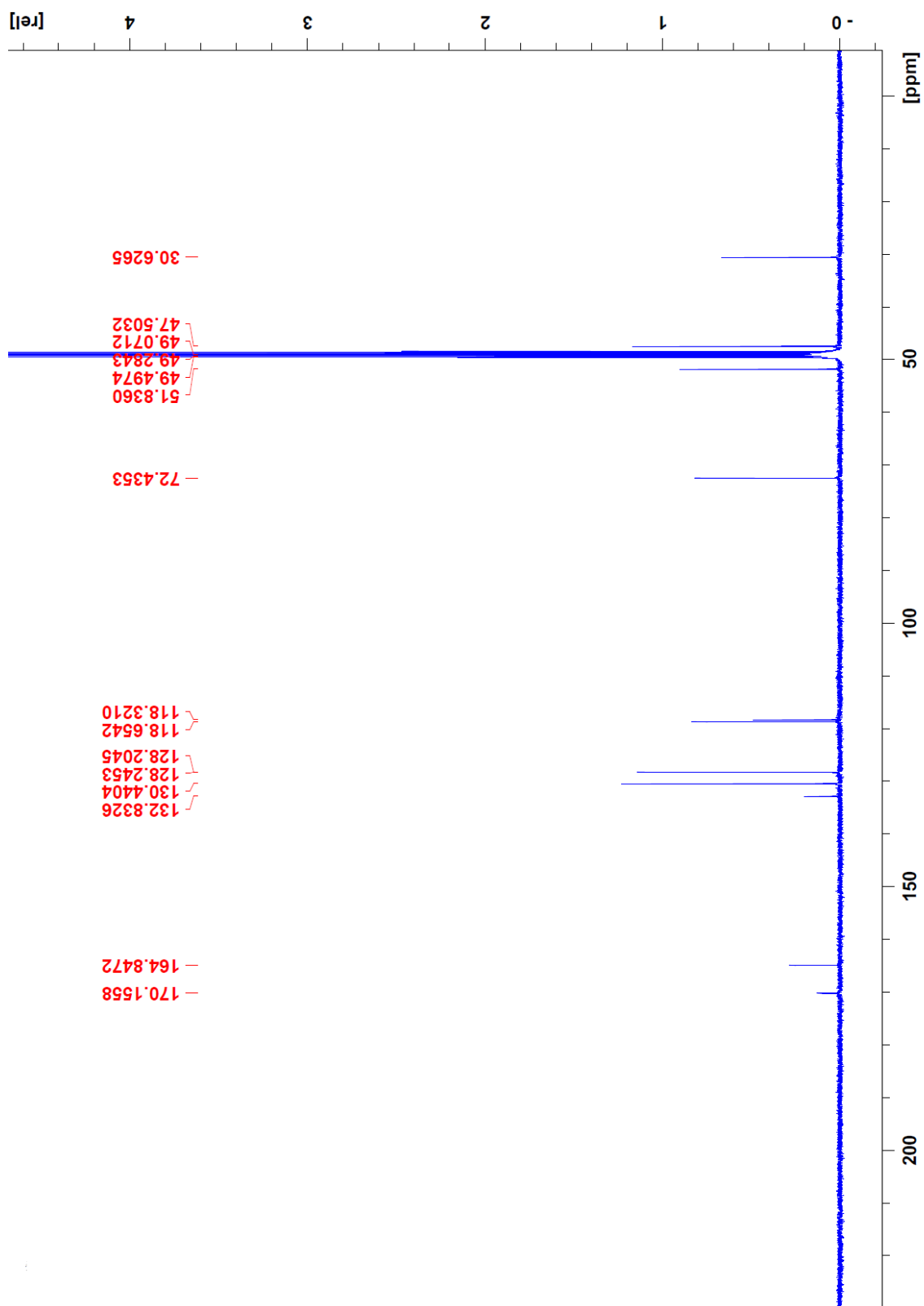


Figure 3.46.  $^{13}\text{C}$ -NMR spectrum (100 MHz,  $\text{CD}_3\text{OD}$ ) of **compound 12** (vasicine).

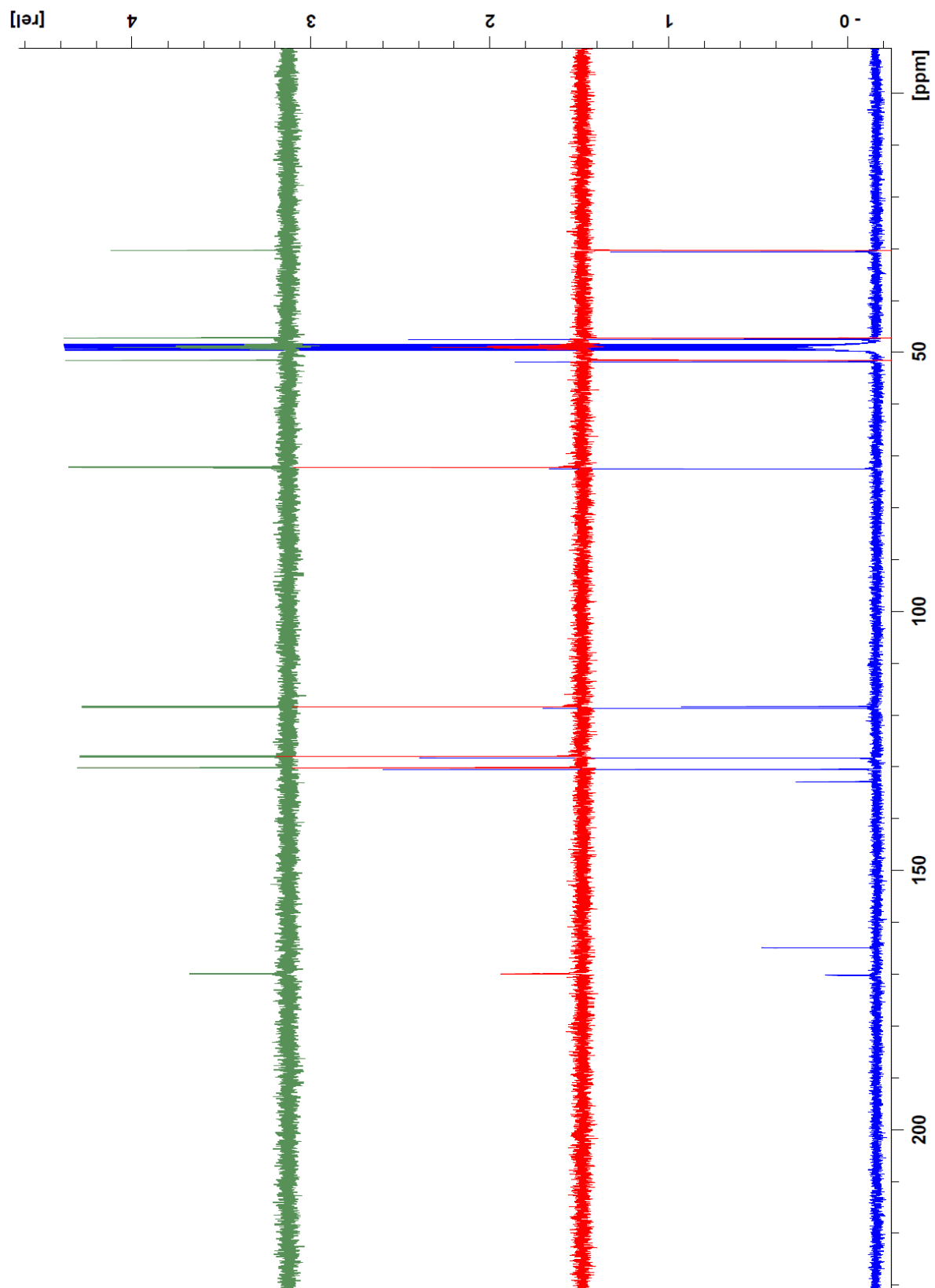


Figure 3.47. Overlay of  $^{13}\text{C}$ -NMR spectrum (blue), DEPT-135 (red) and DEPT-90 (green) (100 MHz, methanol- $d_4$ ) of **compound 12** (vasicine).

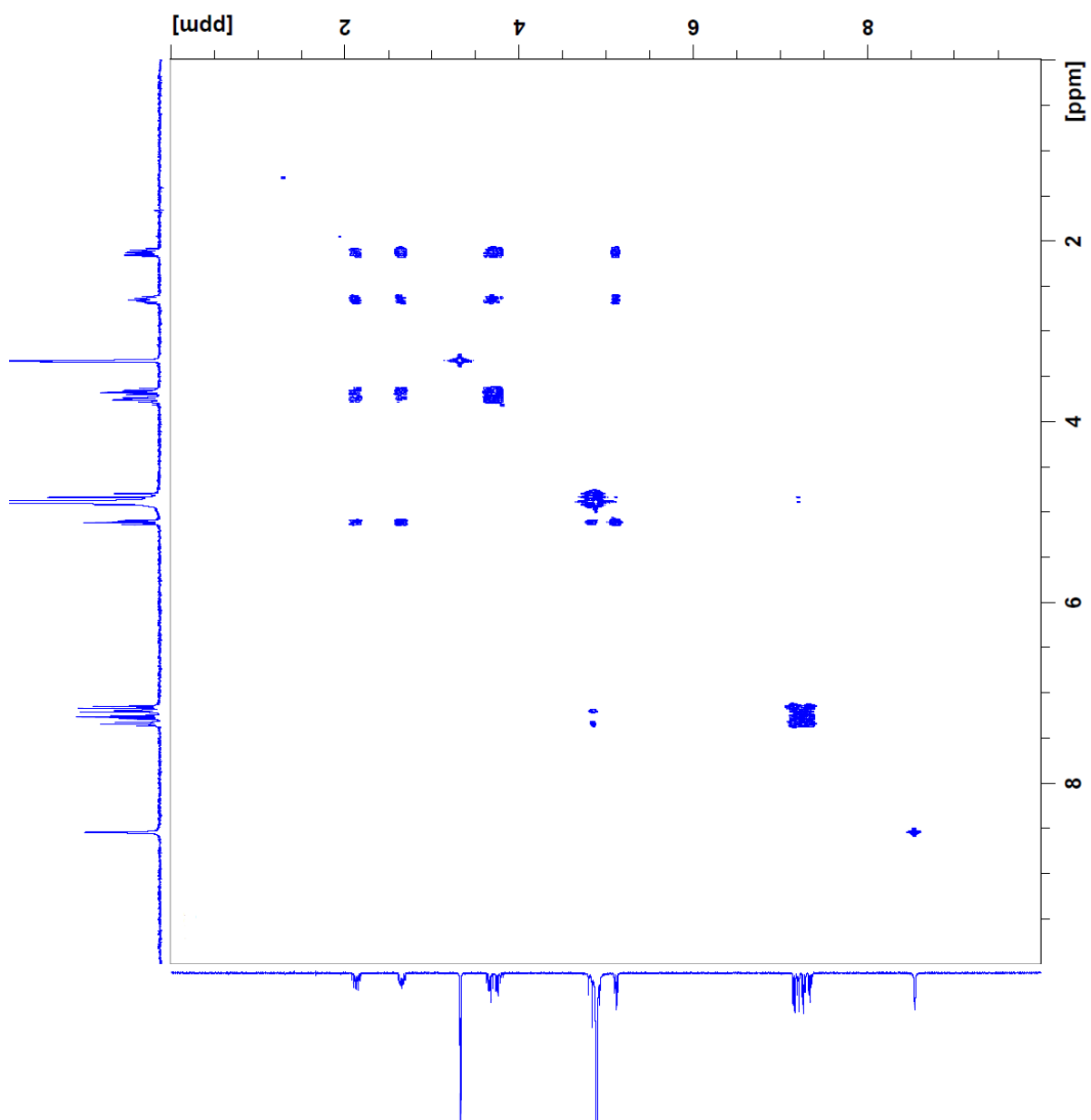


Figure 3.48. COSY spectrum (100 MHz, methanol- $d_4$ ) of **compound 12** (vasicine).

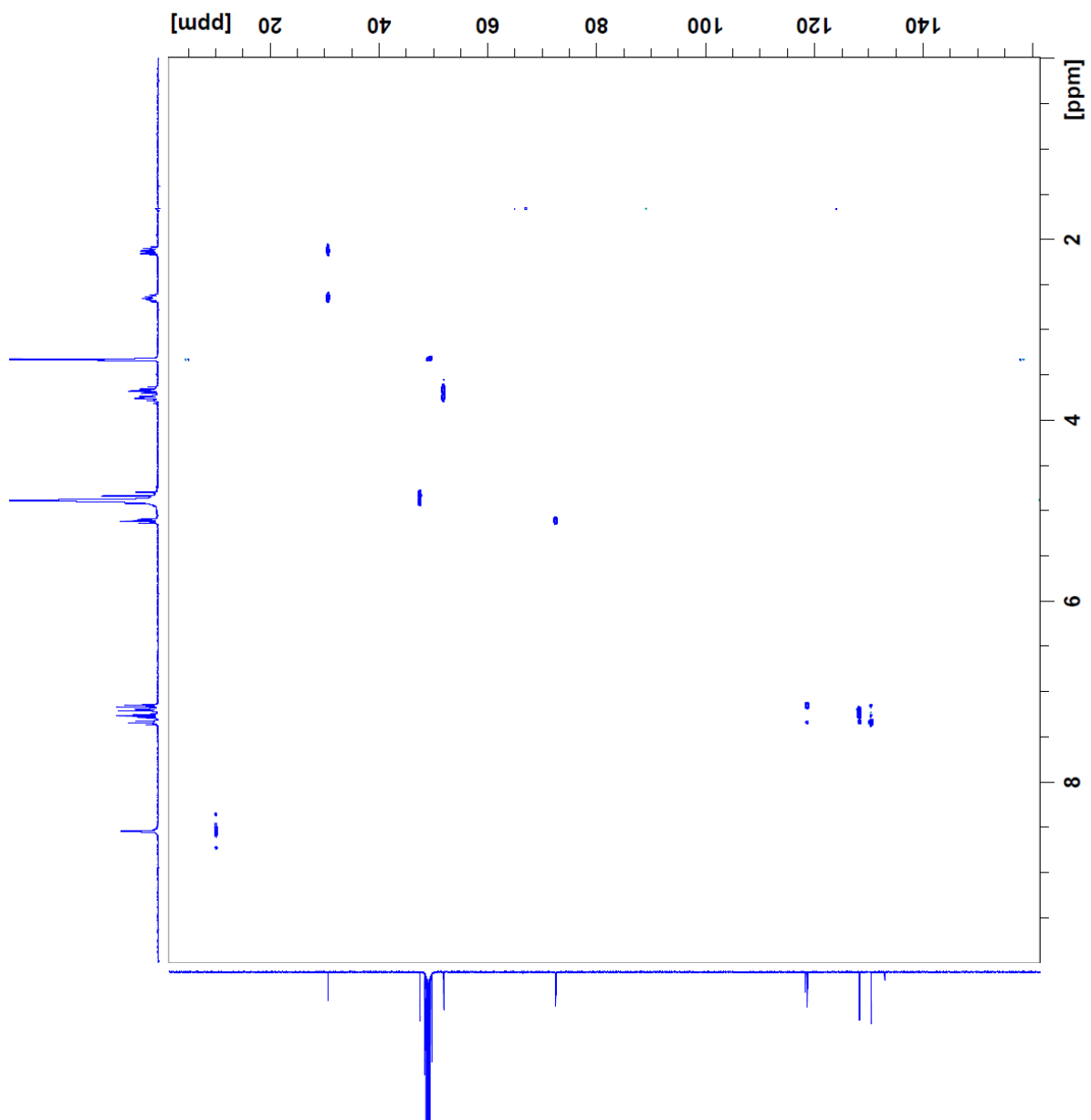


Figure 3.49. HSQC spectrum (400 MHz, methanol- $d_4$ ) of **compound 12** (vasicine).

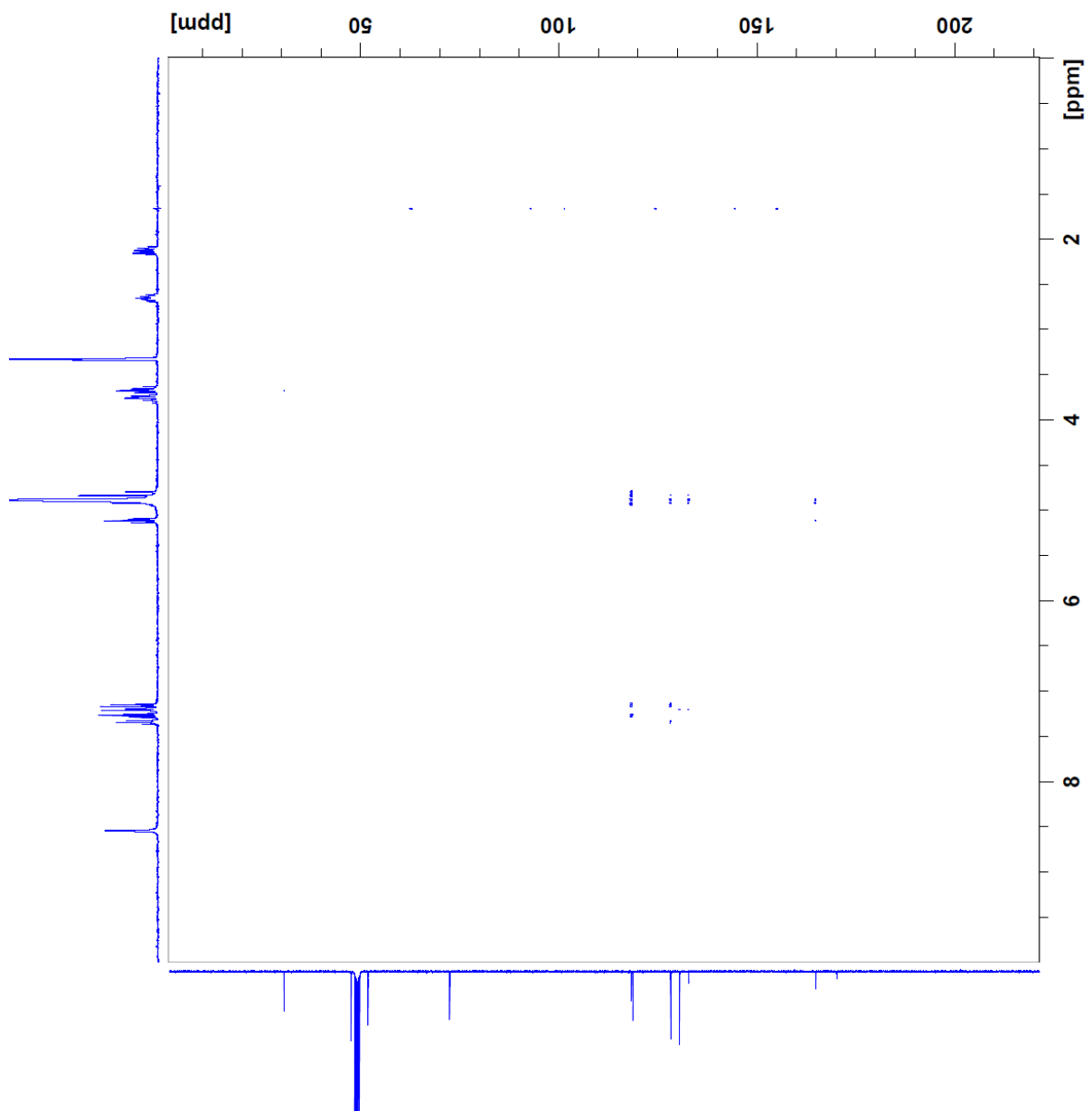


Figure 3.50. HMBC spectrum (400 MHz, methanol-*d*<sub>4</sub>) of **compound 12** (vasicine).



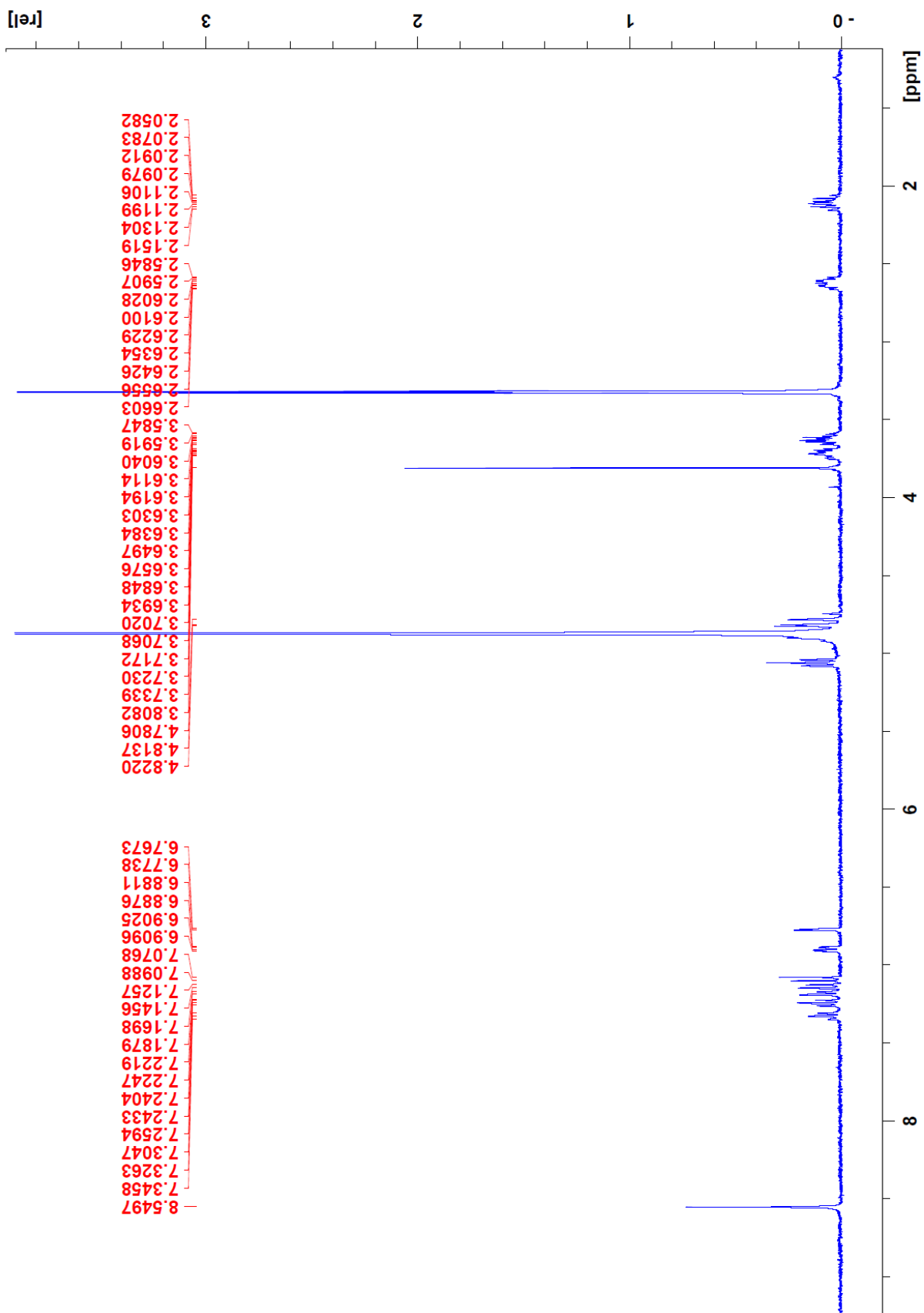


Figure 3.51.  $^1\text{H}$ -NMR spectrum (400 MHz, methanol- $d_4$ ) of **compound 13** (7-methoxyvasicine).

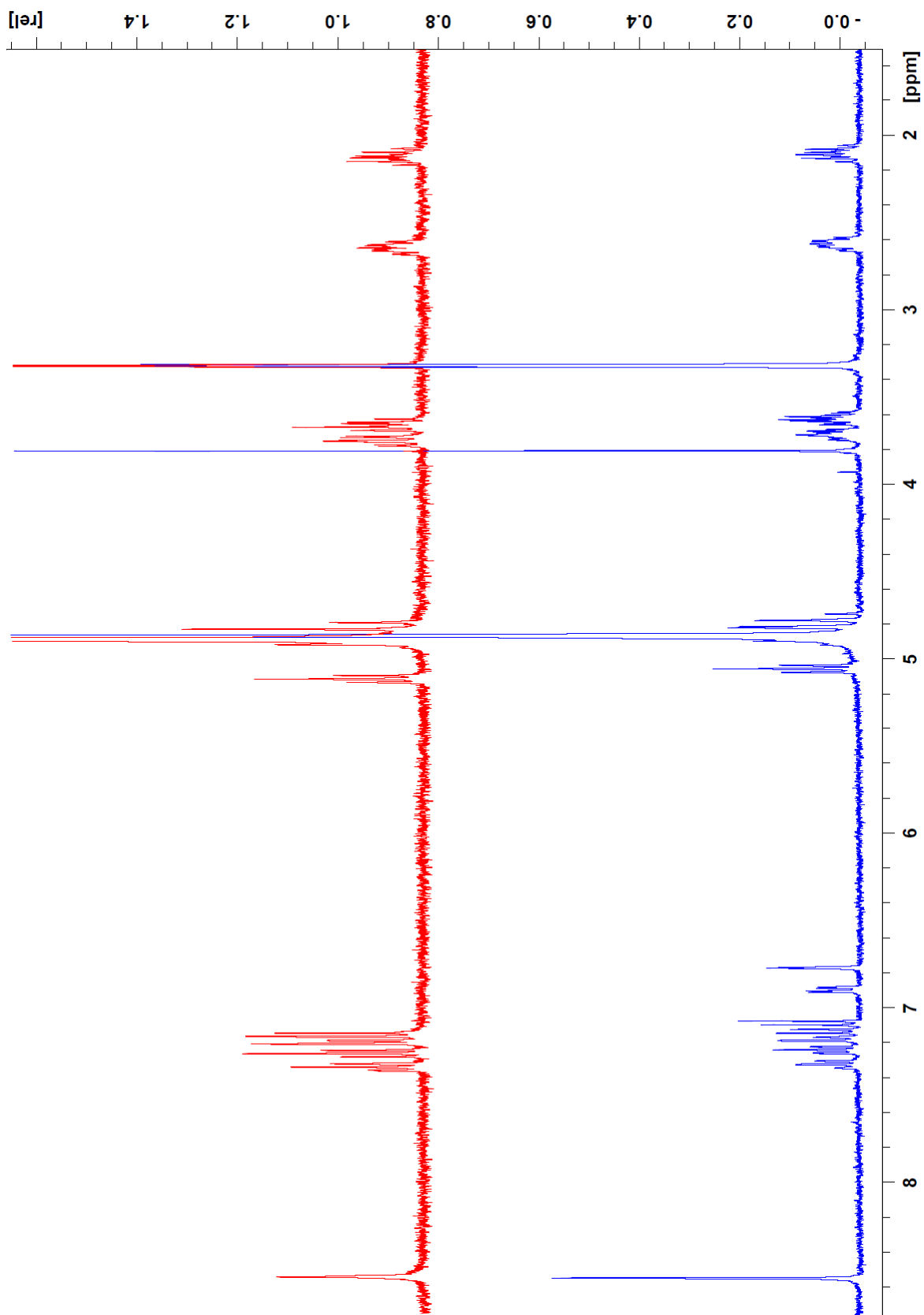


Figure 3.52. Overlapping <sup>1</sup>H-NMR spectra (400 MHz, methanol-d<sub>4</sub>) of **compound 13** (7-methoxy-vasicine) – blue colour, and **compound 12** (vasicine) – red colour.

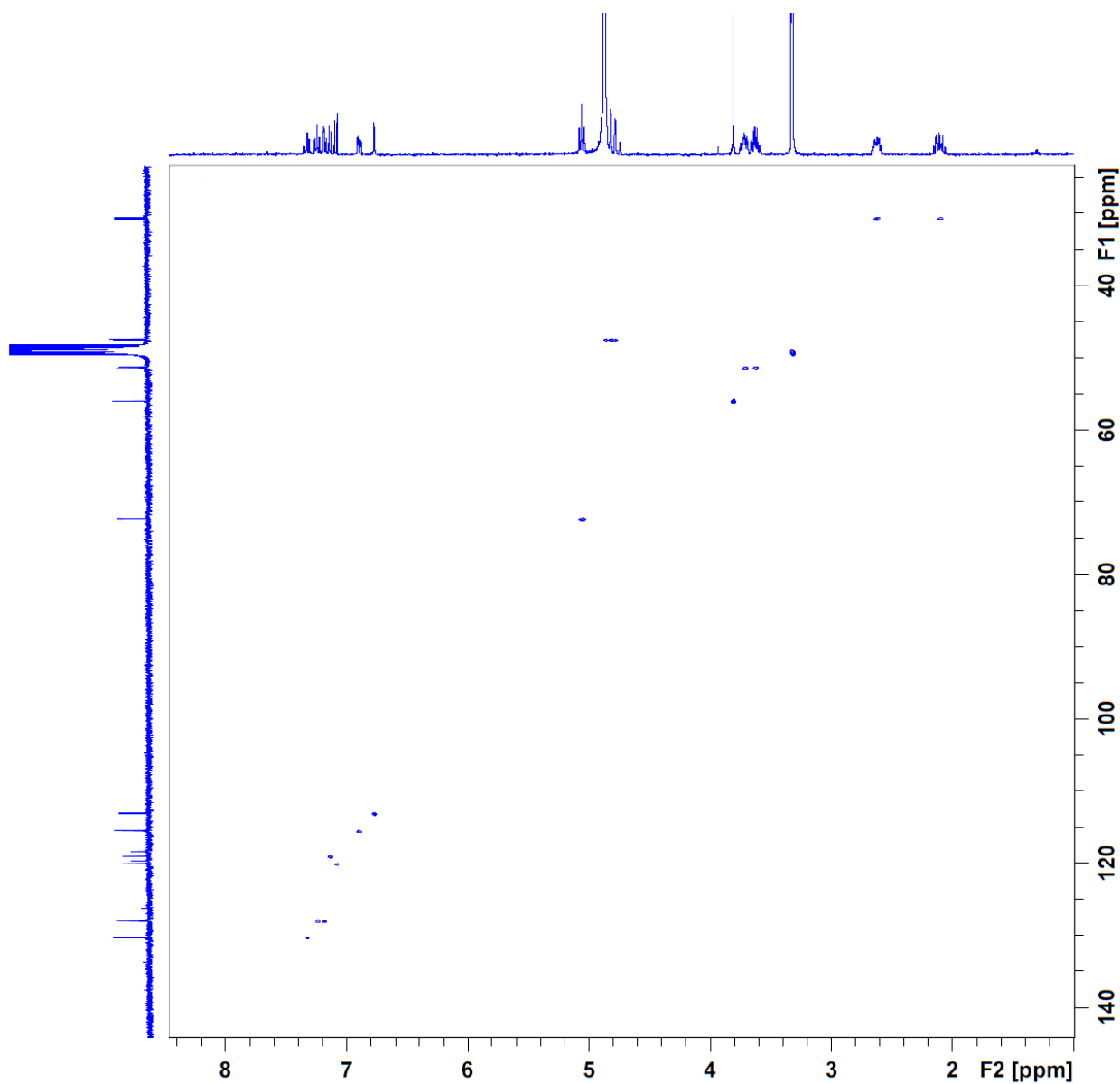


Figure 3.53. HSQC spectrum (400 MHz, methanol- $d_4$ ) of **compound 13** (7-methoxyvasicine).



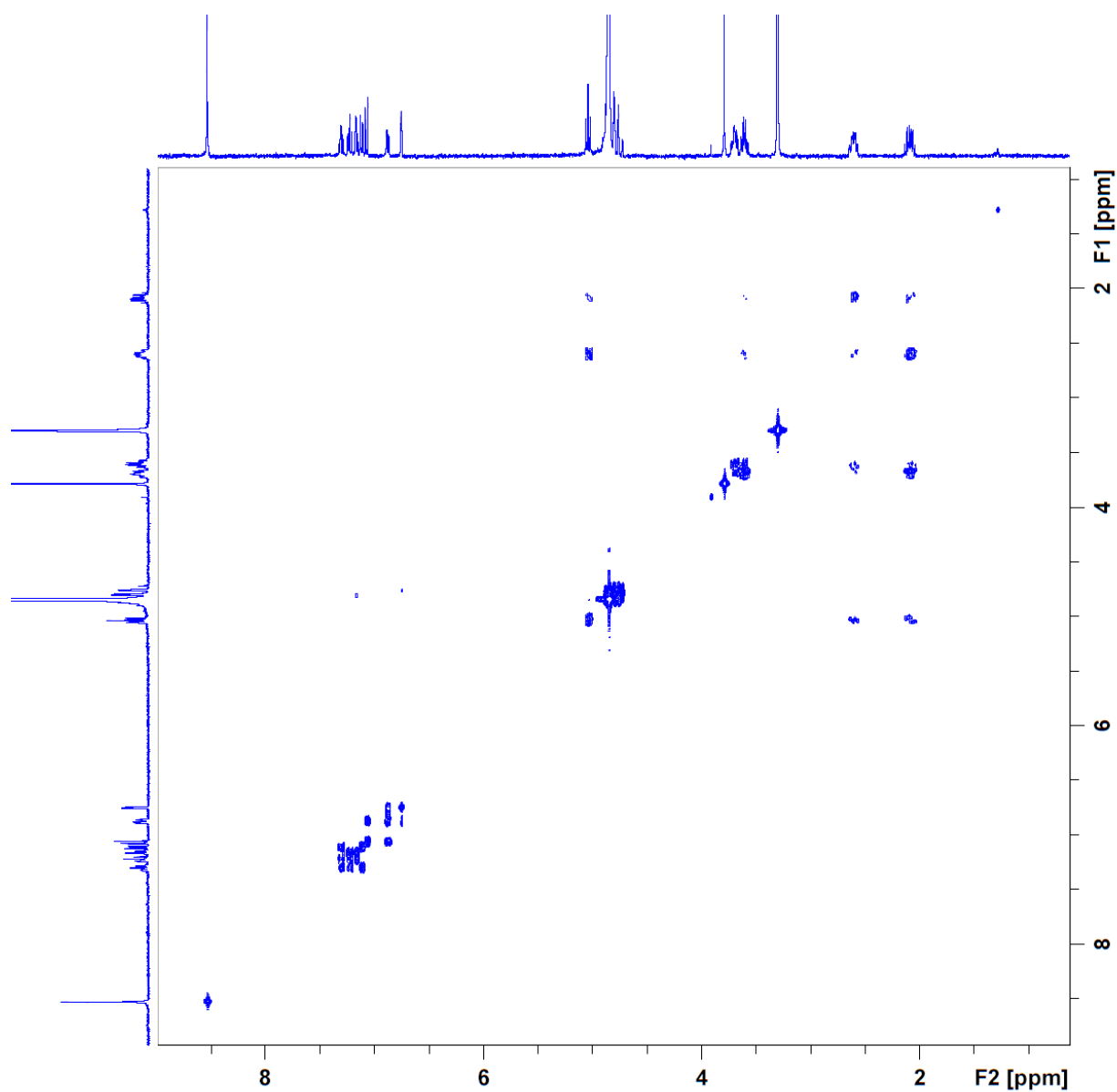


Figure 3.55. COSY spectrum (100 MHz, methanol-*d*<sub>4</sub>) of **compound 13** (7-methoxyvasicine).

	vasicine					7-methoxy-vasicine				
	<sup>1</sup> H ( $\delta$ , ppm)	Multiplicity ( <i>J</i> , Hz)	<sup>13</sup> C ( $\delta$ , ppm)	DEPT		<sup>1</sup> H ( $\delta$ , ppm)	Multiplicity ( <i>J</i> , Hz)	<sup>13</sup> C ( $\delta$ , ppm)	DEPT	
<b>1</b>	1 $\alpha$	3.75	m	51.8	t	1 $\alpha$	3.7	m	51.3	t
	1 $\beta$	3.67				1 $\beta$	3.6			
<b>2</b>	2 $\alpha$	2.12	m	30.6	t	2 $\alpha$	2.1	m	30.7	t
	2 $\beta$	2.64				2 $\beta$	2.6			
<b>3</b>	5.11	dd, <i>J</i> =7.9	72.4	d		5.05	dd, <i>J</i> =8.0	72.2	d	
<b>3a</b>	-		164.8	s		-		163.6	s	
<b>4a</b>	-		132.8	s		-		126.2	s	
<b>5</b>	7.14	d, <i>J</i> =7.8	110.7	d		7.09	d, <i>J</i> =8.8	120.1	d	
<b>6</b>	7.34	ddd, <i>J</i> =7.6, 7.6, 1.2	130.4	d		6.90	dd, <i>J</i> =8.8, 2.7	115.6	d	
<b>7</b>	7.24	ddd, <i>J</i> =1.0, 7.6, 7.6	128.2	d		3.80		160.0	s	
<b>8</b>	7.19	br d, <i>J</i> =7.6	120.2	d		6.77	d, <i>J</i> =2.7	113.1	d	
<b>8a</b>	-		118.3	s		-		119.7	s	
<b>9</b>	9 $\alpha$	4.83	t	47.5	t	9 $\alpha$	4.76	t	47.4	t
	9 $\beta$	4.78				9 $\beta$	4.72			
<b>OCH<sub>3</sub></b>	-	-	-	-	-	3.80	s	56.03	q	

Table 3.5. <sup>1</sup>H- and <sup>13</sup>C-NMR assignments of compounds 12 and 13 in the *Adhatoda vasica* alkaloid fraction.

# Chapter 4

**Method validation *Adhatoda vasica* and  
quantification of vasicine in commercial  
products**

(Manuscript submitted in the *Journal of Herbal Medicine*)





## 1. Objectives

In many countries (India, Pakistan, Nepal, Sri Lanka) herbal formulations containing *Adhatoda vasica* Nees (or *Justicia adhatoda* L., or “Malabar Nut Tree” in English) are used, like *Kada*, *Fermiforte*, *Salus Tuss*, *Kan Jang* and *spirote*, to treat various kinds of respiratory disorders. Moreover, it is frequently included as an ingredient of several proprietary, over the counter (OTC) and polyherbal products for a variety of respiratory ailments including cough, bronchitis, and asthma.<sup>170</sup> Not surprisingly, the frequent ethnobotanical utilization of *Adhatoda vasica* has resulted in its inclusion in the WHO manual “The use of Traditional Medicines in Primary Health Care”.<sup>174</sup> By now, a wide range of phytochemical constituents have been isolated from the leaves of *A. vasica*, for example: alkaloids, phenols, tannins, anthraquinones, saponins, steroids, flavonoids and reducing sugars. However, pharmacologically the most studied chemical component is the bitter quinazoline alkaloid - vasicine.<sup>175</sup> Consequently, a reliable method for the characterization of quinazoline alkaloids, namely vasicine, of *Adhatoda* species is essential for quality control of herbal products.<sup>169</sup> Since vasicine is readily oxidised to vasicinone and the pharmacological effect of these compounds is rather different, it is utterly important to optimize a method for quantification of the quinazoline alkaloids, more particularly vasicine, using HPLC (first objective of the research). Secondly, the validation of this method will ensure an accurate and repeatable determination of vasicine. And, the final objective of the experiment was to test the validated method for quantifying vasicine in commercially available products containing *Adhatoda vasica* leaves powder or extract.

## 2. Materials and Methods

### 2.1 Plant material

The first batch of dried leaves *Adhatoda vasica* Nees and the reference standard (vasicine) were provided by the European Pharmacopoeia (Council of Europe, EDQM: code 0000057451; batch 1502-5546/al). The second batch of *Adhatoda* leaves was collected in Nepal in May 2015 and identified by dr. Atul Upadhyay. Subsequently, the

leaves were air dried and then transferred to the University of Antwerp. The dried leaves were finely pulverized (IKA® M 20 Universal mill, Staufen, Germany) and then sieved through a sieve with a mesh diameter of 355 µm.

## 2.2 Loss on drying

The content of water in the *Adhatoda vasica* **leaves powder** was determined based on the procedure of the European Pharmacopoeia (Method 2.2.32 Loss On Drying, LOD). A sample of 1.0 g powder, was placed in an oven (VWR DRY-line, Leuven, Belgium) for two hours and temperature between 100 °C and 105 °C. Finally, it was cooled down to room temperature in a desiccator and weighted on an analytical balance. The water content was expressed in percentage and calculated by the formula:

$$H(\%) = \frac{m_{before} - m_{after}}{m_{before}} \times 100$$

where H (%) is the water content of the sample;  $m_{before}$  weight of the powder before drying (g); and  $m_{after}$  weight of the powder after 2 h drying (g). Analysis was performed in triplicate. Additionally, for the **dietary supplements** containing plant powder of *Adhatoda vasica* leaves the tests of loss on drying (LOD) was also carried out in the same manner. The experiment was performed in triplicate for each product.

## 2.3 Uniformity of mass of single-dose preparations

For the dietary supplements in the form of tablets/capsules, an additional test of uniformity of mass was carried out according to the European Pharmacopoeia monograph 2.9.5.<sup>176</sup> A total of 20 units taken at random were weighed individually to determine the average mass. Not more than 2 of the individual masses can deviate from the average mass by more than 7.5%, and none can deviate by more than twice that percentage.

## 2.4 Reagents and equipment

All reagents used were of HPLC or analytical grade, unless otherwise stated. Methanol, *n*-hexane, chloroform, absolute ethanol, acetonitrile and glacial acetic acid were purchased from Fisher Scientific, Leicestershire, UK. Potassium dihydrogen phosphate for analysis was acquired from Merck Millipore, Darmstadt, Germany. The sterile and pyrogen free water for HPLC analysis was obtained by a Milli-Q® Integral Water Purification System, Millipore, Bedford MA, USA.

The main equipment used in the method was: heating mantles (Isopad, Labmaster); filters Macherey-Nagel-MN 640 M No.43 with diameter 110 mm (Duren, Germany); Buchi Rotavapor® R-200 (Flawil, Switzerland) with Vacuubrand PC 2001 Vario Vacuum Pump CVC2000 controller (Wertheim, Germany); ultrasonic bath Cleanosonic Branson B3510 (Wareham, Massachusetts, USA); syringe filter, Macherey-Nagel polyamide (nylon) Chromafil® AO-45/25 pore size 0.45 µm, diameter 25 mm (Duren, Germany).

## 2.5 Instrumentation and chromatographic conditions

All analyses were performed on an Agilent Technologies 1260 Infinity HPLC-DAD system (Diegem, Belgium) from the 1200 Infinity Series with degasser, quaternary pump, automatic liquid sampler, thermostatic column compartment and diode array detector (DAD). Agilent OpenLAB CDS ChemStation edition software was used (version A.01.05). The column applied for the method validation was a Purosphere STAR RP-18 Endcapped (250 x 4.6 mm, 5 µm) (Merck, Germany). The mobile phase comprised eluent A: potassium dihydrogen phosphate : acetonitrile : acetic acid (85:15:1, v/v/v), pH 3.9; eluent B: acetonitrile : acetic acid (99:1, v/v). All MS spectra were obtained with a Surveyor LC-MS system equipped with a degasser, a quaternary pump, an autosampler and a DAD (Thermo Fisher), and which was coupled to an LXQ linear ion trap (Thermo Fisher). The LXQ linear ion trap consists of an atmospheric pressure ionization source, ion optics, a mass analyser, and an ion detection system. The column used was Purosphere STAR RP-18 Endcapped (250 x 4.6 mm, 5 µm) (Merck, Germany). The flow rate was 0.7 ml/min, and the solvent program was as follows: A: 0.1% formic acid, B:

acetonitrile; 0.0 min - 10% B, 12.0 min – 10% B, 17.0 min – 50% B, 22.0 – 50% B, 25.0 min – 10% B, 30.0 min – 10% B. The injection volume was 10 µl. All spectra were recorded in the (+) ESI mode scanning in the mass range  $m/z$  100.00 – 500.00. The UV detector was set at 285 nm. All data was acquired and processed using Xcalibur software, version 2.0.

### 3. Method development

#### 3.1 USP method

In general, one of the major drawbacks of developing a reliable method for the quantification of vasicine and vasicinone is the lack of baseline separation between both compounds, resulting in overlapping peaks of the compound of interest. In the current thesis, the starting point for method development was the monograph “Malabar Nut Tree, Leaf” from the United States Pharmacopeia (USP) where the plant material (2.0 g finely powdered *A. vasica* leaves) was extracted with 50.0 ml methanol, using a reflux for 15 min. Afterwards the extract was cooled down to room temperature and the supernatant was decanted. The process was repeated until the last extract was colourless. Those extracts were combined, filtered and concentrated under vacuum. Finally, the volume was adjusted to 25.0 ml with methanol. Then, this sample solution was diluted five times with methanol. Before injection, the diluted sample was filtered through a membrane filter of 0.45 µm. Interestingly, according to the USP the same sample preparation steps could be applied both for thin-layer identification test and for high-pressure liquid chromatography, except from the five-fold dilution step in the HPLC method. The used HPLC conditions for the USP method are included in Table 4.1.

Conditions	USP method
Instrument	Agilent Technologies 1260 Infinity
Injection volume	20 µl
Mobile phase	Buffered solution*/ acetonitrile/ tetrahydrofuran (92:5:3), pH 2.8
Column	4.6 mm x 25 cm, 5 µm packing L10 (Nitrile groups chemically bonded to porous silica particles)
Flow rate	1.0 ml/min
Detector	UV 280 nm

Table 4.1. Instrument conditions for the USP method.

\*The buffer solution was made as follows: dissolve 1.36 g of anhydrous potassium dihydrogen phosphate in 900 ml Milli-Q® water, then add 2.0 ml of 85% *m/m* phosphoric acid, dilute with water to 1000 ml and filter.

### 3.2 Method optimization

The USP method was the starting point for the further method development performed at the research group NatuRA (Natural Products & Food – Research and Analysis). The method optimization investigated the different instrument parameters like columns, mobile phase, the optimal wavelength for UV detection; several extraction procedures and specific conditions for sample preparation.

#### 3.2.1 Chromatographic parameters

In the method optimization three different columns with a length of 25 cm and an internal diameter of 4.6 mm were tested: a Purospher® STAR RP C18 Endcapped (5 µm), a Purospher® STAR RP C8 Endcapped (5 µm) and a Hypersil butyl Genesis RP C4 (5 µm). Additionally, various compositions of the mobile phase were investigated: methanol and water (40/60); eluent A: 0.2% diethylamine and formic acid until pH 3, and eluent B: acetonitrile with 0.2% diethylamine; then, a mobile phase consisting of 0.1 M phosphate

buffer pH 3.9, acetonitrile and glacial acetic acid (85/15/1).<sup>164,170,177</sup> The buffer proved to provide sufficient separation between vasicinone and vasicine.<sup>163</sup> The third mobile phase in combination with C18 column with isocratic elution gave the best separation. However, a gradient elution has also been investigated for achieving a better result. Due to the fact that phosphate buffer can crystallize faster when changing the ratio between eluent A and eluent B, the initial isocratic elution was kept. The optimal wavelength was established at 285 nm for UV detection, and the flow rate was set at 0.7 ml/min.

### 3.2.2 Extraction procedure

Three different **types of extraction** for alkaloids, mainly vasicine, were tested. A general extraction (which referred to the method described in the USP) was compared to a typical alkaloid extraction and an alkaloid micro-extraction. Similarly for all three procedures, the extraction was executed on 2.0 g of sample (finely powdered *A. vasica* leaves) with 50.0 ml methanol under reflux for one hour. The supernatant was filtered and fresh amount of the solvent was added to the remaining powder, the extraction was repeated two more times. The combined methanol extracts were evaporated till dryness. The next steps differed among the several extraction methods and the conditions are summarised in Table 4.2.

<b>General extraction</b>	<b>Typical alkaloid extraction</b>	<b>Alkaloid micro-extraction</b>
<ul style="list-style-type: none"> <li>- Resolve the evaporated sample in 20.0 ml methanol</li> <li>- Filter through 0.45 µm filter before injecting</li> </ul>	<ul style="list-style-type: none"> <li>- Resolve the evaporated sample in 15.0 ml 5% acetic acid</li> <li>- Perform three times liquid-liquid extraction with 10.0 ml hexane</li> <li>- Prepare an aqueous solution alkaline to pH 9.0 with ammonia</li> <li>- Perform three times liquid-liquid extraction with 10.0 ml chloroform</li> <li>- Evaporate the combined chloroform fractions</li> <li>- Resolve in 20.0 ml methanol</li> <li>- Filter through 0.45 µl filter before injecting</li> </ul>	<ul style="list-style-type: none"> <li>- Resolve the evaporated sample in 10.0 ml 5% acetic acid</li> <li>- Transfer into a headspace vial, add 8.0 ml of hexane and close the vial</li> <li>- Place for 15 min in an ultrasonic bath in a horizontal position</li> <li>- Remove the hexane layer and make the aqueous layer alkaline to pH 9.0 with ammonia</li> <li>- Add 8.0 ml of chloroform and place for 30 min in an ultrasonic bath in a horizontal position</li> <li>- Repeat two more times</li> <li>- Evaporate the combined chloroform fractions</li> <li>- Resolve in 20.0 ml methanol</li> <li>- Filter through 0.45 µl filter before injecting</li> </ul>

*Table 4.2. Three different methods for alkaloid extraction.*

It was estimated that the vasicine content was 1.20% when using the alkaloid micro-extraction, and when using the general extraction it was 1.44%, respectively. The conclusion was the amount of vasicine obtained by alkaloid extraction was lower compared to the content obtained by general extraction. In theory, when an alkaloid extraction is performed only the alkaloid fraction is obtained, on the contrary to a general extraction where additional compounds are normally extracted as well. The comparison between the results from the three extraction types are presented in Table 4.3.

Method	Peak area (mAU)
	concentration of the sample $\left(\frac{\text{g}}{\text{ml}}\right) (\times 10^5)$
Alkaloid micro-extraction	0.3427
General extraction	4.1373
Typical alkaloid extraction	3.8364

Table 4.3. Final results from the three extraction procedures.

The value from the alkaloid micro-extraction was about ten times less than the other two methods. Therefore, the alkaloid micro-extraction was considered as the least reliable method. Advantages of the typical alkaloid extraction were the presence of less peaks and subsequently, a better separation in the chromatogram of the sample, however, it was considered as rather labour-intensive and time consuming, consequently, less convincing in perspective to apply the procedure on industrial scale. Also, it contained a liquid-liquid extraction step which might be questioned in regard, if all compounds could be quantitatively transferred. The next step was to compare if the typical alkaloid extraction, would give the same results as the general extraction. Sample of 2 g was treated following the procedure included in Table 4.2. The ratio between peak area and concentration was 8.9% lower for the alkaloid extraction than the general method; and the relative standard deviation was ten times higher for the typical alkaloid extraction (RSD 4.47%) compared to the general (RSD 0.42%). The arguments considered above were the reason to continue the further method optimization using the general extraction procedure.

At first, preliminary validation was carried out according the ICH guidelines on the general extraction method. In the beginning, the calibration model was checked, the repeatability of the method was accepted, and the accuracy was evaluated by the standard addition method (data not included). Unfortunately, the validation procedure revealed a considerable loss of compounds of interest during the sample preparation due to degradation or conversion of vasicine.<sup>178</sup> A possible explanation might be the autooxidation of vasicine to vasicinone that can take place in bright daylight or sunlight.<sup>170</sup> Consequently, all steps in the experimental procedure were performed protected from light.



The chromatograms obtained after the general extraction revealed a considerably high peak area for vasicine, therefore the **amount of the sample** was reduced from 2.0 g to 1.0 g. Another change was concerning the **solvent composition** used to make the final dilution of the sample for injection. In the preliminary experiments, the peak obtained using pure methanol gave fronting. As a result, in order to achieve a symmetrical peak shape the percentage of the organic solvent was brought as close as possible to the percentage of the organic solvent in the mobile phase. Particularly, pure methanol, 50% methanol, pure water and methanol : water (40 : 60) were examined. The most promising results were accomplished with the latter composition of the solvent mixture where the fronting from the previous results was avoided.

The next experiment focused on multiple injections of samples prepared with the general extraction scheme. Merging of the peaks was observed after the multiple injections, and also, it was speculated that compounds were retained on the column. Consequently, the **composition of the mobile phase** and the **type of elution** was investigated. Two mobile phases were used: the already described eluent A (0.1 M potassium dihydrogen phosphate, acetonitrile and glacial acetic acid (85/15/1)), and as an eluent B acetonitrile and glacial acetic acid (99/1). Due to the risk of precipitation when using a gradient elution, it was confirmed that the maximum percentage of B where the precipitation did not take place was 60%. As a result, a washing step was implemented to the already existing isocratic elution. Regarding the chromatographic run, after 12 minutes all peak of interest were eluted with 100% eluent A, from 12<sup>th</sup> till 17<sup>th</sup> min the mobile phase was changed to 50% eluent B and it was kept for 5min. At the 22<sup>nd</sup> min the mobile phase was restored back to 100% A over a period of 3 min.

Other factor that required optimisation were the **reflux conditions**. In order to establish an extraction till exhaustion of the sample, different time periods (15 min, 30 min), extraction solvents (methanol, ethanol) and extraction volumes were evaluated. The initially described conditions in the USP method included three times reflux for 15 min each. The question was, if three time was enough for exhaustive extraction of the sample, and if it was necessary to increase the duration of the reflux. Two sets of samples were prepared: first one – refluxing 15 min, second one – 30 min, both repeated four times. There was no big difference between the results from samples refluxed 15 or 30 min.

However, there was a difference in the amount recovered with the fourth time reflux, which was intentionally not combined with the rest of the extracts. It was smaller for the longer refluxing than for the shorter period (data not presented). Moreover, when ethanol was used as extraction solvent the detected amount of vasicine was lower compared to the samples extracted with methanol (data not shown). In the end, it was concluded that refluxing three times during 30 min with a volume of 50.0 ml methanol was sufficient for extracting 1.0 g sample.

### 3.3 Final method

A standard solution was made by dissolving 10.0 mg vasicine in 10.0 ml pure methanol. The solution was sonicated for 15 min and then, cooled down to room temperature. Of this solution 2.0 ml was taken and diluted till 25.0 ml with methanol : water (40 : 60). The standard had a final concentration of 80 µg/ml.

Finely powdered 1.0 g dried leaves were placed into a round bottom flask of 250 ml. Then, 50.0 ml pure methanol was added and 30 min reflux was performed using a heating mantle and a condenser. After cooling down to room temperature, the supernatant was decanted through a filter paper into a new round bottom flask of 250 ml. The reflux procedure was repeated two more times. The combined extracts were concentrated under vacuum until the volume was less than 25 ml. The concentrated extract was transferred to a 25.0 ml volumetric flask. The 250 ml flask was rinsed with methanol, which was also transferred to the measuring flask and the volume was adjusted with methanol till 25.0 ml. Finally, the methanol solution was diluted five times with methanol : water (40 : 60). The aqueous solution was filtered through a syringe filter into an HPLC vial ready for analysis. The conditions for the sample preparation and the chromatographic analysis are summarised in Table 4.4.

<b>Standard preparation</b>	<ul style="list-style-type: none"> <li>- Dissolve 10.0 mg vasicine in methanol (1 mg/ml)</li> <li>- Solution sonicated for 15 min, then cooled down to room temperature</li> <li>- Dilute 2.0 ml of the solution to 25.0 ml with a mixture of methanol and water (40 : 60) (v/v)</li> </ul>																		
<b>Sample preparation</b>	<ul style="list-style-type: none"> <li>- 1.0 g sample of dried leaves <i>A. vasica</i> (355 µm)</li> <li>- Extract with 50.0 ml methanol under reflux for 30 min using heating mantle and condenser</li> <li>- Filter the extract and collect the filtrate</li> <li>- Repeat the extraction two more times</li> <li>- Concentrate under vacuum the combined filtrates till volume less than 25 ml</li> <li>- Transfer to a volumetric flask (25 ml) and adjust the volume with methanol</li> <li>- Dilute five times with methanol : water (40 : 60)</li> <li>- Filter through a 0.45 µl syringe filter before injecting</li> </ul>																		
<b>HPLC conditions</b>	<ul style="list-style-type: none"> <li>- Instrument: Agilent Technologies 1260 Infinity</li> <li>- Injection volume: 20 µl</li> <li>- Mobile phase A: potassium dihydrogen phosphate (0.1 M)/ acetonitrile/ glacial acetic acid (85:15:1)</li> <li>- Mobile phase B: acetonitrile/ glacial acetic acid (99:1)</li> <li>- Gradient: Isocratic elution with a washing step:</li> </ul> <table border="1" style="margin-left: auto; margin-right: auto;"> <thead> <tr> <th>min</th> <th>% A</th> <th>% B</th> </tr> </thead> <tbody> <tr> <td><b>0</b></td> <td>100</td> <td>0</td> </tr> <tr> <td><b>12</b></td> <td>100</td> <td>0</td> </tr> <tr> <td><b>17</b></td> <td>50</td> <td>50</td> </tr> <tr> <td><b>22</b></td> <td>50</td> <td>50</td> </tr> <tr> <td><b>25</b></td> <td>100</td> <td>0</td> </tr> </tbody> </table> <ul style="list-style-type: none"> <li>- Run time: 30 min</li> <li>- Column: Purosphere STAR RP-18 Endcapped (250 x 4.6 mm, 5 µm) (Merck, Germany)</li> <li>- Column temperature: 20 °C</li> <li>- Flow: 0.7 ml/min</li> <li>- Detection wavelength: 285 nm</li> </ul>	min	% A	% B	<b>0</b>	100	0	<b>12</b>	100	0	<b>17</b>	50	50	<b>22</b>	50	50	<b>25</b>	100	0
min	% A	% B																	
<b>0</b>	100	0																	
<b>12</b>	100	0																	
<b>17</b>	50	50																	
<b>22</b>	50	50																	
<b>25</b>	100	0																	

Table 4.4. Optimized sample preparation and chromatographic conditions.

The content of vasicine is expressed in percentage (equal to g/100 g) by the formula:

$$\text{vasicine content (\%)} = \frac{x}{A_{st}} \times \frac{A_p}{m - \left(m \times \frac{H}{100}\right)} \times 0,0125$$

where  $x$  is the amount of vasicine in the standard solution in  $\mu\text{g/ml}$ ;  $A_{st}$  is the peak area of vasicine in the standard solution;  $A_p$  is the peak are of vasicine in sample solution;  $m$  is the weighted amount of the finely powdered leaves of *A. vasica* in grams;  $H$  is the water content in percentage of the powdered leaves determined by loss on drying.

#### 4. Method validation

##### 4.1 Materials and methods

In the beginning, the method was validated on a fresh batch of dried, powdered leaves of *Adhatoda vasica* EDQM based on the optimized procedures developed so far. The ICH guidelines on the validation of analytical methods (ICH 1994, 1996, 2002) were followed.<sup>179,180,181</sup> The calibration model, repeatability, accuracy and specificity were investigated. For the statistical analysis Excel 2010 (Microsoft Office Microsoft corporation, USA) was applied. All results were expressed as percentage, where  $n$  represented the number of values. A 5% level of significance was selected.

##### 4.1.1 Calibration model

A stock solution containing 10.0 mg vasicine in 10.0 ml absolute methanol was prepared (1 mg/ml, as level of the expected amount). From this solution eight different dilutions were made in a concentration range between 5  $\mu\text{g/ml}$  (as 5% level) and 200  $\mu\text{g/ml}$  (as 200% level), using methanol : water (40 : 60). Each concentration was injected in duplicate and regression analysis was performed.

#### 4.1.2 Precision

In order to verify the precision of the injector one sample was injected six times. Consequently, the standard deviation and the relative standard deviation were estimated with a view to evaluate the injection repeatability.

Regarding the repeatability and intermediate precision, six separately prepared samples (1.0 g), which correspond to the 100% level, were analysed in one day. The procedure was repeated on two additional days. Each sample was injected once. The vasicine standard (concentration between 70 and 80 µg/ml), which was used to estimate the amount of vasicine, was freshly prepared every day and injected at the beginning (in duplicate) and at the end of the sequence. The mean, the (relative) standard deviation and the 95% confidence interval were calculated for each day, and also the overall mean, confidence interval and the relative standard deviation. The 95% confidence interval was calculated by the formula:

$$CI = mean \pm \frac{[t(0,05; n - 1) \times S]}{\sqrt{n}}$$

where  $CI$  is the 95% confidential interval;  $S$  is the standard deviation;  $t(p, df)$  included  $p$  (probability) equal to 0.05 when a CI of 95% is used and  $df$  (degrees of freedom)  $n-1$ .

The data, which was collected in three different days, was analysed by an ANOVA single factor test. To test the homogeneity of variance on the different days, a Cochran test was performed in advance. The C-value for the Cochran test was calculated by the formula:

$$C = \frac{S_{max}^2}{\sum_j S_j^2}$$

where  $C$  is the C-value from the Cochran test;  $S_{max}^2$  is the maximum variance of the three days;  $j$  is a single day and  $\sum_j S_j^2$  is the sum of the variances of the three days.

Theoretically, the ANOVA single factor test calculates the mean squares between groups and within groups. These values were used to calculate the within-day and between-day coefficients of variations:

$$S_{within} = \sqrt{MS_{within}}$$

$$RSD_{within} = S_{within} \times \frac{100}{\langle x \rangle}$$

$$S_{between} = \sqrt{\frac{MS_{between} - MS_{within}}{n} + MS_{within}}$$

$$RSD_{between} = S_{between} \times \frac{100}{\langle x \rangle}$$

where *MS* is the mean square; *within* referred to the same day; *between* referred to different days; *RSD* is the relative standard deviation,  $\langle x \rangle$  is the average of the vasicine content and *n* is the number of values in each group.

In order to check the linearity of the method, which corresponds to the repeatability of different concentration levels, six samples containing half of the amount dry leaves powder (50% or 0.5 g) and six samples with one and a half the amount (150% or 1.5 g) were prepared. Then, they were analyzed by the optimized method and a single-point calibration was used to calculate the vasicine content. These results were compared to the one from the 100% level from the different days and similar calculations were applied for the intermediate precision as well.

Because the EDQM batch had completely been used during the precision experiment, new plant material was used for the further analysis, namely, *A. vasica* leaves collected from Nepal (May 2015). Extensive preliminary research on the *Adhatoda* leaves from Nepal was required, which included analysis on different levels (50%, 100%, 150%, in triplicate on the same day) and different days. Additionally, a second analyst repeated three samples of 100%. For each day and concentration level the average vasicine amount, the standard deviation, the relative standard deviation and the 95% confidence interval were determined.

### 4.1.3 Accuracy

In order to determine the accuracy of the method samples were prepared in triplicate, using the *Adhatoda* leaves collected in Nepal, and a recovery experiment was performed by standard addition method. Different amounts of the vasicine standard were added to the 50% level sample to obtain  $\pm 75\%$ ,  $\pm 100\%$  and  $\pm 125\%$  of the vasicine concentration. The preparation on each level was done in triplicate and the mean recovery percentage of the different concentrations, the RSD% and the 95% confidence interval were investigated.

In particular, for the purpose of the analysis, a stock solution of 45.0 mg vasicine standard was dissolved in 20.0 ml absolute methanol with a final concentration of 2.5 mg/ml. To prepare the desired vasicine concentration levels of  $\pm 75\%$ ,  $\pm 100\%$  and  $\pm 125\%$ , 1.0 ml, 2.0 ml and 3.0 ml of the stock solution, was added to the samples, respectively. The sample preparation included the optimized method and each solution was injected once. The vasicine standard solution (concentration between 70 and 80  $\mu\text{g/ml}$ ) was prepared from the stock solution and was used for the single point calibration.

The recovery of the single-point standard addition is presented by the formula:

$$\text{Recovery}(\%) = \frac{X_{\text{after}} - X_{\text{before}}}{X_{\text{added}}} \times 100$$

where  $X_{\text{after}}$  (g/100 g) is the amount of vasicine calculated based on the obtained peak area and on the single point calibration;  $X_{\text{before}}$  (g/100 g) is the average amount of vasicine obtained from the precision experiment and  $X_{\text{added}}$  (g/100 g) is the added amount of vasicine.

The mean recovery percentage of the different concentrations, the RSD% and the 95% confidence interval were estimated. The latter is presented by the formula:

$$CI = \text{mean recovery percentage} \pm S \times \left[ \frac{t(p, df)}{\sqrt{n}} \right]$$

where  $CI$  is the 95% confidence interval;  $S$  is the standard deviation of the nine samples;  $t(p, df)$  includes  $p$  (probability) equal to 0.05 when a CI of 95% was used and  $df$  (degree, of freedom)  $n-1$ ; and  $n$  is the number of samples.

#### 4.1.4 Specificity

In order to unambiguously verify the specificity for the compound of interest, an additional MS analysis was performed. The LC/MS analysis of the standard solution vasicine and solutions of the two samples (both from the EDQM and Nepal) were executed employing a Surveyor LC system coupled to an LXQ linear ion trap and a Purosphere STAR RP-18 Endcapped column. For any commercial product, particularly, the specificity of the method was determined by observing interference of any encountered ingredient present in the formulation.

### 4.2 Results and discussion

#### 4.2.1 Loss on drying

A water content of  $(7.07 \pm 0.05)\%$  was determined for the batch of powdered leaves used in the validation of the method.

#### 4.2.2 Calibration model

The vasicine standard dilutions were analyzed on eight different concentration levels, ranging from 5.125  $\mu\text{g/ml}$  to 205.00  $\mu\text{g/ml}$ . A calibration curve was generated, and the equation and determination coefficient ( $R^2$ ) were calculated (Figure 4.1).



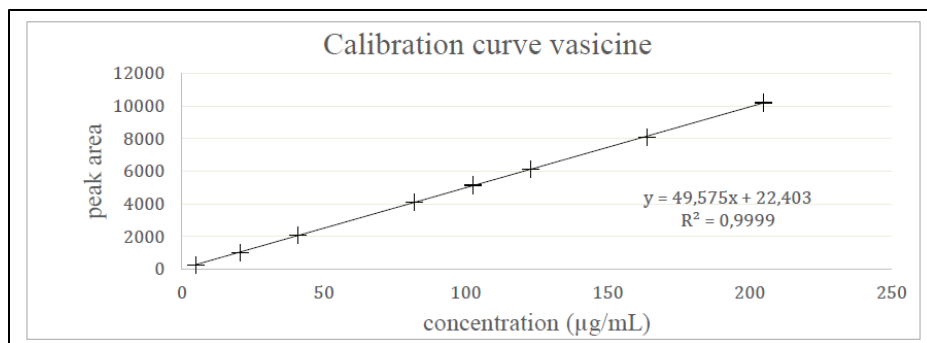


Figure 4.1. Linear calibration curve of vasicine standard.

The regression line was presented by the equation:  $y = 49,58 x + 22,40$  and the calculated  $R^2$  (0.99992) was higher than 0.99, revealing a linear correlation between the concentration of vasicine and the obtained signal. Moreover, a Student's t-test was performed to obtain additional information on the slope of the curve and the intercept. Through this test the 95% confidence interval on the intercept and the significance of the regression coefficient was studied. Regarding the intercept, the calculated (1.629) value was smaller than the t-critical value (2.145), which implies that the point (0.0) was included in the 95% confidence interval, as a consequence a single point calibration was justified. The t-value on the slope was 409.9 which was larger than the t-critical value of 2.145, therefore the null hypothesis should be rejected and the slope differed from 0. In the residual plot (Figure 4.2) no trend could be observed and the residuals were randomly scattered and homoscedastic, therefore, a linear model was applicable. The maximum deviation was established at 1.48%, which is lower than the accepted 5% limit.

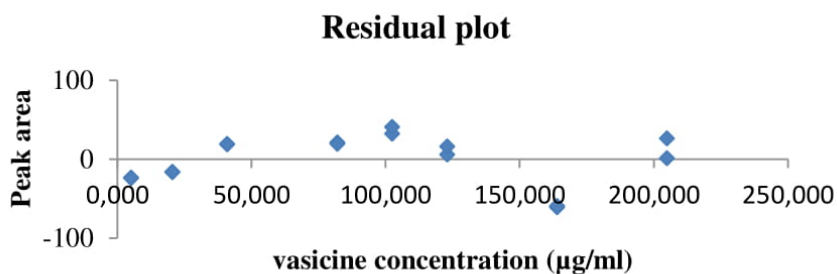


Figure 4.2. Residual plot for vasicine.

#### 4.2.3 Repeatability – Intermediate precision

In order to evaluate the repeatability of the method the analysis was performed six times in the same day, and for intermediate precision – in three different days on different concentration levels, therefore to prove that the uncertainty of the measurement was equal in the whole range of the method. Regarding the intermediate precision, eighteen samples of 1.0 g powdered leaves of *A. vasica* equally divided over three days were analysed. The variation within each day and the variation between days was compared. The average vasicine content for each day and the relative standard deviation are presented in Table 4.5:

	100% level day1	100% level day 2	100% level day 3
<b>Average</b>	0.9467	0.9451	1.0016
<b>STDEV</b>	0.0153	0.0074	0.0248
<b>RSD %</b>	1.62%	0.79%	2.48%

Table 4.5. Results from the intermediate precision on different days.

The variances of the different days were checked by means of a Cochran test which revealed a value of 0.680 below the critical value of 0.707 (C-value), therefore the variance can be considered as equal. Based on the ANOVA single factor there was a difference between the three days (  $F = 20.64 > 3.682$  (critical F-value)). However, the RSD%<sub>between</sub> (3.7%) was calculated to be smaller than the RSD%<sub>max</sub> (= 5.0%), thus the method was considered as precise (Table 4.6).

	Within day precision	Between day precision
<b>Standard deviation</b>	0.017%	0.036%
<b>RSD</b>	1.80%	3.72%

Table 4.6. RSD values for within day precision and between day precision.

It could be concluded that the eighteen samples analysed over three different days do not differ significantly from each other in terms of average vasicine concentration.

#### 4.2.4 Repeatability - Linearity

The repeatability on three different concentration levels (linearity) was compared. The average vasicine content for each concentration level and the relative standard deviation are presented in Table 4.7:

	50% level	100% level	150% level
<b>Average</b>	1.0104	1.0016	1.0633
<b>STDEV</b>	0.0139	0.0248	0.0188
<b>RSD %</b>	1.37%	2.48%	1.77%

Table 4.7. Results from the intermediate precision on different concentration levels.

In the same manner as for the intermediate precision the Cochran value was calculated:  $0.530 < 0.707$ , which allowed to conclude that the variances of the different concentration levels were considered as equal. In the ANOVA single factor for the thirty values of the three different concentration levels the F-value was higher than the critical value ( $F = 17.25 > 3.682$ ). Based on the statistical analysis, the results from the three different days and levels were significantly different but the RSD<sub>between levels</sub> (Table 4.8) was in the same order as the RSD<sub>between days</sub>, and smaller than RSD<sub>max</sub> which is  $\frac{2}{3} \times \text{RSD}_{\text{Horwitz}} (= 4.0\%)$ . There was no concentration-related difference in the results, therefore, the method was considered as precise.

	Within level precision	Between level precision
<b>Standard deviation</b>	0.020%	0.038%
<b>RSD</b>	1.9%	3.7%

Table 4.8. RSD values for within and between level precision.

In conclusion, the variation of the method for the three different days and levels was accepted as equal. Both for the intermediate precision as for the repeatability on different concentration levels the average vasicine amount, standard deviation and relative standard deviation were calculated. The average vasicine content calculated with the 18 values of the intermediate precision was established at  $0.96 \pm 0.03\%$  (RSD 3.28%). The average vasicine content calculated with the 30 values obtained through the repeatability test on different concentration levels was  $0.99 \pm 0.05\%$  (RSD 4.40%). In both cases the relative standard deviation was less than 5%.

#### 4.2.5 Additional test on a new batch

The water content for the batch collected in Nepal was evaluated with a loss on drying test and was determined as  $[7.40 \pm 0.03\%]$ . The average vasicine amount for the six samples of the 50% level was estimated at  $1.15 \pm 0.01$  g/100 g; the average vasicine content for the nine samples of the 100% level was calculated as  $1.13 \pm 0.01$  g/100 g; and for the six samples of the 150% the average was  $1.12 \pm 0.01$  g/100 g. In total, the average vasicine content for the 21 values was calculated as  $1.14 \pm 0.01$  g/100 g with a relative standard deviation of 1.23% (for details see Attachment 1). The Cochran test revealed:  $0.506 < 0.561$  and the ANOVA test showed  $F = 6.443 > 2.848$ . The calculated  $RSD\%_{\text{between}}$  was 1.0%, which was smaller than the  $RSD\%_{\text{max}}$ , as a result it was confirmed that there was no significant difference between the different days. When another analyst conducted the method, the same concentration of vasicine was recorded. The result demonstrated that there was no influence by the analyst or by different concentration levels.

#### 4.2.6 Accuracy of the method

The accuracy was analysed, using three concentration levels (Table 4.9) by spiking the sample with vasicine reference standard. On average,  $102.34 \pm 4.29\%$  of the added vasicine was recovered. The confidence interval was calculated to be 99.04 – 105.64%, which included 100%, therefore, the method could be considered as accurate.

<b>Concentration</b>	<b>Recovery (%)</b>
Level 1	102.45
50% plant material + 25% vasicine	111.48
RS	107.27
Level 2	100.72
50% plant material + 50% vasicine	98.70
RS	98.94
Level 3	100.76
50% plant material + 75% vasicine	101.36
RS	99.39
<b>Average</b>	102.34%
<b>SD</b>	4.29%
<b>95% CI</b>	99.04% - 105.64%

Table 4.9. Results on the accuracy by spiking with vasicine.

#### 4.2.7 Specificity - selectivity

The specificity and selectivity of the quantification method of vasicine was investigated based on its HPLC-DAD analysis. The peak of vasicine in the test solutions, prepared from the *Adhatoda vasica* leaves from Nepal and the EDQM sample, showed the same UV spectrum, with an UV max at 222 nm and 285 nm, as the peak of vasicine in the reference solution. The presence of vasicine in samples from different extracts was confirmed by comparison of the chromatogram of the vasicine standard and the extract (Figure 4.3). Based on their retention time and overlying their UV-spectra the identity of the peak was confirmed, and no co-elution of vasicine and other compounds was detected.

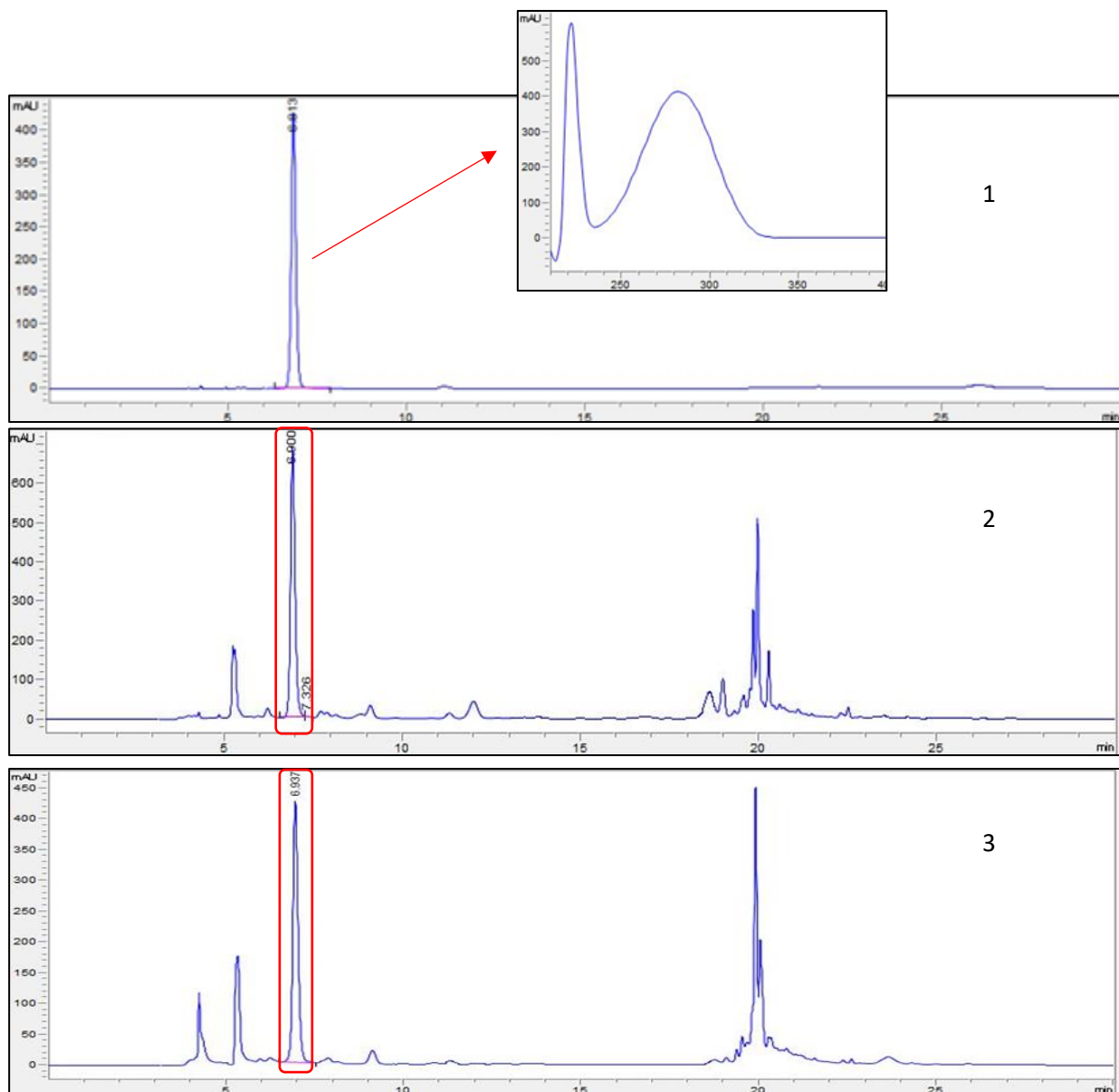


Figure 4.3. Chromatogram of the reference solution vasicine with an UV maximum at 222 nm (1), the *Adhatoda vasica* EDQM sample - test solution (2), and the *Adhatoda vasica* sample from Nepal - test solution (3).

In order to unambiguously verify the specificity for the compound of interest, an additional MS analysis was performed. The LC/MS analysis of the standard solution vasicine (Figure 4.4) and solutions of the two samples (an EDQM sample solution, Figure 4.5 and the solution from the Nepal sample, Figure 4.6) was performed.

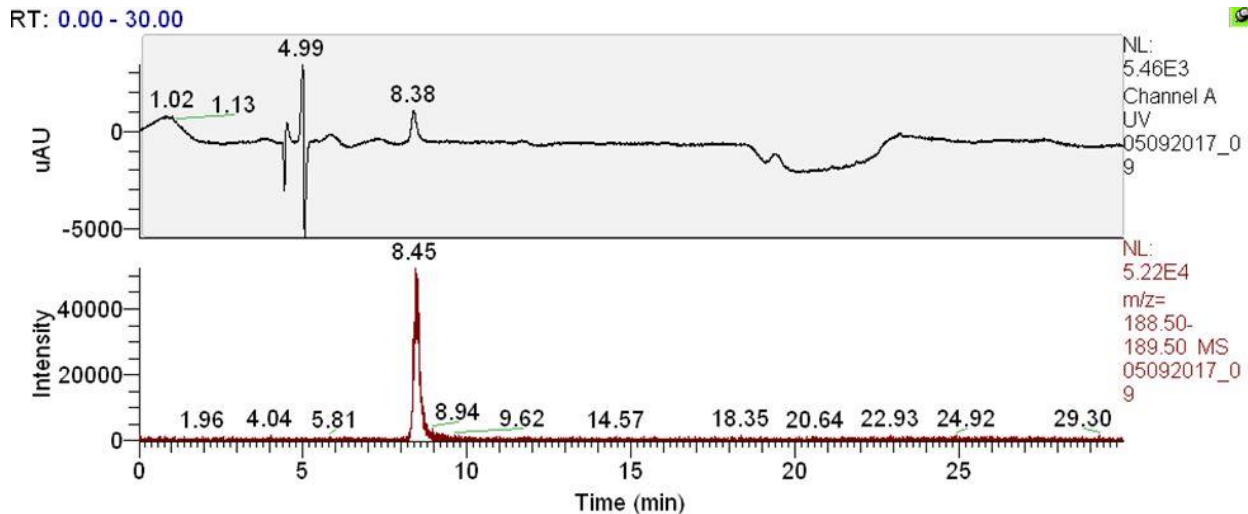


Figure 4.4. Both UV and extracted ion chromatogram ( $m/z$  189  $[M+H]^+$ ) of the standard vasicine solution.

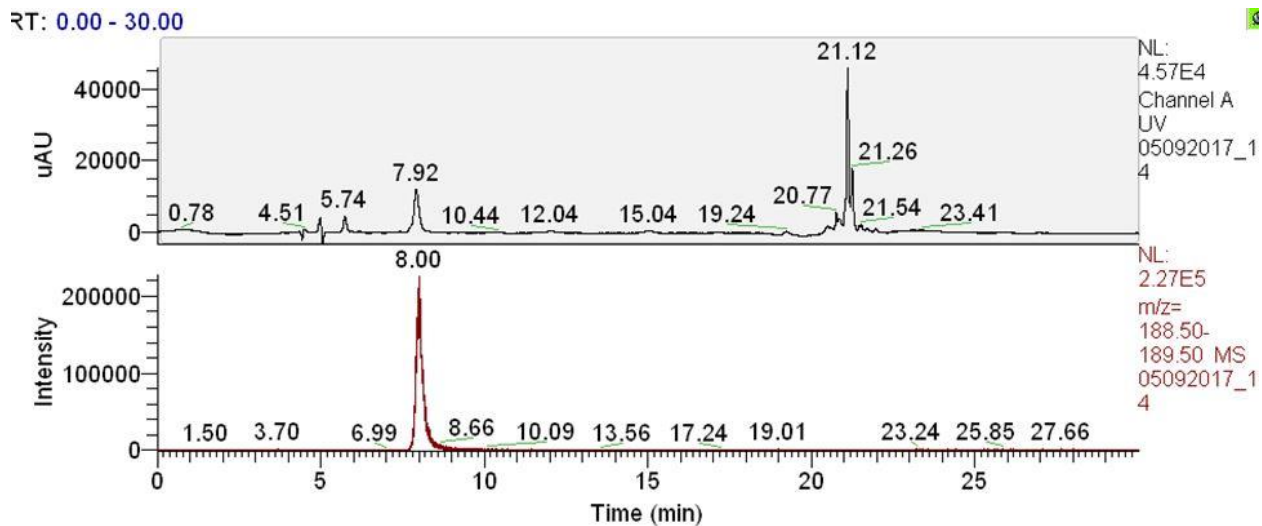


Figure 4.5. Both UV and extracted ion chromatogram ( $m/z$  189  $[M+H]^+$ ) of the EDQM sample solution.

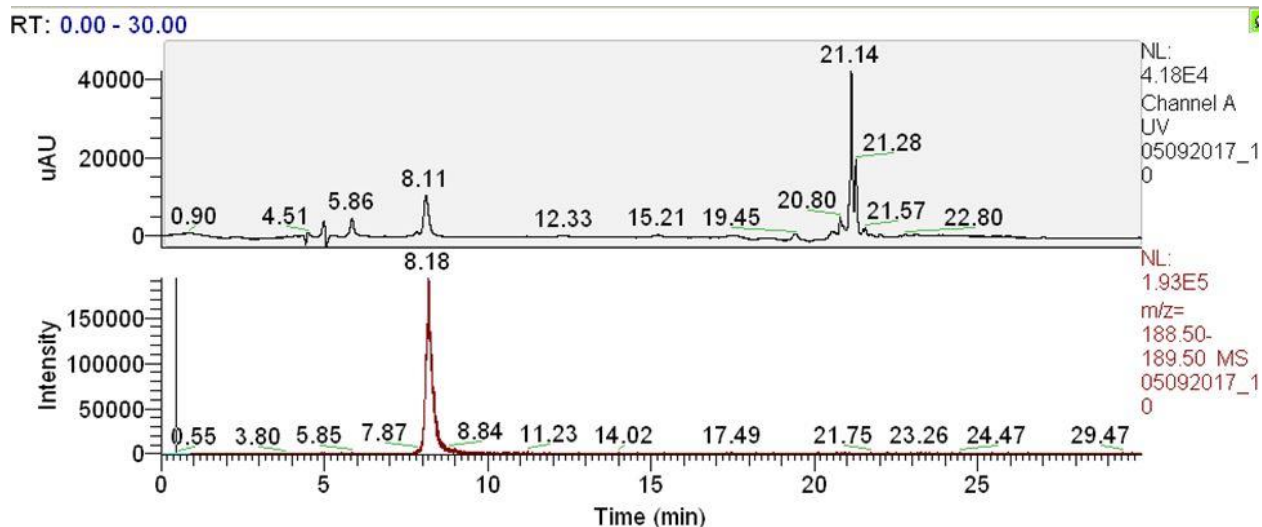


Figure 4.6. Both UV and extracted ion chromatogram ( $m/z$  189  $[M+H]^+$ ) of the Nepal sample solution.

The peak resulting from the vasicine standard ( $m/z$  189  $[M+H]^+$ ) as the peak with a pseudo molecular ion of  $m/z$  189  $[M+H]^+$  were found at the same retention time in the chromatogram for both test samples of EDQM leaves powder and the leaves powder from Nepal. Therefore, it was concluded that vasicine could be clearly discovered in the composition of the analysed plant material, and most importantly, unambiguously confirmed that no co-eluting compounds were present.



## 5. Quantification of vasicine in commercial products

After being finalized, the validated method was applied for quantifying the amount of vasicine in commercial products following the established experimental procedure.

### 5.1 Materials and methods

*Adhatoda vasica* dry leaves powder was obtained from several commercial sources. Firstly, plant powder supplements, which are referred in the thesis as preparation A, preparation B and preparation C. Suggested use for preparation A by the manufacturer was: ½ to 1 teaspoon with warm water, once or twice daily; for preparation B: ¼ to ½ teaspoon with warm water, once or twice daily; and preparation C: ½ to 1 teaspoon two times per day powder with water. Secondly, dietary supplements containing plant(s) powder(s) or plant extract(s): preparation D (capsules, containing seven plant extracts where the amount of *Adhatoda* extract per capsule was 14 mg); preparation E (tablets, containing seventeen plant powders where the amount of *Adhatoda vasica* powder per tablet was 65 mg); preparation F (capsules, containing only *Adhatoda* extract and the declared amount of extract was 400 mg per capsule).

The sample preparation from plant powder followed the procedure described in the Method development (section 3 in this chapter). As for the sample preparation from dietary supplements: The content of two capsules / two tablet masses of the dietary supplement and 50 ml methanol were placed in a 250 ml round-bottom flask and the further steps were the same as for the plant powder. The samples were tested in triplo. The applied chromatographic conditions were previously described in the Final method, section 3.3 (see Table 4.4, “HPLC conditions”). For the quantification of vasicine in samples two reference solutions (a) were used during each measurement and they were injected in the beginning and at the end of the analysis. The area of the vasicine standard was calculated as a mean value of the mean area values of two reference injections at the beginning of the analysis and at the end of the analysis:

$$Area = \frac{\left[ \frac{VR1 + VR2}{2} \right] + VRF}{2}$$

where *VR1* is the area of vasicine reference solution 1<sup>st</sup> injection, *VR2* the area of vasicine reference solution 2<sup>nd</sup> injection and *VRF* the of vasicine reference solution final injection. Then, the area of the standard could be used in calculating the Relative Response Factor (RRF):

$$RRF = \frac{mass * purity}{dilution\ factor * Area * 100}$$

where the mass of the reference product is expressed in grams (g) and the purity of the reference product is presented in percentage (%).

Consequently, the mean Relative Response Factor ( $RRF_{mean}$ ) was used for further calculating the percentage of vasicine in each sample:

$$result\% = \frac{Area * RRF_{mean.} * dilution\ factor * 100}{mass}$$

using the area of vasicine in the tested sample, the  $RRF_{mean}$ , the dilution factor and the mass of the tested sample expressed in grams (g). The final percentages were calculated taking into account the loss on drying (LOD) of the powder:

$$Result\% = \frac{result\% * 100}{100 - LOD}$$

More detailed information on the LOD data for individual samples can be found in Attachment 2.

## 5.2 Validation within flexible scope

Physicochemical analysis according official monographs are developed and validated for a specific analyte in a specific matrix. When such an analyte needs to be determined in a different matrix a validation within a flexible scope (re-validation or validation in lesser extent) should be completed. Therefore, validation with a flexible scope was performed to analyse vasicine with the validated method but present in a different matrix, namely, several commercial products. It was carried out for

preparation D regarding precision and accuracy. The methods and materials, as well as the chromatographic parameters and conditions, were the same as the previously discussed in the method validation part. Also, the preparation of the reference and the test solutions was performed in the same manner as before.

### 5.3 Results and discussion

In contrast to the *Adhatoda* leaves powder, the commercial products like capsules and tablets, can contain other constituents such as different plant extracts and/ or powders, which might influence aspects in the analytical method (i.e., the extraction process, the chromatographic separation). Therefore, it is of high importance to investigate, if the composition of the commercial products would not have an effect on the performance (precision and accuracy) of the validated method. The so called “Flexible scope” or “Flexible validation” was executed for preparation D to analyse the effect of the discussed factors. The standard procedure followed in the precision experiment normally includes analysis of the sample on 3 different concentration levels. In particular, two samples of preparation D on the lowest level and on the highest level, together with three samples on the 100% level of the method were analysed. The mean values, as well as the standard deviation (S) and the relative standard deviation (RSD%) were obtained. The percent vasicine at different concentration levels was calculated: for the 50% level it was  $0.114 \pm 0.003$  (RSD 2.77%), for the 100% level it was  $0.116 \pm 0.005$  (RSD 4.66%) and for the 150% level  $0.121 \pm 0.001$  (RSD 1.23%). The range  $[x_{\max}-x_{\min}]$  of the 7 results should fall within the critical range (95% probability level) and the range  $[x_{\max}-x_{\min}]$  of the 3 results at the 100% levels should fall within the critical range (95% probability level). The total RSD% value (4.40%) from the method validation for repeatability in different concentration levels reported previously was used for calculating the critical range. In the current case, the result could be confirm because for both groups of samples the critical differences were smaller than the critical ranges (see Table 4.6).

<b>&lt;x&gt; (3) =</b>	0.116	RSD method	4.40
<b>s (3)=</b>	0.005	CR 0.95 (3)=	0.0183
		max-min=	<b>0.0100</b>
<b>&lt;x&gt; (7) =</b>	0.117	CR 0.95 (7)=	0.0235
<b>s (7)=</b>	0.005	max-min=	<b>0.0130</b>
<b>RSD%</b>	3.92		

Table 4.6. Critical range values and range for the 3 results at 100% level and all 7 results values.

The accuracy was tested on the 100% concentration level in triplicate. To 50% of the sample  $\pm$  50% standard was added. The obtained recovery values should fall within the accuracy range of the validated method. On average,  $104.8 \pm 6.0\%$  of the added vasicine was recovered. The confidence interval was calculated to be 89.9 - 119.7%, which included the 100% and the method could be considered as accurate. In order to check the precision of the results obtained during the recovery in regard to the general precision of the whole method, an F-test was performed. All 30 values from the total validation were used to calculate the mean, the standard deviation and the variance of the precision ( $0.99\% \pm 0.05$ ,  $2.50E-03$ ). For the validation within the flexible scope only 3 values were used, however, also here the mean the standard deviation and the variance were calculated ( $1.04\% \pm 0.06$ ,  $3.53E-03$ ). The ratio between the variance recovery and the variance precision gave an F-value of 1.41. Theoretically, if the variance of the precision is smaller than the variance of the recovery value, the method is not accepted as accurate. Nevertheless, then the F-value should be compared to a concrete F-critical value and if it is smaller, the procedure is accepted as accurate. In the current test, the F-value was smaller than the F-critical ( $1.41 < 3.328$ ), therefore the procedure was concluded as accurate regarding the specificity-selectivity (Figure 4.7). Additionally, Figure 4.7 presents the chromatogram from preparation D with the UV-spectrum of vasicine (UV maximum at 222 nm).

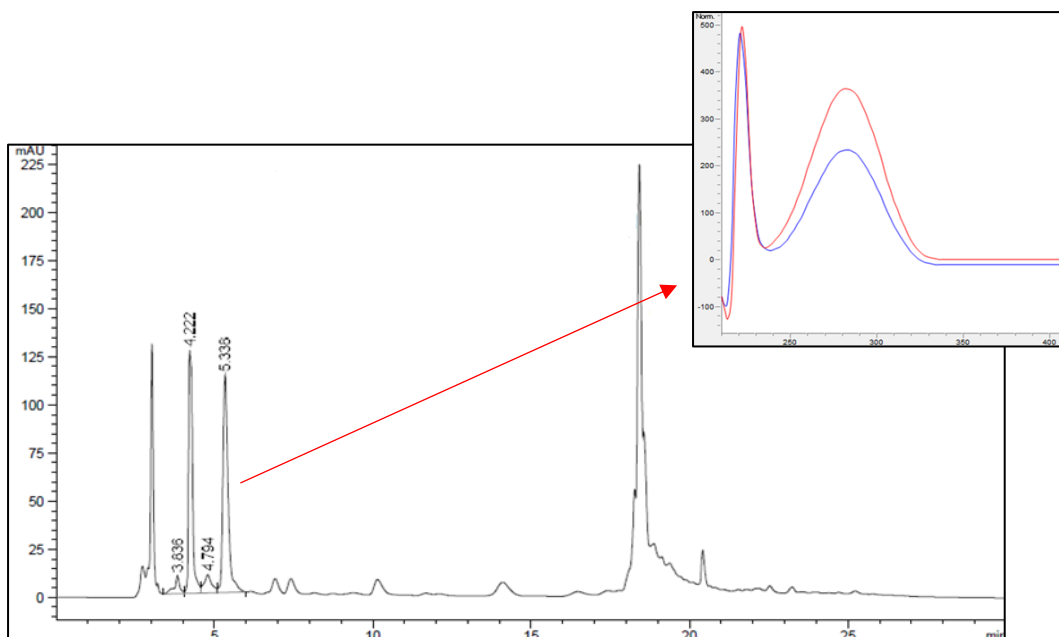


Figure 4.7. Chromatogram from preparation D and comparison between the UV spectrum of vasicine in the standard solution (red) and test solution (blue).

The spectra from both the standard and the vasicine peak in the tested sample were overlaying. Therefore, this proved that the vasicine was present in the tested samples, and most importantly, that the baseline separation of chemical compounds was successful. Regarding preparation E and F, the findings followed a similar pattern (the chromatograms of preparation E and preparation F are presented in Attachment 3 and 4).

The validated method was applied for quantifying vasicine in six commercial products. Attachment 5 contains the results from the uniformity of mass performed for the different dosage forms where the average mass value of one capsule from preparation D was 357.8 mg; for preparation E the average mass value of one tablet was 241.4 mg; and for preparation F the average mass value of one capsule was 406.9 mg. The results of all preparations containing *A. vasica* leaves powder (A – C) and the summary of the obtained results for the dosage forms: the amount of *Adhatoda* extract in each test, the amount of vasicine per tablet and the amount of vasicine in extract in percent for preparation D - E, are included in Table 4.7.

	result (%)	LOD 2h (%)	Result (%)
<b>Preparation A</b>	<b>0.333</b> , 0.007, 2.21	11.63	<b>0.377</b> , 0.008, 2.21
<x>, s, RSD%			
<b>Preparation B</b>	<b>0.778</b> , 0.007, 0.93	6.94	<b>0.836</b> , 0.008, 0.93
<x>, s, RSD%			
<b>Preparation C</b>	<b>0.470</b> , 0.002, 0.51	3.74	<b>0.488</b> , 0.002, 0.51
<x>, s, RSD%			
	result (%)	result (mg)	Result (%)
<b>Preparation D</b>		vasicine	vasicine
		per capsule	in extract
<x>, s, RSD%	<b>0.093</b> , 0.001, 0.84	<b>0.332</b> , 0.002, 0.49	<b>2.371</b> , 0.012, 0.49
<b>Preparation E</b>		vasicine	vasicine
		per tablet	in plant powder
<x>, s, RSD%	<b>0.150</b> , 0.002, 1.62	<b>0.360</b> , 0.003, 0.71	<b>0.554</b> , 0.004, 0.71
<b>Preparation F</b>		vasicine	vasicine
		per capsule	in extract
<x>, s, RSD%	<b>0.134</b> , 0.006, 4.14	<b>0.537</b> , 0.008, 1.54	<b>0.134</b> , 0.002, 1.54

Table 4.7. Vasicine content in three commercial products of *Adhatoda vasica* powder, and vasicine content in formulated products: preparation D - containing *Adhatoda vasica* extract in capsules, preparation E - containing powdered *Adhatoda vasica* plant material in tablets, preparation F – containing *Adhatoda vasica* extract in capsules.

On average, the analysis showed precise and reproducible results of the vasicine amount within a wide range of contents. However, in the six food supplements that were investigated in this work, a substantial difference in the amount of vasicine (Table 4.8) could be observed between the leaves powders and the dosage forms, and within the samples of each group (results ranging from 0.13% till 2.37%). Concerning the powders, a possible explanation might be the different origin of the plant material. Many factors like climate condition, time the material was collected, way of drying, transportation and storage might have an effect on the vasicine content in the final product. In regard to the dosage forms, which contained *A. vasica* extract (preparation D and F), a limiting factor could be the way of extracting the plant material – the extraction solvent, taking into consideration the effect of bright daylight or sunlight on vasicine stability.

<b>Preparation</b>	<b>A</b>	<b>B</b>	<b>C</b>	<b>D</b>	<b>E</b>	<b>F</b>
<b>Vasicine [%]</b>	0.377	0.836	0.488	2.371	0.554	0.134
				per extract	per powder	per extract
<b>s</b>	0.008	0.008	0.002	0.012	0.004	0.002
<b>RSD</b>	2.21	0.93	0.51	0.49	0.71	1.54
<b>Product characteristic</b>	Plant powder	Plant powder	Plant powder	Mix of plant extracts	Mix of plant powders	Plant extract

Table 4.8. Mean value of vasicine content in *A. vasica* - derived products.

Nevertheless, after comparison between the amount of vasicine found in each product (preparation D - F) and the recommended dose by the manufacturer, it was observed that the vasicine intake between the several dosage forms, was approximately in the same range – from 0.996 to 1.074 mg/day (Table 4.9). However, the amount of vasicine, which was administered in the body with the plant powders was significantly different, ranging between 6.71 to 40.60 mg. Despite that the values were higher compared to the vasicine intake with the dosage forms, the manufacturer did not provide additional information about the exact amount of vasicine which is absorbed in the body. Therefore, evaluating the quality and the suggested dose for those plant powders can be made after a detailed study of their bioavailability.

<b>Preparation</b>	<b>Content manufacturer</b>	<b>Dosage manufacturer</b>	<b>Result from the analysis (vasicine, mg)</b>	<b>Intake (vasicine, mg)</b>
<b>A</b>	leaves powder	1/2 teaspoon - 1 teaspoon/1-2 times per day	3.77 mg/1 g powder	6.71 mg – 26.84 mg/day
<b>B</b>	leaves powder	1/4 - 1/2 teaspoon/1-2 times per day	8.36 mg/1 g powder	8.44 mg – 33.94 mg/day
<b>C</b>	leaves powder	1/2-1 teaspoon/2 times per day	4.88 mg/1 g powder	20.30 mg – 40.60 mg/day
<b>D</b>	14 mg extr.	2-3 caps/day for 2-3 months	0.332 mg/caps	0.996 mg/day
<b>E</b>	65 mg powder	3 tabs/day	0.360 mg/tab	1.08 mg/day
<b>F</b>	400 mg extr.	2 caps/day	0.537 mg/caps	1.074 mg/day

*Table 4.9. Comparison between the vasicine intake for the investigated dosage forms containing extract or powder of A. vasica.*

In summary, based on the results obtained in the course of the analysis, the validated method can be applied for unambiguous quantification of vasicine in plant-derived products which would be used to investigate the quality and the supplement intake prescribed by the manufacturer.



## 6. Conclusion

Firstly, a method was optimized for the determination of vasicine in the leaves of *Adhatoda vasica*. The optimization was based on a monograph from the USP and further developed in the NatuRA lab. In particular, the adaptations of the USP method considered some instrument parameters like the column and the mobile phase; also considerable efforts were made for finding the optimal extraction conditions and sample preparation. Due to the risk for autooxidation of vasicine (the main quinazoline alkaloid) to vasicinone that can take place in bright daylight or sunlight, all steps in the experimental procedure were performed protected from light. This consideration was necessary because of their completely different pharmacological activity. After establishing the final method, the procedure was validated according the ICH guidelines regarding linearity, precision, accuracy and specificity. The calibration model was found to be linear in the concentration range of 5.125 to 205 µg/ml. The intermediate precision was determined on eighteen samples of 1.0 g equally divided on three days. The average vasicine content was calculated to be 0.96 g/100g with a relative standard deviation of 0.03%. The precision at different concentration levels was estimated by testing six samples of 0.5 g and six samples of 1.5 g. Those values were compared with the values for the intermediate precision. Regarding the precision at different concentration levels, the average vasicine content of 0.99 g/100g with a RSD% of 0.05% was obtained. The average recovery was found to be 102.34% with a RSD of 4.29%. Finally, the specificity and the selectivity of the method was investigated by applying UV and MS detection. The latter confirm the good chromatographic separation of vasicine without the presence of co-eluting compounds.

Secondly, the study aimed to test whether the validated method for quantification of vasicine in plant material, was applicable for the quantitative determination of vasicine in commercially available products. The test was carried out on six commonly available supplements which contained *Adhatoda vasica* leaves powder, or dosage forms (tablets or capsules) containing *A. vasica* powder or extract. The percentage vasicine in each one of them was successfully obtained. Additionally, to be able unambiguously to apply the method for investigating vasicine in various matrices, a validation within a flexible scope

was required, which was based on an in house protocol in the NatuRA lab. As a result, it was confirmed that the validated method was still precise and accurate for vasicine quantification in matrices that differ from the one used to perform the validation. The experimental conditions were proved to ensure good baseline separation between vasicine and vasicinone, and no co-elution of other compounds in both chromatograms for leaves powder samples and dosage forms products occurred. Based on the presented results, the established method can be efficiently used for the quantification of vasicine in various commercial products in the future. Consequently, providing better understanding of the recommended dosage and the quality of the products. Moreover, the validated method can be applied to determine the different amount of vasicine between the plant parts of *A. vasica*, or plant parts of *A. vasica* collected from different geographical locations, and also, the vasicine content in other plants which have been reported to contain the compound in their phytochemical composition.

## 7. Attachment

### Attachment 1

Vasicine content (g/100g)							
	50% day 1	50% day 2	100% day 1	100% day 2	100% another analyst	150% day 1	150% day 2
<i>Sample 1</i>	1.1601	1.1470	1.1277	1.1403	1.1544	1.1183	1.1259
<i>Sample 2</i>	1.1602	1.1370	1.1343	1.1317	1.1225	1.1251	1.1229
<i>Sample 3</i>	1.1536	1.1617	1.1332	1.1326	1.1339	1.1192	1.1347
<b>Average</b>	1.1580	1.149	1.1318	1.135	1.137	1.1208	1.1278
<b>STDEV</b>	0.0038	0.012	0.0036	0.0047	0.016	0.0037	0.0061
<b>RSD%</b>	0.33%	1.08%	0.32%	0.42%	1.42%	0.33%	0.54%
<b>CI (-)</b>	1.1485	1.1176	1.1229	1.1231	1.0967	1.1117	1.1127
<b>CI (+)</b>	1.1674	1.1795	1.1406	1.1467	1.1771	1.1300	1.1430

Table 4.10. Result for the precision tests.

## Attachment 2

	Mass of weighing bottle [g]			Mass of substance [g]	LOD [g]	LOD [%]
	Empty	Full	After 2 h drying			
1. Preparation A	26.4323	27.4673	27.3466	0.9960	0.1159	11.64
2. Preparation A	25.6119	26.6259	26.5115	1.0350	0.1207	11.66
3. Preparation A	25.8823	26.8783	26.7624	1.0176	0.1180	11.60
1. Preparation B	25.8823	26.8850	26.8148	1.0027	0.0702	7.00
2. Preparation B	25.6120	26.6126	26.5433	1.0006	0.0693	6.93
3. Preparation B	25.4323	27.4605	27.3889	1.0282	0.0707	6.88
1. Preparation C	25.9074	26.9351	26.8964	1.0277	0.0387	3.77
2. Preparation C	25.6116	26.6216	26.5840	1.0100	0.0376	3.72
3. Preparation C	25.8824	26.9053	26.8671	1.0229	0.0382	3.73

Table 4.11. Raw data loss on drying.

### Attachment 3

	Preparation D [mg]	Preparation E [mg]	Preparation F [mg]
1	0.3623	0.2329	0.3992
2	0.3531	0.2370	0.4016
3	0.3593	0.2345	0.3900
4	0.3530	0.2462	0.4035
5	0.3606	0.2345	0.3856
6	0.3709	0.2423	0.4519
7	0.3340	0.2465	0.4292
8	0.3643	0.2477	0.4195
9	0.3405	0.2383	0.3700
10	0.3525	0.2455	0.4055
11	0.3501	0.2528	0.3787
12	0.3530	0.2391	0.4305
13	0.3473	0.2355	0.4016
14	0.3727	0.2414	0.4117
15	0.3733	0.2511	0.3972
16	0.3673	0.2420	0.3957
17	0.3341	0.2455	0.4326
18	0.3636	0.2397	0.4244
19	0.3869	0.2415	0.3777
20	0.3563	0.2335	0.4325
<b>Mean</b>	0.3578	0.2414	0.4069

Table 4.12. Uniformity of mass for preparation D, E and F.

In preparation D, one value exceeded the range (No. 19 – 8.15% more than average value). In preparation E, all values are within the range of limit. In preparation F, two values deviate from the range (No. 6 – 11.06% more than average value; No. 9 – 9.07% less than average value). In general, all samples meet the requirements of the European Pharmacopoeia.

## Attachment 4

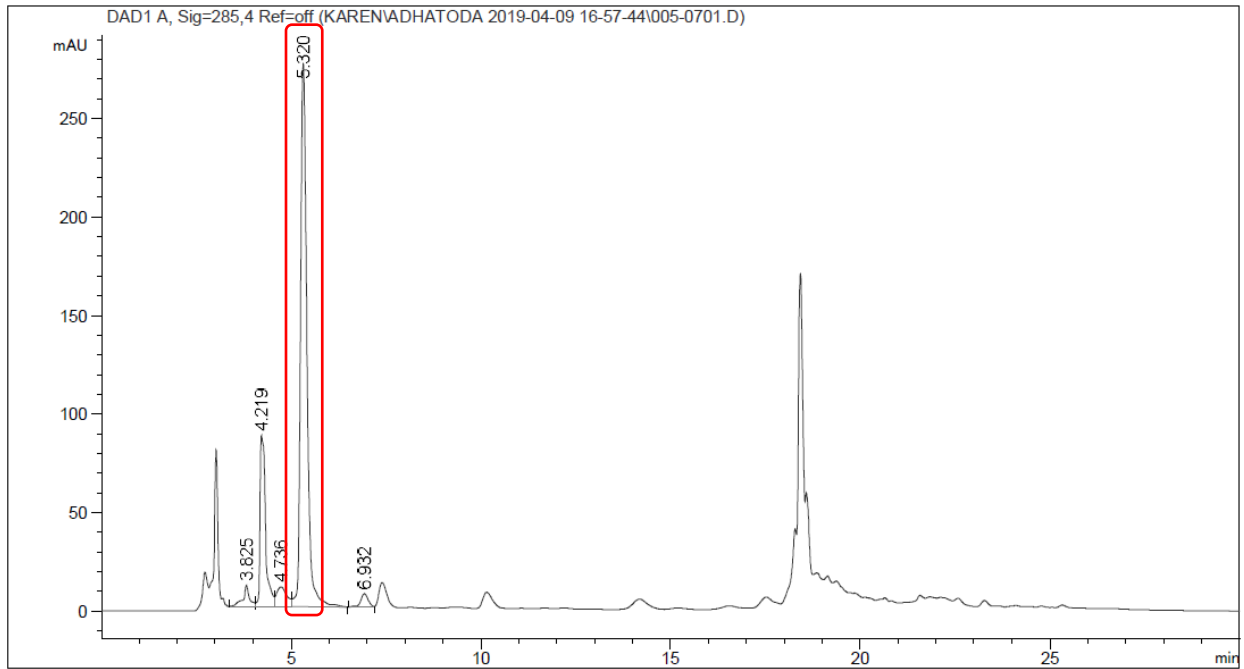


Table 4.13. Chromatogram obtained from preparation E.

## Attachment 5

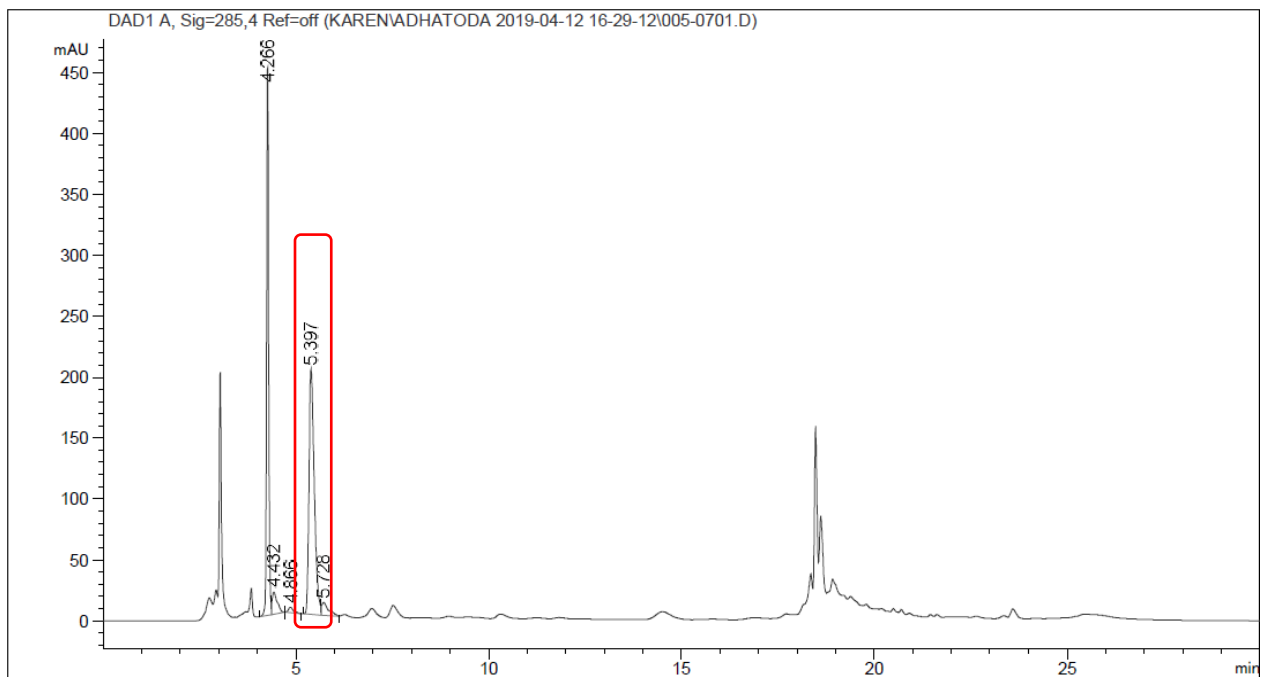


Table 4.14. Chromatogram obtained from preparation F.

# Chapter 5

General assays for detecting AGEs inhibition





## 1. To set the scene

The non-enzymatic protein glycosylation contributes to the pathogenesis of many diseases and the process of normal aging. As one would expect, any inhibitor of glycation can be beneficial for prevention and treatment of pathological conditions and to increase the lifespan. The research in this direction has resulted in establishing *in vitro* models which were used to evaluate the inhibiting properties of various natural compounds. The extrapolation of *in vitro* studies to *in vivo* models is not straightforward due to differences in the conditions of glycation and bioavailability problems.<sup>48</sup> Nevertheless, results obtained in these models permit preliminary screening for potential inhibitors of glycation. The existing methods for measuring AGEs inhibition include: specific fluorescence at defined excitation and emission wavelength; immunochemical (ELISA) and immunohistochemical assays; instrumental methods as high-performance liquid chromatography (HPLC), gas chromatography coupled with mass spectrometry (GS-MS), and liquid chromatography coupled with tandem mass spectrometry (LC-MS/MS). The most abundant ways for AGEs quantification include spectrophotometric measurement of the characteristic increase in absorbance (300 - 400 nm) or fluorescence measurement at particular excitation and emission wavelengths.<sup>182</sup> There are several *in vitro* model systems, which are used to investigate the inhibitory effect of natural products on individual stages of protein glycation process such as the bovine serum albumin (BSA) – methylglyoxal (MGO) assay, BSA – glucose assay and N-acetyl-glycyl-lysine-methyl ester (Gk – peptide) – ribose assay. *In vitro* the phenomenon of glycation is simulated by reaction mixtures including protein and sugar. While sugars (glucose, ribose) and dicarbonyl compounds (MGO) are used as glycated agents, BSA and Gk-peptide represent the amine source. Although Gk is not found in physiological or food systems, it still can serve as a target for glycating agents. In the mentioned techniques, the degree of glycation is analyzed by the development of the characteristic fluorescence signal.<sup>61</sup> The theoretical background for each one is discussed briefly: Serum albumins are the major soluble protein constituents of the circulatory system and have many physiological functions (depot proteins, transporters, metabolism of various exogenous ligands).<sup>183</sup> More specifically, BSA has been the most abundant protein in *in*

*vitro* models due to its structural homology with human serum albumin (HSA). Being a major binding protein for drugs and other physiological substances, BSA is considered as a model protein for studying drug-protein interaction *in vitro*.<sup>183</sup> The **BSA/ glucose experiment** is based on the formation of AGEs by a reaction between BSA, as the model protein, and glucose as the glycating agent. The products are characterized by their specific intrinsic fluorescence after an incubation period of 7 days.<sup>33,61</sup> Alternatively, the **Gk-peptide/ ribose assay** is used to evaluate the ability of the test compounds to inhibit the cross-linking of Gk-peptide - the synthetic peptide, containing a lysine residue, in the presence of ribose, after 24 h incubation.<sup>38,61</sup> Rahbar *et al.* pointed out that co-incubation of Gk-peptide with ribose increases the late glycation products formation. The procedure is expected to generate peptides with advanced Maillard reaction products with dimerization through lysine-lysine cross-linking.<sup>61</sup>

Additionally, other spectroscopic methods include the fructosamine assay and the dicarbonyl entrapment method. Ketoamines (fructosamines) are Amadori products which are formed in the early stages of the glycation process as derivatives of the non-enzymatic reaction between a sugar (usually glucose) and a protein (usually albumin). In the **fructosamine determination assay**, if the tested compounds are able to significantly reduce the amount of fructosamine, it can be deduced that their mode of action relies either on inhibition of the Schiff base or the Amadori products formation. Carbonyl stress is caused by a generalized increase in the concentration of reactive carbonyl precursors of AGEs. Among those,  $\alpha$ -dicarbonyl compounds play a very prominent role.<sup>184</sup> In order to evaluate the **dicarbonyl entrapment** properties of test compounds, the loss of glyoxal in the course of the reaction is monitored in the presence of Girard reagent T (trimethylaminoacetohydrazide chloride), a quaternary ammonium derivative.<sup>60</sup> Under mild acid or alkaline conditions, the reagent reacts with ketones and aldehydes containing  $\alpha$ -dicarbonyl functional group to produce water-soluble compounds which strongly absorb UV light.<sup>185</sup> The reaction is non-enzymatic and, yet, it is very rapid and sensitive. In general, aminoguanidine is the first choice for a positive control in the dicarbonyl assay because dicarbonyl sugar derivatives react rapidly and irreversibly with aminoguanidine to give stable 3-aminotriazine derivatives.<sup>186</sup>

The research line on investigation of AGEs inhibiting properties of natural compounds was initially started in the host institution by Dr. Atul Upadhyay.<sup>99</sup> The reported promising results and the already optimized experimental procedures by Dr. Upadhyay, served as a starting point for evaluating the anti-AGEs activity of isolated pure compounds from *Citrus* species and *Adhatoda vasica* (see Chapter 3). These test models included the bovine serum albumin (BSA)/glucose assay, the fructosamine assay and dicarbonyl entrapment measurement. The complete methodology of these assays is discussed below.

## 2. Materials and methods

### 2.1 Solvents and reagents

Dimethyl sulfoxide (DMSO) and sodium hydroxide were analytical grade and were purchased from Fisher Scientific (Hampton, NH, USA). Bovine serum albumin (98%), nitroblue tetrazolium chloride, sodium azide (99.5%), Girard's reagent T, D-glucose (>99.5%), glyoxal (40 wt. % in water), aminoguanidine were ordered from Sigma Aldrich (Overijse, Belgium). Mangiferin was provided by prof. Wim Vanden Berghe from the PPES (Proteinsciences, Proteomics & Epigenetics Signaling) lab, department of Biomedical Sciences, University of Antwerpen. Sodium dihydrogen phosphate dihydrate was from Merck (Darmstadt, Germany), sodium bicarbonate and sodium formate were from Acros Organic (New Jersey, USA). The Ac-Gly-Lys-OMe acetate salt (Gk-peptide) was provided by Bachem, California, USA. Thiamine was ordered from ChemCruz, (Dallas, Texas) and pyridoxamine dihydrochloride was from Carl Roth (Karlsruhe, Germany). Water was obtained by a Milli-Q system from Millipore (Bedford, USA) and was filtered through a 0.22 µm membrane filter.

### 2.2 Instruments

Measurements of the pH were achieved with SensION (Hach). Incubation at 37 °C was done in a REV SCI (Incufridge) machine. For the AGEs experiments using fluorometry

the fluorescence signal was detected on a Tecan™ Infinite M200 (Giessen, the Netherlands). Black flat bottom 96-well plate were purchased from Greiner Bio-One, Kremsmünster, Austria; and transparent flat-bottom 96-well plate, Thermo Fisher Scientific, Roskilde, Denmark. For the dicarbonyl entrapment experiment a Lambda 35 double beam UV/ VIS spectrophotometer (Perkin-Elmer, Waltham, USA) equipped with a deuterium and a Tungsten lamp was used (UV WinLab™ 6.4 Software).

## 2.3 Methods

### 2.3.1 BSA / glucose assay

As stated in the introduction of the chapter, bovine serum albumin (BSA) derivatives, modified by methylglyoxal and glucose *in vitro*, have been used in many studies as model AGE proteins.<sup>187</sup> The BSA/glucose procedure in the current experiment was similar in many respects to the conditions proposed by Derbré *et al.*<sup>75</sup> Sodium phosphate buffer (500 ml, 50 mM) was prepared (pH 7.4) containing 0.02% (m/V) sodium azide in order to prevent bacterial growth. A 10 ml solution of BSA with a final concentration of 22.2 mg/ml and a 10 ml solution of glucose (1111.1 mM final concentration) were made in phosphate buffer. Aminoguanidine was used as a positive control with final concentrations between 0.1 mM and 10 mM (all solutions were prepared in DMSO).<sup>188</sup> The reaction mixture contained 135  $\mu$ l of the BSA solution, 135  $\mu$ l of the glucose solution and 30  $\mu$ l of the aminoguanidine solution, or test compound in DMSO (*test*, in the formula). The control samples consisted of BSA solution, glucose solution and only DMSO (*control*, in the formula). All samples were incubated at 37 °C for 7 days. The blank samples, where no AGEs formation should be observed, were used to compensate for the possible interference of the fluorescence signal by the test compounds. They were prepared as a parallel set of the previously discussed samples but the incubation was performed at 4 °C instead (*test*, *blank* and *control*, *blank*, respectively, in the formula), a temperature at which no AGEs are formed.<sup>60</sup> Every concentration of the positive control, test compound and blank samples was tested in triplicate. After the incubation, 150  $\mu$ l of the solutions were pipetted into a black flat bottom 96-well plate. The fluorescence intensity of the

reaction products (AGEs) was measured. Measurements were conducted at room temperature with two sets of wavelengths:  $\lambda_{exc}$  of 370 nm and  $\lambda_{em}$  of 440 nm (indicative for vesperlysine-like AGEs as vesperlysine-A, -B, -C, crossline); and  $\lambda_{exc}$  of 335 nm and  $\lambda_{em}$  of 385 nm (indicative for the amount of pentosidine-like AGEs such as pentosidine and argpyrimidine).<sup>188</sup> The percentage inhibition of AGEs formation was calculated using the following formula:

$$\% inhibition = \left( 1 - \frac{RFU_{test} - RFU_{test,blank}}{RFU_{control} - RFU_{control,blank}} \right) \times 100$$

where RFU was the amount of relative fluorescence units.<sup>60</sup>

It is worth to mention that normally DMSO does not inhibit the amount of AGEs formed when its concentration in the incubated mixture remains less than 10% v/v. On the contrary, a level of 30% DMSO can induce the formation of AGEs.<sup>75</sup>

A possible drawback of the described method could be an eventual interference of the test compound with the fluorescence measurement. For example, quenching of the fluorescence signal due to complex formation or interaction between the test molecule and any of the components in the incubation mixture; or autofluorescence characteristics of the molecule itself.<sup>189</sup> As a result, those factors can hinder the accurate measurement of potential anti-AGEs activity. Regarding the use of the method for plant extracts, many secondary metabolites have UV maxima between 300 nm and 400 nm, therefore interference with intrinsic AGEs fluorescence should be considered.<sup>188</sup> Theoretically, interferences can be excluded by using the *test blank* presented in the formula. However, since the quenching and / or the autofluorescence affected the measured fluorescent signal to a great extent, this was not considered appropriate.

The pure compounds tested in the BSA/glucose experiment were vasicine (*Adhatoda vasica*) and nobiletin (*Citrus sinensis*), which were isolated and identified previously (see Chapter 3). Their test concentrations ranged from 0.1 to 5 mM.

### 2.3.2 Fructosamine assay

The chemistry of the fructosamine assay was introduced in details by Baker *et al.*<sup>190</sup> Particularly, the Amadori products reduce the nitro blue tetrazolium (NBT) reagent to a tetrazinoyl radical (NBT<sup>•+</sup>), which disproportionates to a highly colored formazan dye (MF<sup>+</sup>) detected at a characteristic wavelength (530 nm) (Figure 5.1). The first step includes a rearrangement reaction forming the C1-C2 eneaminol, which after the loss of a proton yields the eneaminol anion, and an electron is transferred from the C2 oxygen atom to NBT<sup>2+</sup>, forming NBT<sup>•+</sup>. During this process, it is converted to an eneaminol radical, which then contributes a second electron for reduction of another molecule of NBT<sup>2+</sup>, followed by hydrolysis of the ketoimine adduct to form glucosone. Further enolization and oxidation of glucosone may contribute to the enhanced color typical for the fructosamine assay. In summary, fructosamine reacts with NBT, resulting in oxidation of fructosamine to fructosimine and reduction of NBT to a monoformazan dye.<sup>191</sup> The formation rate of formazan is proportional to the concentration of fructosamine in the samples and a spectrophotometer is used to follow the increase in absorbance at 530 nm over successive 5-min intervals between 0 and 35 min.<sup>190</sup>

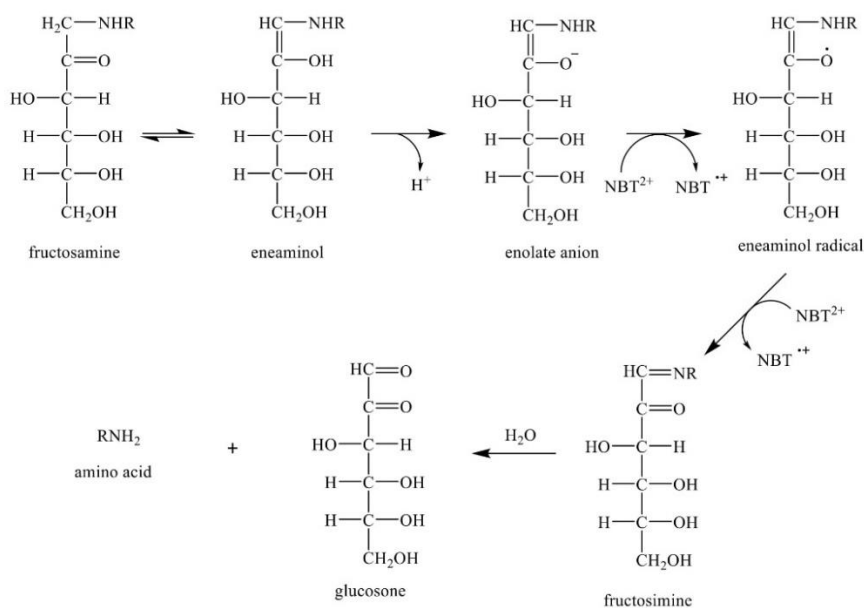


Figure 5.1. Reaction mechanism for formation of glucosone during the fructosamine assay.<sup>190</sup>

For the particular purposes of the research project, the assay was performed using an *in vitro* model where the samples include BSA, glucose and the test compound, following the procedure described by Chompoo *et al.*<sup>192</sup> Aminoguanidine was used as a positive control; the control samples contained DMSO (*control*, in the formula) instead of test compound solution (*test*, in the formula).<sup>99,190</sup> The *control* sample represented the maximum quantity of AGEs formed during the incubation period at 37 °C. Similarly to the BSA/glucose assay, blank samples, where no AGEs are expected, were incubated at 4 °C (for the test compounds *test*, *blank* in the formula; *control*, *blank* only contains DMSO). For all of them the incubation time was 7 days. Then, 100 mM sodium bicarbonate buffer (pH 10.35 at 37 °C) was used to prepare the coloring reagent, i.e. 300 µM nitro blue tetrazolium chloride (NBT) just before measurement. The experiment was performed in transparent flat-bottom 96-well plates where 40 µl of the sample and 160 µl of the freshly made NBT solution were added to each plate. During a 20 min incubation time at 37 °C, the UV absorbance at 530 nm was followed using a Tecan spectrophotometer.<sup>191</sup> To take into account any VIS-absorbance of compounds in the reaction mixture, the absorbance values at 4 °C (no AGEs, namely *control*, *blank*) were subtracted from those at the 37 °C (maximum AGEs formed, namely *control*), resulting in only the formazan VIS-absorbance.

$$\% \textit{ inhibition} = \left( 1 - \frac{A_{\textit{test}} - A_{\textit{test,blank}}}{A_{\textit{control}} - A_{\textit{control,blank}}} \right) \times 100$$

In the formula A is the detected absorbance.

In many published studies, the use of aminoguanidine as a positive control is considered as a critical part in the assay. Aminoguanidine is a hydrazine compound that forms stable hydrazine derivatives with dicarbonyl moieties, in other words, it is inhibiting another part of the AGEs formation and it is not feasible to be used as a positive control in this assay. Moreover, it has been reported that high concentrations of aminoguanidine can actually lead to an increase in the fructosamine formation.<sup>190</sup> Therefore, beside evaluating the fructosamine inhibiting properties of test compounds, a separate investigation for a new positive control in the assay was carried out. The test compounds in the fructosamine experiment were vasicine (concentration range 0.1 to 5 mM) from *Adhatoda vasica* and

nobiletin (concentration range 0.5 to 5 mM) from *Citrus sinensis*, which were previously obtained (see Chapter 3). All samples were prepared and measured in triplicate. Based on literature, pyridoxamine (concentration range 15 to 25 mM), thiamine (concentration range 15 to 25 mM) and mangiferin (concentration range 0.1 to 10 mM, and 1.5 to 5 mM), were selected as potential candidates for a positive control.<sup>50,193,194</sup>

### 2.3.3 Dicarbonyl measurement

In order to study the dicarbonyl entrapment properties of test compounds, the loss of glyoxal (GO) during the course of the reaction is monitored. Aminoguanidine, the agent used as a positive control in the experiment, forms adducts with GO and, therefore, the relative amount of reactive GO left decreases sharply within the first two hours. During the GO-BSA interaction, aminoguanidine entraps GO and the amount of reactive GO remaining for the interaction with BSA to form AGEs is much less, and hence, the formation of the GO-BSA complex is reduced. When a test compound cannot entrap GO the amount of reactive GO left for the formation of Girard-T ((carboxymethyl)trimethylammonium chloride hydrazide) adduct is higher (Figure 5.2). The maximum absorbance is reached after 10 min and the product is stable for at least 30 min.

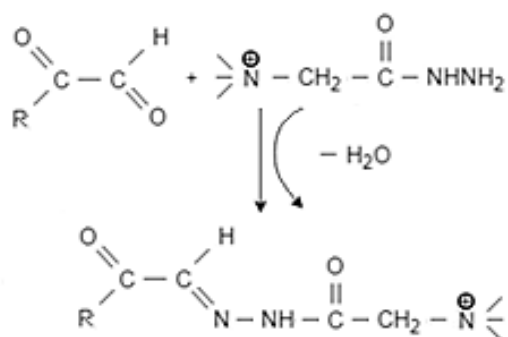


Figure 5.2. Reaction between  $\alpha$ -dicarbonyl and the Girard-T reagent.<sup>184</sup>

The fact that conversion to triazine derivatives in AGEs formation is rapid, that these produced triazines are stable, and that aminoguanidine reacts only slowly and reversibly



with D-glucose, confirms that it would be useful as a reagent to react with dicarbonyl intermediates produced in the Maillard reaction and to allow their quantitation during such reactions.

Normally, the GO entrapment assay is performed in a two-steps procedure following Upadhyay *et al.* with slight modifications.<sup>60</sup> To begin with, to 1000  $\mu\text{l}$  GO (1.1 mM solution in sodium phosphate buffer, see the BSA/glucose experiment), 200  $\mu\text{l}$  of the test compound or aminoguanidine (1 mM solution in DMSO) and 800  $\mu\text{l}$  sodium phosphate buffer was added (*test* in the formula). The *test blank* samples contained only 200  $\mu\text{l}$  test compound or aminoguanidine and 1800  $\mu\text{l}$  sodium phosphate buffer. The *control* sample was prepared using 1000  $\mu\text{l}$  GO, 800  $\mu\text{l}$  sodium phosphate buffer and 200  $\mu\text{l}$  DMSO. All samples were incubated at 37 °C and at time points 0, 5, 10, 15, 30, 45, 60, 75, and 90 min, 100  $\mu\text{l}$  sample was taken and then frozen at -80 °C until further processing. The test was performed in triplicate for each time point.

In the second part of the test, 850  $\mu\text{l}$  of sodium formate buffer (500 mM, pH 2.9) and 50  $\mu\text{l}$  of a 500 mM solution of Girard – T reagent in sodium formate buffer were added to each sample (final volume 1.0 ml). Afterwards, they were incubated for 10 min at room temperature, which was followed by measuring the UV absorbance at 290 nm using a Genesys-10 UV spectrophotometer (Thermo Fisher Scientific). One sample was prepared by adding 200  $\mu\text{l}$  DMSO to 1800  $\mu\text{l}$  phosphate buffer, kept at room temperature, and used to set the spectrophotometer to zero (solvent control). The percent of GO entrapment was calculated by the following formula:<sup>60</sup>

$$\% \text{ GO entrapment} = \left( 1 - \frac{A_{\text{test}} - A_{\text{test,blank}}}{A_{\text{control}}} \right) \times 100$$

where A was the absorbance being measured. The *test blank* sample was used to subtract the VIS absorbance of the test compound in order to obtain the absorbance that is only caused by the reaction product between GO and the Girard-T reagent.

The test compounds in the dicarbonyl entrapment assay were vasicine (from *Adhatoda vasica*) and nobiletin (from *Citrus sinensis*), which were isolated and identified previously (see Chapter 3). Their test range was between 0.1 to 10 mM (final concentration) for

vasicine, and between 0.1 to 5 mM for nobiletin (final concentration). Aminoguanidine was tested in a final concentration range of 0.01 – 5.0 mM.

## 2.4 Statistical analysis

The statistical analysis of the data was performed using SPSS (IBM Corporation, Armonk, NY USA) 26 version software. One-way Analysis of Variances (ANOVA) ( $p < 0.05$ ) and Kruskal-Wallis H test were used to determine the significance of differences between means.

## 3. Results and discussion

### 3.1 BSA/ glucose assay

The first compound tested in the BSA/glucose experimental model was vasicine. Figure 5.3 shows the fluorescence results for the different concentrations of aminoguanidine, as a positive control, and vasicine being tested with the first set of wavelengths, where the “control” presents the maximum AGEs formed, and the “control blank” refers to the non-AGEs forming samples.

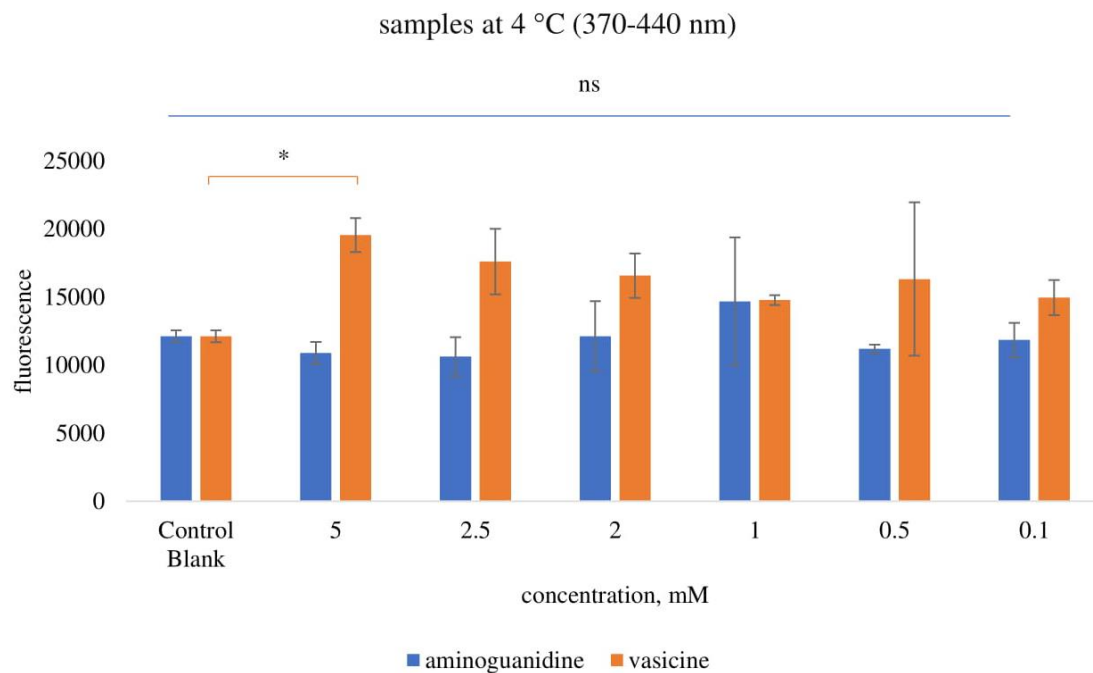
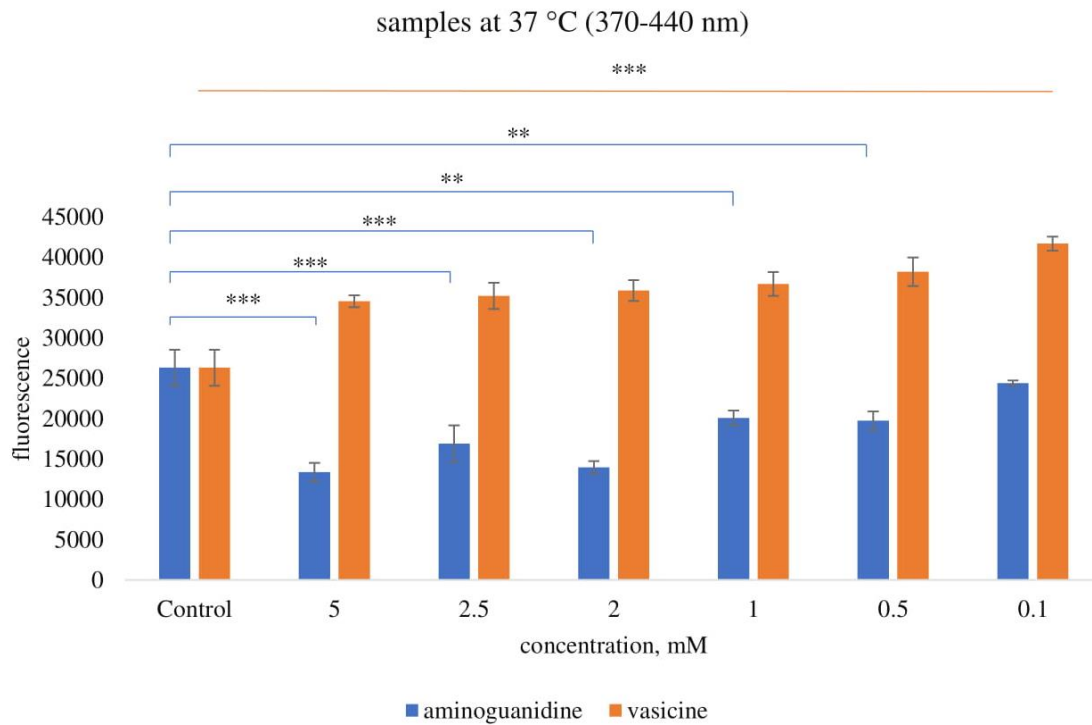


Figure 5.3. Effect of aminoguanidine and vasicine on AGEs formation in BSA/ glucose assay (370-440 nm). The figures represent mean  $\pm$  SD of three replicates, and the experiment was performed only once ( $n=1$ ). The statistically significant difference between samples is included: \* -  $p < 0.05$ , \*\* -  $p < 0.01$ , \*\*\* -  $p < 0.001$ , ns - not significant.

The data from the 370 – 440 nm experiments showed that the fluorescence signal, indicating the presence of AGEs, for all concentrations of vasicine was much higher than the control samples at 4 °C and 37 °C. Since at 4 °C formation of AGEs was not expected, the fluorescence values higher than the blank, seem to indicate autofluorescence properties of the test compound. Similarly, since the 37 °C control sample normally contain the maximum level of AGEs (no inhibitor present), again it was speculated that the test compound possessed autofluorescence properties. This idea was also confirmed by the results at 37 °C were all concentrations had higher fluorescence than the control, which should have the highest value in those incubation conditions. However, although vasicine might have autofluorescence properties, the test samples incubated at 37 °C showed a concentration dependent decrease of the fluorescence signal, suggesting that the test compound indeed had anti-AGEs properties but the current method was inadequate to calculate an IC<sub>50</sub>. Therefore, the activity of vasicine against AGEs formation had to be investigated through another technique. Statistically significant differences between groups regarding vasicine incubated samples at 37 °C (370 – 440 nm) was shown by one way – ANOVA ( $p < 0.001$ ). A Bonferroni post hoc test was performed to ascertain which pairs of groups differ significantly from one another, which revealed the presence of statistically significant differences between the control and all concentrations of vasicine ( $p < 0.001$ ) (Figure 5.3). After a Bonferroni's multiple comparison test regarding the vasicine samples incubated at 4 °C (370 – 440 nm) a statistically significant difference was found between the control blank and 5 mM vasicine,  $p = 0.027$  (Figure 5.3).

Additionally, the results from the other set of wavelengths are presented in Figure 5.4.

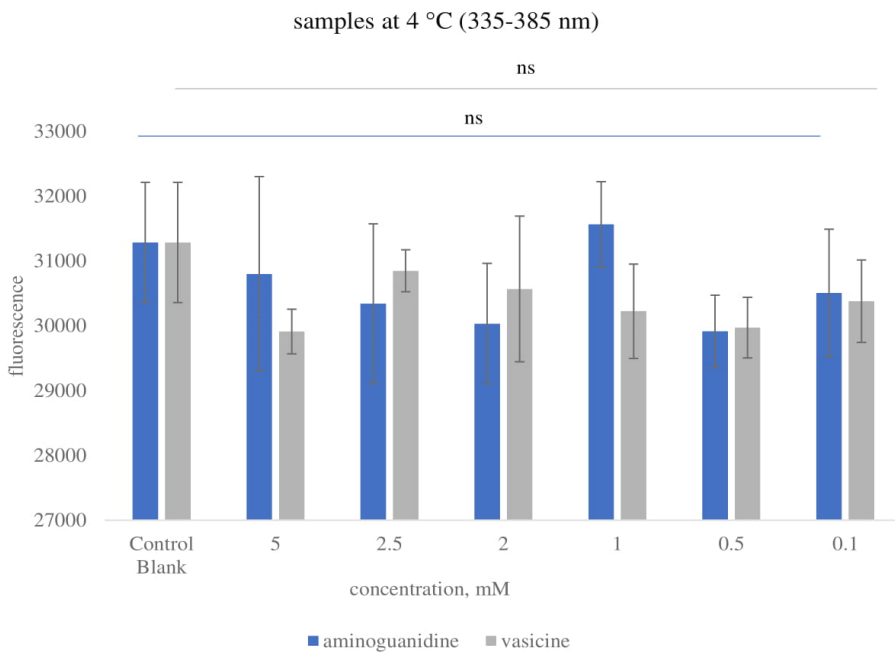
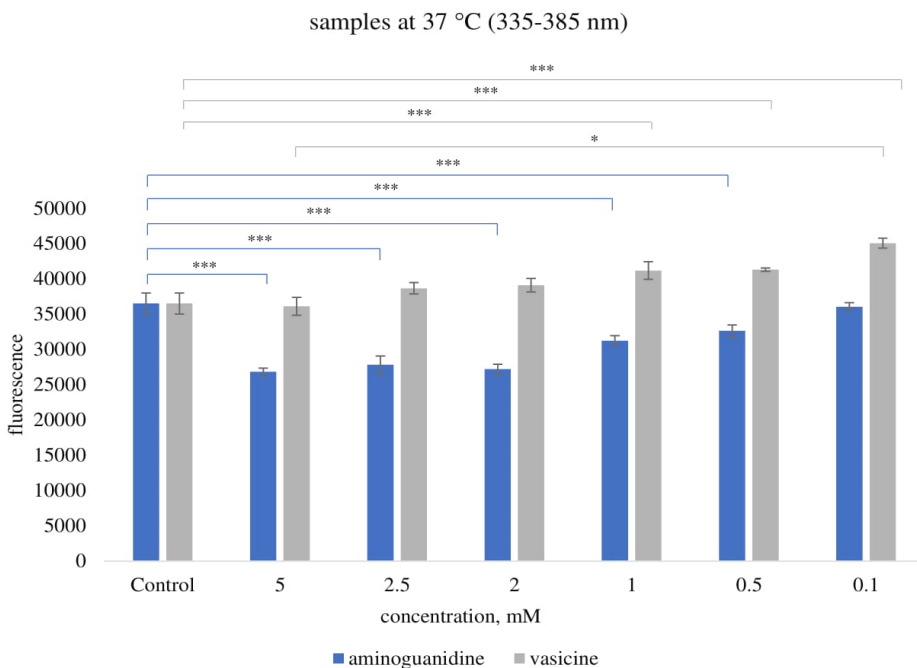


Figure 5.4. Effect of aminoguanidine and vasicine on AGEs formation in BSA/ glucose assay (335-385 nm). The figures represent mean  $\pm$  SD of three replicates and the experiment was performed only once ( $n=1$ ). The statistically significant difference between samples is included: \* -  $p < 0.05$ , \*\* -  $p < 0.01$ , \*\*\* -  $p < 0.001$ , ns - not significant.

Although the fluorescence at 4 °C showed inconsistent results for all different concentrations of vasicine, at 37 °C the same concentration dependent decrease was detected but with a fluorescence signal higher than the control. Statistically significant differences between groups regarding vasicine samples incubated at 37 °C (335 – 385 nm) were shown by one way – ANOVA ( $p < 0.001$ ). A Bonferroni post hoc test was performed to ascertain which pairs of groups differ significantly from one another, which revealed the presence of statistically significant differences between many groups (e.g., between the control and 0.1 mM, 0.5 mM and 1 mM vasicine,  $p < 0.001$ ) (Figure 5.4). A Kruskal-Wallis H test was conducted in order to determine, if there were statistically significant differences between the several concentrations of vasicine. Dunnett multiple comparison showed that there were statistically significant differences between 5 mM and 0.1 mM vasicine ( $p < 0.05$ ). Concerning the vasicine samples incubated at 4 °C (335 – 385 nm), no statistical significance was found between the values (Figure 5.4).

Regarding the positive control samples with aminoguanidine incubated at 37 °C (370-440 nm wavelength), a dose-dependent decrease was observed and the values for all concentrations were lower than the control. At 4 °C although fluctuation of the values was present, they were below the value of the *control blank*, therefore it was concluded that no AGEs were formed in any of the samples. The observations for aminoguanidine samples measured at 335-385 nm were the same as at the previous wavelength. Statistically significant differences between groups regarding aminoguanidine samples incubated at 37 °C (370 – 440 nm) were shown by one way – ANOVA ( $p < 0.001$ ). A Bonferroni post hoc test was performed to ascertain which pairs of groups differ significantly from one another, which revealed the presence of statistically significant differences between the control and all concentrations of aminoguanidine except 0.1 mM (e.g., between the control and 0.5 mM aminoguanidine,  $p = 0.017$ , control and 2 mM, 2.5 mM, 5 mM,  $p < 0.001$ ) (Figure 5.3). Statistically significant differences between groups regarding aminoguanidine samples incubated at 37 °C (335 – 385 nm) were shown by one way – ANOVA ( $p < 0.001$ ). A Bonferroni post hoc test was performed to ascertain which pairs of groups differ significantly from one another, which revealed the presence of statistically significant differences between the control and all concentrations of aminoguanidine ( $p < 0.001$ ) except the 0.1 mM concentration (see Figure 5.4). However,

no statistically significant differences between groups regarding aminoguanidine samples incubated at 4 °C (370 – 440 nm) ( $p < 0.387$ ) and at 4 °C (335 – 385 nm) ( $p < 0.403$ ) were found by the one way – ANOVA (Figure 5.3 and Figure 5.4).

In summary, vasicine clearly showed inhibition of the formation of AGEs in the BSA/glucose assay, but calculation of an actual % inhibition is not possible due to its autofluorescent properties. The percent inhibition for both compounds in the two wavelengths was calculated and the data from the 370-440 nm was used to obtain the  $IC_{50}$  value for aminoguanidine (Figure 5.5) which was around 2 mM. The second wavelength could not be used to monitor the activity of the compound because the values for aminoguanidine were higher than 100% (Figure 5.6).

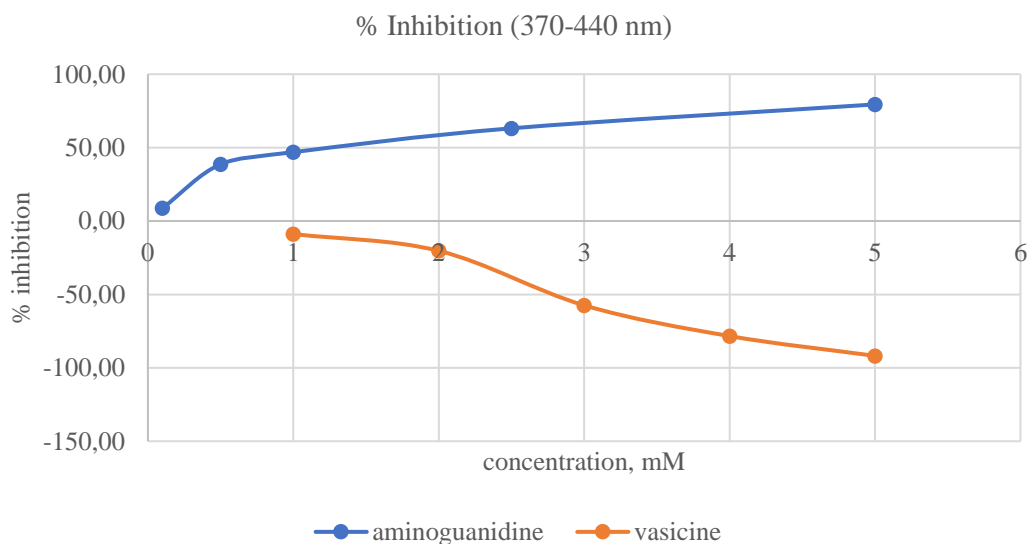


Figure 5.5. Results for the calculated percent inhibition for aminoguanidine and vasicine tested in the BSA/glucose experiment (370-440 nm).

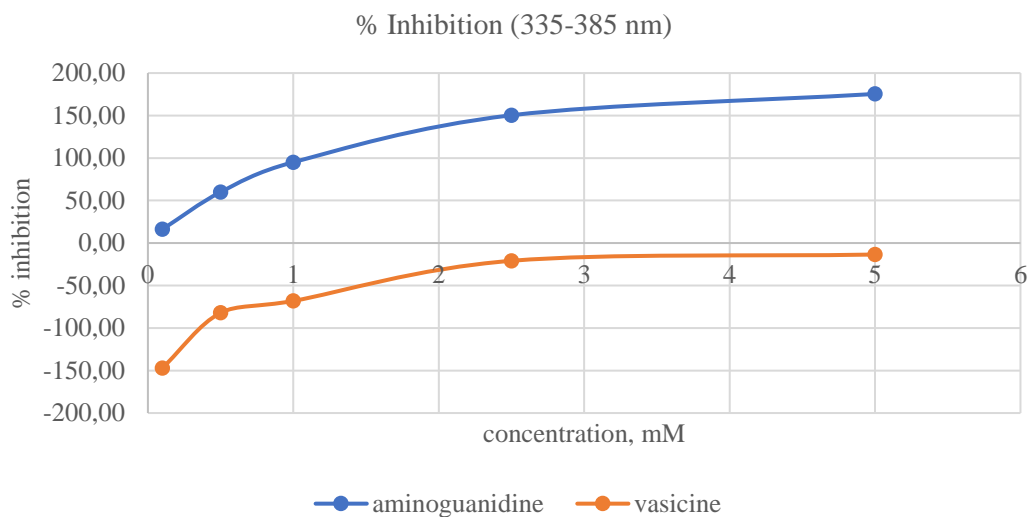


Figure 5.6. Results for the calculated percent inhibition for aminoguanidine and vasicine tested in the BSA/glucose experiment (335-385 nm).

Three different hypotheses could be raised why this autofluorescence occurs: (1) due to a complex formation between vasicine and the protein (BSA), or (2) between vasicine and the sugar (glucose), or (3) as a property of the test molecule itself. Therefore, in order to address this question, another experiment was conducted where vasicine was incubated in a mixture containing only BSA in buffer solution (Figure 5.8), or only glucose (Figure 5.9), or without the presence of any protein or sugar but only in buffer (Figure 5.7). The samples were treated according to the established procedure for the BSA/glucose assay.



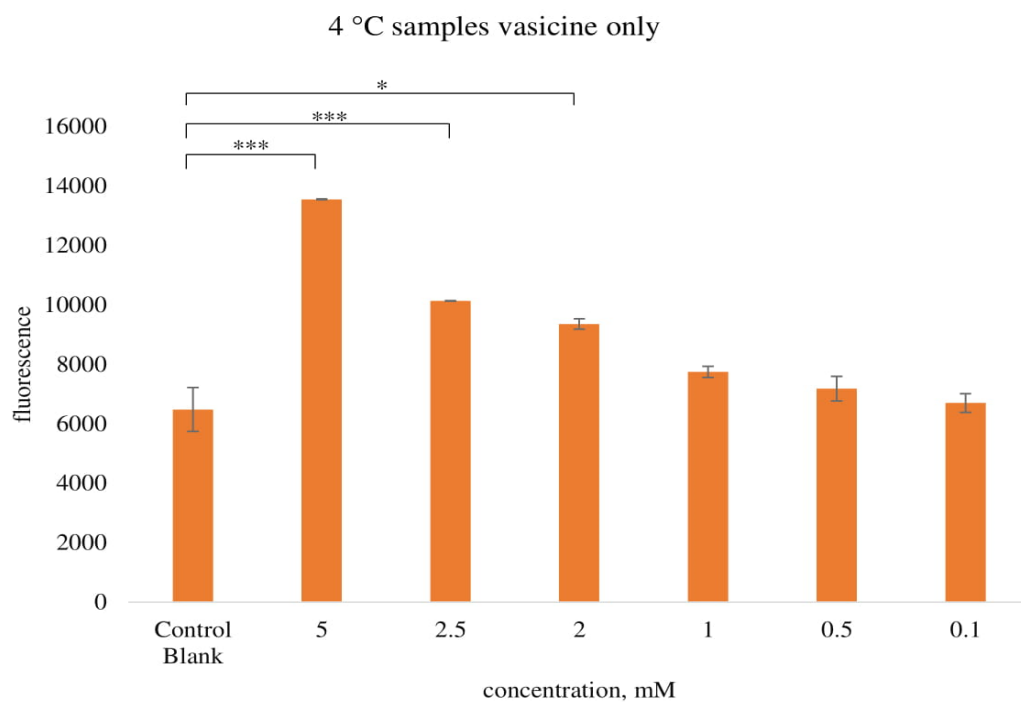
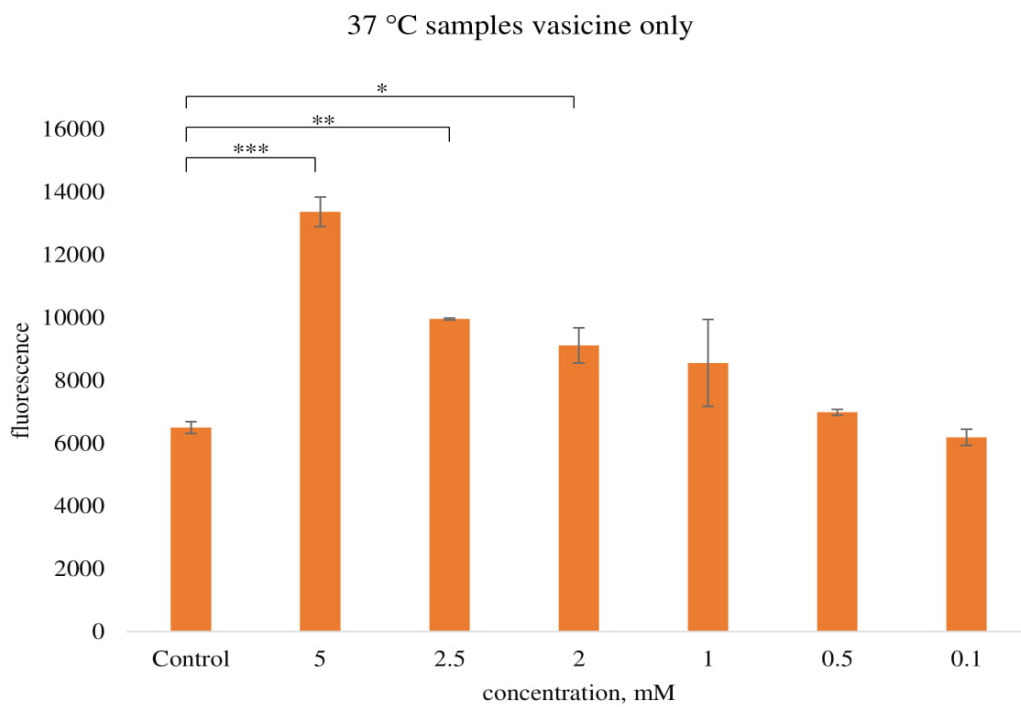
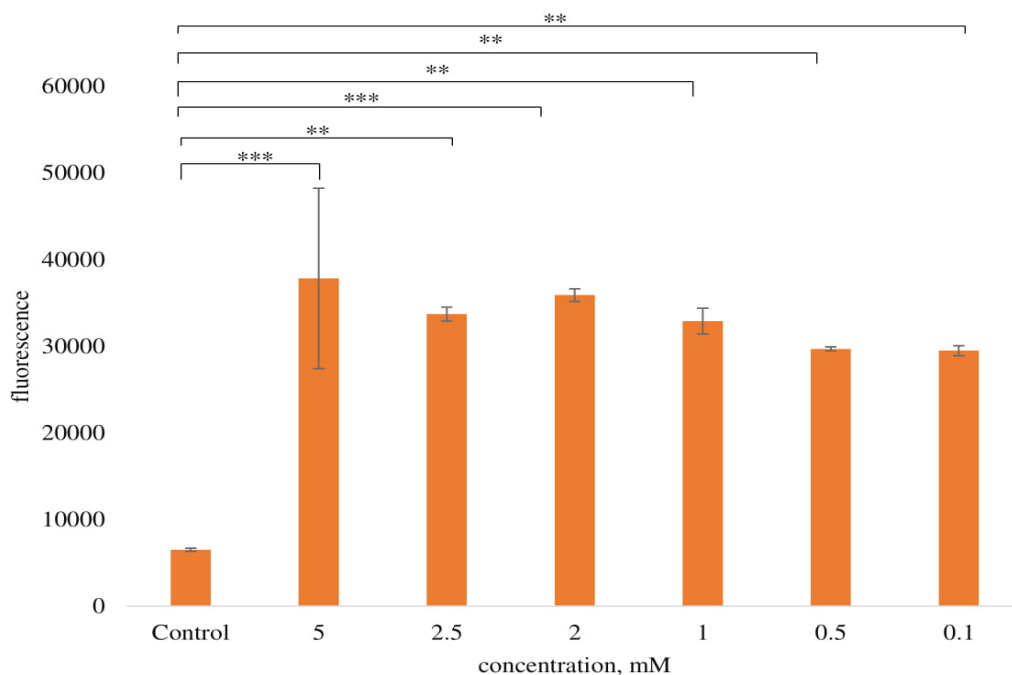


Figure 5.7. Samples containing different concentrations of vasicine only in buffer measured at 370 – 440 nm. The figures represent mean  $\pm$  SD of three replicates and the experiment was performed only once ( $n=1$ ). The statistically significant difference between samples is included: \* -  $p < 0.05$ , \*\* -  $p < 0.01$ , \*\*\* -  $p < 0.001$ , ns - not significant.

Figure 5.7 shows that the graphs from testing only vasicine at different concentrations in buffer solution followed similar pattern for both temperatures. The values were higher than the control (only DMSO in phosphate buffer) and in general an increase of the signal was observed with an increasing concentration of the compound. Also, it could be concluded that the autofluorescence of vasicine was not temperature dependent. Statistically significant differences between groups regarding vasicine in buffer solution incubated at 37 °C (370 – 440 nm) were shown by one way – ANOVA ( $p < 0.001$ ). A Bonferroni post hoc test was performed to ascertain which pairs of groups differ significantly from one another, which revealed the presence of statistically significant differences for instance between control and 2.5 mM vasicine,  $p = 0.015$ , control and 5 mM vasicine,  $p < 0.001$  (Figure 5.7). Statistically significant differences between groups regarding samples with only vasicine in buffer solution incubated at 4 °C (370 – 440 nm) was shown by one way – ANOVA ( $p < 0.001$ ). A Bonferroni post hoc test was performed and it revealed the presence of statistically significant differences between the control blank and 2 mM vasicine,  $p = 0.002$ , control blank and 2.5 mM vasicine,  $p < 0.001$  and control blank and 5 mM vasicine,  $p < 0.001$ . For the rest of the groups no significant difference was observed (Figure 5.7).

37 °C samples vasicine and BSA



4 °C samples vasicine and BSA

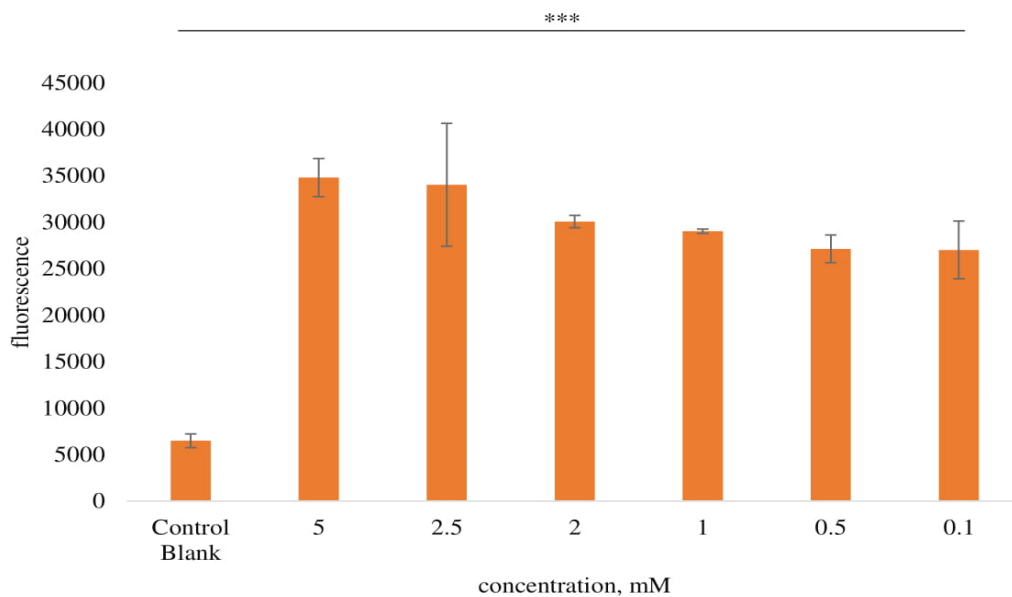
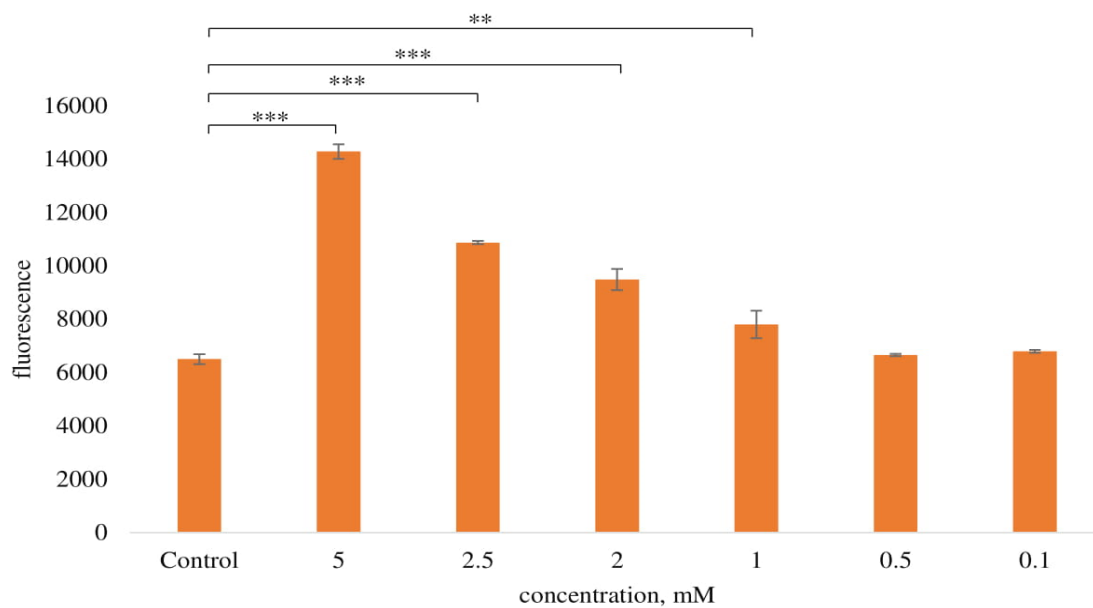


Figure 5.8. Samples containing different concentrations of vasicine with BSA in buffer measured at 370 – 440 nm. The figures represent mean  $\pm$  SD of three replicates and the experiment was performed only once. The statistically significant difference between samples is included: \* -  $p < 0.05$ , \*\* -  $p < 0.01$ , \*\*\* -  $p < 0.001$ , ns - not significant.

The samples which contained vasicine only in a BSA buffer solution (Figure 5.8), though concentration dependent, demonstrated excessively higher values than the control (DMSO and buffer). The result for the test solutions may be explained by the high fluorescence of BSA itself, in contrast to the *control / control blank* samples (containing only DMSO in buffer for both temperatures) where it was absent. Statistically significant differences between groups regarding vasicine and BSA at 37 °C (370 – 440 nm) were shown by one way – ANOVA ( $p = 0.001$ ). A Bonferroni post hoc test revealed the presence of statistically significant differences between the control and all concentrations of vasicine in the presence of BSA (control and 0.1 mM, 0.5 mM vasicine,  $p = 0.003$ ; control and 1 mM, 2.5 mM vasicine,  $p = 0.001$ ; control and 2 mM, 5 mM vasicine,  $p < 0.001$ ) (Figure 5.8). Statistically significant differences between groups regarding vasicine and BSA samples at 4 °C (370 – 440 nm) were presented by one way – ANOVA ( $p < 0.001$ ). A Bonferroni post hoc test revealed the presence of statistically significant differences between the control blank and all concentration of vasicine in the presence of BSA,  $p < 0.001$  (Figure 5.8).

### 37 °C samples vasicine and glucose



### 4 °C samples vasicine and glucose

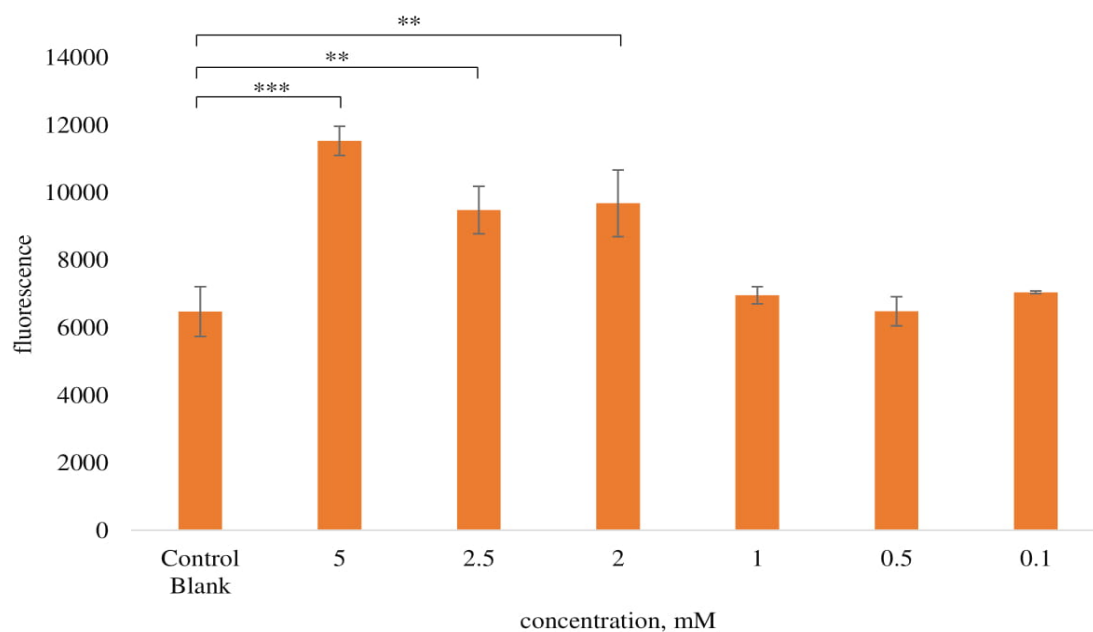


Figure 5.9. Samples containing different concentrations vasicine and glucose in buffer measured at 370 – 440 nm. The figures represent mean  $\pm$  SD of three replicates and the experiment was performed only once. The statistically significant difference between samples is included: \* -  $p < 0.05$ , \*\* -  $p < 0.01$ , \*\*\* -  $p < 0.001$ , ns - not significant.

The outcome from the samples with vasicine and glucose buffer solution was similar to those containing only vasicine (Figure 5.9). Statistically significant differences between groups regarding vasicine and glucose at 37 °C (370 – 440 nm) were shown by one way – ANOVA ( $p < 0.001$ ). A Bonferroni post hoc test revealed the presence of statistically significant differences between the control and 1 mM concentrations of vasicine in the presence of glucose,  $p = 0.046$ , between the control and 2 mM vasicine,  $p < 0.001$ , control and 2.5 mM vasicine,  $p < 0.001$  and control and 5 mM vasicine,  $p < 0.001$  (Figure 5.9). Statistically significant differences between groups regarding vasicine and glucose at 4 °C (370 – 440 nm) were shown by one way – ANOVA ( $p < 0.001$ ). A Bonferroni post hoc test revealed the presence of statistically significant differences between the control blank and 2 mM concentration of vasicine in the presence of glucose,  $p = 0.020$ , control blank and 2.5 mM,  $p = 0.030$  and control blank and 5 mM,  $p < 0.001$  (Figure 5.9). The graphs from the autofluorescence study for vasicine at 370 – 440 nm are summarized in Figure 5.10.

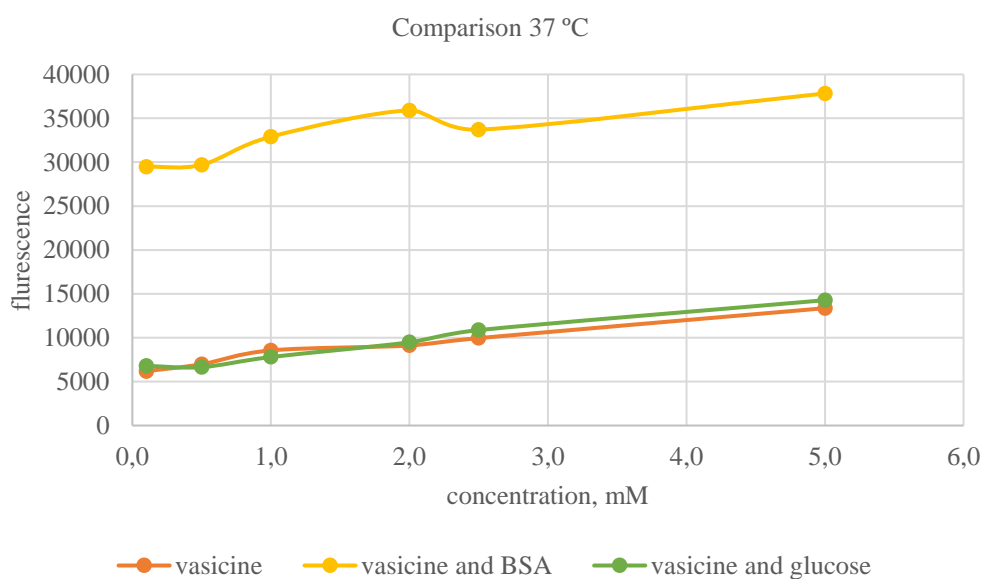


Figure 5.10. Comparison between the different sample sets at 37 °C in the autofluorescence study for vasicine measured at 370 - 440 nm wavelength.

However, interesting observations were made when the same samples were analyzed at the other set of wavelength namely, 335 – 385 nm (Figure 5.11 – 5.13).

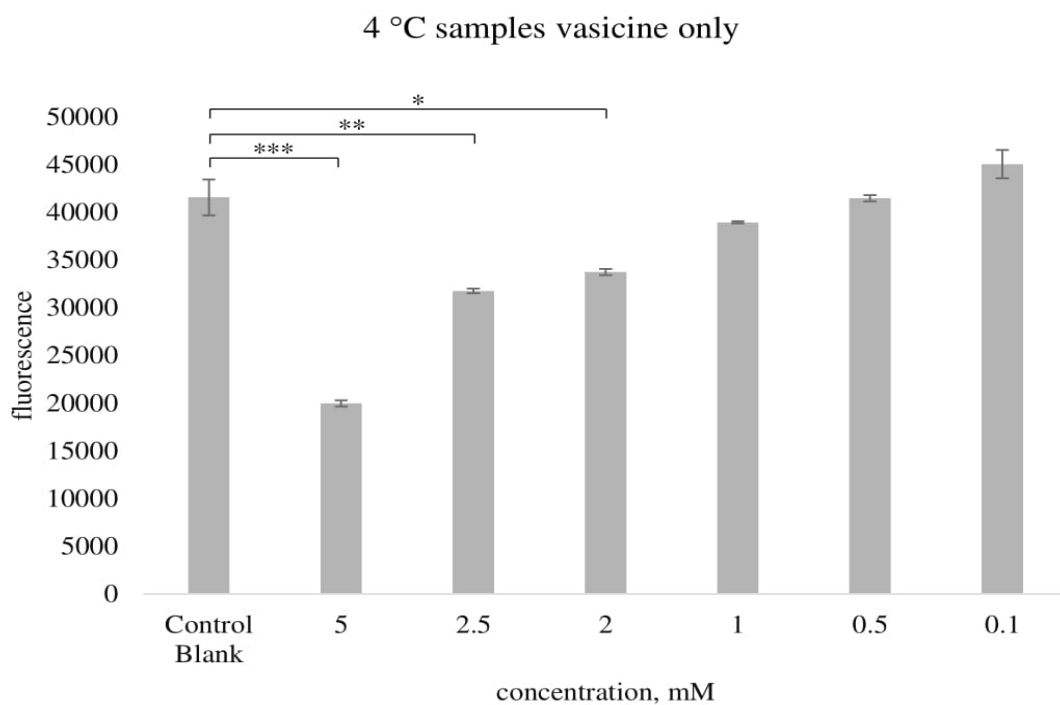
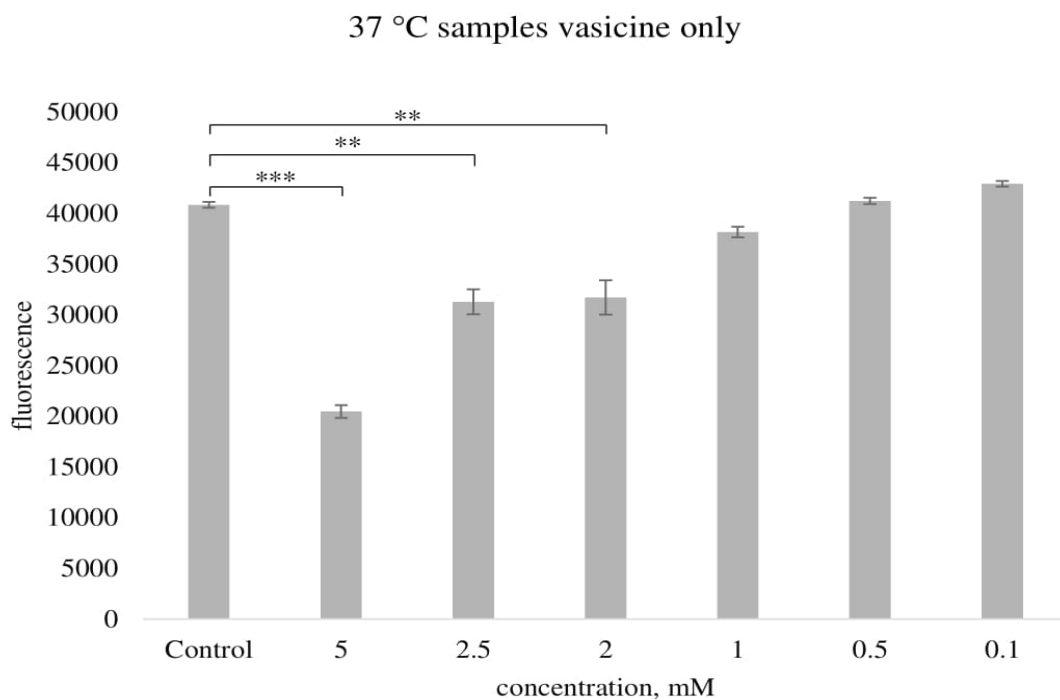
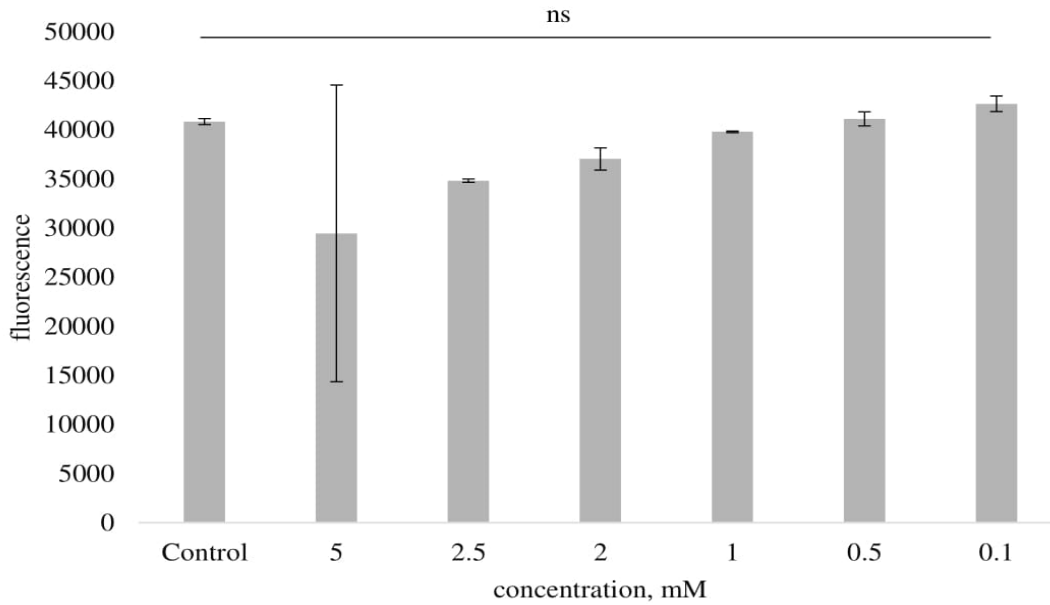


Figure 5.11. Samples containing different concentrations of vasicine only in buffer measured at 335 – 385 nm. The figures represent mean  $\pm$  SD of three replicates and the experiment was performed only once ( $n=1$ ). The statistically significant difference between samples is included: \* -  $p < 0.05$ , \*\* -  $p < 0.01$ , \*\*\* -  $p < 0.001$ , ns - not significant.

The control contained only DMSO in phosphate buffer incubated at 37 °C and the control blank had the same composition though incubated at 4 °C. For samples containing only vasicine in phosphate buffer, for both - after incubation at 4 °C as well as at 37 °C, a concentration dependent decrease of the signal was observed when increasing the concentration. The effect could be related to quenching of the fluorescence signal by the test compound. Statistically significant differences between groups regarding vasicine in buffer solution incubated at 37 °C (335 – 385 nm) were shown by one way – ANOVA ( $p < 0.001$ ). A Bonferroni post hoc test was performed to ascertain which pairs of groups differ significantly from one another, which revealed the presence of statistically significant differences for instance between control and 2 mM vasicine,  $p = 0.003$ , control and 2.5 mM vasicine,  $p = 0.002$ , control and 5 mM vasicine,  $p < 0.001$  (Figure 5.11). Statistically significant differences between groups regarding samples with vasicine only in buffer solution incubated at 4 °C (335 – 385 nm) was shown by one way – ANOVA ( $p < 0.001$ ). A Bonferroni post hoc test was performed and it revealed the presence of statistically significant differences between the control blank and 2 mM vasicine,  $p = 0.012$ , control blank and 2.5 mM vasicine,  $p = 0.003$  and control blank and 5 mM vasicine,  $p < 0.001$ . For the rest of the groups no significant difference was observed (Figure 5.11).



### 37 °C samples vasicine and BSA



### 4 °C samples vasicine and BSA

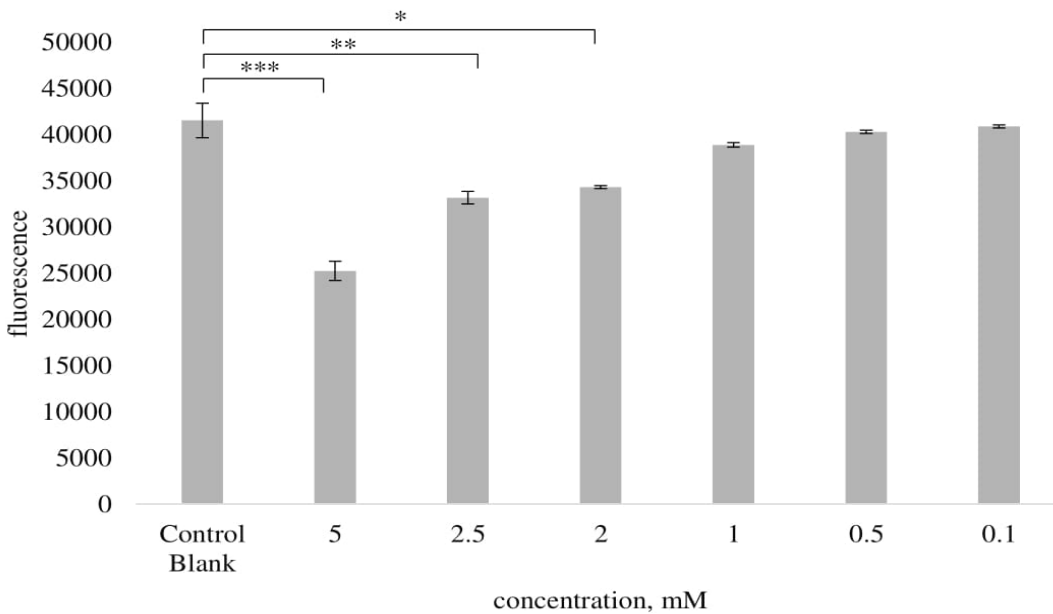


Figure 5.12. Samples containing different concentrations vasicine and BSA in buffer measured at 335 – 385 nm. The figures represent mean  $\pm$  SD of three replicates and the experiment was performed only once ( $n=1$ ). The statistically significant difference between samples is included: \* -  $p < 0.05$ , \*\* -  $p < 0.01$ , \*\*\* -  $p < 0.001$ , ns - not significant.

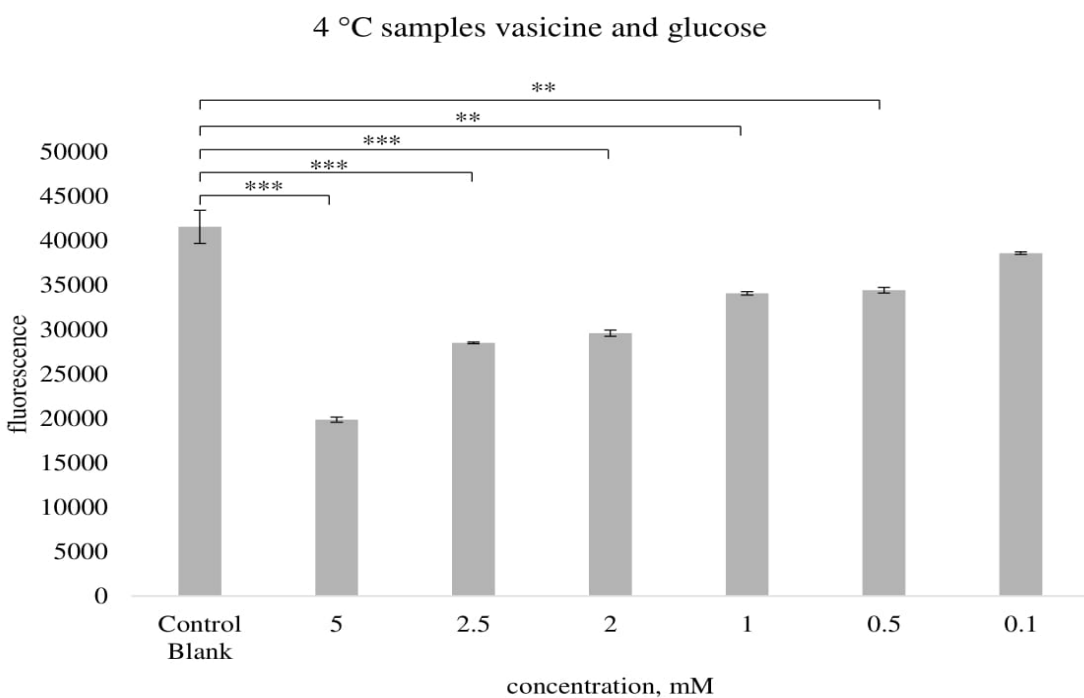
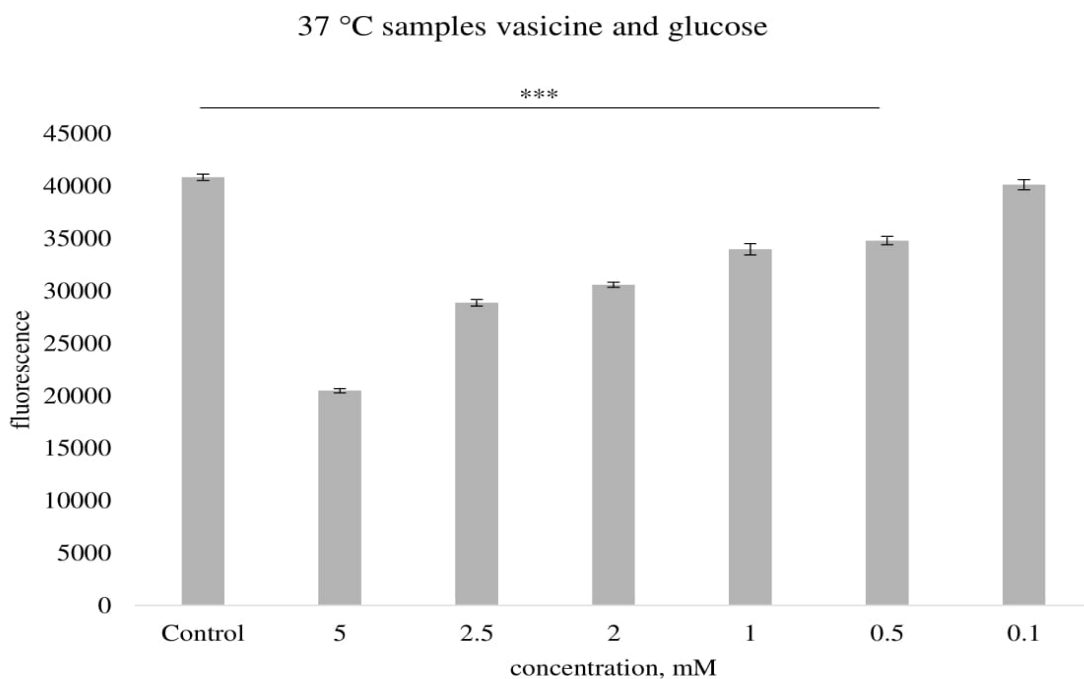


Figure 5.13. Samples containing different concentrations of vasicine and glucose in buffer measured at 335 – 385 nm. The figures represent mean  $\pm$  SD of three replicates and the experiment was performed only once ( $n=1$ ). The statistically significant difference between samples is included: \* -  $p < 0.05$ , \*\* -  $p < 0.01$ , \*\*\* -  $p < 0.001$ , ns - not significant.

For the samples with only BSA or only glucose and vasicine, the results were similar and led to the same conclusion as for vasicine alone. By definition, fluorescence quenching is the decrease of the quantum yield of fluorescence from a fluorophore induced by a variety of molecular interactions with a quencher molecule. The quenching can be dynamic, where a random non interactive collision of small molecules deactivates the excited state of the fluorophore, or static, resulting from the formation of a ground-state complex between the fluorophore and the quencher. In summary, a molecular contact is required between the fluorophore and the quencher for fluorescence quenching to occur.<sup>195</sup> The extent of dynamic quenching depends on the accessibility of the fluorophore to the quencher. In this case, the first group of samples, where the effect was observed, contained only vasicine solution in phosphate buffer, therefore, it can be concluded that there might be an interaction between the vasicine molecules and the phosphate buffer, or between two molecules vasicine that leads to quenching of the signal. Surprisingly, the presence of a protein or a sugar does not play a role in this phenomenon since these samples gave the same results as the one containing only vasicine. Statistically significant differences between groups regarding vasicine and BSA samples at 37 °C (335 – 385 nm) by one way – ANOVA were not observed (Figure 5.12). Statistically significant differences between groups regarding vasicine and BSA samples at 4 °C (335 – 385 nm) were presented by one way – ANOVA ( $p < 0.001$ ). A Bonferroni post hoc test revealed the presence of statistically significant differences between the control blank and 2 mM vasicine in the presence of BSA,  $p = 0.012$ , control blank and 2.5 mM vasicine,  $p = 0.005$  and control blank and 5 mM vasicine,  $p < 0.001$  (Figure 5.12). Statistically significant differences between groups regarding vasicine and glucose at 37 °C (335 – 385 nm) were shown by one way – ANOVA ( $p < 0.001$ ). A Bonferroni post hoc test revealed the presence of statistically significant differences between the control and all concentrations of vasicine in the presence of glucose ( $p < 0.001$ ), except with 0.1 mM vasicine (Figure 5.13). Statistically significant differences between groups regarding vasicine and glucose at 4 °C (335 – 385 nm) were shown by one way – ANOVA ( $p < 0.001$ ). A Bonferroni post hoc test revealed the presence of statistically significant differences between the control blank and 0.5 mM concentration of vasicine in the presence of glucose,  $p = 0.005$ , control blank and 1 mM,  $p = 0.004$ , control blank and 2

mM,  $p < 0.001$ , control blank and 2.5 mM,  $p < 0.001$  and control blank and 5 mM,  $p < 0.001$  (Figure 5.13). Figure 5.14 summarises the comparison between all different sets of samples which revealed the quenching properties of vasicine at 335-385 nm wavelength.

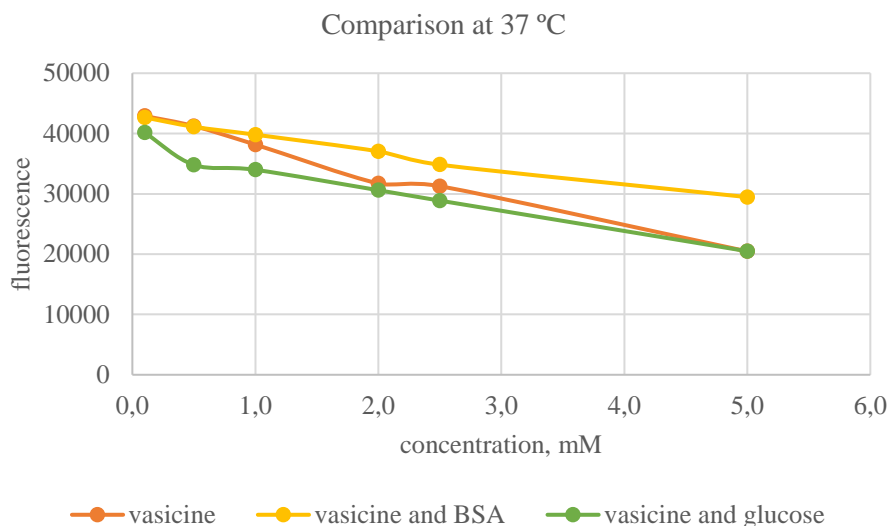


Figure 5.14. Comparison between the different sample sets at 37 °C in the autofluorescence study for vasicine measured at 335-385 nm wavelength.

Different concentrations of nobiletin were tested in the BSA/glucose experiment too. The problem with this compound was its rather poor solubility. In general, it has already been reported that the overall solubility of PMFs is rather low.<sup>120</sup> After addition of the higher concentrations nobiletin to the reaction mixture and after completing the incubation, clear crystals from the compound could be observed, except for the lowest concentration of 0.1 mM nobiletin. However, the test was performed further, and for the 0.1 mM concentration was discovered that the values at 37 °C and at 4 °C (370-440 nm) were higher than the respective control samples. Based on this, quenching properties of the nobiletin molecule were speculated. As a result, the activity of nobiletin could not be evaluated in this assay. As an opportunity to eliminate the effect of the quenching in the test, an alternative approach has been introduced by some researchers.<sup>192,196</sup> It was referred to like the **BSA/glucose precipitation assay** where the samples are treated with trichloroacetic acid (TCA), in order to precipitate the proteins in the reaction mixture and, consequently, to eliminate their interference on the fluorescence measurement. The supernatant

containing the glucose, inhibitor and interfering substances is discarded after centrifugation. The precipitate, containing AGEs-BSA, is used. The true inhibition activity is estimated by subtracting the quenching effect from the apparent inhibitory activity. In spite of the presence of many interfering substances (e.g. chlorophyll, phycobiliprotein - autofluorescent substance), the method has found application mainly in investigating plant extracts for AGEs inhibition.<sup>197</sup> Therefore, physical removal of autofluorescent and quenching material from the reaction mixture was achieved by the addition of TCA. Despite the attempt to apply the suggested technique in the current work, satisfactory results were not achieved.

### 3.2 Fructosamine assay

Through the fructosamine assay more information can be obtained about a potential activity of the test compound on the early stages of the glycation process when Amadori products (e.g. fructosamines) are formed. However, in the current thesis several issues were addressed in order to improve the assay. These included: the choice of a reliable positive control and its optimal concentration; the incubation time for the *in vitro* samples; and the duration for measuring the absorbance at 530 nm.

The preliminary results for aminoguanidine and mangiferin, where the samples were incubated using the conditions included in point 2.3.1 of the chapter (incubation for 7 days etc.), are presented in Figure 5.15. Aminoguanidine showed a higher absorbance than the control sample which resulted in negative values for the percentage of inhibition. For mangiferin, a dose-dependent relationship could be observed and further calculations for the inhibition of fructosamine formation could be made.

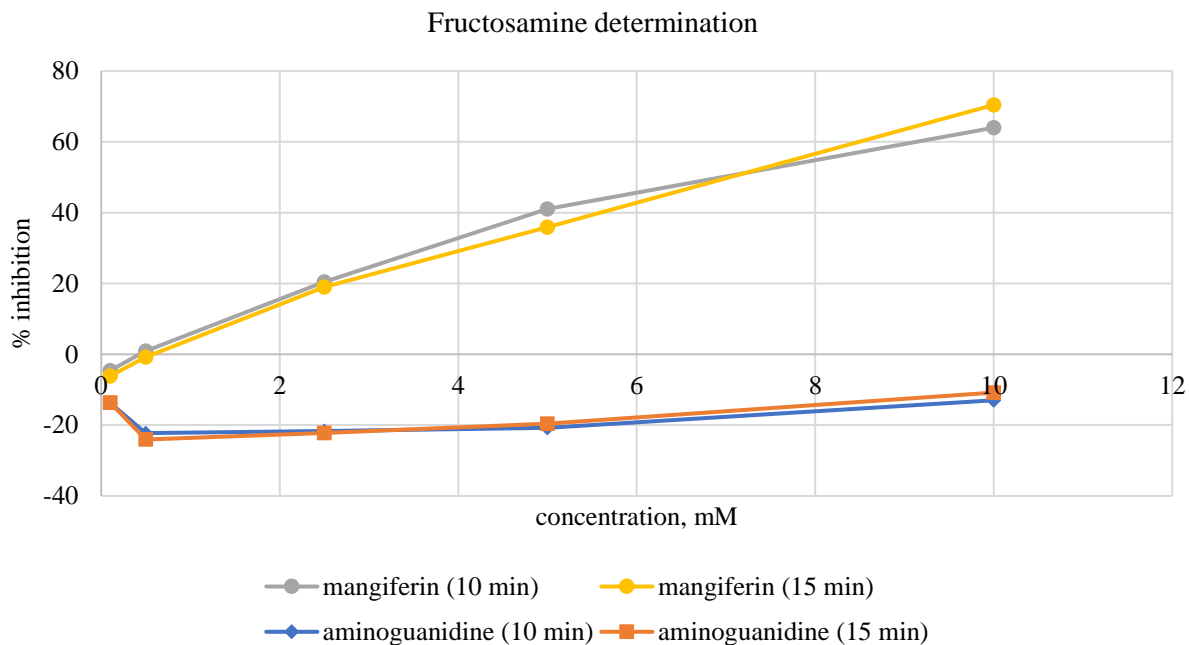


Figure 5.15. Results from aminoguanidine and mangiferin percent inhibition on fructosamine formation. Preliminary test for mangiferin as a potential positive control in the fructosamine assay (absorbance measured at 530 nm, after 10 min and after 15 min). The experiment was performed only once ( $n=1$ ).

Mangiferin at 10 mM showed an inhibition around 67%, at 5 mM around 40% and at 2.5 mM around 20%, consequently, an  $IC_{50}$  value of 6.25 mM could be obtained by interpolation between 10 and 5 mM. As a result, the compound was considered as a potential candidate for a positive control. As mentioned, the mechanism of action for aminoguanidine was proved to be trapping of dicarbonyl compounds which was in line with the obtained preliminary results. The optimization continued by using pyridoxamine (15 to 25 mM), thiamine (15 to 25 mM) and mangiferin (1.5 to 5 mM) in the further tests for a positive control. Another step to be considered was the incubation time of the samples with the dye at 37 °C when the absorbance was detected at 530 nm. The suggested conditions by Chompoo *et al.* were to measure the absorbance in 5-min intervals during 20 min; however, the time was prolonged to 35 min instead, based on another research paper.<sup>190</sup> As a result, the duration when the dye was stable could be analyzed more precisely. Lastly, the incubation time for fructosamine formation was studied. Although 7 days incubation was used for the samples in the BSA/glucose assay,

a screening experiment for 12 days was carried out to monitor specifically the required time for fructosamine formation. The incubation was performed as described before (see the *control* in the BSA/ glucose experiment) and samples were collected each day. Therefore, a time profile for the fructosamine formation was built (Figure 5.16). From the figure is visible that the plateau in the formation of fructosamine was reached after the ninth day. As a result 9 days was chosen for the next screening experiment concerning the positive control candidates.

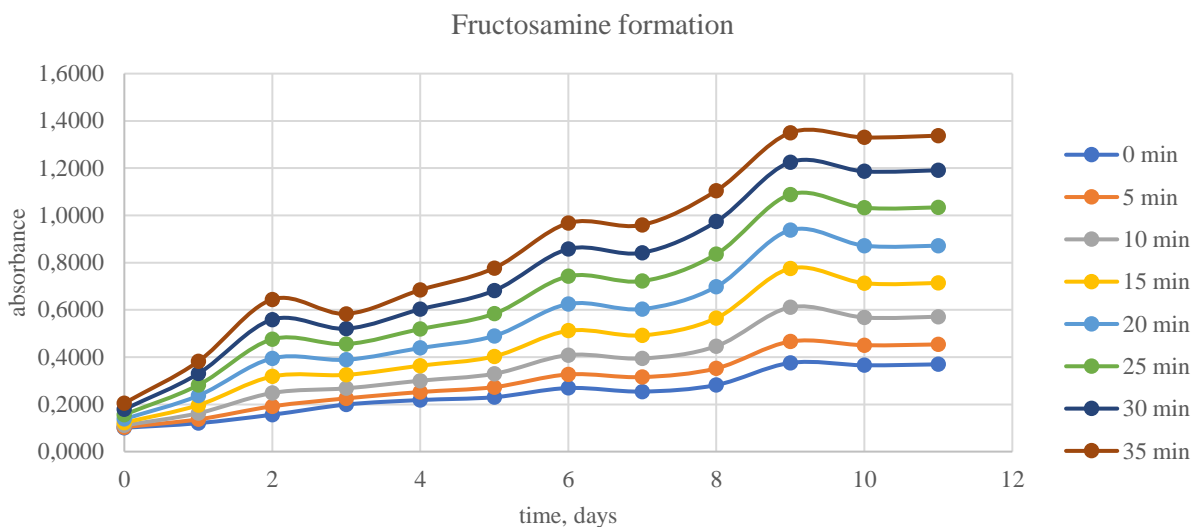


Figure 5.16. Monitoring the fructosamine formation without the presence of inhibitor during 12 days incubation time. The absorbance was measured at 530 nm after adding the dye to each sample in 5-min interval in duration of 35 min at 37 °C. The experiment was performed only once (n=1).

Inhibition curves of the positive control candidates (Figure 5.17 and Figure 5.18) were established.

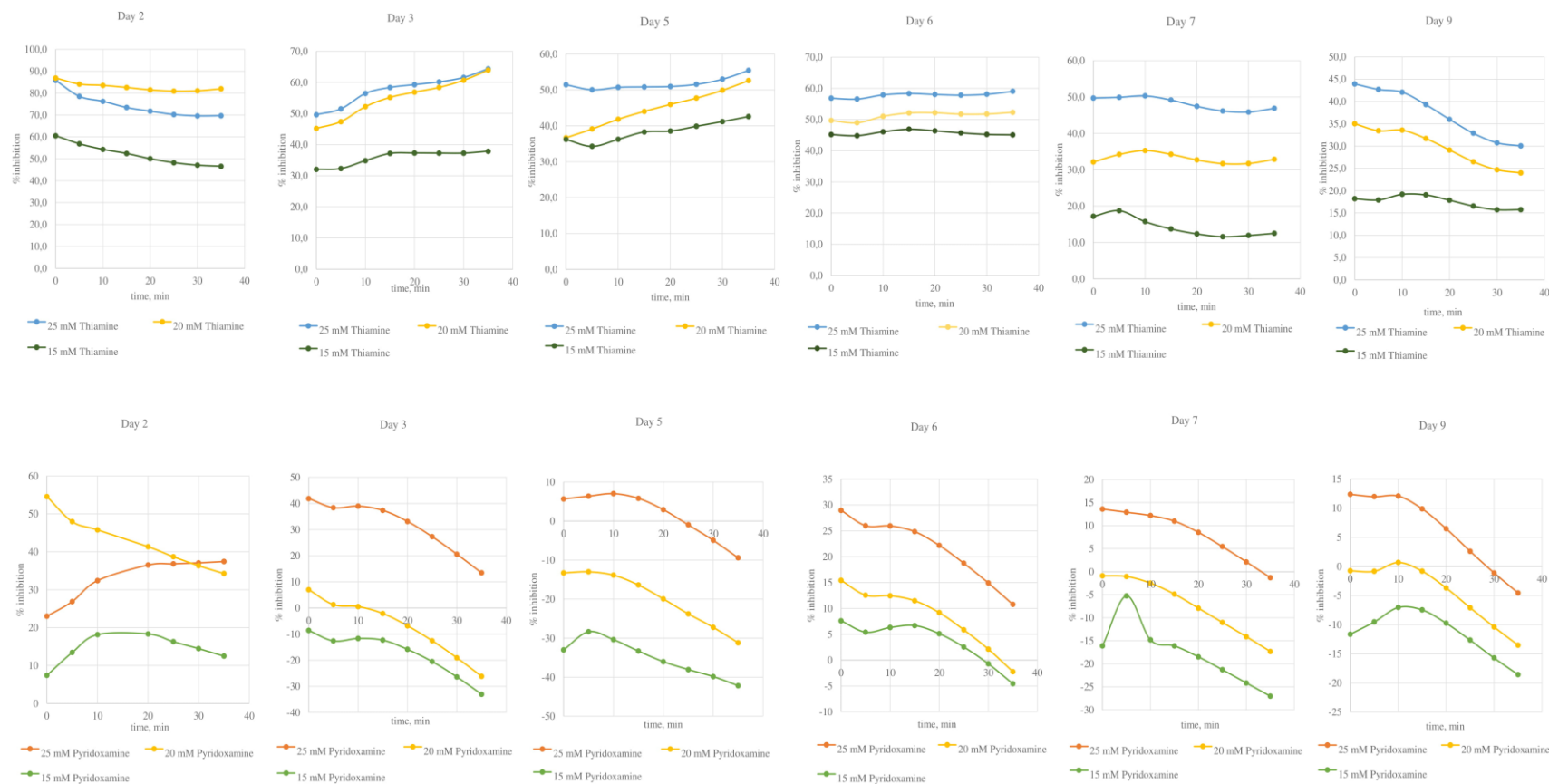


Figure 5.17. Monitoring the fructosamine formation in the presence of different concentrations thiamine and pyridoxamine as potential inhibitors during 9 days incubation time and measuring the absorbance (530 nm) after adding the dye to each sample in 5-min interval for 35 min measurement at 37 °C. The experiment was performed only once (n=1).



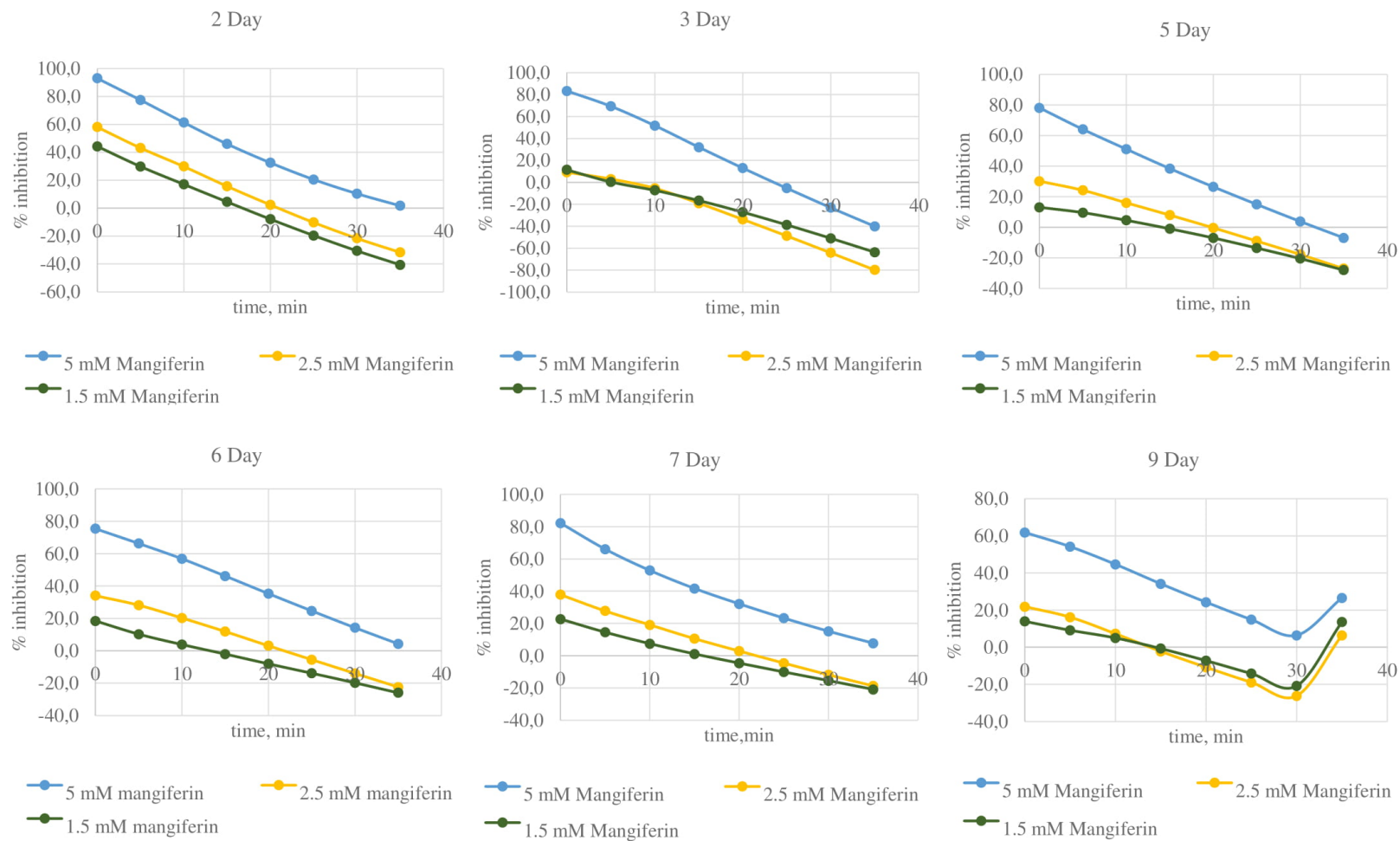


Figure 5.18. Monitoring the fructosamine formation in the presence of different concentrations mangiferin as potential inhibitor during 9 days incubation time and measuring the absorbance (530 nm) after adding the dye to each sample in 5-min interval for 35 min measurement at 37 °C. The experiment was performed only once (n=1).

For thiamine the highest % inhibition and clear concentration dependent decrease was observed on day 6 (25 mM gave 56.8%, 20 mM gave 49.7% and 15 mM – 45.2%). The percentages were kept during the whole 35 min measurement time. As a result it could be concluded that the  $IC_{50}$  for thiamine, in the fructosamine assay performed with incubation of six days, was 20 mM. For pyridoxamine the results from the incubation showed the highest % inhibition and dose-dependent decrease on day 6 of the incubation: around 25% for the 25 mM concentration, 12% for the 20 mM and negative results for the lowest concentration. Moreover, the percentage was decreasing after 15 min. The  $IC_{50}$  value for pyridoxamine was not reached with the tested concentrations. For mangiferin the highest inhibition and concentration dependent pattern were discovered at day 7; unfortunately, no plateau could be reached. However, considering the preliminary results where the  $IC_{50}$  value was around 6 mM and the obtained data after 10 min of measurement (5 mM gave 52.9% inhibition, 2.5 mM – 20%, and 1.5 mM – 7%), 5 mM mangiferin was the accepted  $IC_{50}$  value which could be measured after 7 days incubation. In conclusion, pyridoxamine had the lowest activity, it had never reached the 50% inhibition. Mangiferin, on the other hand, showed high activity in a rather short reaction time, in contrast to thiamine, which had good activity, but independent from the reaction time. In general, a short reaction time was preferred for mangiferin due to activity loss with longer incubation.

Regarding the test compounds, again with nobiletin solubility problems were encountered, and therefore the experiment could not be performed accurately. Then, 5 mM mangiferin, in the role of a positive control, and 0.1 till 5 mM vasicine (final concentrations) were tested in the assay (Figure 5.19).

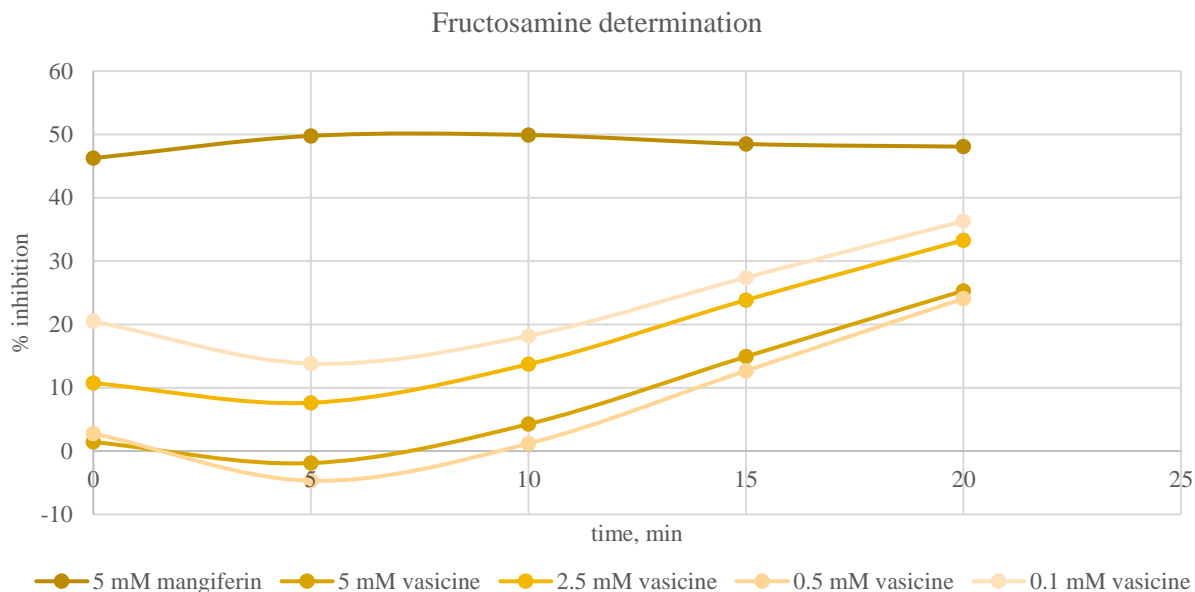


Figure 5.19. Results from different concentrations vasicine and 5mM mangiferin tested in the fructosamine assay. The experiment was performed only once (n=1).

For mangiferin the 50% inhibition was reached after 10 min while vasicine at that point had a considerably lower percentage of inhibition. The increase in the percentage of inhibition of vasicine in time could be explained by the interference between vasicine and the dye.

In summary, though some of the isolated pure compounds from the research project (see Chapter 3) did not prove satisfactory activity in the fructosamine determination assay, two compounds were introduced as promising positive controls in the very same experiment, namely, mangiferin and thiamine.

### 3.3 Dicarbonyl measurement

Initially, the experimental procedure was based on an article where the incubation time with the Girard-T reagent was set to 1 h before measurement.<sup>60</sup> However, the time was changed to 10 min due to another article where the reaction between GO and Girard-T was suggested to be completed in that time (reaching maximum absorbance); and that the product was stable for at least 30 min.<sup>185</sup> In our case, the dicarbonyl entrapment assay

was performed for the pure compounds vasicine and nobiletin. Different concentrations of the test compounds and aminoguanidine, as the positive control, were examined. After initial investigation of the positive control aminoguanidine (final concentrations between 0.05 and 2.5 mM) it was found that with 1 mM aminoguanidine, the absorbance was in the linear range of the detector. For the test compounds the selected concentrations were: 1 mM for vasicine; 0.5 mM for nobiletin. In the end, the dicarbonyl entrapment test was performed and the results are shown in Figure 5.20.

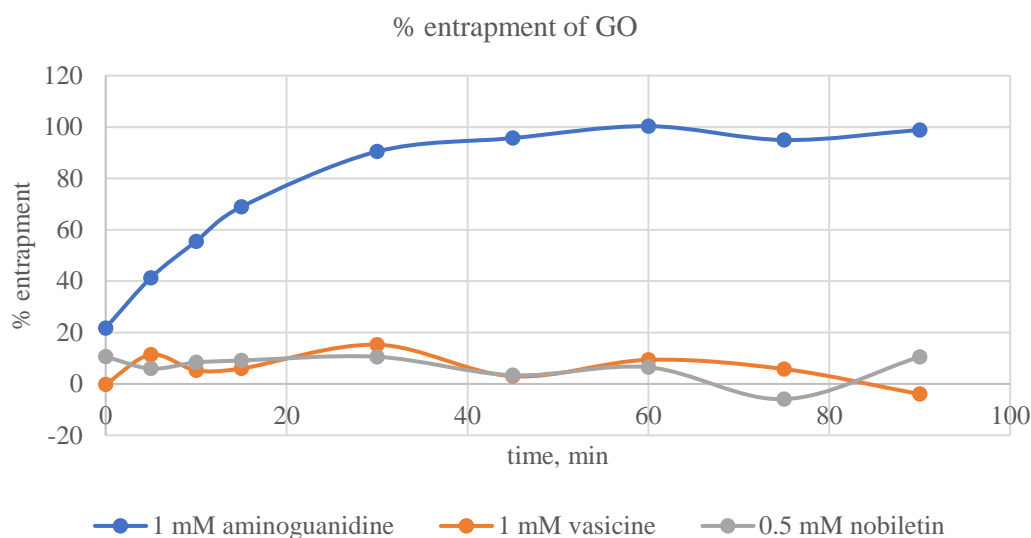


Figure 5.20. Results from the dicarbonyl entrapment experiment for 1 mM vasicine and 0.5 mM nobiletin. The UV absorbance was measured at 290 nm. The experiment was performed only once (n=1).

For aminoguanidine a reduction of GO with 41.3% could be observed after five min and after 30 min it had reached a plateau phase where almost all GO was entrapped. The result could confirm the expected mechanism of action for aminoguanidine - trapping of GO over time. On the contrary, for the other compounds the absorbance remained the same during the whole experiment, so no entrapment could be calculated. The compounds were considered as not active in this assay. In summary, vasicine and nobiletin did not show the same pattern as aminoguanidine in the assay as inhibitors of

the dicarbonyl intermediates. However, another mechanism of action for those compounds as AGEs inhibitors might be possible.

#### *4. Conclusion*

In conclusion, there are few *in vitro* model systems which are used to evaluate the inhibitory effect of test compounds on the glycation process, such as: the BSA/glucose experiment, determining the fructosamine adduct formation, and the dicarbonyl entrapment assay. To date, many natural products and plant extracts have been extensively studied using the mentioned techniques. However, most of these tests suffer from different drawbacks. For example, accurate measurements in the BSA/glucose test have often been hampered by extreme autofluorescence of the test compounds, or complex formation between test compound and the protein which resulted in quenching of the fluorescence signal. So far, other experiments regarding the early stages of AGEs formation have been confined primary to the need of optimizing the experimental conditions for each compound being tested.

Therefore, the drawbacks of the assays discussed above could be circumvented by establishing a reliable and universal method for unambiguous detection of AGEs inhibitors.



# **Chapter 6**

**From vial to file: Development and validation of a  
UPLC/ MS method for quantifying AGEs  
inhibition**





## 1. *The pirouette of ideas*

In the beginning, the early assessment of AGEs was limited to detection and quantification of those with intense intrinsic fluorescence like pentosidine and argpyrimidine. Nevertheless, fluorescence properties do not definitely correlate to a high functional or pathogenic role in the human body. Therefore, a lot of efforts were made for the establishment of more universal and reliable techniques covering a broad range of detectable AGEs. Though, quantification of AGEs with instrumental methods, such as liquid chromatography, requires a completely different sample preparation and performance of the analysis. For instance, the sample preparation should minimize interferences generated from chemical characteristics of the test molecules or the eventual binding ability of some small molecules to the proteins in the reaction mixture. For the purpose of the current project, an attempt to develop and to validate a method for the quantification of N<sup>ε</sup>-(carboxymethyl)lysine (CML) in *in vitro* samples has been conducted. Consequently, many factors had to be taken into consideration when establishing each step of the analytical protocol.

The initial choice that defines the whole direction of the analytical procedure was the careful **selection of the AGE of interest**. N<sup>ε</sup>-(Carboxymethyl)lysine (CML) is a well-characterized and extensively studied product in the field of advanced glycation. It has been analyzed as an indicator of the Maillard reaction in food products, also in biological systems as a lysine residue in proteins formed by both glycooxidation and lipid peroxidation pathways.<sup>40,198-199</sup> A number of analytical techniques for the quantification of CML in biological matrixes have been proposed based on instrumental methods like isotope dilution LC-MS/MS analysis, HPLC with a derivatization reaction with *ortho*-phthalaldehyde (OPA) or 6-aminoquinolyl-*N*-hydroxy-succinimidyl-carbamate (AQC), or immunochemical methods.<sup>198,200-201,187</sup> It was firstly isolated and described from glycated proteins *in vivo* and is considered to be the most abundant AGE in the human body; e.g. it was detected in tissues of lens crystallin, skin collagen and in urine.<sup>202</sup> Increases in the concentration of CML have been observed in the blood and tissues of patients with diabetes mellitus, in the intracellular neurofibrillary deposits in Alzheimer's disease and in atherosclerotic plaques.<sup>203-204</sup> Moreover, high serum levels of CML have been discovered

in patients on dialysis and with diabetic nephropathy.<sup>59</sup> As a result, investigating the concentration of CML *in vitro*, and inhibition of its formation, was considered as a promising starting point for the analytical procedure.

Another major question was **which CML fraction** was going to be used for the analysis. In biological systems AGEs exist in two forms: free AGEs (glycated amino acids) and protein-bound AGEs (protein glycation adducts).<sup>205</sup> The physiological effects of both are most likely different, therefore, scientists emphasize that it is important to quantify them separately.<sup>10,23</sup> CML exists as free form or bound to lysine residues within peptides and proteins.<sup>22</sup> The choice which fraction to be measured had a crucial impact on the further sample preparation steps.

In order to facilitate the quantification of free AGEs, proteins and the protein-bound AGEs should be removed from the reaction mixture. Generally, proteins are removed from the samples by precipitation with organic solvents, change in pH, addition of salts, and ultrafiltration.<sup>206</sup> On the other hand, a standard approach in the sample preparation for instrumental analysis of protein-bound AGEs, involves their enzymatic or chemical release from the proteins in the mixture. Therefore, the role of the **hydrolysis step** is crucial in the characterization of protein-bound AGEs in complex matrices. Nevertheless, it requires lengthy and multiple preparation steps. So far, two hydrolyzation methods have been described: The **enzymatic hydrolysis** procedure is recommended for analyzing acid unstable AGEs, e.g. pyrraline and *N*<sup>ε</sup>-fructosyllysine. It requires a cocktail of enzymes, firstly introduced by Thornalley *et al.*, which included pepsin, pronase E, aminopeptidase and prolidase.<sup>207,208</sup> Also other methods were described based on the use of proteinase K or trypsin.<sup>209,210</sup> **Acid hydrolysis** is performed by heating the sample with 6 M hydrochloric acid for 24 h at a temperature of 100 °C in Eppendorf polypropylene vials. To be certain that CML is not produced from Amadori rearrangement products (ARPs) during acid hydrolysis, the samples can be stabilized by inserting a sodium borohydride reduction step.<sup>198,211</sup> In the current research project, this step was not included because of the simplicity of the matrix compared to those reported in the papers. In the latter cases, the analysis was conducted on food or biological samples, in contrast to the *in vitro* model used in this thesis.

In order to obtain accurate data for the level of CML in the hydrolysed sample, a suitable **cleaning step** is essential to remove interferences and matrix effects, and to maximize the sensitivity of the final LC/MS analysis. Various types of cartridges for solid phase extraction can be used in the clean-up step of protein hydrolysates. For example, Supelco C18 cartridges, Oasis HLB 6cc, MCX cartridges or P3 plates (protein precipitation plates).<sup>198,208,211-212</sup>

Last but not least, the selected **instrument** to perform the measurement plays a crucial role. In literature, the analysis of CML based on liquid chromatography coupled with tandem mass spectrometry (LC-MS/MS) ensures its quantification in quite low amount.<sup>182</sup> Although CML has hydrophilic characteristics, reverse phase chromatography with triple quadrupole detection is normally used.<sup>211</sup> In general, this is due to the addition of ion-pairing reagents like nonafluoropentanoic acid (NFPA) during the sample preparation and as a modifier of the mobile phase which resulted in increased affinity of CML to the column, increased purity of the spectrum and vastly increased MS signal.<sup>198</sup> However, despite its good compatibility with LC-MS, the high concentration of NFPA results in a mobile phase with very low pH (approximately 2), therefore it leads to rapid deterioration of the column.<sup>213</sup> Another approach, mentioned above, which ensures CML quantification with reverse phase chromatography, is a preliminary derivatization reaction. During the method development presented in the thesis, a derivatization step with hydrochloric acid and *n*-butanol (1:3) was required to perform the measurement using a TQD detection system.<sup>214</sup> This derivatization reaction involves butyl esterification of the amino acid, adding 56 mass units (see Figure 6.1):

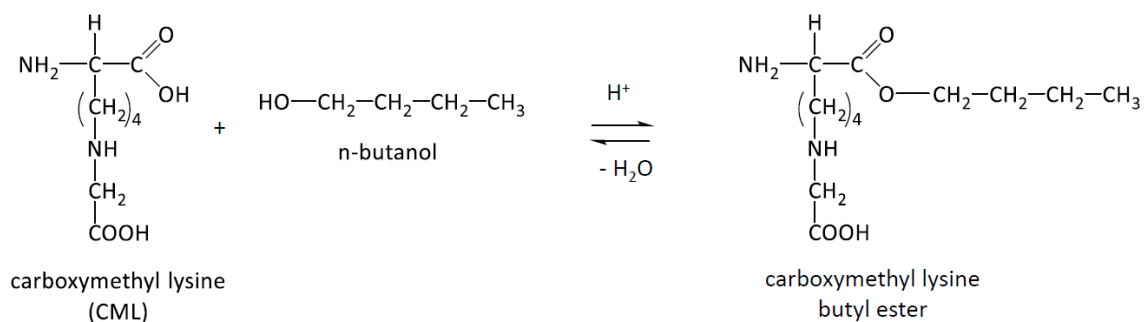


Figure 6.1. Derivatization reaction for CML.

Additionally, since CML is a highly polar compound, reversed-phase chromatography (such as C<sub>18</sub>) can be replaced by hydrophilic interaction liquid chromatography (HILIC) which will improve its retention. Alternatively, if HILIC separation is used instead of reversed-phase chromatography, non-derivatized AGEs are retained without any mobile phase modifier and the drawbacks with the ion-pairing reagents can be avoided.<sup>215</sup>

The use of an **internal standard** for the precise quantification of CML in the samples employing MS detection is advisable. Possible reasons to add an internal standard could be: compensation for sample to sample recovery differences during preparation and sample extraction; differences in actual injection volume between injections; compensation for variability in instrument performance or response due to matrix effects.<sup>216-217</sup> As a rule, an equal amount of internal standard is added to the samples for analysis, and it is presumed that the initial ratio between the compound of interest and this standard does not change because both experience the same losses during the sample preparation step. In the end, both compounds are analyzed and the ratio of their signals is calculated; thus, the internal standard corrects for variations in the analyte.<sup>218</sup> In LC-MS/MS analysis of small molecules the internal standard could be stable-isotope labelled forms of the analyte, for example d<sub>2</sub>-CML or d<sub>4</sub>-CML, or structural analogues, in the case of CML: (S-(4-pyridylethyl)-L-cysteine (PEC); or α-aminobutyric acid.<sup>187,219</sup>

In summary, all factors described above should be delicately balanced in order to achieve the optimal conditions in every aspect of the analytical procedure during method development.

## 2. Reagents and equipment

### 2.1 Solvents and reagents

The solvents acetonitrile, isopropanol, *n*-butanol (99%), dimethyl sulfoxide (DMSO), sodium hydroxide were analytical grade and were purchased from Fisher Scientific (Hampton, NH, USA) or from Acros Organics (Geel, Belgium). The reagents formic acid (99+%) and trifluoroacetic acid (p.a. 99%) were obtained from Acros Organics. Bovine serum albumin (98%), sodium azide (99.5%), aminoguanidine, D-glucose (>99.5%), D-ribose (>99%) were ordered from Sigma Aldrich. Sodium dihydrogen phosphate was from Merck (Darmstadt, Germany). The Ac-Gly-Lys-OMe acetate salt (Gk-peptide) was provided by Bachem, California, USA. For the UPLC/MS experiments on AGEs the standard N- $\epsilon$ -carboxymethyl-L-lysine (CML) was purchased from Polypeptide Group (Strasbourg France); the internal standards S- $\beta$ (4-pyridylethyl)-L-cysteine (PEC) was from Santa Cruz Biotechnology (Dallas, Texas); and d<sub>2</sub>-CML and d<sub>4</sub>-CML were from Iris Biotech GMBH (Marktredwitz, Germany). Water was obtained by a Milli-Q system from Millipore (Bedford, USA) and was filtered through a 0.22  $\mu$ M membrane filter.

### 2.2 General apparatus

Ultrasonication was performed with a Branson 3510 ultrasound bath. Also, a small centrifuge Sigma 1-15 PK (Fisher Bioblock Scientific, Merelbeke, Belgium), a vacuum centrifuge Savant equipped with Refrigerator Vapor Trap (RVT) 400 and SpeedVac Concentrator (SPD) 121P (Thermo Scientific, Massachusetts, USA) were used. Measurements of the pH were achieved with SensION (Hach, Mechelen, Belgium). Incubation at 37 °C was done in a REV SCI (Incufridge) machine and the heating plate (dry bath FB 15101) used for the hydrolysis step was from Fisher Scientific.

## 2.3 Instruments

### Protein crash technique

The removal of proteins – the prime interfering compounds in *in vitro* samples, was achieved on P3 (Protein Precipitation Plates) cartridges equipped with 96 deep-well collection plates (2 ml) (Porvair Sciences, Wrexham, United Kingdom). These plates ensure quantification of the small molecules in those samples after the proteins are “crashed” out of the solution.<sup>220</sup> The method is described as a simple extraction based on precipitating the proteins with acetonitrile.<sup>212</sup>

### UPLC (Ultra-Performance Liquid Chromatography)

Ultra-Performance Liquid Chromatography (UPLC) was performed using a Waters Acquity<sup>®</sup> system (Waters Assoc, Milford, MA) that comprised a binary solvent manager, sample manager, column manager and UV detector. MassLynx version 4.1 software was applied. The chromatographic conditions were optimized on different columns: an Acquity UPLC BEH C18 column (100 mm x 2.1 mm, 1.7 µm) (Waters) and an Acquity UPLC BEH Amide column (100 x 2.1 mm, 1.7µm) (Waters). The used UPLC systems were coupled to different mass spectrometers.

### Triple Quadrupole Detector (TQD)

An Acquity Ultra-performance Liquid Chromatography system (Waters) with a sample manager, binary solvent manager, diode array detection (DAD) and a triple quadrupole detector was used. MassLynx version 4.1 software was used.

### Quadrupole Time-of-flight (QTof) mass spectrometer

An ACQUITY Ultra-performance Liquid Chromatography system (Waters Corporation, MA, USA) coupled to a Waters<sup>®</sup> Xevo G2-XS QTof mass spectrometer (Waters, UK) operating with MassLynx 4.1 software was employed. The Xevo<sup>®</sup> G2-XS QTof Mass Spectrometry system is a hybrid, quadrupole, orthogonal acceleration, time-of-flight (Tof) mass spectrometer which is equipped with a LockSpray<sup>™</sup> (ESI) source (Figure 6.2).<sup>221</sup>

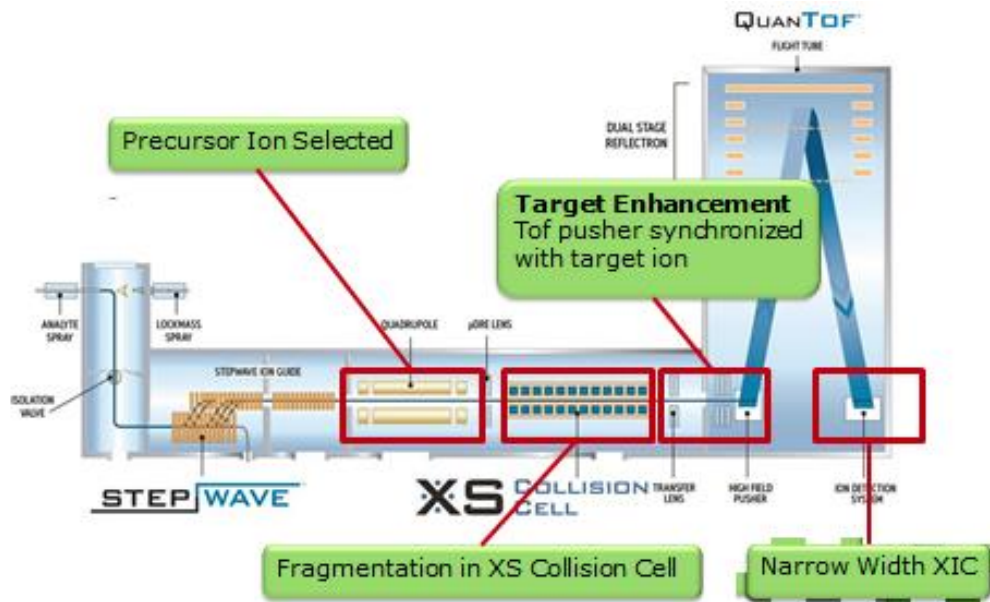


Figure 6.2. Main modules in the Xevo® G2-XS QToF Mass Spectrometry system.

QToF provides accurate mass spectra using internal mass calibration during acquisition and mass drift compensation (collected in single MS mode and applied to the MS-MS as a rolling average). The ion optics operate in the following sequence: the samples from the LC are introduced under atmospheric pressure into the high performance ZSpray™ dual-orthogonal electrospray ionization source; the ions pass through the sample cone and into the vacuum system; the ions pass through the StepWave™ ion guide to the quadrupole; the mass-separated ions pass the XS Collision Cell; the ions, focused by the transfer lenses, move into the QuanTof analyser; they are orthogonally accelerated up by high voltage pulse in a flight tube; finally, they are reflected back towards the detector (Figure 6.2).<sup>222</sup>

## 2.4 Statistical analysis

Statistical analysis was carried out by one-way analysis of variance (ANOVA) followed by Dunnett's post hoc test using a PC running GraphPad Prism software, version 8.4.2 (GraphPad Software, Inc., La Jolla, CA, USA).

## 2.5 Test compounds

The commercial products, which were tested in the final method, were: silymarin, apigenin, (-) epi-catechin, quercetin, rutin, curcumin, (+) catechin, pyridoxamine, metformin, cyanidin, ginkgolide A and amentoflavone. They were purchased from Sigma Aldrich (Missouri, USA) and were tested in 0.1 mM final concentration (for ginkgolide A and for amentoflavone also 1 mM final concentration was tested). The isolated pure compounds (see Chapter 3) analyzed with the method were: bilobetin (1 mM and 0.1 mM final concentrations), ginkgetin/isoginkgetin mixture (1 mM and 0.1 mM final concentrations), vasicine (2, 1, 0.5 and 0.1 mM final concentrations), nobiletin (3, 2.5, 0.5 mM and 0.1 mM final concentrations), 5-demethylnobiletin (0.1 mM final concentration), sinensetin (0.1 mM final concentration), 4',5,6,7-tetramethoxyflavone (0.1 mM final concentration), tangeretin (0.1 mM final concentration) and heptamethoxyflavone (0.1 mM final concentration). All solutions were prepared in DMSO.

## 3. Method development

### 3.1 The starting point of the method development

The first attempt to develop a reliable instrumental method for measuring AGEs inhibition was based on previously described work by Schalkwijk *et. al.*, who used an Ultrahigh-Performance Liquid Chromatography (UPLC) instrument coupled to a triple quadrupole mass spectrometry detector (TQD) to quantify plasma levels of free and protein-bound CML.<sup>90</sup> Initially, for the precise quantification of the AGE of interest, an internal standard S- $\beta$ (4-pyridylethyl)-L-cysteine (PEC) was chosen in consistency with the procedure of Crabb *et. al.*<sup>219</sup>

The stock solutions of the standards CML and PEC were prepared in Milli-Q water with a final concentration of 1 mM.<sup>223</sup> Afterwards, each stock solution was further diluted with water to obtain a concentration between 50 nM and 2500 nM. Samples were prepared by following the general incubation procedure, previously described in Chapter 5 for the BSA/glucose experiment.<sup>224</sup> The sample preparation steps aimed to measure **the free**



**AGEs** as discussed by Schalkwijk.<sup>225</sup> This procedure required a derivatization reaction with hydrochloric acid and *n*-butanol (1:3).<sup>226</sup> First, 75  $\mu$ l of incubated sample were mixed with 15  $\mu$ l of the internal standard (2500 nM PEC). Then, proteins were precipitated by adding 600  $\mu$ l of methanol and acetonitrile (1:3) during vortex mixing. After centrifugation at 20 °C for 20 min at 14 000 rpm the supernatant was taken. The latter was further dried under nitrogen at 70 °C and derivatization was carried out for 90 min at 70 °C in derivatization vials. In the end, the derivatized samples were dried and dissolved in 150  $\mu$ l water, then transferred into glass vials ready to be submitted for analysis. The same derivatization step was performed on the samples for the calibration curve.

The **measurement** was carried out on an Acquity UPLC system using a TQD MS as a detector. The MS method development started with direct infusion of individual derivatized standards (CML, PEC) into the ESI source. Multiple reaction monitoring (MRM) was carried out in ESI positive ion mode. For each compound the optimal cone voltage was determined as well as the MRM transitions with their respective collision energy values. The main precursor ion from the derivatized CML adduct was a sodium adduct  $m/z$  317  $[M + Na]^+$  and the main product ion was  $m/z$  186  $[M + Na]^+$ . The main MRM transition for the derivatized PEC was  $m/z$  283  $[M + Na]^+$  to  $m/z$  110  $[M + Na]^+$ . Other instrumental parameters could be defined as follows: capillary voltage 2.0 V, cone voltage 30 V, source temperature 120 °C, desolvation temperature 450 °C, gas desolvation gas flow 800 L/h, cone gas flow 40 L/h. Chromatographic separation was performed on an Acquity UPLC BEH C18 column (50 x 2.1 mm, 1.7 $\mu$ m). The used mobile phase consisted of ammonia (5 mmol/l) in water (mobile phase A) and acetonitrile (mobile phase B) at a flow rate of 0.8 ml/min. The gradient elution began with 1% B, then for 2 min it increased to 3% B, and for 7 more min to 40% B. At 9.10 min the percentage of B was 55% and it was kept constant till the twelfth minute. Finally the composition of the mobile phase was restored to the initial conditions.<sup>225</sup> The column temperature was set at 45 °C and the injection volume was 10  $\mu$ l.

In general, the derivatization reaction is utterly important when CML is measured with LC-UV due to the lack of chromophores in the structure. In the TQD measurement the derivatization with hydrochloric acid and *n*-butanol (1:3) was used to increase the ESI sensitivity by improving the ionization, and the polarity of the reverse phase.<sup>227</sup> However,

the results obtained by this method showed no consistency after repeated injection, and no concentration-dependent results between different standards could be obtained. Also, changes in chromatographic conditions and mass spectrometric parameters could not resolve this issue and reproducible results were not obtained.

### 3.2 Method optimisation

Because of the lack of reproducible results, a more sensitive high resolution MS system was chosen in order to be able to measure in full scan mode. An Ultrahigh-Performance Liquid Chromatography (UPLC) instrument coupled to a Quadrupole time-of-flight mass spectrometer (QToF) was used for further analysis. The optimization of the analytical procedure continued as follows: The **sample preparation** included the already described derivatization step with hydrochloric acid and *n*-butanol (1:3). The UHPLC-MS analysis was carried out on an ACQUITY UPLC system coupled to a Xevo QToF MS system. The experiment was performed on an Acquity UPLC BEH C18 column (50 x 2.1 mm, 1.7 $\mu$ m) and the mobile phase consisted of water with 0.1% formic acid and acetonitrile with 0.1% formic acid. The gradient elution started with 1% B for 2.5 min, then rising to 40% B by the eleventh minute. At 11.10 min the percentage of B was 55%, which was kept till the fifteenth minute. Next, for 3 min the starting percentages were restored. The flow rate was reduced to 0.6 ml/min and the column temperature was kept at 40 °C. The injection volume was 10  $\mu$ l. Electrospray in the negative ionization mode (ESI) was applied with sample cone set at 40 V. A solution of sodium formate was used to calibrate the mass spectrometer. Leucine enkephalin was used as a lock mass.

The signal measured for CML and PEC after the derivatization were  $m/z$  317.2440 [M + Na]<sup>+</sup> and  $m/z$  283.1480 [M + Na]<sup>+</sup>, respectively. Measurements were performed in full scan. Despite the fact that generating the product ions will increase the specificity of the measurements, the sensitivity was poor after fragmentation. Though following the above described procedure, no persistent result could be obtained. Problems might be caused by an incomplete derivatization reaction since no particular pattern was shown.

### 3.2.1 Change of chromatographic conditions

In order to avoid the derivatization reaction, but to sustain an optimal chromatographic separation and mass spectrometric detection, the possibility of hydrophilic interaction chromatography (HILIC) was investigated. This is a potent and favourable technique to resolve highly polar molecules, e.g. amino acids and amino acid-like compounds such as CML. The applied mobile phase was based on the article of Danaceau *et. al.* and consisted of 10 mM ammonium formate with pH 3 (eluent A) and 85% acetonitrile in 10 mM ammonium formate (eluent B), using gradient elution: starting percentage 85% B for 6.0 min, then the percentage of B was reduced to 67.4% till the 10.0 minute. From 10.0 to 12.0 min the percentage B was further decreased to 55.6%. Next, between 12.1 min and 18.0 min the percentage was kept at 85% B.<sup>228</sup> For improved retention, selectivity and separation of polar AGEs, the Acquity UPLC BEH Amide **column** (100 x 2.1 mm, 1.7µm) (Waters) was selected. The previous stock solutions of CML and PEC, and their further dilutions described before were prepared in Milli-Q water. However, one of the most important parameters to obtain suitable peak shapes in HILIC mode is the nature of the solvent. Therefore, a crucial aspect in the further method development based on the HILIC mode was the way how those standard dilutions were made. Generally, samples that contain a high percentage of water would elute rapidly on a HILIC column and peak splitting could occur.<sup>229</sup> As a result, finding the right composition and proportion for the **dilution mixture** was critical for the analysis. For instance, the content of acetonitrile will depend on the polarity of the compound. To begin with, a high content of acetonitrile in water was tested to eliminate potential peak splitting.<sup>230</sup> However, with 95% acetonitrile, peak splitting was not observed but the response was rather low. A possible explanation may be the decreased solubility of the compound of interest; therefore, isopropanol was included in the dilution mixture.<sup>230</sup> In the end, a composition of 45% isopropanol, 45% acetonitrile and 10% water resulted in no splitting and good intensity of the signal (Figure 6.3).

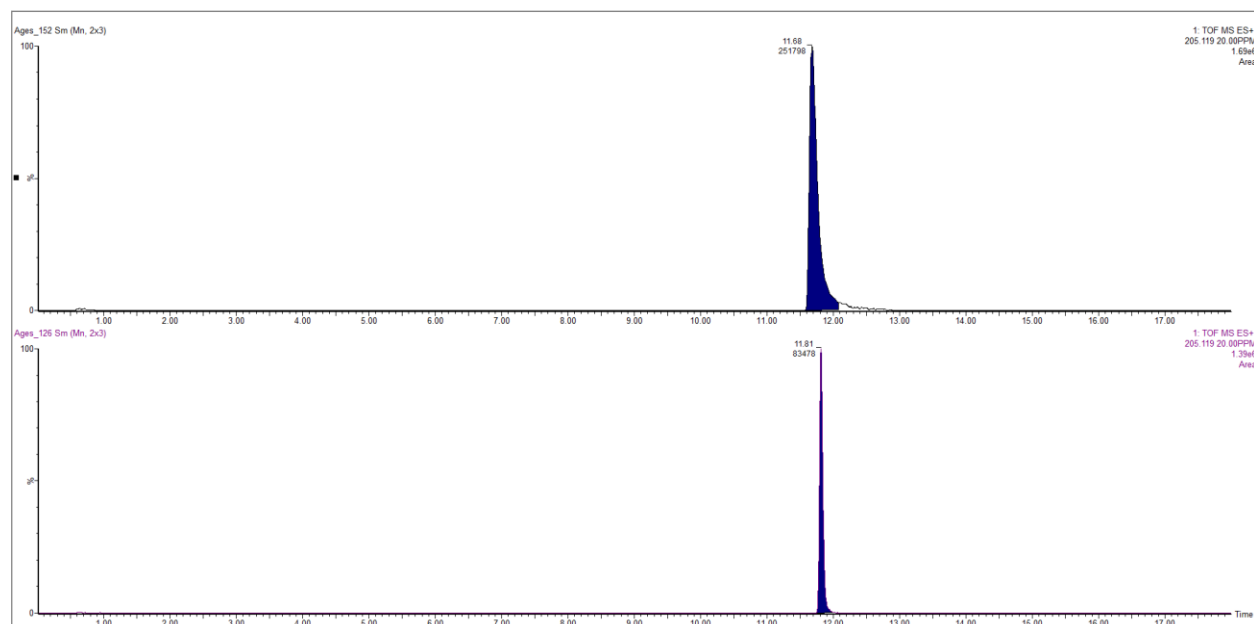


Figure 6.3. Extracted ion chromatogram for  $m/z$  205.119  $[M+H]^+$  for 2500 nM CML standard solutions (from bottom to top) prepared in 95% acetonitrile and in isopropanol : acetonitrile : water (45:45:10) mixture.

Even though the standards were completely soluble in the mixture isopropanol, acetonitrile and water (45:45:10) and chromatograms showed peaks with a nice shape, their signal revealed no linear concentration dependent relation. The highest concentrations gave relatively good response, in contrast to the lowest one where the response trend was completely lost (Figure 6.4 (2)). A probable explanation might be the attachment of CML to glass vials. This can be related to a study by Kalasin and Santore, who demonstrated that also small amounts of fibrinogen could be adsorbed onto a negatively charged silica surface.<sup>231</sup> Therefore, the adhesion properties of peptides and proteins could be a reason for inaccurate results and wrong conclusions in certain experiments.<sup>232</sup> In the current test, the proportion of CML attached to the glass surface was not significant at the highest concentrations of the standard; while at the lowest concentrations, most of the compound present in the solution can be attached to the glass. To reduce surface binding of proteins several approaches have been described, such as adding Tween-20 or salt in a high concentration, addition of bovine serum albumin (BSA), using coated tubes with polyethylene glycol (PEG) or siliconizing agents, or designing a solvent system that reduces the tendency of proteins to interact with the

surface.<sup>233-234</sup> Although including BSA to the solvents or using it to coat surfaces seems to be the easiest approach, it is not feasible in some experiments such as purification of peptides/proteins for mass spectrometric analyses, and it is considered as rather labour intensive.<sup>232</sup> In conclusion, the phenomenon of glass adhesion required the glass vials to be replaced by **polypropylene vials** (Varian 0.1 ml screw top vial kit, 99788790). This step was of great importance and remained crucial for the positive outcome of the whole experimental procedure. Figure 6.4 shows the comparison between the response for 2500 nM and 1000 nM CML in polypropylene vials (1) and in glass vials (2).

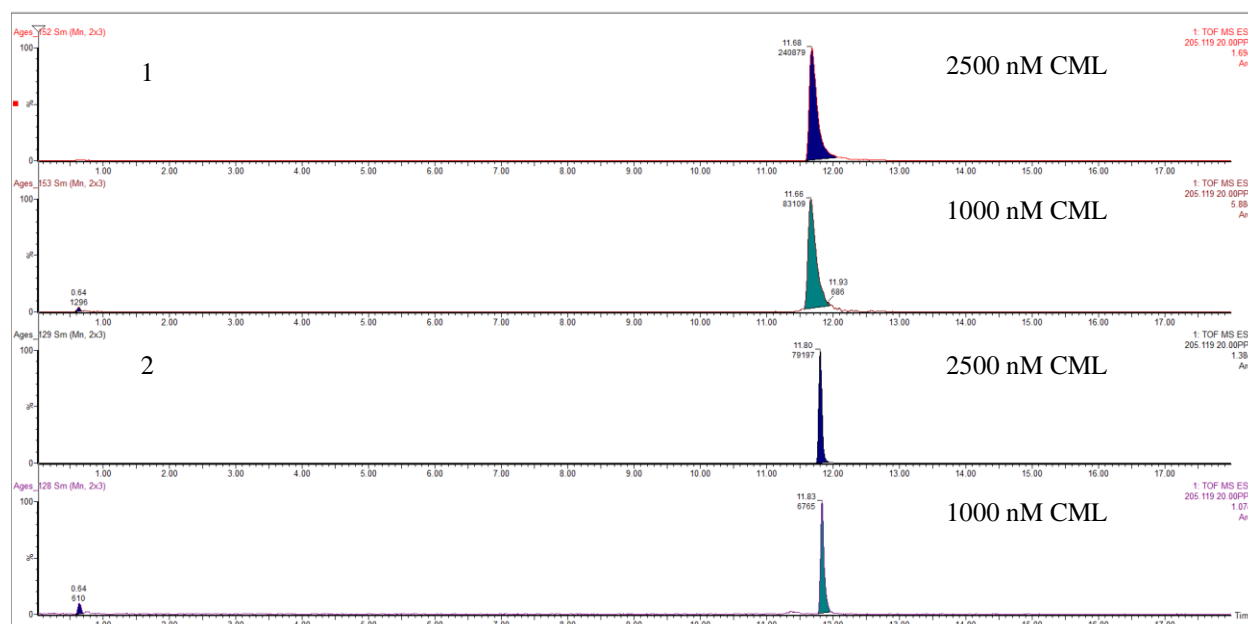
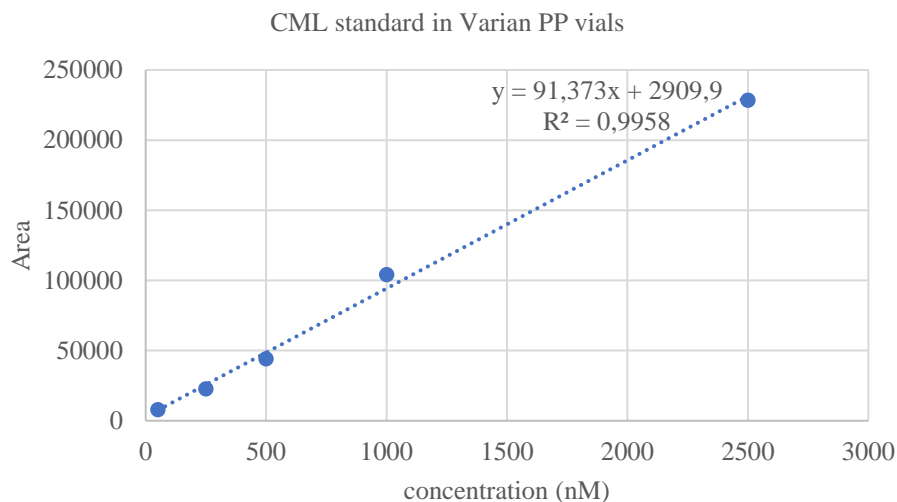


Figure 6.4. Extracted ion chromatograms comparing the intensity between 2500 nM and 1000 nM standard solutions CML prepared in polypropylene vials (1) and in glass vials (2).

The intensity for both concentrations measured in the polypropylene vials was much higher and a clear signal vs. concentration response was discovered compared to the same dilutions prepared in the glass vials. After selecting the polypropylene vials for the following experiments, standard dilutions of CML in isopropanol, acetonitrile and water (45:45:10) mixture were analyzed and the calibration curve is shown in Figure 6.5.



*Figure 6.5. Calibration curve for single standard dilutions CML prepared in Varian polypropylene vials and eluted with mobile phase containing 85% acetonitrile in 10 mM ammonium formate as eluent A and 10 mM ammonium formate pH 3 as eluent B.*

A linear response was observed for the standard dilutions of CML (Figure 6.5). However, in the same conditions a bad peak splitting was observed for the internal standard PEC. Consequently, several other chromatographic systems were tested as an alternative, for example: acetonitrile : water : 1 M ammonium acetate (90 : 9.9 : 0.1) as A, and water : acetonitrile: 1 M ammonium acetate (90 : 9.9 : 0.1) as B.<sup>235</sup> The pH was adjusted to 5.78. Unfortunately the compound did not provide satisfactory results (Figure 6.6).

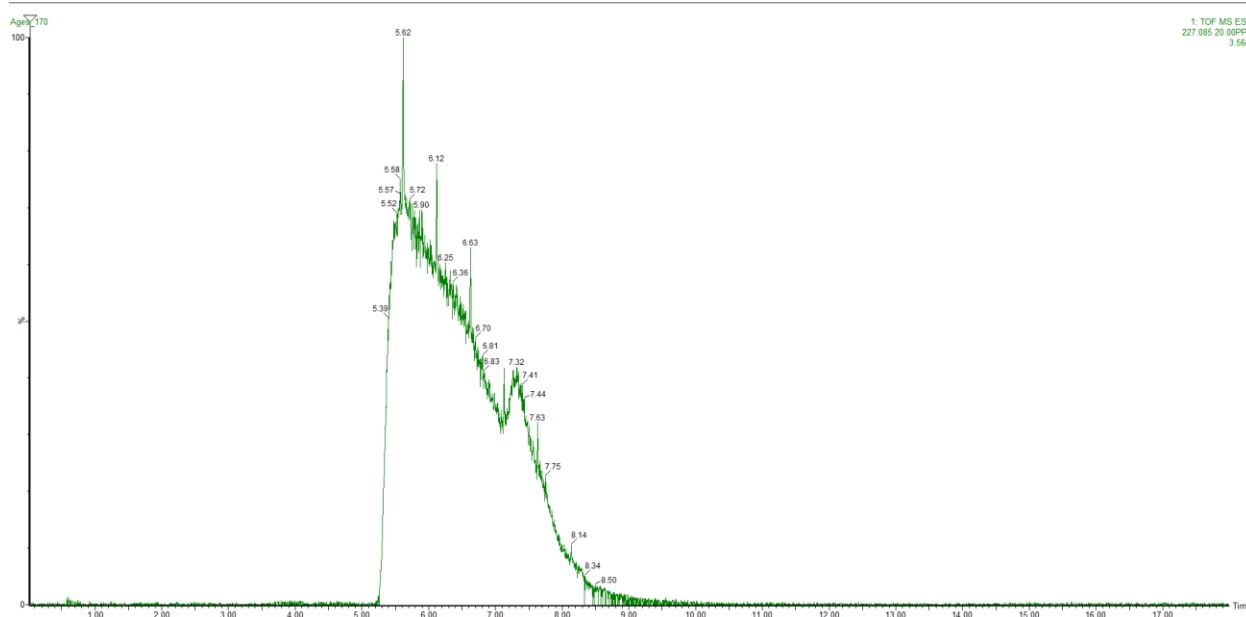


Figure 6.6. Standard solution of 2500 nM PEC in isopropanol : acetonitrile : water (45:45:10) mixture analysed in Varian polypropylene vials. The mobile phase contained acetonitrile:water:1M ammonium acetate (90:5:5) as eluent A and water:acetonitrile:1M ammonium acetate (90:5:5) as eluent B.

As an alternative, the mobile phase containing water with 0.1% formic acid (eluent A) and acetonitrile with 0.1% formic acid (eluent B), which was used previously with the BEH C18 column, was proposed again and the conditions were optimized as shown in Table 6.1:

Conditions	Parameters																								
Instrument	ACQUITY Ultra-Performance Liquid Chromatography system coupled to a Xevo G2-XS QToF MS system																								
Column	Acquity UPLC BEH Amide column (100 x 2.1 mm, 1.7µm)																								
Injection volume	10 µl																								
Mobile phase	water with 0.1% formic acid (eluent A) acetonitrile with 0.1% formic acid (eluent B)																								
	<table border="1"> <thead> <tr> <th>time, min</th> <th>%A</th> <th>%B</th> </tr> </thead> <tbody> <tr> <td>0.00</td> <td>15</td> <td>85</td> </tr> <tr> <td>6.00</td> <td>15</td> <td>85</td> </tr> <tr> <td>6.10</td> <td>20.9</td> <td>79.1</td> </tr> <tr> <td>10.00</td> <td>32.6</td> <td>67.4</td> </tr> <tr> <td>12.00</td> <td>44.4</td> <td>55.6</td> </tr> <tr> <td>12.10</td> <td>15</td> <td>85</td> </tr> <tr> <td>18.00</td> <td>15</td> <td>85</td> </tr> </tbody> </table>	time, min	%A	%B	0.00	15	85	6.00	15	85	6.10	20.9	79.1	10.00	32.6	67.4	12.00	44.4	55.6	12.10	15	85	18.00	15	85
time, min	%A	%B																							
0.00	15	85																							
6.00	15	85																							
6.10	20.9	79.1																							
10.00	32.6	67.4																							
12.00	44.4	55.6																							
12.10	15	85																							
18.00	15	85																							
Flow rate	0.4 ml/min																								
ESI mode	negative																								
Tune parameters	Source: sample cone 40V, capillary 1.01kV; Temperature: source 120 °C, desolvation 550 °C; Gas flow: gas cone 50 L/h, desolvation gas 1000 L/h																								

Table 6.1. Optimized instrumental conditions.

The results from testing standard solutions of 2500 nM CML and PEC in the isopropanol, acetonitrile and water (45:45:10) mixture with the new chromatographic conditions are presented in Figure 6.7:



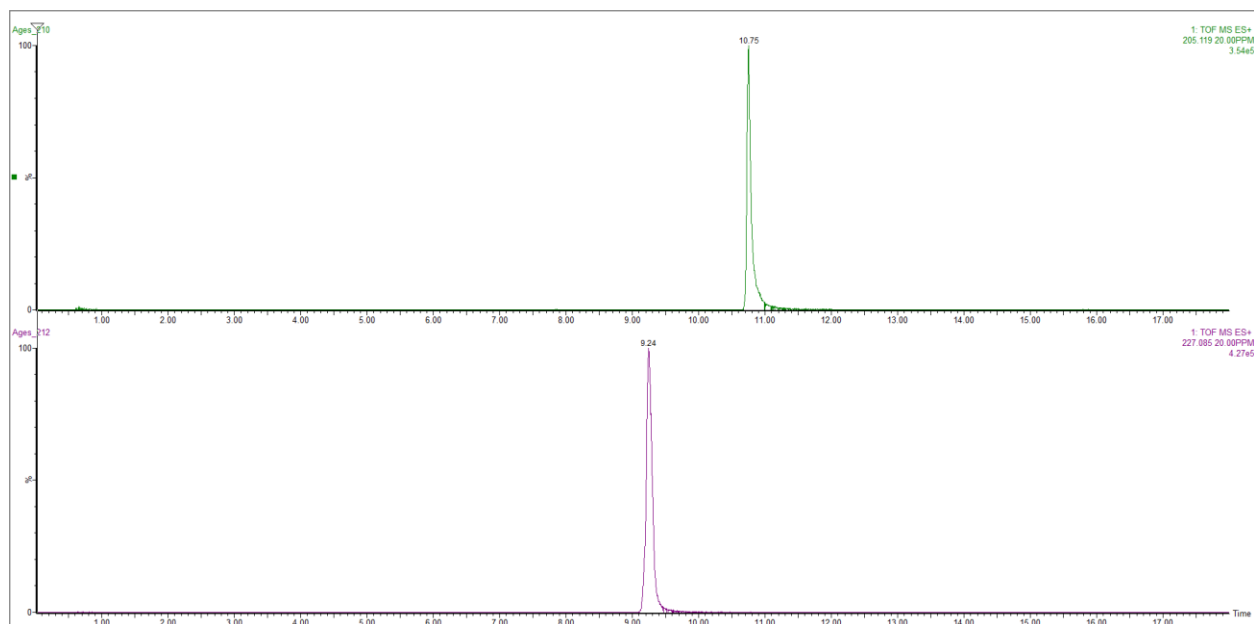


Figure 6.7. Standard solutions of 2500 nM CML and PEC prepared in Varian polypropylene vials eluted using 0.1% formic acid in water (eluent A) and 0.1% formic acid in acetonitrile (eluent B).

The CML and the PEC standards showed optimal results and a calibration curve including several standard dilutions could be generated (Figure 6.8).

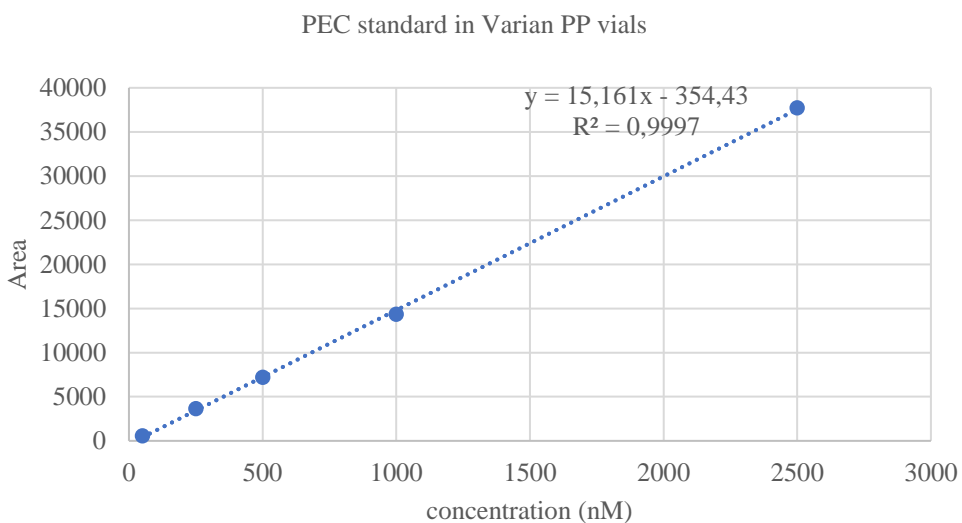
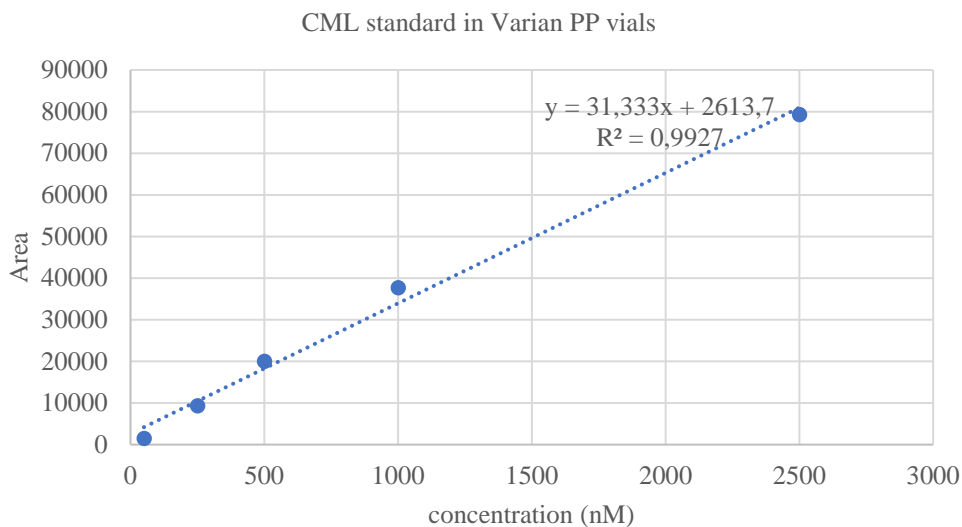


Figure 6.8. Calibration curves of single standard dilutions CML and PEC prepared in Varian polypropylene vials eluted with 0.1% formic acid in water (eluent A) and 0.1% formic acid in acetonitrile (eluent B).

Then, the calibration standards had to be prepared in the same matrix as the samples in the intended incubation conditions namely, containing BSA and glucose in a concentration similar as described in the BSA/ glucose assay (see Chapter 5), applying 2500 nM PEC as an internal standard. The following sample preparation procedure was applied: to 75  $\mu$ l of the incubated sample 15  $\mu$ l internal standard was added; then proteins were precipitated by adding 600  $\mu$ l of methanol and acetonitrile (1:3) while vortexing; after

centrifugation at 20 °C for 20 min at 14 000 rpm the supernatant was taken and dried under vacuum; finally, the sample dissolved in the isopropanol, acetonitrile and water (45:45:10) mixture was ready for analysis. A problem occurred at the final step where, although peak shapes remained good, the dried samples were not completely dissolved in the isopropanol, acetonitrile and water (45:45:10) mixture before analysis; therefore, accurate quantification data could not be provided. Optimizing the content of the incubation solutions and addition of a cleaning step before injection of the sample appeared as new challenges in the method development process.

### 3.2.2 Conditions for sample incubation and sample preparation

In the beginning of the chapter, where the starting point of the method development was discussed, it was emphasized that the analytical method was developed for quantifying the free AGEs fraction.<sup>90,219</sup> The sample preparation procedures for the *in vitro* model, including the one adapted for HILIC mode, are summarized in Table 6.2.

Regarding the sample incubation, the **incubation mixture** containing bovine serum albumin (BSA) at a final concentration of 10 mg/mL and glucose at a final concentration of 500 mM was incubated for 7 days at 37 °C in order to form the maximum amount of AGEs. Next to this, a calibration curve containing samples with different concentrations of CML standard and fixed concentration of the internal standard (2500 nM PEC) in the incubation mixture was prepared. To begin with, the **sample preparation** for free AGEs determination was considered to be improved by optimizing the precipitation step (Table 6.2, column 1). Acetonitrile, and an isopropanol : acetonitrile : water (45:45:10) mixture were tested but no significant difference was observed. Another question that raised was, if it was necessary to dry the samples or if they could directly be injected for analysis. With the second precipitation mixture (isopropanol : acetonitrile : water) they could be directly submitted for analysis. However, the data from the calibration curve samples and from the incubated samples were still inconsistent: no clear concentration-dependent response for CML. Also, the chromatographic peaks from the internal standard (PEC) showed either peak splitting after precipitation with acetonitrile or low response after precipitation with the isopropanol mixture.

Since sample clean up by precipitation was resulting in unpredictable results and additionally, **protein-bound AGEs** were not measured, a hydrolysis step was included as discussed above. This hydrolysis step might be carried out before or after the precipitation (Table 6.2). In contrast to several other AGEs, CML is an acid stable compound.<sup>198</sup> This facilitated its analysis by using 6 M hydrochloric acid for the hydrolysis. In addition, acid hydrolysis is easier, less expensive and more reliable than, for example, enzymatic hydrolysis.<sup>40</sup> However, in general, after hydrolysis the samples are considered as too “dirty” to be submitted for MS analysis directly. In order to improve the condition of the samples two different compositions of the incubation mixture were used, namely, the standard BSA (66.5 kDa)/ glucose mixture and a protein with much lower molecular weight, *i.e.* the Gk-peptide (*N*-acetyl-glycyl-lysine methyl ester, 259.31 g/mol) with ribose as the sugar component. It was speculated that the use of a lower molecular weight protein will result in relatively “cleaner” hydrolysates. Nevertheless, the **sample cleaning** procedure had yet to be optimized.

Measuring free AGEs	Measuring protein-bound AGEs (first approach)	Measuring protein-bound AGEs (second approach)
<ul style="list-style-type: none"> <li>• 75 µl sample (mixture of a protein –BSA, a sugar – Glu (see Chapter 5), and the standard CML solution for the calibration curve; or test compound in DMSO)</li> <li>• addition of 15 µl internal standard</li> <li>• protein precipitation</li> <li>• vortex</li> <li>• centrifugation</li> <li>• the supernatant is taken</li> <li>• dried under nitrogen</li> <li>• reaction of derivatization</li> <li>• dried under nitrogen</li> <li>• dissolve in water</li> <li>• transfer in glass vials</li> <li>• injecting 10 µl for analysis</li> </ul>	<ul style="list-style-type: none"> <li>• 75 µl sample (mixture of a protein – BSA or Gk-peptide, a sugar - Glu or Rib (see Chapter 5), and the standard CML solution for the calibration curve; or test compound in DMSO)</li> <li>• addition of 15 µl internal standard</li> <li>• protein precipitation</li> <li>• vortex</li> <li>• centrifugation</li> <li>• remove supernatant</li> <li>• acid hydrolysis of the remaining pellet</li> <li>• dry under vacuum</li> <li>• reconstitution in water</li> <li>• transfer in polypropylene vials</li> <li>• injecting 10 µl for analysis</li> </ul>	<ul style="list-style-type: none"> <li>• 75 µl sample (mixture of a protein –BSA or Gk-peptide, a sugar - Glu or Rib (see Chapter 5), and the standard CML solution for the calibration curve; or test compound in DMSO)</li> <li>• addition of 15 µl internal standard</li> <li>• acid hydrolysis of the sample</li> <li>• drying under vacuum</li> <li>• reconstitution in isopropanol:acetonitrile:water (45:45:10)</li> <li>• vortex</li> <li>• centrifugation</li> <li>• transfer in polypropylene vials</li> <li>• injecting 10 µl for analysis</li> </ul>

Table 6.2. Sample preparation standard procedures for measuring free AGEs or protein-bound AGEs.

Based on preliminary research, several solid phase extraction models were tested as a cleaning-up step: protein precipitation plates P3 (317100/240100, Porvair), Oasis® PRiME HLB cartridges (186008057, Waters) and iSPE®-HILIC cartridges (200.001.0025, Hilicon). Therefore simple elution of the different standard solutions of CML prepared in the isopropanol mixture was performed. The results obtained after clean-up step with the P3 plates suggested the best recovery. Then, parallel sample sets containing Gk-peptide / ribose or BSA / glucose with standard dilutions of CML at different concentrations, and 2500 nM PEC as an internal standard, were made. After acid hydrolysis, the different samples were eluted through the P3 plate. Only for CML in the Gk-peptide / ribose batch a calibration curve could be obtained (Figure 6.9). The signal for the internal standard was lost and the results from the BSA / glucose mixture did not show a concentration dependent response.

In conclusion, **Gk-peptide and ribose** were selected as preferable incubation mixture for AGEs formation in the *in vitro* model. The small molecular weight of the peptide in the reaction mixture resulted in optimal conditions for the acid hydrolysis which favours the further sample preparation step. Moreover, at this point of the research the decision was made to focus only on quantifying the “total” AGEs and to make no distinction between the free and the protein-bound AGEs. The amount of the free fraction was considered considerably lower than the bound fraction, due to the simplicity of the incubation model in contrast to biological models generally used in other research methods.

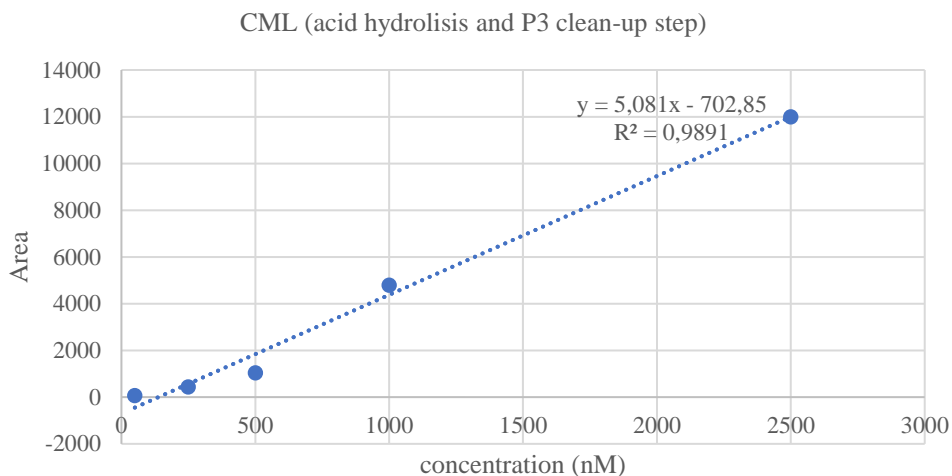


Figure 6.9. Calibration curve of single standard dilutions CML after acid hydrolysis and P3 plate clean-up step.

The new conditions for the sample preparation for the total CML level can be summarized as follows:

- 75 µl sample = incubation mixture containing Gk-peptide (5 mg/ml) and Rib (3 mg/ml), and the standard CML solution for the calibration curve or test compound in DMSO, incubated at 37 °C for 24 h
- addition of 15 µl internal standard (2500 nM PEC)
- hydrolysis of the sample with 6 M hydrochloric acid
- drying the hydrolysate in a vacuum centrifuge
- reconstitution in Milli-Q water
- cleaning through P3 cartridges, elution with acetonitrile
- drying the collected sample in a vacuum centrifuge
- reconstitution in isopropanol : acetonitrile : water (45:45:10) mixture
- transfer the sample in polypropylene vials
- injecting 10 µl for analysis

The necessity to reconstitute the acid hydrolysate in water and the use of acetonitrile for the elution through the P3 cartridges was based on the guidelines for the protein precipitation plates from the manufacturer.<sup>236</sup>

### 3.2.3 A deuterated internal standard

A remaining issue in the procedure was the response of the internal standard (2500 nM PEC) and the inability to obtain reliable quantification data. As a result, the development focused on the choice of N- $\epsilon$ -carboxy[D<sub>2</sub>]methyl-L-lysine (d<sub>2</sub>-CML) as more promising candidate due to the general assumption that an analyte and stable isotope labelled internal standard have identical physicochemical properties.<sup>237</sup>

The preliminary analyses included the injection of standard solutions of CML and d<sub>2</sub>-CML in different concentrations prepared in the isopropanol : acetonitrile : water (45:45:10) mixture (Figure 6.10).

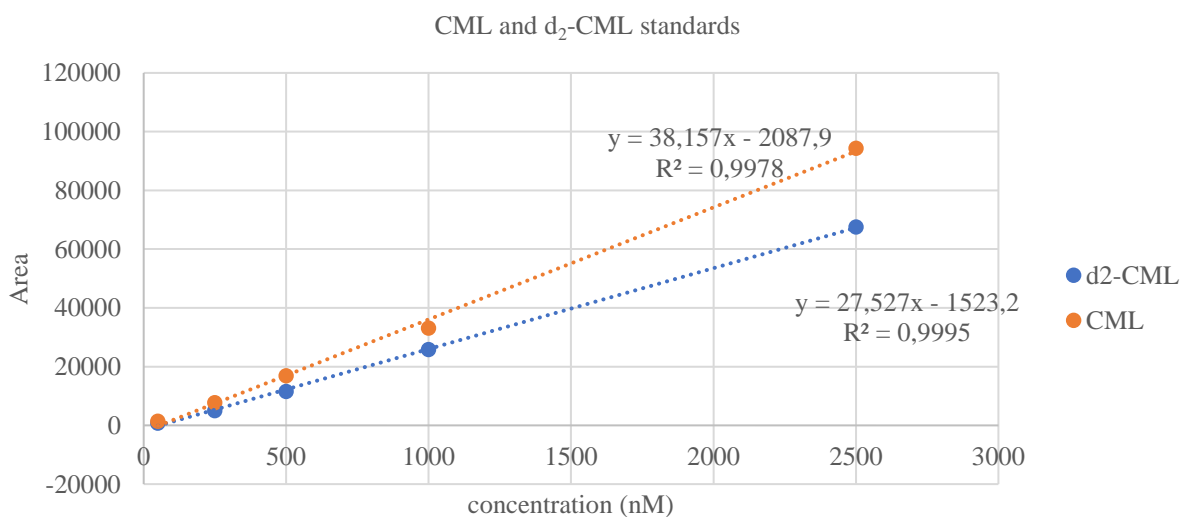


Figure 6.10. Comparison between calibration curves of single standard dilutions CML and d<sub>2</sub>-CML samples prepared in isopropanol:acetonitrile:water (45:45:10) mixture.



Further on, samples containing the Gk-peptide / ribose mixture with standard solutions of CML and 2400 nM d<sub>2</sub>-CML as an internal standard, were used for the calibration curve (Figure 6.11):

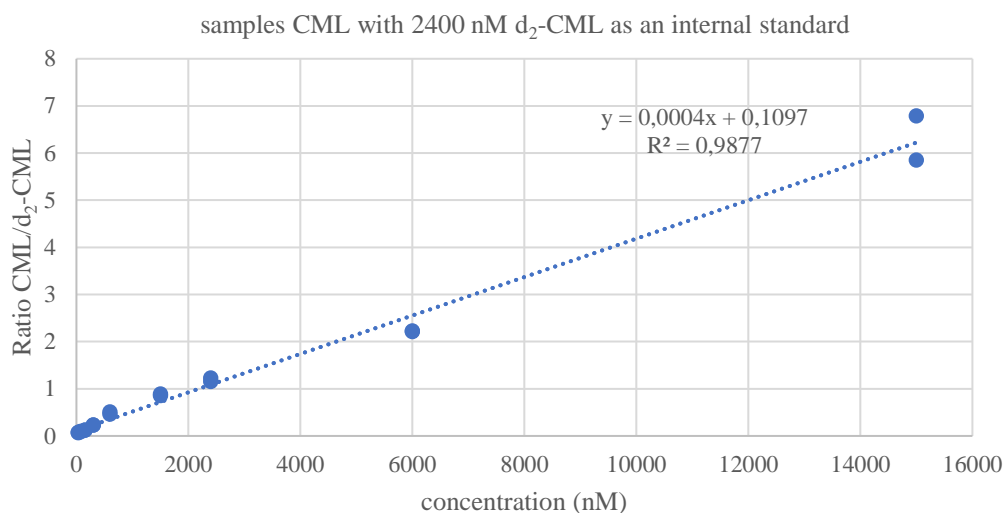


Figure 6.11. Calibration curve of samples containing CML standard solutions and an internal standard 2400 nM d<sub>2</sub>-CML prepared in Gk-peptide / ribose reaction mixture. Samples were prepared in diplo.

The sample preparation steps were executed as described above. For incubating real samples with Gk-peptide/ ribose, the protocol of the BSA / glucose experiment was applied, in which the incubation time was set on 7 days. With the new composition of the reaction mixture, the amount of CML formed was excessively high (area more than 500 000), and as a result it caused suppression of the d<sub>2</sub>-CML molecular ion signal (Figure 6.12A). Therefore, the same samples were prepared again but instead of 7 days the incubation was carried for just 24 h.<sup>38,61</sup> In this case, the area for the CML signal was considerably lower (around 100 000), which enabled the detection of the signal for the internal standard (Figure 6.12B).

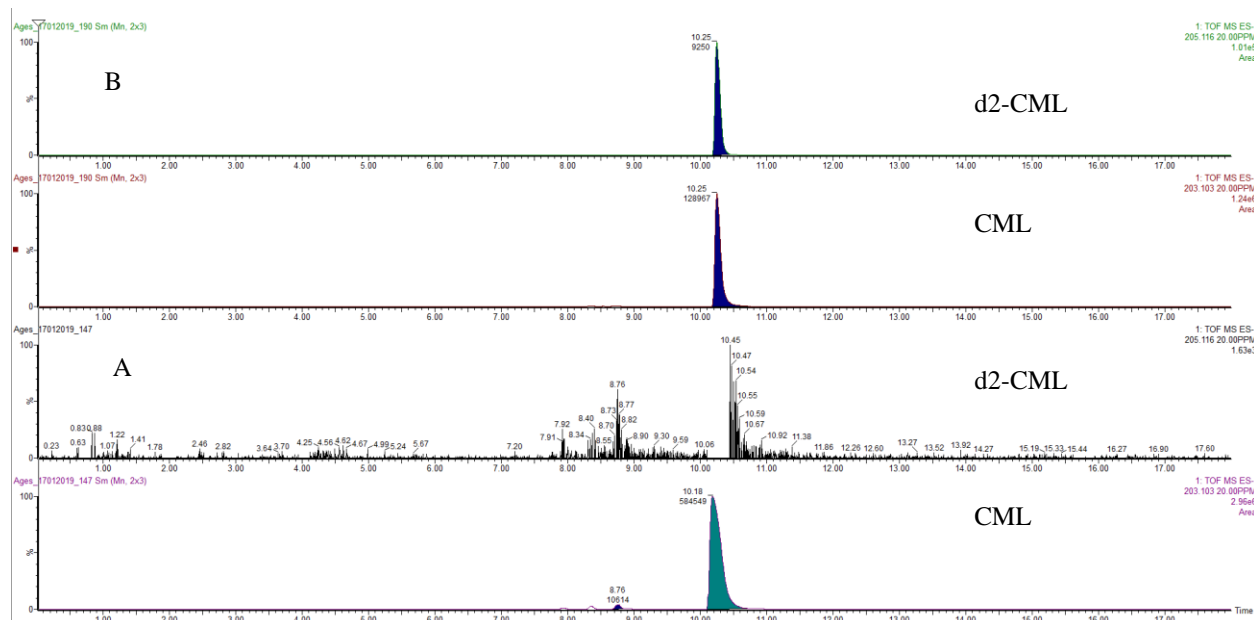


Figure 6.12. Results for CML and  $d_2$ -CML respond obtained from 7 days incubated samples (A); and results for CML and  $d_2$ -CML respond obtained from 24 h incubated samples.

### 3.2.4 Gk-peptide / ribose samples: optimization of stock solution concentrations and incubation time

To tackle this problem of the high CML signals, different concentrations of Gk- and ribose solutions were examined, as well as the duration of the incubation by checking several time points.

The test solutions of the protein and the sugar in the reaction mixture were as follows:

	Initial concentration	New concentration 1	New concentration 2
Gk-peptide	111.1 mg / 10 ml (final concentration 5 mg/ml)	55.55 mg / 10 ml (final concentration 2.5 mg/ml)	37.04 mg / 10 ml (final concentration 1.7 mg/ml)
ribose	66.7 mg/ 10 ml (final concentration 3 mg/ml)	33.35 mg/ 10 ml (final concentration 1.5 mg/ml)	22.24 mg/ 10 ml (final concentration 1 mg/ml)

The incubation time of CML formation with the suggested reduced concentrations of Gk-peptide and ribose was set at 34 h and a sample was taken every 2 h. 2400 nM  $d_2$ -CML

was used as an internal standard. In order to perform quantification of CML a calibration curve was built. The amount of CML formation in the tested conditions is shown in Figure 6.13.

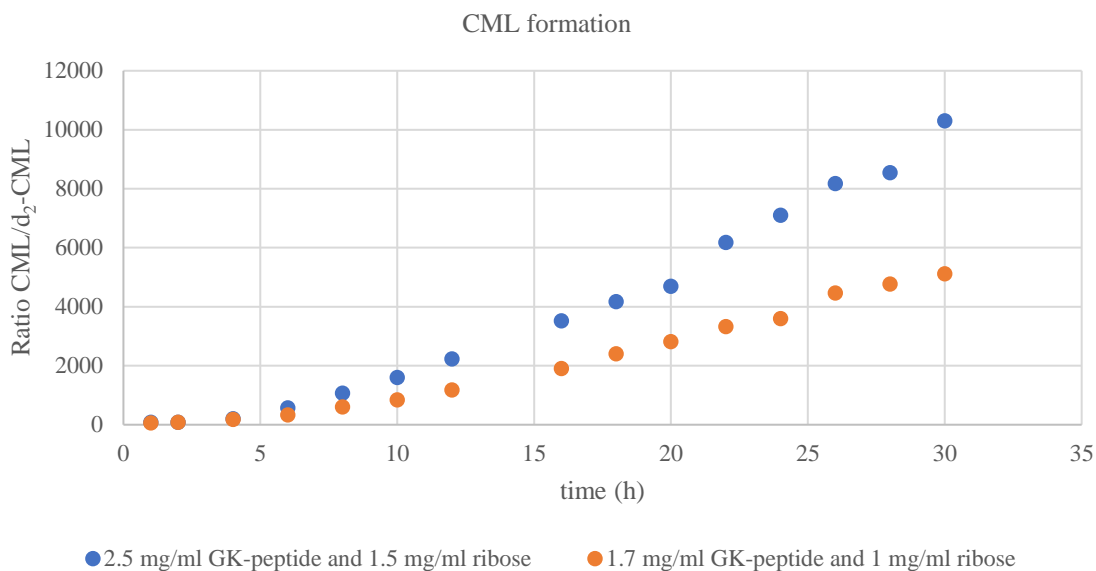


Figure 6.13. Time profile of CML formation with different concentrations of Gk-peptide and ribose incubated for 34 h at 37 °C, and sample was taken in every 2 h.

In conclusion, **1.7 mg/ml Gk-peptide** and **1 mg/ml ribose** were selected as the starting concentrations used for the incubation mixture. In this conditions, although the amount of CML formed was rather low, it was considered to be sufficient to perform tests on the anti-AGEs activity of test compounds later on. Regarding the 2.5 mg/ml Gk-peptide and 1.7 mg/ml ribose incubation mixture, the amount of CML formed quickly reached a level where suppression of the intensity of the internal standard might occur. Therefore a balance between sufficient CML formation where AGEs inhibition can be tested, and sufficient intensity of the internal standard had to be established. In addition, **24 h** was chosen as the most optimal incubation time. It was considered as the moment just before the plateau in the CML formation was reached.

After establishing the conditions discussed so far, the method validation was approached following the FDA Guidelines of Bioanalytical Method Validation regarding linearity, precision and quality control.<sup>238</sup>

## 4. Method validation

### 4.1 Materials and methods

Based on the FDA Guidelines, the linearity of the method was determined by the analysis of 8 different concentrations of CML (75, 150, 300, 750, 1500, 2500, 3500 and 5000 nM) and using 2400 nM  $d_2$ -CML as an internal standard. A calibration curve was established and the samples were quantified by reference to the external standard calibration curve. Consequently, the lowest concentration of the calibration curve was set as 75 nM CML which was determined based on the balance between a good peak shape and high signal to noise ratio. For evaluating the between-day variation 18 samples were prepared and analyzed on 3 different days in triplicate. These samples included the eight different concentrations of CML standard; three quality control samples; three concentrations of aminoguanidine (2.5 mM, 10 mM and 20 mM final concentration) and pyridoxamine (10 mM, 25 mM and 50 mM final concentration), tested as candidates for a positive control; and one sample representing the maximum amount of AGEs formed. The quality control samples contained standard solutions of 75, 2500 and 5000 nM CML prepared in triplicate from a different stock solution than the one used for the calibration curve samples.

The summary of the protocol for the HILIC UPLC method coupled to a Xevo QTof MS system used for the method validation is presented in Table 6.3. To assess the inhibitory effect on CML formation both aminoguanidine at concentrations of 2.5, 10 and 20 mM and pyridoxamine at 10, 25 and 50 mM were used. The results of the test compounds were compared to samples which were considered to contain the maximal amount of AGEs formed in the present conditions. The latter consisted of Gk-peptide, ribose and 10% DMSO.

<b>Standard preparation</b>	<ul style="list-style-type: none"> <li>- Prepare stock solutions of CML and d<sub>2</sub>-CML in Milli-Q water (1 mM)</li> <li>- Obtain standard dilutions between 50 and 2400 nM in a mixture of acetonitrile-isopropanol-water (45:45:10)</li> </ul>	<table border="1"> <thead> <tr> <th>min</th> <th>% A</th> <th>% B</th> </tr> </thead> <tbody> <tr> <td>0.00</td> <td>15</td> <td>85</td> </tr> <tr> <td>6.00</td> <td>15</td> <td>85</td> </tr> <tr> <td>6.10</td> <td>20.9</td> <td>79.1</td> </tr> <tr> <td>10.00</td> <td>32.6</td> <td>67.4</td> </tr> <tr> <td>12.00</td> <td>44.4</td> <td>55.6</td> </tr> <tr> <td>12.10</td> <td>15</td> <td>85</td> </tr> <tr> <td>18.00</td> <td>15</td> <td>85</td> </tr> </tbody> </table>	min	% A	% B	0.00	15	85	6.00	15	85	6.10	20.9	79.1	10.00	32.6	67.4	12.00	44.4	55.6	12.10	15	85	18.00	15	85
min	% A		% B																							
0.00	15		85																							
6.00	15	85																								
6.10	20.9	79.1																								
10.00	32.6	67.4																								
12.00	44.4	55.6																								
12.10	15	85																								
18.00	15	85																								
<b>Sample preparation</b>	<ul style="list-style-type: none"> <li>- 75 µl from the incubated sample: incubation mixture containing Gk-peptide (1.7 mg/ml), Rib (1 mg/ml) and the standard CML solution for the calibration curve dissolved in isopropanol : acetonitrile : water (45:45:10) mixture; or test compound/aminoguanidine in DMSO (test sample/ positive control); or just DMSO (negative control sample)</li> <li>- addition of 15 µl internal standard (2400 nM d<sub>2</sub>-CML)</li> <li>- hydrolysis of the sample with 6 M hydrochloric acid (1 ml) for 1 h</li> <li>- drying the hydrolysate in a vacuum centrifuge</li> <li>- reconstitution in 200 µl Milli-Q water</li> <li>- cleaning 100 µl hydrolysate through P3 cartridges with addition of 300 µl acetonitrile</li> <li>- drying of the collected sample in a vacuum centrifuge</li> <li>- reconstitution in 200 µl isopropanol : acetonitrile : water (45:45:10) mixture</li> </ul>																									
<b>UPLC conditions</b>	<ul style="list-style-type: none"> <li>- Instrument: ACQUITY UPLC system coupled to a Xevo G2-XS QToF MS system, operating in negative ion mode</li> <li>- Injection volume: 10 µl</li> <li>- Mobile phase A: water and 0.1% formic acid</li> <li>- Mobile phase B: acetonitrile and 0.1% formic acid</li> <li>- Column: Acquity UPLC BEH Amide column (100 x 2.1 mm, 1.7 µm)</li> <li>- Column temperature: 40 °C</li> <li>- Flow: 0.4 ml/min</li> <li>- Tune parameters: sample cone 40 V, capillary 1 V; Temperature: source 120 °C, desolvation 550 °C; Gas flow: gas cone 50 L/h, desolvation gas 1000 L/h</li> </ul>																									

Table 6.3. Summarized conditions used during the method validation (where DMSO had a final concentration of 10%).

## 4.2 Results and discussion

### 4.2.1 Between-day precision with d<sub>2</sub>-CML as an internal standard

The calibration curves of CML ( $R^2 > 0.9182$  on day 1, 0.9064 on day 2, 0.9070 on day 3) and the results for the determination of the between-day precision of CML in *in vitro* samples with d<sub>2</sub>-CML as an internal standard are presented in Figure 6.14.

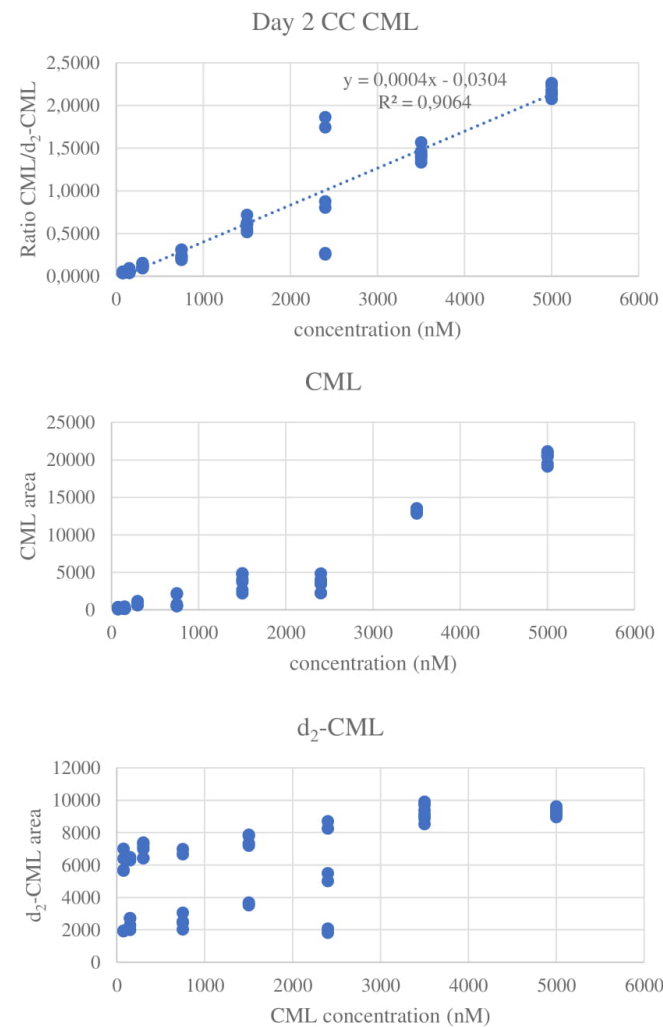
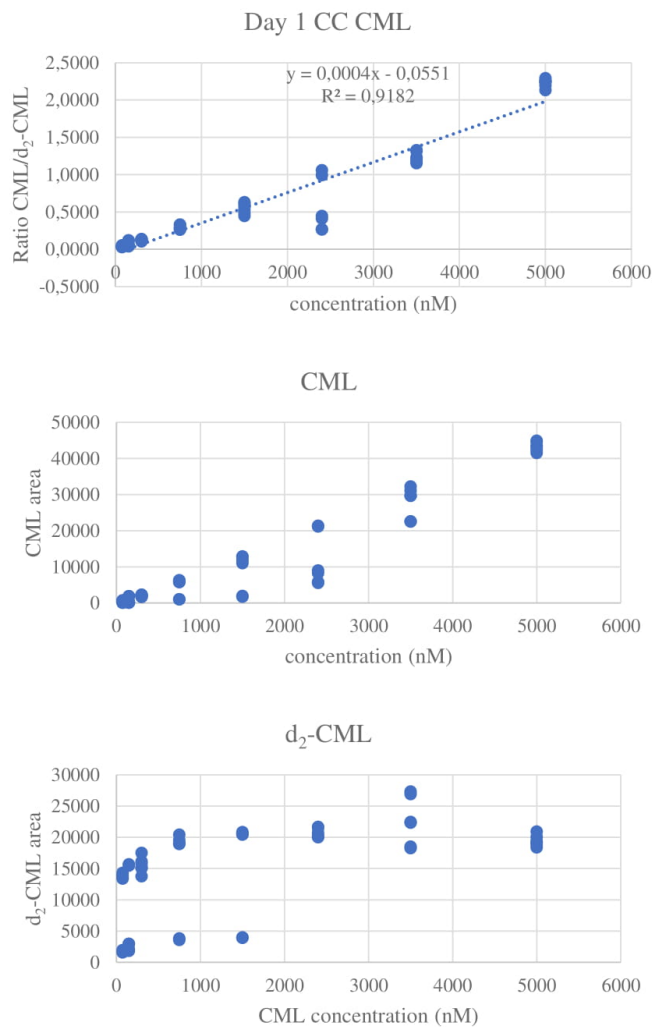


Figure 6.14. Calibration curves (CC) for CML in *in vitro* samples with d<sub>2</sub>-CML as an internal standard (Ratio, CML area, d<sub>2</sub>-CML area with increasing concentration of CML). Samples were prepared in triplicate and were measured in “Varian” vials.

The samples that contained a known AGEs inhibitor, aminoguanidine, showed a gradual concentration dependent decrease in the AGEs formation, in contrast to pyridoxamine which was extremely potent in the applied concentrations (Figure 6.15). The control samples on day 3 had a lower value than normally expected in comparison to the previous two measurements (data not presented). Therefore, the last experiment had to be performed again.

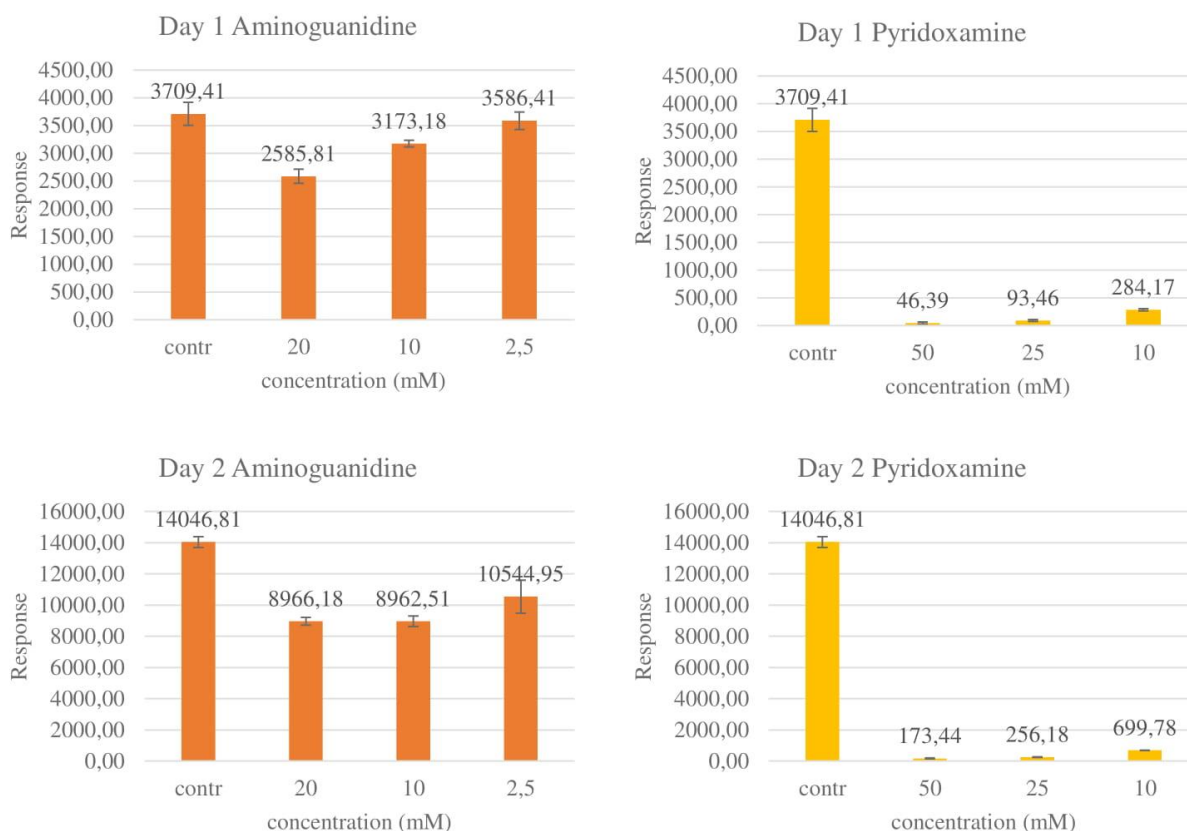


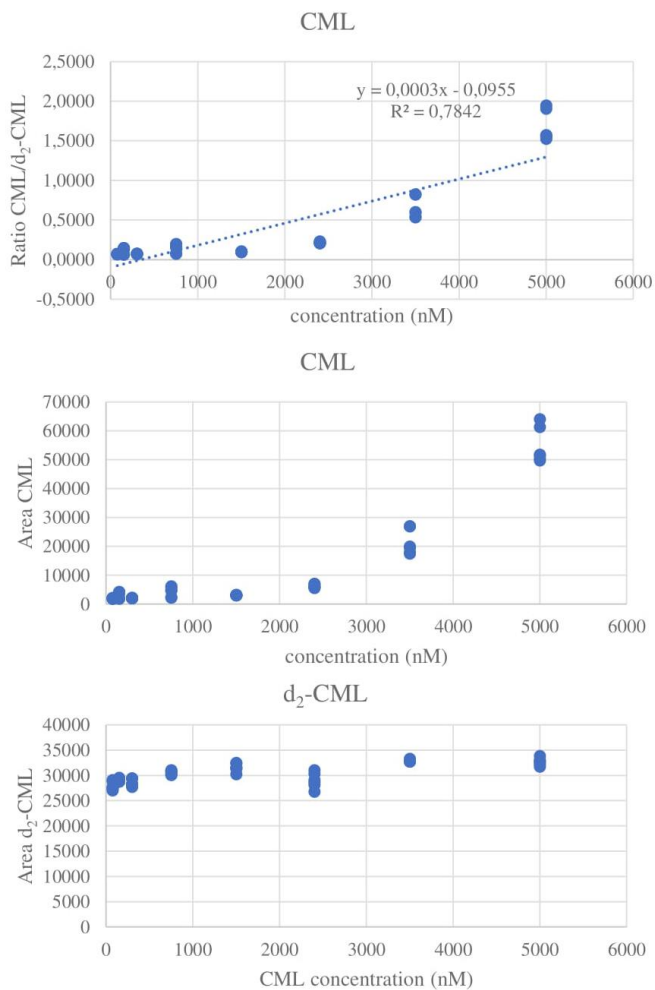
Figure 6.15. Inhibitory effect on AGEs formation of pyridoxamine and aminoguanidine on day 1 and day 2 where the figures represent mean  $\pm$  SD of three replicates and the experiment was performed only once. The response was obtained based on the ratio CML/d<sub>2</sub>-CML from the incubated samples, and the slope and the intercept values from the linear equation from the calibration curve samples.

Unfortunately, at a given moment the stock of the “Varian” vials was finished and the company was out of business. Therefore, there was an urgent need for new vials suitable



for the analysis. Several vials were tested: LCGC Certified Clear Glass 12x32 mm Screw Neck Vial, Total Recovery, with Cap and Pre-slit, PTFE/Silicone Septum, 1ml volume (186000385C, Waters), TruView LCMS Certified Clear Glass 12x32 mm Screw Neck Vial, with Cap and Pre-slit, PTFE/Silicone Septum, 2ml volume (186005666CV, Waters), polypropylene Screw neck vials 0.300 ml (702226, Macherey-Nagel GmbH & Co.KG), Polypropylene 12 x 32 mm Screw Neck Vial, with Cap and Preslit PTFE/Silicone Septum, 0.700 ml volume (186005221, Waters) and Screw top 12x32 mm polypropylene vials, certified, 0.250 ml (5190-2242, Agilent). The linearity experiment was performed for incubated samples using different test vials (Figure 6.16). The results from the tests carried out using standard solutions of CML and d<sub>2</sub>-CML prepared in the isopropanol : acetonitrile : water (45:45:10) mixture are presented in Figure 6.17.

0.7 ml polypropylene vials, 186005221 (Waters)



0.3 ml polypropylene vials, 702226 (Macherey-Nagel GmbH&Co.KG)

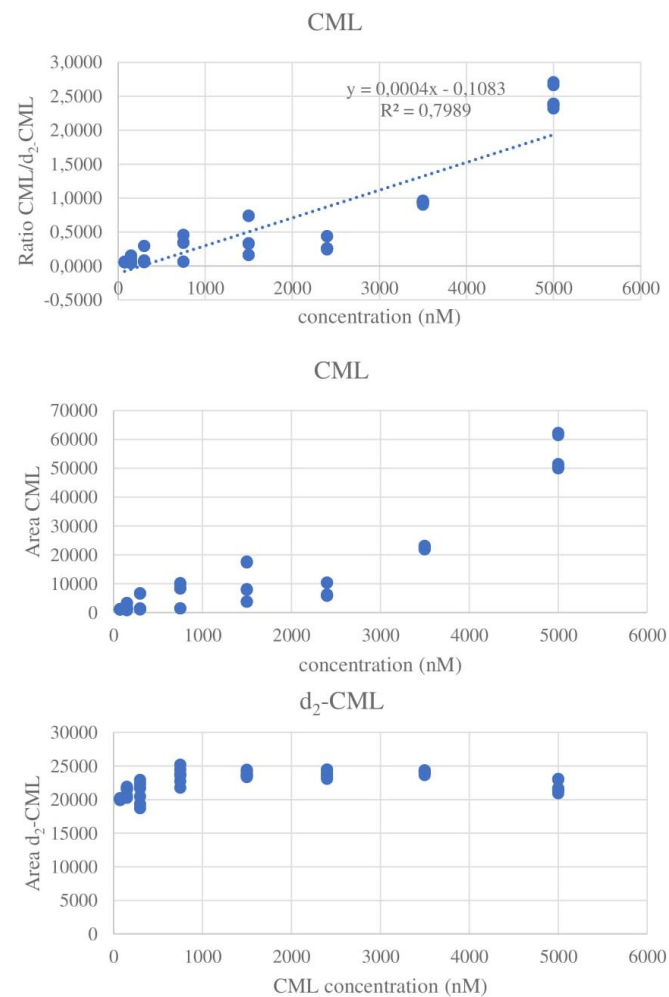
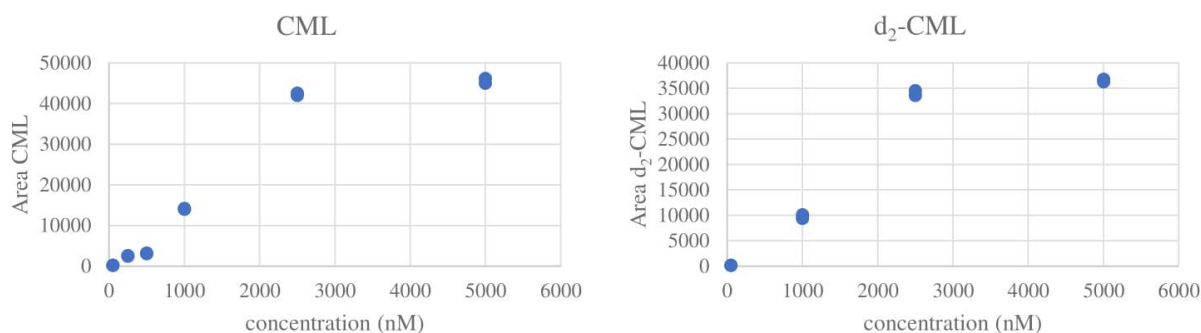


Figure 6.16. Linearity experiment for incubated samples performed with two different polypropylene vials and d<sub>2</sub>-CML used as an internal standard.

### 1.0 ml Total Recovery vials, 186000385C (Waters)



### 0.250 ml polypropylene vials, 5190-2242 (Agilent)

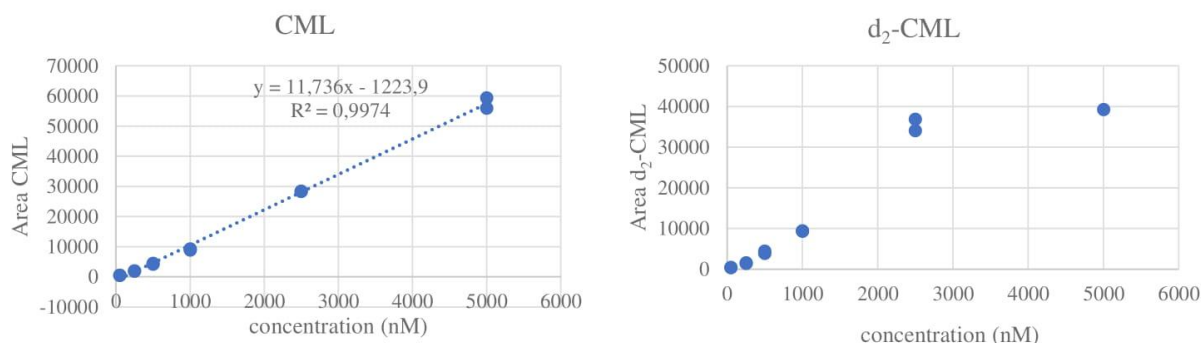


Figure 6.17. Results from standards CML and d<sub>2</sub>-CML prepared individually with isopropanol:acetonitrile:water (45:45:10) mixture in different test vials

As seen from the graphs in Figure 6.16, no linear response for the incubated samples analyzed in Waters 0.700 ml polypropylene vials (186005221) and Macherey-Nagel, 0.300 ml polypropylene vials (702226) was found. Only the graphs from the d<sub>2</sub>-CML, showed consistent results. Moreover, regarding the calibration curves from the CML and d<sub>2</sub>-CML standards investigated in the Total recovery vials from Waters (186000385C), a plateau response was observed. Similarly, for the d<sub>2</sub>-CML measured in polypropylene vials from Agilent (5190-2242) also a plateau was reached starting from 2500 nM CML,

in contrast to the CML samples where a calibration curve could be generated. Based on the results, the Agilent vials were considered as the best choice with regard to effectiveness and price. Additionally, a decision to change the internal standard from d<sub>2</sub>- to d<sub>4</sub>-CML was taken. Since a compound and its stable isotope labelled internal standard will theoretically co-elute, it is important that the mass difference between the compounds is at least 3 mass units, in order to be able to separate them in the mass analyser. When the difference is less than 3 mass units (as it was the case with d<sub>2</sub>-CML), the isotope peak of the analyte might interfere with the signal of the internal standard.<sup>237</sup>

#### 4.2.2 New internal standard: d<sub>4</sub>-CML

The final attempt to improve the precision of the method was to include another deuterated form of CML as an internal standard such as N-ε-carboxy[4,4,5,5-D<sub>4</sub>]methyl-L-lysine (d<sub>4</sub>-CML). The preliminary test, where only standard dilutions of d<sub>4</sub>-CML prepared in the isopropanol : acetonitrile : water (45:45:10) mixture were analyzed, is shown in Figure 6.18.

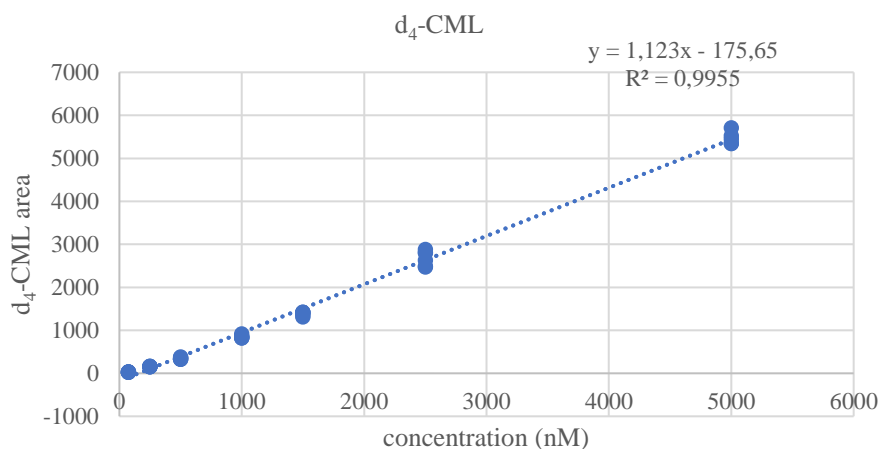


Figure 6.18. Calibration curve of standard dilutions of d<sub>4</sub>-CML prepared in the isopropanol:acetonitrile:water (45:45:10) mixture. Samples were made in triplicate.

Then, the calibration curve samples had to be prepared in the same biological matrix as the samples in the intended study, namely, containing protein (Gk-peptide, 1.7 mg/ml),

sugar (D-ribose 1 mg/ml), standard dilutions of CML (75 nM – 2500 nM final concentration) and 1000 nM d<sub>4</sub>-CML internal standard (Figure 6.19).

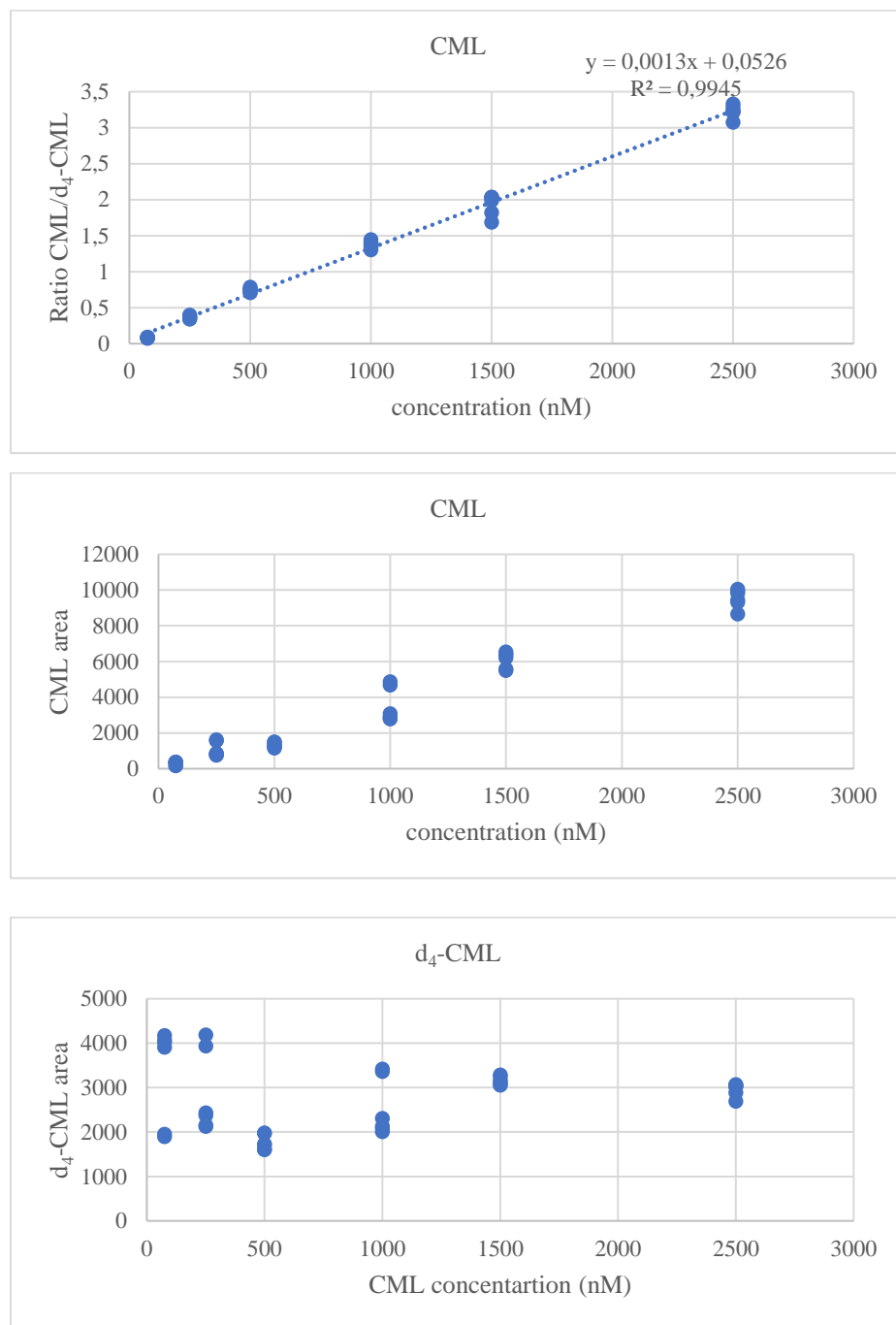


Figure 6.19. Calibration curve samples containing protein (Gk-peptide, 1.7 mg/ml), sugar (1 mg/ml), standard dilutions of CML (75 nM – 2500 nM final concentrations) and 1000 nM d<sub>4</sub>-CML as an internal standard. Samples were prepared in triplicate.

Some general observations after those preliminary tests were made: From the data after injecting standard dilutions of d<sub>4</sub>-CML prepared in isopropanol : acetonitrile : water (45:45:10) mixture, the response for the 1000 nM concentration was around 800. However, the samples which were prepared with the Gk-peptide/ ribose mixture, standard dilutions of CML and 1000 nM d<sub>4</sub>-CML internal standard, showed inconsistent response for the deuterated standard. Moreover, the average response for the 1000 nM internal standard included in all samples was higher than the 800 value obtained before. Bearing in mind that the latter samples had experienced several sample preparation steps where expectable losses were considered (data not included), these results could not be explained.

Nevertheless, the optimal concentration of d<sub>4</sub>-CML as an internal standard was yet to be examined. Additionally, several sets of samples were prepared varying the initial concentration of Gk-peptide and ribose in the incubation mixture, in order to check whether a higher concentration of formed CML could affect the response of d<sub>4</sub>-CML. These included: 1.7 mg/ml for the protein and 1 mg/ml for the sugar (condition 1), or 0.85 mg/ml protein and 0.50 mg/ml, sugar respectively (condition 2). The selected concentration of d<sub>4</sub>-CML added to each sample was 1000 nM or 2000 nM, respectively. After preparing the two mixtures, they were incubated at 37 °C for 16 h, and samples were taken every hour. The results from using 1.7 mg/ml protein and 1 mg/ml sugar (condition 1) for the incubation mixture and 2000 nM d<sub>4</sub>-CML as an internal standard are shown in Figure 6.20. The first group of graphs (A) represents the results from the CML calibration curve samples prepared in Gk-peptide/ ribose mixture after carrying out the sample preparation steps. A linear response could be generated and the graph investigating only the d<sub>4</sub>-CML results had the expected pattern. However, for the incubated samples the linear response was lost (Figure 6.20B). And although the CML was gradually generated in time, the values for the internal standard only, were inconsistent - random excessively high values were measured.

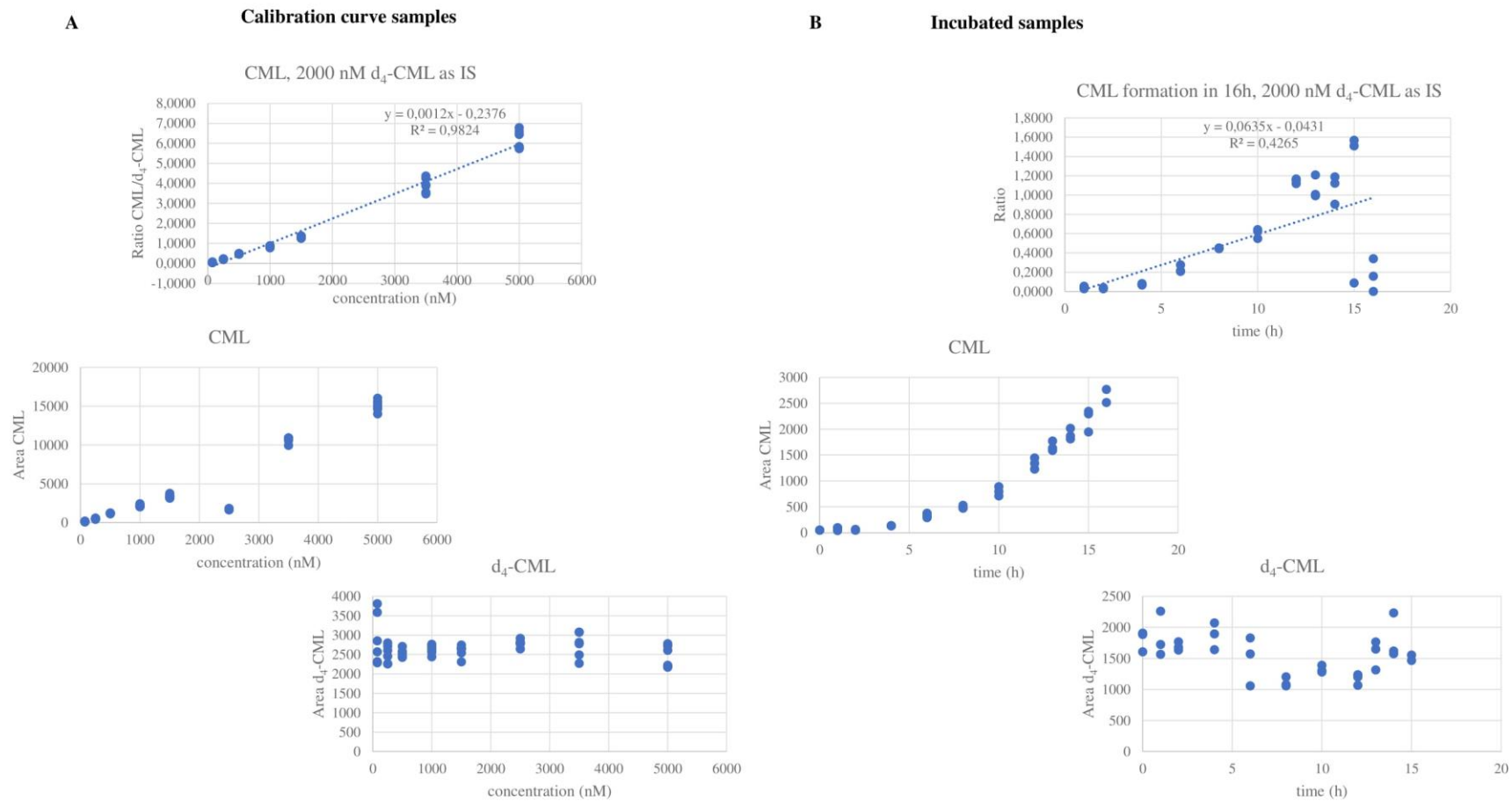


Figure 6.20. Results from the incubation mixture with conditions 1 (1.7 mg/ml protein and 1 mg/ml sugar) and 2000 nM d<sub>4</sub>-CML as an internal standard (IS). Calibration curve samples (A) and samples incubated for 16 h (B). All samples were prepared in triplicate.

The data for the samples containing 1000 nM d<sub>4</sub>-standard is not presented. The same relatively low response for the 1000 nM d<sub>4</sub>-CML was measured with incubation conditions 1 (1.7 mg/ml for the Gk-peptide and 1 mg/ml for the ribose); or inconsistency in the response was detected after applying the incubation conditions 2 (0.85 mg/ml protein and 0.50 mg/ml sugar). Although all samples had followed the same sample preparation steps and were measured in the same instrumental conditions, the unexpected results could not be explained. Nevertheless, the 2000 nM d<sub>4</sub>-CML concentration was selected for proceeding the experiment.

Recently, there has been increasing attention for the adequate monitoring of internal standard response for LC-MS/MS analysis. The variable response of the internal standard in the current method was similar as the one previously reported by Aimin Tan *et al.*<sup>239</sup> The gradual decrease and randomly scattered low internal standard values has been explained by autosampler needle blockage. However, in our results the internal standard in the calibration samples was not affected and a matrix-related issue was also considered.

According to the Waters Comprehensive Guide to HILIC, one of the parameters that is often overlooked when working with HILIC mode is the needle wash solvent.<sup>230</sup> Therefore, the composition of the needle wash solvent set up in the instrument (i.e., strong/ weak needle wash, purge solvent, etc.) was reconsidered. The weak wash was changed from water : methanol : acetonitrile : isopropanol (25:25:25:25) with 0.02% formic acid to just 90% acetonitrile in water. Based on the mentioned guide, it was recommended to accommodate the composition of this wash solvent to match that of the initial mobile phase conditions (90 – 95% acetonitrile). Otherwise retention may be altered or completely lost. Moreover, the amount of washing solvent used after each injection was increased (from 200 to 400 µl), as well as the blank samples used between the different samples (from isopropanol : acetonitrile : water (45:45:10) to 90% acetonitrile); and a switch from partial to full loop was applied.

The optimal amount of CML formed, which would not affect the response of the internal standard, was reinvestigated. The two incubation conditions described above were used to monitor its concentration over a period of 36 h and by taking a sample every hour. Condition 1 included the use of 1.7 mg/ml for the Gk-peptide and 1 mg/ml for the ribose



(Figure 6.21A); and condition 2: 0.85 mg/ml of the protein and 0.50 mg/ml for the sugar, respectively (Figure 6.21B).

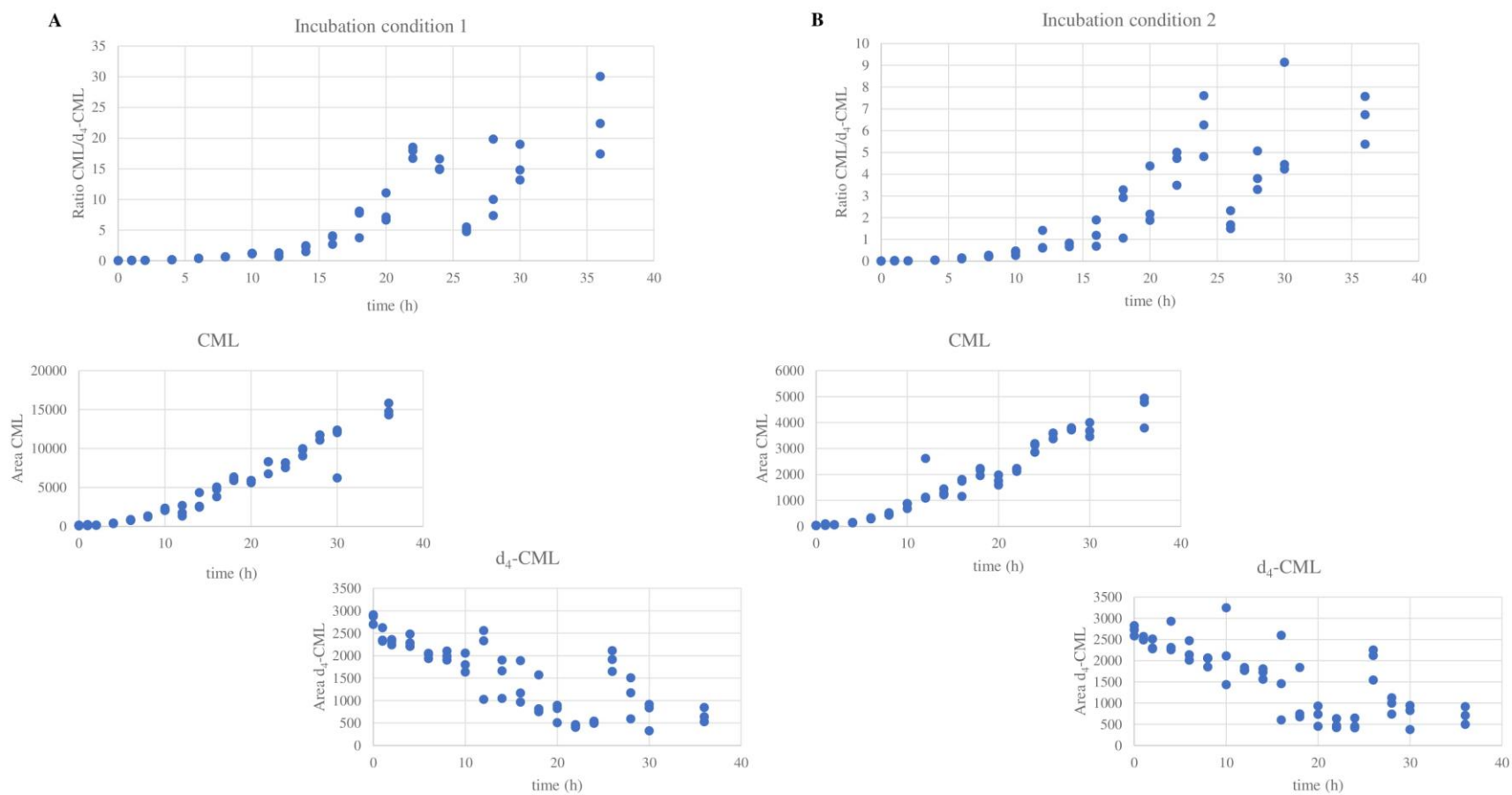


Figure 6.21. Results for CML formation in two sets of incubation conditions during 36 h. 2000 nM d<sub>4</sub>-CML was used as an internal standard (IS) and the injection volume was 10 μl. All samples were made in triplicate.

The first graphs from Figure 21A and B represent the CML formation as a function of time, and the ratio between the CML response and the d<sub>4</sub>-CML (2000 nM) internal standard. By applying both incubation conditions the CML formation was gradually increasing in time (graphs based on the correlation between time and the area of the CML signal). However, the results from the deuterated standard remained as before. Despite the implemented changes, the response of the internal standard did not show an optimal pattern. A blockage of the needle was excluded as a potential problem. However, based on the results, it was decided to maintain the concentration of the components in the incubation mixture as before, namely, 1.7 mg/ml for the protein and 1 mg/ml for ribose. It was not beneficial to decrease these concentrations due to the really low amount of CML formed, which might hinder the adequate measurement of inhibitory properties of test compounds afterwards.

Additionally, the injection volume was investigated with regard to the previously suspected matrix effect. The initial injection volume was set at 10 µl (Figure 6.21). However, smaller sample volumes were tested, namely, injecting 5 µl and 2 µl. After injecting 5 µl of sample (Figure 6.22), the response for the internal standard was better and enabled the generation of a calibration curve.

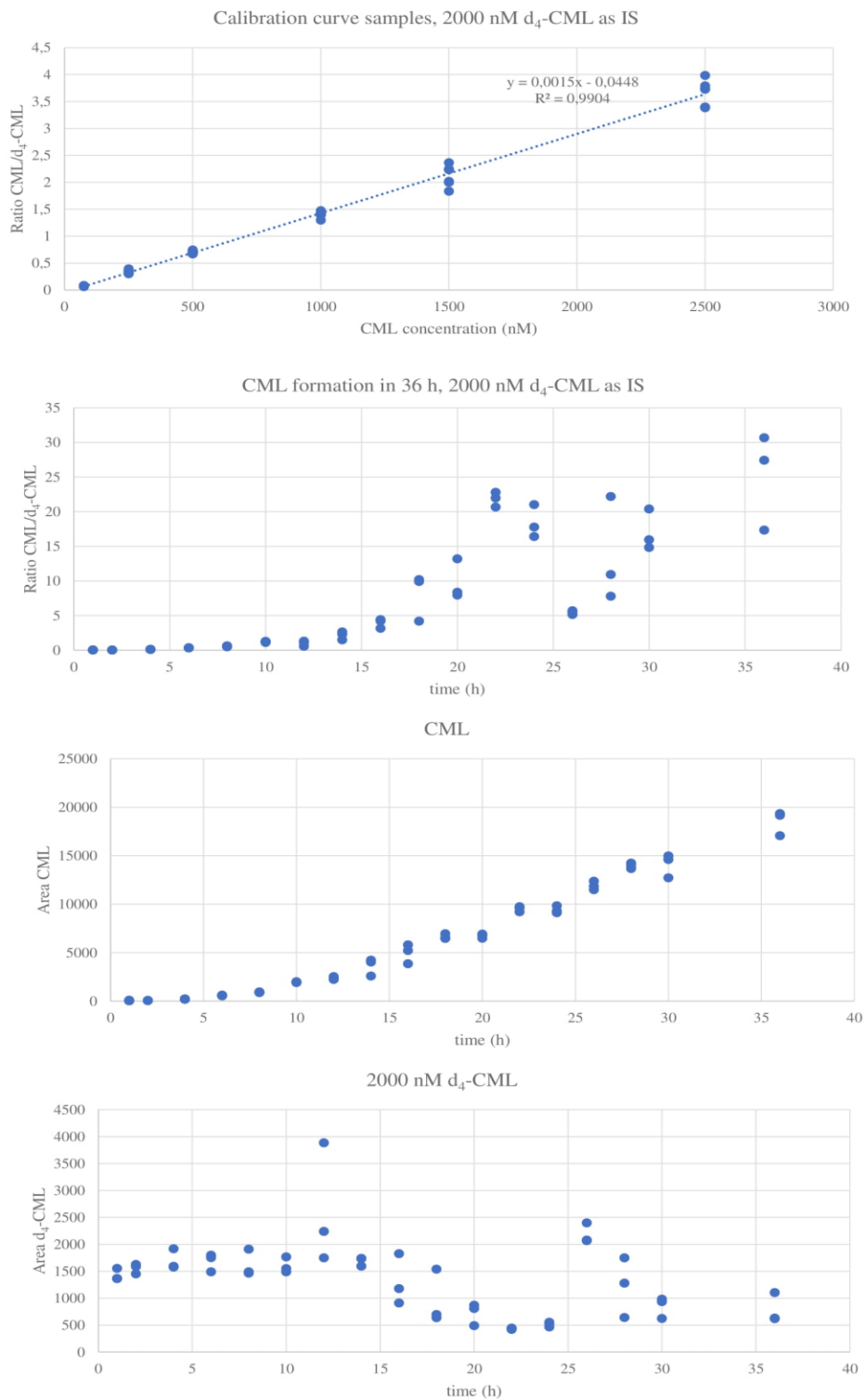
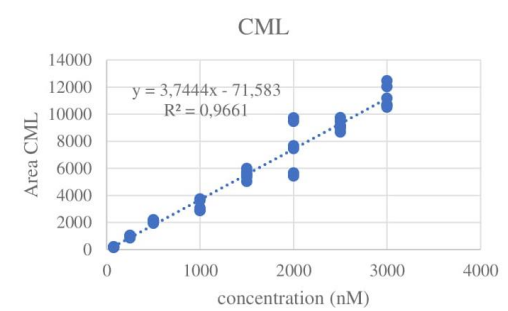
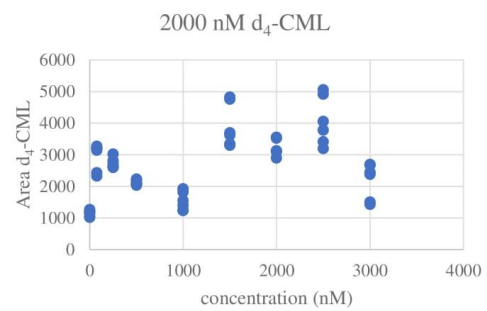
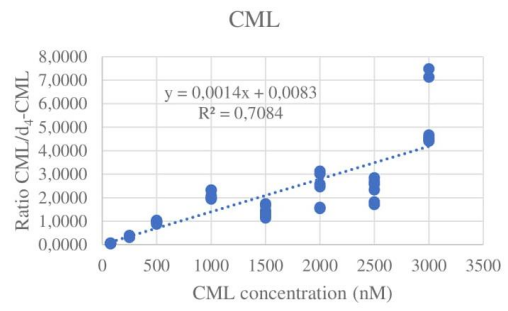


Figure 6.22. Results for monitoring CML formation, using incubation conditions 1, during 36 h. 2000 nM d<sub>4</sub>-CML was used as an internal standard (IS) and the injection volume was 5 μl. Samples were prepared in triplicate.

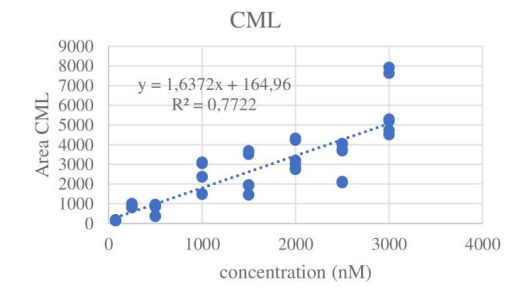
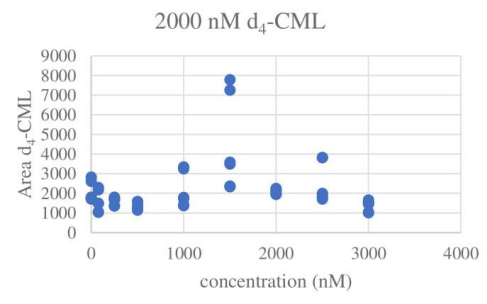
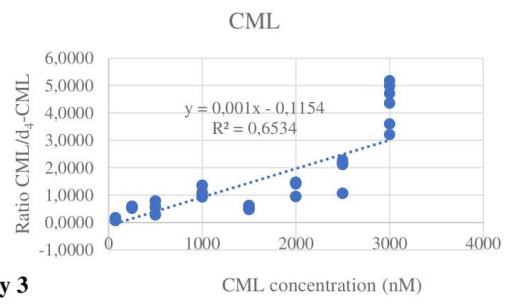
The data for the experiment in which 2  $\mu\text{l}$  was injected are not shown. Not surprisingly, the signal of the internal standard was particularly low in this case, which might affect the precise quantification. In summary, after detailed investigation, the following conditions were selected: incubation conditions 1, 2000 nM  $d_4$ -CML as an internal standard, incubation time 14 h and injection volume 5  $\mu\text{l}$ .

After the applied changes, the between-day precision was determined. Unfortunately, the three days data sets still showed considerable inconsistency in the response of the internal standard (Figure 6.23). In spite of reducing the injection volume and setting the detector to collect the data only in the time period when the peaks of interest were eluted, the internal standard behaviour remained unclear. However, in the end, the calibration curve was constructed without the ratio between CML and  $d_4$ -CML, but only based on the area of CML. Even then, good linear response was achieved only for day 1 samples ( $R^2$  value 0.9661). For the other two days (day 2 -  $R^2$  value 0.7722, and day 3 -  $R^2$  value of 0.6675) a calibration curve was not obtained.

**Day 1**



**Day 2**



**Day 3**

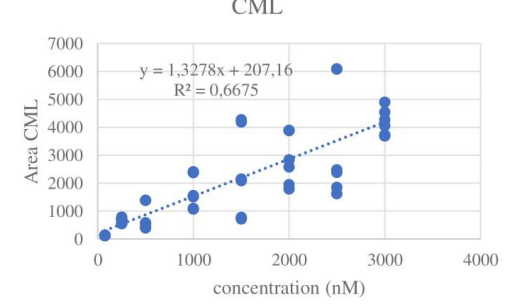
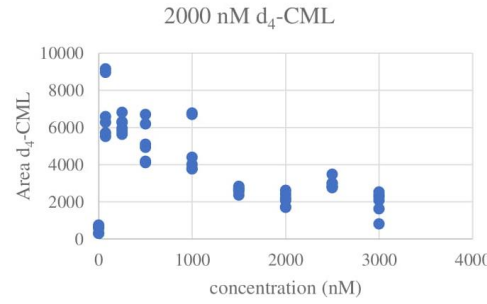
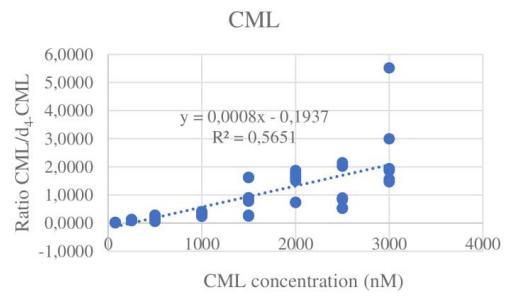


Figure 6.23. Between-day precision results of samples (in triplicate) with 2000 nM d<sub>4</sub>-CML as an internal standard.

In addition, during the test aminoguanidine was used as a positive control in concentrations of 2.5, 10, 20, 25 and 30 mM, and for all days a concentration dependent decrease of AGEs formation was observed. As a result, 20 mM aminoguanidine, which showed about 50% inhibition (Figure 6.24), was selected as a positive control in the current assay for the future testing of natural products.

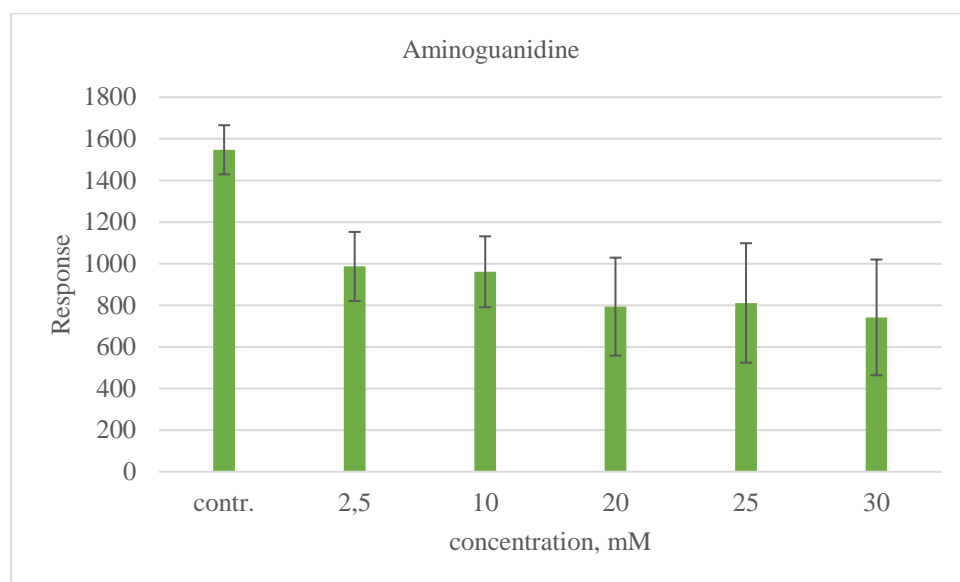


Figure 6.24. Effect on AGEs inhibition from testing different concentrations aminoguanidine as a candidate for a positive control. The figures represent mean  $\pm$  SD of three replicates and the experiment was performed only once. The response was obtained based on the ratio CML/d<sub>4</sub>-CML from the incubated samples, and the slope and the intercept values from the linear equation from the calibration curve samples (day 1).

### 5. Results from isolated pure compounds and commercial standards tested in the method

The final step in the experimental workflow was to investigate some of the isolated natural products (see Chapter 3) and selected commercially available pure compounds in the current method in order to evaluate their AGEs inhibiting properties. Due to the above mentioned issues with the internal standard, the results for AGEs inhibition were based only on the decreased area of CML formation in the incubation mixture while the tested compounds were present. The results are included in Figure 6.25 and Figure 6.26.

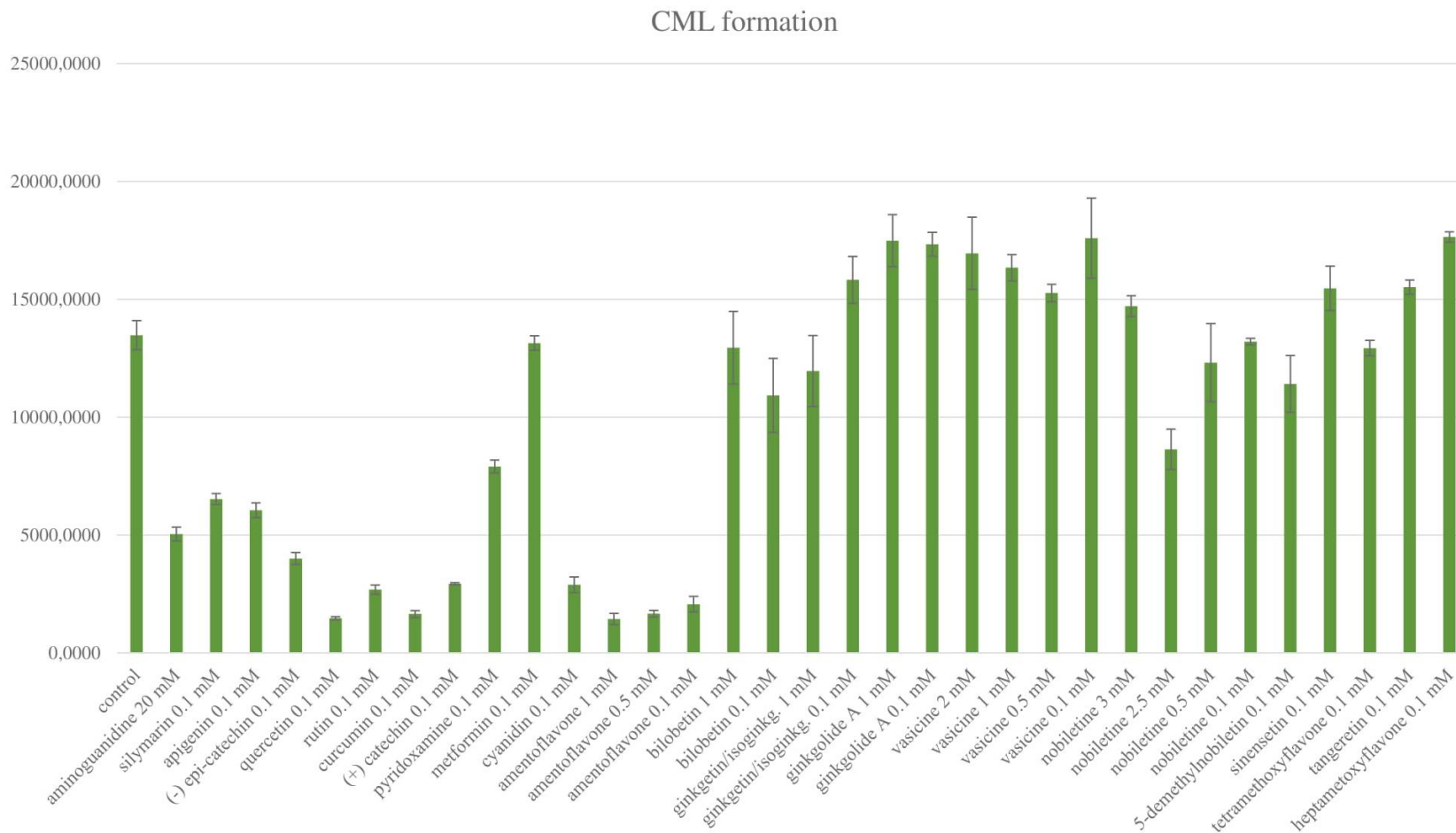


Figure 6.25. Isolated natural products and commercially available pure compounds and their effect on the CML formation.



From the figure it could be easily observed that several commercially obtained natural products showed significant decrease in AGEs formation, for example: 0.1 mM silymarin and 0.1 mM apigenin demonstrated activity similar to the positive control, while 0.1 mM (-) epi-catechin, 0.1 mM quercetin, 0.1 mM curcumin, 0.1 mM rutin, 0.1 mM (+) catechin, 0.1 mM cyanidin, and the three different concentrations of amentoflavone inhibited CML formation to a greater extent than aminoguanidine. From the other standard compounds, 0.1 mM pyridoxamine proved more potent activity than metformin tested in the same concentration. From the isolated compounds the mixture ginkgetin/isoginkgetin, 2.5 mM nobiletin and 0.1 mM 5-demethylnobiletin had a moderate anti-AGEs activity but further tests are required to calculate the  $IC_{50}$  value. Statistically significant differences between groups regarding the commercially obtained natural product standards was shown by one way – ANOVA. The Bonferroni multiple comparisons test was performed to ascertain which pairs of groups differ significantly from one another and presence of statistically significant differences was found between many of them like: control and aminoguanidine,  $p < 0.001$ , control and 0.1 mM silymarin, 0.1 mM apigenin, 0.1 mM (-) epi-catechin, 0.1 mM quercetin, 0.1 mM rutin, 0.1 mM curcumin, 0.1 mM (+) catechin, 0.1 mM pyridoxamine and 0.1 mM cyanidin (for all  $p < 0.001$ ) (Figure 6.26). Many test compounds showed activity at 0.1 mM, and were much more active than the positive control aminoguanidine tested at 20 mM concentration.

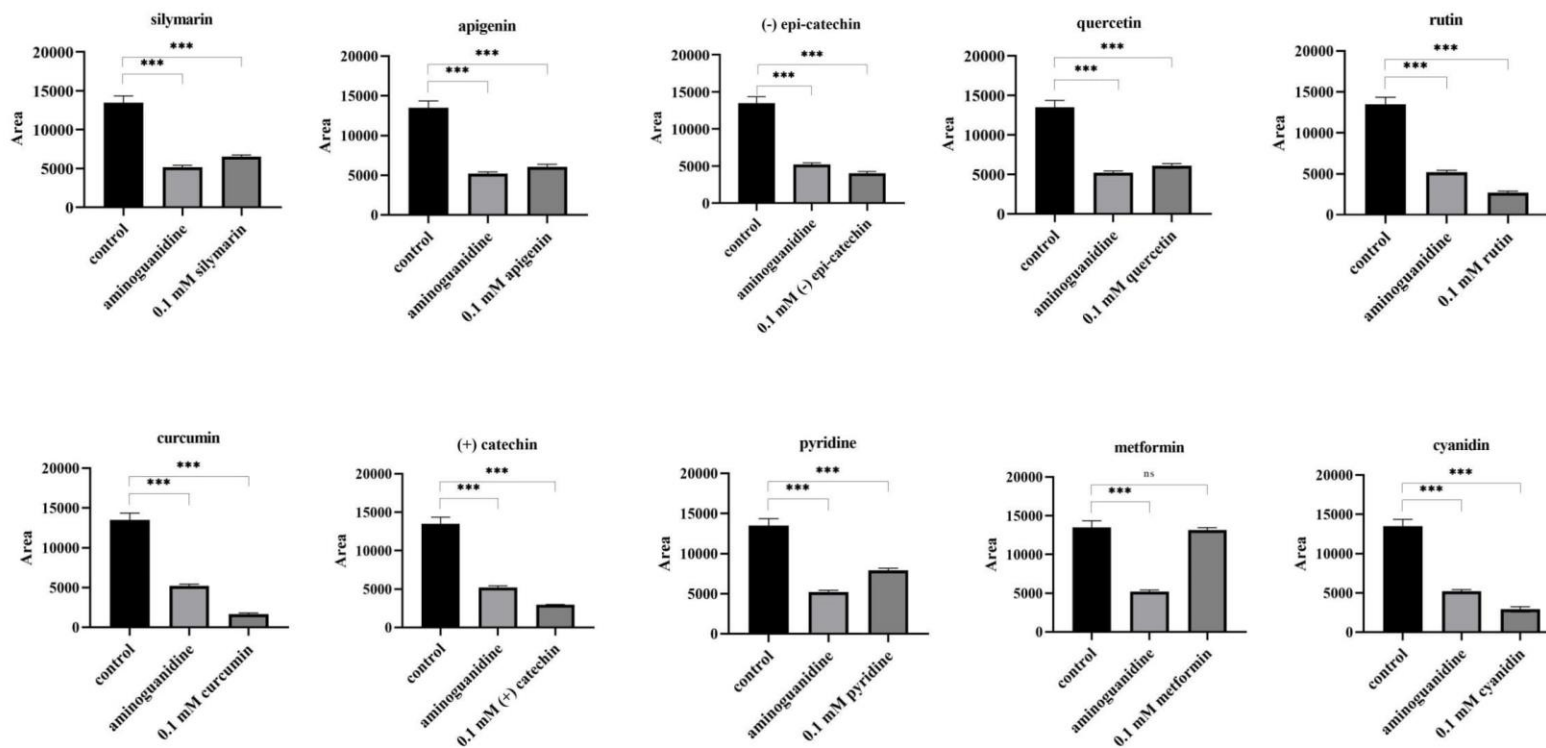


Figure 6.26. Statistically significant differences for commercially obtained natural products tested for reducing the CML formation (\*  $p < 0.05$ , \*\*  $p < 0.01$ , \*\*\*  $p < 0.001$ ). Samples were prepared in triplicate and the experiment was performed only once.

One way – ANOVA was performed ( $p < 0.001$ ) to study the statistically significant differences between groups regarding the isolated pure compounds from *Citrus* species, *Ginkgo biloba* and *Adhatoda vasica*. After Bonferroni multiple comparison test statistically significant inhibition of AGEs was seen between control and 2.5 mM nobiletin,  $p < 0.001$ ; control and 0.1 mM 5-demethylnobiletin (Figure 6.27).

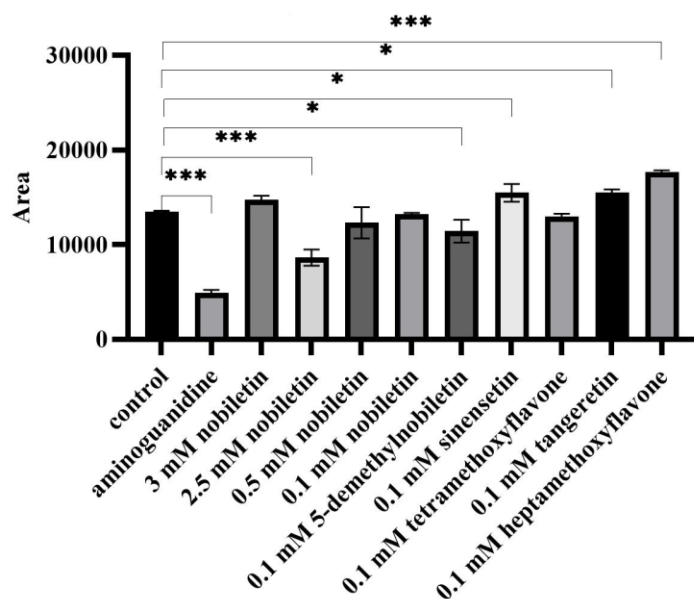


Figure 6.27. Statistically significant difference for polymethoxylated flavonoids tested for reducing CML formation (\*  $p < 0.05$ , \*\*  $p < 0.01$ , \*\*\*  $p < 0.001$ ). Samples were prepared in triplicate and the experiment was performed only once.

The Bonferroni test revealed statistically significant inhibition of AGEs also for the tested biflavonoids: control and 1 mM, 0.5 mM, 0.1 mM amentoflavone,  $p < 0.001$ ; and control and 0.1 mM bilobetin,  $p = 0.035$ ; for the rest of the samples no statistically significant difference was found (see Figure 6.28).

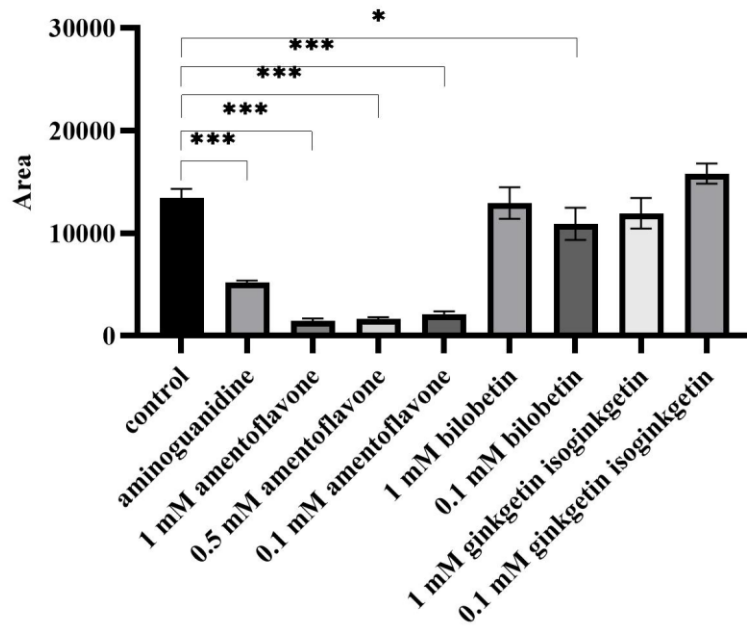


Figure 6.28. Statistically significant differences for biflavonoids tested for reducing CML formation (\*  $p < 0.05$ , \*\*  $p < 0.01$ , \*\*\*  $p < 0.001$ ). Samples were prepared in triplicate and the experiment was performed only once.

Vasicine showed no AGEs inhibition (Figure 6.29).

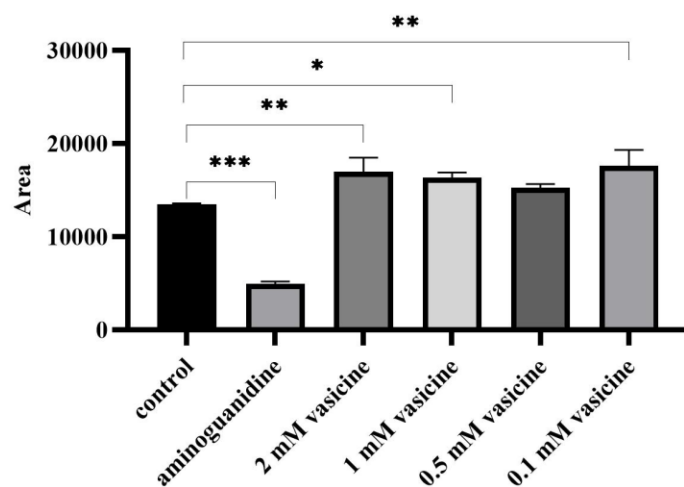


Figure 6.29. Statistically significant differences for different concentrations vasicine tested for reducing CML formation (\*  $p < 0.05$ , \*\*  $p < 0.01$ , \*\*\*  $p < 0.001$ ). Samples were prepared in triplicate and the experiment was performed only once.

However, during this last experiment a new aspect concerning the future testing of compounds and extracts in the assay was noted, namely, the solubility of test products in DMSO, which would limit the highest possible test concentration, and the solubility of the test products in the incubation mixture. For instance, the commercial products (without pyridoxamine and metformin) were tested also in a final concentration of 1 mM; however, after their addition to the incubation solution, precipitation was observed which required performing further analysis of a lower concentration. For all concentrations of nobiletin (except the 0.1 mM final concentration), samples showed precipitation of the compound after incubation overnight. Nevertheless, the sample preparation was continued and after adding the acid for hydrolysis, the sample turned to an intense yellow solution (compound finally dissolved). The obtained activity should not be considered as accurate, if the compounds were not completely dissolved. The rest of the polymethoxylated flavonoids showed no change of color after adding the acid. Presumably, the measured activity could be considered as accurate.

## 6. Conclusion

During this research project numerous steps were taken in order to develop an analytical procedure which can address the demand for reliable quantification of AGEs levels in biological samples. By implementation of mass spectrometry, analysis of the lysine derivative - N-(carboxymethyl)-lysine (CML) in *in vitro* models was performed. CML, one of the most abundant AGEs *in vivo*, as well as *in vitro*, was a logical choice for the developed method the far-sighted goal of which was the precise and unambiguous quantification of the AGEs inhibiting properties of selected natural products. The current chapter was a narrative description of all the steps that were taken in the development of the analytical protocol. In summary, determination of the CML levels was achieved through: an UPLC/ QToF Xevo MS detection system connected to a BEH Amide column, and gradient elution with water with 0.1% formic acid (eluent A) and acetonitrile with 0.1% formic acid (eluent B), using 2000 nM d<sub>4</sub>-CML as an internal standard. The samples were generated by incubating Gk-peptide (1.7 mg/ml) and ribose (1 mg/ml) for 14 h at 37 °C; then the sample preparation steps included acid hydrolysis with 6M hydrochloric acid at 100 °C for 24 h; and a cleaning step through P3 cartridges. Before analysis the samples were reconstituted in isopropanol:acetonitrile:water (45:45:10) and placed in polypropylene vials ready for analysis. All the steps are summarized in Figures 6.30 and 6.31.

The following challenge was to test the current method for investigating the AGEs inhibition of isolated pure compounds (see Chapter 3) and some commercially available standards. 20 mM aminoguanidine was applied as a positive control. From the isolated compounds the mixture ginkgetin/isoginkgetin 1 mM and 5-demethylnobiletin 0.1 mM demonstrated moderate activity in the method, and extra tests are necessary to obtain the IC<sub>50</sub> concentration. The overall results from the commercially obtained standards were in line with reported findings in literature concerning their eventual anti-AGEs activity. However, the solubility of the natural products or plant extracts will be an important issue in the future application of the analytical method.

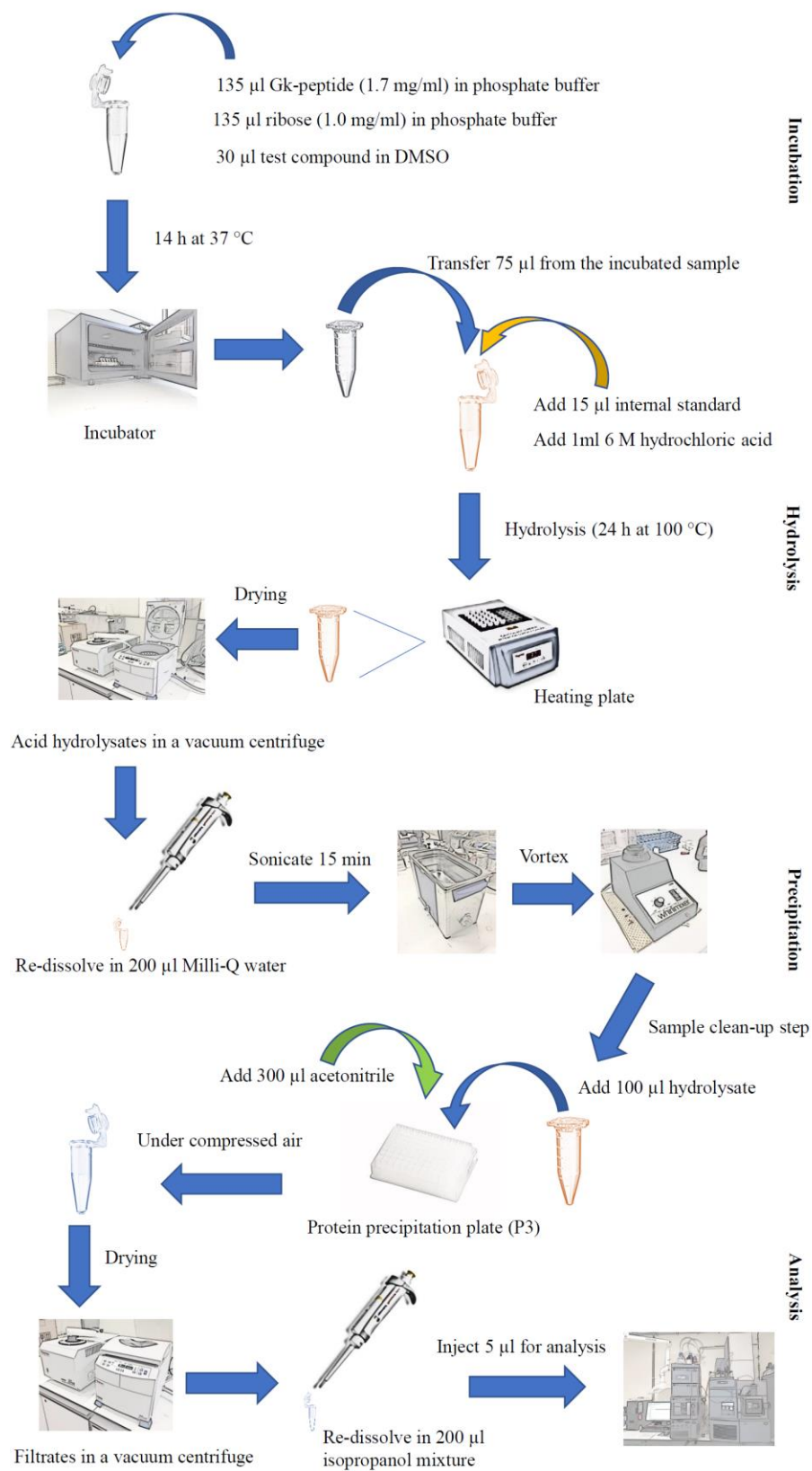


Figure 6.30. General scheme of the sample preparation steps.

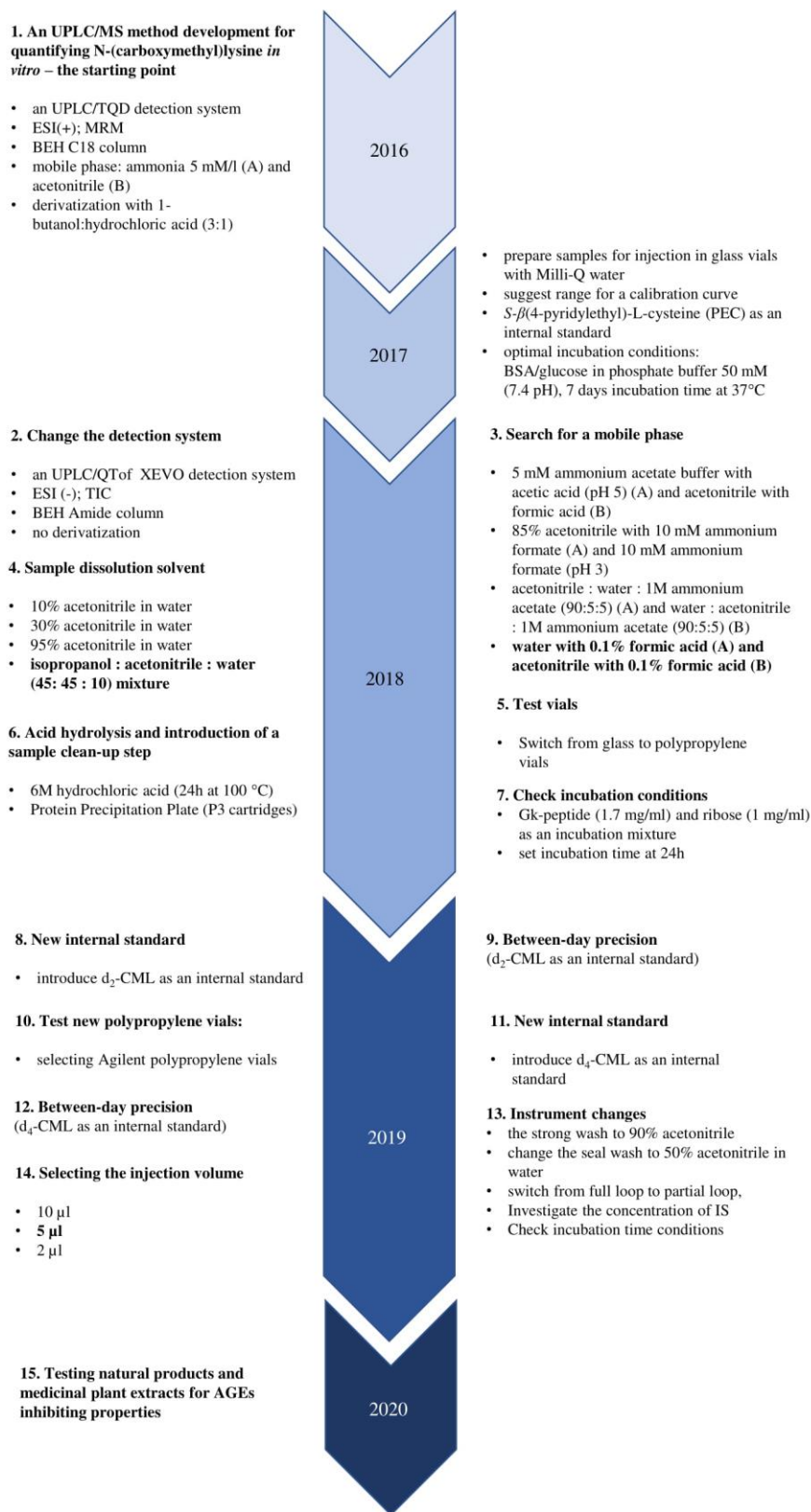


Figure 6.31. Timeline of the development and the validation of the method.



# Chapter 7

## The autophagy experiment



## 1. Introduction

The purpose of autophagy is to serve as a dynamic recycling process that produces new building blocks and energy for cellular renovation and homeostasis.<sup>87</sup> Autophagy can be activated in response to adverse environmental conditions, such as the deprivation of nutrients or growth factors. Autophagy also plays a role in the development and defence against microbial infections, and regulation of organelle homeostasis.<sup>240</sup> Therefore, dysregulation of autophagy can be involved in the pathogenesis of many human diseases like neurodegenerative diseases, heart diseases, cancer and aging.<sup>241</sup> Autophagy is a dynamic multistep process, therefore a combination of approaches should be implemented to identify and quantify autophagic activity in different systems including steady-state and flux measurements.<sup>81</sup> Generally, the assays used to determine the amount of autophagosomes, involve the detection of the LC3 protein. LC3 is the commonly used name for microtubule-associated protein light chain 3, an ubiquitin-like molecule that is the mammalian homologue of the autophagy-related protein 8 (Atg8) in yeast. The LC3 family contains four different known isoforms, namely, LC3A, LC3B, LC3B<sub>2</sub> and LC3C. Generally, LC3B is the most studied form in autophagy assays. Following translation, the unprocessed form of LC3 (proLC3) is cleaved by Atg4 protease, resulting in the LC3-I form (non-lipidated) with a carboxyterminal exposed glycine. Upon induction of autophagy, the exposed glycine of LC3-I is conjugated by Atg7, Atg3 and by Atg12-Atg5-Atg16L multimers (Figure 7.1) to the highly lipophilic phosphatidylethanolamine (PE) moiety, generating LC3-II (lipidated form).<sup>242</sup> LC3-II appears to be degraded and / or dissociated after autophagosome fusion with lysosomes, leaving less LC3 on the autolysosome membrane. As LC3-II is present on phagophores and autophagosomes, it serves as an indicator of autophagosome formation because it is the only well-characterized protein that is specifically localized in autophagic structures throughout the process from phagophore to lysosomal degradation.<sup>243</sup> Therefore, the level of LC3-II is widely used as a marker for monitoring the autophagic process.<sup>119</sup> The endogenous LC3 is detected as two individual bands in SDS-Page (sodium dodecyl sulphate polyacrylamide gel electrophoresis) and immunoblotting, representing the accurate number of autophagosomes. One band refers to the non-lipidated LC3-I form

(16-18 kDa), and the other represents the lipidated LC3-II form (14-16 kDa). Although LC3-II has larger molecular weight due to the PE-conjugation, it is still moving faster during the electrophoresis due to higher hydrophobicity.<sup>244</sup> Monitoring the autophagic flux by the turnover of LC3 using immunoblotting is one of the most common assays.<sup>243</sup> Another autophagic flux assay includes the determination of free GFP (green fluorescent protein) fragments resulting from the degradation of the GFP-fused LC3 (GFP – LC3) within the autolysosome.<sup>241</sup> When GFP – LC3 is expressed in cultured cells, punctate signals are observed by fluorescence microscopy, which represents isolation membranes and autophagosomes. Previous studies showed that GFP is more resistant than LC3 in response to lysosomal degradation and thus the determination of free GFP has been applied to study the autophagic flux.<sup>241</sup> However, these approaches are time-consuming and labour intensive and the results are often variable in different experimental settings and hard to interpret. Therefore, it is of utmost importance to perform different experimental procedures to confirm autophagy modulation properties of test compounds.<sup>243,245</sup>

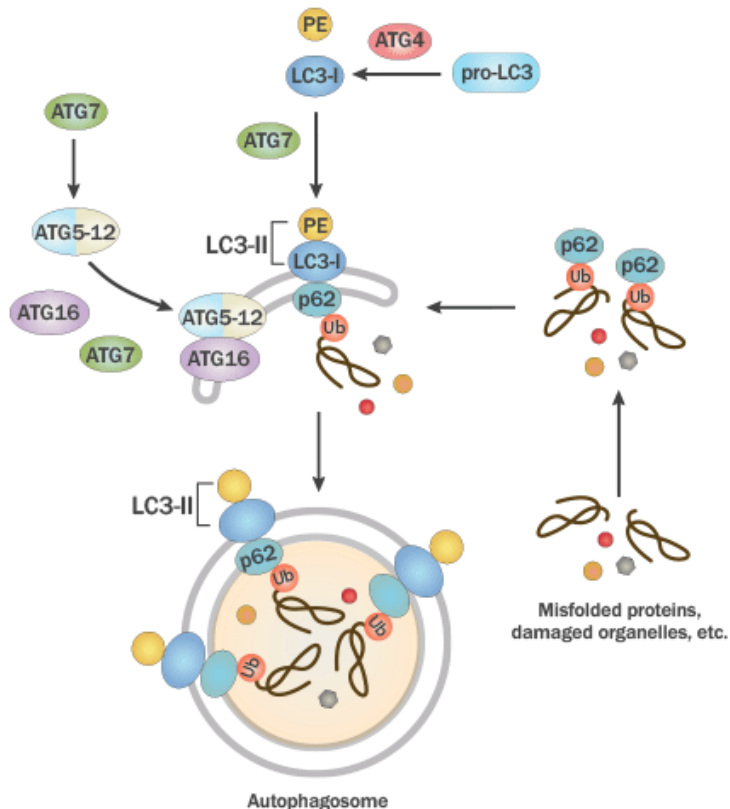


Figure 7.1. Transformation of LC3: Atg4 cleaves pro-LC3 to form LC3-I which then gets conjugated to PE (by Atg7) for the generation of LC3-II. The latter gets recruited to the autophagosomal membrane, helping its elongation. Atg7 also mediates Atg5-Atg12-Atg16 complex formation, which along with LC3-II is critical for the autophagosome formation. Adaptor protein p62 binds to ubiquitinated proteins and LC3-II for mediating autophagy via localizing into autophagic compartments, transporting ubiquitinated proteins and organelles for degradation.<sup>81</sup>

**Western blotting (immunoblotting)** is a widely used technique for protein detection and quantification e.g. for the LC3 protein. Western blot analysis measures the conversion of LC3 from unlipidated LC3-I to the lipidated form LC3-II. An increased conversion ratio corresponds to an increased autophagosome number. The quantification should be based mainly on the comparison between the LC3-II level and the level of a housekeeping protein (e.g.  $\beta$  – actin); however, expressing the result by using the ratio between LC3-II and LC3-I is considered as not accurate since LC3-II tends to be more sensitive to be detected by immunoblotting than LC3-I.<sup>246</sup> The increased LC3-II levels can be associated with either enhanced autophagosome synthesis or reduced autophagosome turnover. In order to better interpret the changes in levels of processed LC3-II, the experiments were

performed with and without the addition of bafilomycin A<sub>1</sub>, a lysosomal protease inhibitor which blocks the fusion of autophagosomes with lysosomes, leading to an increase in LC3.<sup>94,243,246</sup> The autophagic flux includes the complete processing of cargo, from its sequestration to its degradation and recycling of basic components back to the cytosol. The western blot analysis can be used to estimate the autophagic flux by monitoring the accumulation of autophagosomes. Some pharmacological compounds like bafilomycin A<sub>1</sub> and chloroquine (inhibitors of lysosome acidification) are used to block the autophagic flux and to prevent LC3-II degradation, whereas degradation of LC3-I is not affected.<sup>94,246</sup> The difference in the amount of LC3-II measured in the presence and the absence of these compounds ensures the measurement of the autophagic flux. Moreover, the assays provide the possibility to distinguish the agents which can induce or inhibit the autophagy flux. As a positive control everolimus is used, an established autophagy activator.<sup>81,247</sup> In order to interpret the result obtained with western blot analysis, it should be noted that the obtained data is semi-quantitative. Firstly, this is due to variation in the loading and the transfer rates between the separate lanes in a sample, and secondly, the generated signal is not linear across the concentration range.<sup>248</sup>

A number of methods based on commercially available kits have been developed to determine the autophagic flux using **flow cytometry**. The approach is particularly useful for cells that grow in suspension.<sup>85</sup> In contrast to other dyes, the Cyto-ID fluorescence dye specifically marks autophagic compartments with minimal staining of lysosomes or endosomes. As a result, this leads to much lower background staining in non-autophagic cells and ensures a rapid and quantitative monitoring of the autophagic flux.<sup>249</sup> The assay shows advantages compared to the general LC3B-based assays where only autophagosomes are measured and not most autophagic compartments. Additionally, the pixel limits of the immunoblots may provide inaccurate quantification.<sup>250</sup>

## 2. Materials and Methods

### 2.1 Materials

#### 2.1.1 Cell culture

In order to perform the autophagy experiments, several cell types were used: Jurkat T cells, HEK 293 T and L 929 cells. The **Jurkat T** cells are obtained from peripheral blood and originate from a human leukemic T cell line, have good response to autophagy modulators and are cultivated in suspension.<sup>251</sup> The Jurkat T cells growth medium contained: 500 ml RPMI medium 1640 + Glutamax™ with indicator (Phenol red), Gibco (Dublin, Ireland); 5 ml Penicillin (10000 Units/ml)/ Streptomycin (10000 µg/ml), Gibco; 1 ml Polymyxin B (PMB, 10000 Units/ml), Gibco; 50 ml Heat Inactivated Fetal Bovine Serum (HI-FBS), Sigma-Aldrich (Darmstadt, Germany). **HEK 293 T** is a cell line established from primary embryonic kidney cells, which was transformed with sheared human adenovirus type 5 DNA.<sup>252,253</sup> They are a popular choice for experimental models because of their quick and easy reproduction and maintenance; amenability to transfection using a wide variety of methods; high efficiency of transfection and protein production; faithful translation and processing of proteins; and small cell size with minimal processes appropriate for voltage-clamp experimentation.<sup>254</sup> The HEK 293T cells growth medium consisted of: 500 ml RPMI medium 1640, Gibco; 5 ml Penicillin (10000 Units/ml) / Streptomycin (10000 µg/ml), Gibco; 1 ml Polymyxin B (PMB, 10000 Units/ml), Gibco; 50 ml Heat Inactivated Fetal Bovine Serum (HI-FBS), Sigma-Aldrich. The **L 929** cell line was derived from normal subcutaneous connectivity tissue and has a fibroblast morphology.<sup>255</sup> The L929 cells growth medium contained: 500 ml DMEM medium, Gibco; 5 ml Penicillin (10000 Units/ml) / Streptomycin (10000 µg/ml), Gibco; 1 ml Polymyxin B (PMB, 10000 Units/ml), Gibco; 50 ml Heat Inactivated Fetal Bovine Serum (HI-FBS), Sigma-Aldrich. The cells were grown according a protocol established in the host pharmacology lab. The conditions for plating out the cells were previously investigated and selected.

General materials and reagents used in the cell culture experiments were: Cellstar® Cell Culture Flasks of 250 ml with standard cap (T75) from Greiner Bio-one (Vilvoorde,

Belgium); Dulbecco's Phosphate-Buffer Saline (DPBS) and the trypsin solutions from Gibco; Cellstar® Cell Culture 12-well Plate, sterile (665 180) and Cellstar® Cell Culture 12-well Plate for suspension culture, sterile (665 102) purchased from Greiner Bio-one; dimethyl sulfoxide (DMSO) from Sigma-Aldrich.

Regarding the instruments, centrifuge: 5810 Eppendorf; microscope: Olympus CK 30; incubator: Binder; Countess™ II Automated Cell Counter, Invitrogen (California, USA) were used.

### 2.1.2 Western blot

Tween 20 and mouse monoclonal antibody for  $\beta$ -actin (clone AC-15, Sigma-Aldrich, A5441) were obtained from Sigma-Aldrich. The everolimus was from Novartis (Basel, Switzerland) and the bafilomycin A was from Santa Cruz Biotechnology (Texas, USA). The composition of the different buffer solutions was: Laemmli buffer: 950  $\mu$ l Laemmli sample buffer (Bio-Rad, California, USA) and 50  $\mu$ l  $\beta$ -mercaptoethanol; Running buffer: MES SDS-Page running buffer (diluted from 20x stock) (Invitrogen); Transfer buffer (for 2 liters): 28.8 g glycine (Sigma-Aldrich), 6 g Tris (Acros Organics, New Jersey, USA), to 400 ml methanol Millipore® water was added till 2 liters; 10x PBS (phosphate-buffer saline, Bio-Rad Laboratories) (for 1 liter): 80 g sodium chloride (Sigma-Aldrich), 2 g potassium chloride (Sigma-Aldrich), 11.5 g disodium hydrogen phosphate (Sigma-Aldrich), 2 g potassium dihydrogen phosphate (Sigma-Aldrich) and the pH was adjusted to 7.4 with hydrochloric acid (Sigma-Aldrich); Blocking buffer: 20 ml Odyssey® blocking buffer (PBS) LI-COR® Biosciences (Nebraska, USA) with 100 ml Millipore® water. Other materials, which were used, were: Bolt™ 12% Bis-Tris plus Gel (Novex, Massachusetts, USA), PageRuler™, prestained protein ladder (Thermo Scientific, Massachusetts, USA), Immobilon – FL PVDF membrane (Millipore, Massachusetts, USA), double Whatmann filter paper, methanol (Merck, Darmstadt, Germany), mouse monoclonal antibody for LC3 (anti-LC3B, clone 5F10, 0231-100/LC3-5F10) (Nanotools, Teningen, Germany), IR-Dye labelled goat anti-mouse (IgG, 926-68070, LI-COR Biosciences), Dulbecco's Phosphate-Buffer Saline (DPBS) solution (Gibco). The IR fluorescence detection was performed on



an Odyssey SA infrared imaging system (LI-COR Biosciences). The intensity of the protein bands was quantified using Image Studio software (LI-COR Biosciences).

### 2.1.3 Cyto-ID Detection Kit

In the protocol CYTO-ID® Green Autophagy Detection Reagent from Enzo Life Sciences (New York, USA) was used. The RPMI 1640 medium with and without the presence of phenol red indicator was purchased from Thermo Fisher Scientific (Waltham, USA). Dimethyl sulfoxide (DMSO) was ordered from Sigma-Aldrich. The Cellstar® Cell Culture 12-well Plate for suspension culture, sterile (665 102) were purchased from Greiner Bio-one. And the chloroquine, the 10x Assay buffer, as well as the Green Detection Reagent were from Enzo Life Sciences. The fluorescent dye solution was made by adding 10 µl of the reagent to 10 ml RPMI without the presence of phenol red indicator, supplemented with 5% FBS. The flow cytometer used in the experiment was BD Accuri™ C6 Flow Cytometer (BD Biosciences, USA), using 488 nm laser source.

## 2.2 Methods

### 2.2.1 Maintaining cell cultures

Cell culture is one of the major model systems to study the autophagy flux and to discover novel compounds as autophagy modulators.<sup>252</sup> In order to ensure a healthy and constant growth of the cells, their medium should be refreshed on regular bases. This is performed in a sterile laminar airflow (LAF) cabinet. Before proceeding with further steps, the cell culture flask is inspected under the microscope for possible contamination and general condition of the cells. For adherent cells and suspension cell, the following procedure can differ. Regarding adhesion cells (e.g. L 929 cell line), in the LAF, the medium is aspirated from the side of the flask by a Pasteur pipette and then the cells are washed only with DPBS solution in order to remove any traces of the medium. After discarding the DPBS, pre-warmed trypsin solution (0.25%) is added for 2-3 min to detach the cells. The step is monitored under the microscope, approximately till 80% of the cells release from the

surface. By adding the pre-warmed medium, the trypsin is inactivated and the cell suspension is collected in a tube which is further centrifuged for 4 min at 1700 rpm (or 559 x g). In the end the medium is aspirated and the cells are resuspended with fresh medium so as to obtain the desired cell concentration. Then, the cells are incubated at 37 °C, 5 % CO<sub>2</sub>. The procedure concerning suspension cells does not require the use of trypsin solution. At first, the cell suspension is transferred into a tube and then centrifuged for 5 min at 1500 rpm (or 435 x g). The medium is aspirated and then pre-warmed medium is used to resuspend the cells. The amount of added medium depends on the required cell concentration. In general, the cells can be either used for experiments or for future culturing. In the latter scenario, 20 ml fresh growing medium is added to the cells, they are transferred to a new cell culture flask with marked date, passage number and type of cells, and finally placed in the incubator.

The counting of the cells was performed with a Countess™ II Automated Cell Counter. The living cells are distinguished from the dead cells by trypan blue (0.4%). The dye stains the dead cells the membrane of which is normally compromised. Following the established procedure, 15 µl of the trypan blue is mixed with 15 µl cell suspension in an Eppendorf vial, and then 10 µl of the mixture is pipetted onto a disposable cell counting slide. The slide is inserted into the automated cell counter and the cells are captured and counted by an image analysis algorithm using brightfield.

To test whether the cells HEK 293T and L 929 treated with the selected compounds show any autophagy modulation properties, 250 000 cells/ml were seeded and treated for 18 h in a 12-well plate prior to western blotting. For the HEK cells RPMI medium (with 10% FBS, P/S, PMB, see 2.2.1) was used and the L 929 cells were incubated in DMEM medium (with 10% FBS, P/S, PMB, see 2.2.1). All test compounds were dissolved in DMSO (10 µM final concentration). The blank contained medium and DMSO and the positive control samples were treated with everolimus (10 µM final concentration). Two sets of test were prepared, namely, bafilomycin A (100 nM final concentration) - treated and untreated cells.<sup>256</sup> After that, the cells were lysed and collected with Laemmli buffer. Finally, the samples were further heat-denatured for 5 min in boiling water.<sup>257</sup>

### 2.2.2 Western blotting

By definition, western blotting involves the separation and identification of a protein mixture based on their molecular weight through gel electrophoresis with subsequent transfer to a suitable membrane (e.g. polyvinylidene fluoride, PVDF). After proteins have been transferred onto the membrane, they can be directly identified through their reaction with specific antibodies (immunodetection).<sup>258</sup> Firstly, a primary antibody is added, which is specific for the target protein, then, by using a labelled secondary antibody, a quantitative signal can be generated. The precise quantification of the signal can be done for instance by fluorescent sensitive dye.

#### *Electrophoresis*

In the beginning, the obtained lysates from the cell culture samples were loaded on an Invitrogen, Bolt™ 12% Bis-Tris Plus SDS-polyacrylamide gel cassette, which was placed in a tank filled with running buffer. The loading of the gel was as follows: 3 µl from the pre-stained protein ladder were pipetted in the first slot, the second was filled only with 12 µl Laemmli buffer, then 12 µl from the denatured test samples. The gel electrophoresis was performed at 165 V until the front reached the bottom of the cassette.

#### *Blotting*

Then, the proteins were transferred to an Immobilon FL PVDF Transfer membrane (pre-treated with methanol, washed with water and pre-soaked in transfer buffer) according to an established procedure. The process is known as blotting and it was achieved by electrophoretic elution in a tank filled with transfer buffer. The construction of the blotting sandwich is presented in Figure 7.2.<sup>258</sup>

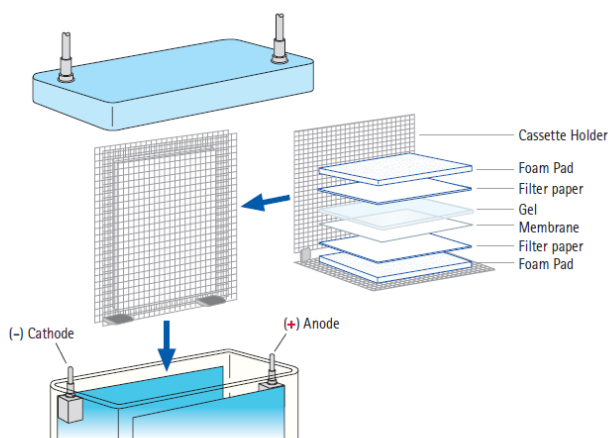


Figure 7.2. Tank (wet) transfer system.<sup>258</sup>

It contained a fiber mat (pre-soaked in transfer buffer), one double Whatmann filter (pre-soaked in transfer buffer), Immobilon FL PVDF membrane, the gel, again one double Whatmann filter, and a fiber mat. Air bubbles were removed before the transfer. With the tank transfer the gel/membrane stack was completely immersed in a buffer reservoir filled with transfer buffer, and a current was applied (100 V for 50 min). Further on, the membrane was incubated for one hour with LI-COR blocking buffer in Phosphate-buffered saline (PBS) (1:5 dilution) without added Tween at room temperature on a shaker. After blocking, the membrane was probed overnight at 4 °C on a shaker with primary antibodies (1:1000 dilution prepared in PBS with 0.1% Tween for the LC3 antibody, and 1:5000 for the  $\beta$ -actin antibody) in LI-COR blocking buffer in PBS (1:5 dilution) supplemented with 0.1% Tween.<sup>259</sup> Then, after several washing steps of the membrane with PBS with 0.1% Tween, followed one hour incubation at room temperature on a shaker with IR fluorescent dye secondary antibodies (1:20000 in PBS with 0.1% Tween) in LI-COR blocking buffer (1:5 dilution) with 0.01% SDS to reduce the background autofluorescence. In the final step, the membrane was washed with PBS with 0.1% Tween, finally, only with PBS, and was ready for analysis by the Odyssey SA infrared imaging system.

### *Measurement and interpretation of the results*

The 700 channel (red) displayed the anti-mouse antibody and the 800 channel (green) displayed the anti-rabbit antibody. LC3-I and its lipidated form LC3-II poses different electrophoretic mobility where the lipidated form is moving faster in the gel, despite its larger molecular weight. LC3-II can be found at 14-16 kDa while LC3-I at 16-18 kDa.<sup>81</sup> As mentioned before, in the assay, the difference in the LC3-II signal is observed in the presence and in the absence of bafilomycin (inhibitor of lysosome acidification). When the autophagy flux is induced, an increase in the LC3-II signal should be observed in the presence of bafilomycin. If the ratio between the LC3-II over the  $\beta$ -actin signal is increasing, there is an activity. The measurement of the signal was carried out in Pixels. The interpretation of the result was possible due to the inclusion of molecular weight (MW) standards on the gel. It facilitates the estimation of the size of the proteins of interest after the resolution by electrophoresis.

### *Test compounds*

In the western blot analysis the following groups of compounds were tested: isolated polymethoxylated flavonoids from *Citrus* species (see Chapter 3), including 4',5,6,7-tetra-methoxyflavone; sinensetin; tangeretin; 5-demethylnobiletin; nobiletin; heptamethoxyflavone were initially tested in 10  $\mu$ M final concentration; additionally, sinensetin, nobiletin, and heptamethoxyflavone were also examined at 30  $\mu$ M final concentration; and commercially available amentoflavone in a concentration range between 10 and 100  $\mu$ M (10  $\mu$ M, 20  $\mu$ M, 25  $\mu$ M, 50  $\mu$ M, 75  $\mu$ M and 100  $\mu$ M final concentration).

### 2.2.3 Cyto ID Detection Kit

Realizing the need for a robust method to label autophagic compartments with minimal staining of lysosomes and endosomes, scientists developed a fluorescence dye, which is a novel approach for detecting autophagy. The CYTO-ID<sup>®</sup> Autophagy Detection Kit is a non-transfection, quantitative assay for monitoring autophagy and estimating autophagic flux in live cells.<sup>80</sup> The commercially available kit - Enzo Life Science Cyto-ID<sup>®</sup> Autophagy

Detection Kit, was used for detection of autophagy in live cells by flow cytometry. The detection reagent becomes brightly fluorescent in vesicles produced during autophagy and has been validated under a wide range of conditions known to modulate autophagy pathways. The assay provides rapid, specific and quantitative approach for monitoring autophagic activity at the cellular level, and in the current project, was applied for Jurkat cells. Everolimus (a well-known inducer of autophagy) was used as a positive control. The live cell analysis kit provided a convenient approach for analysing of the regulation of autophagic activity at the cellular level.

### *Cell treatment*

The cells used in the experiment were Jurkat cells which are human T lymphocyte cells. The required amount of 500 000 cells/ml was seeded and treated for **16 h** in a 12-well plate for suspension. For the Jurkat cells RPMI medium (with 10% FBS, P/S, PMB, see 2.2.1) was used. All test compounds were dissolved in DMSO (10  $\mu$ M final concentration). The blank sample contained medium and DMSO and the positive control samples were treated with everolimus (10  $\mu$ M final concentration). Two sets of wells were prepared, namely, chloroquine (50  $\mu$ M final concentration) - treated and untreated cells. The role of chloroquine in the assay is similar to the role of bafilomycin A<sub>1</sub> in the western blot analysis, namely, blocking the degradation of the autophagosomes which leads to their accumulation.

### *Flow cytometry analysis*

After the incubation, the cells were collected by centrifugation at 1000 rpm (or 187 x g) for 5 min. The upper layer was discarded. Then, the cells were washed with RPMI without phenol red indicator and re-suspended. Again the cells were centrifuged and the upper layer was discarded. Subsequently, they were resuspended in the same manner in RPMI without phenol red, and the CYTO-ID<sup>®</sup> Green stain solution was added to each sample. At this point it is important to achieve mono-disperse cell suspension by gently pipetting up and down repeatedly.<sup>249</sup> All samples were covered with aluminium foil due to the light sensitivity of the reagent. The samples were gently vortexed and incubated for 30 min at 37 °C in the dark. After that the cells were collected by centrifugation and washed with 1x

Assay buffer. Finally, they were resuspended again in the assay buffer and the green fluorescence was analyzed in the FL1 channel of a flow cytometer. The calculation of the results was based on the percentage value of AAF (Autophagy Activity Factor), which is directly correlated to autophagy activity within a cell population:

$$AAF = \left( \frac{FL1_{treated} - FL1_{control}}{FL1_{treated}} \right) \times 100$$

where  $FL1_{treated}$  is the mean fluorescence intensity of treated sample,  $FL1_{control}$  is the mean fluorescence intensity of control sample containing only DMSO.

### *Test compounds*

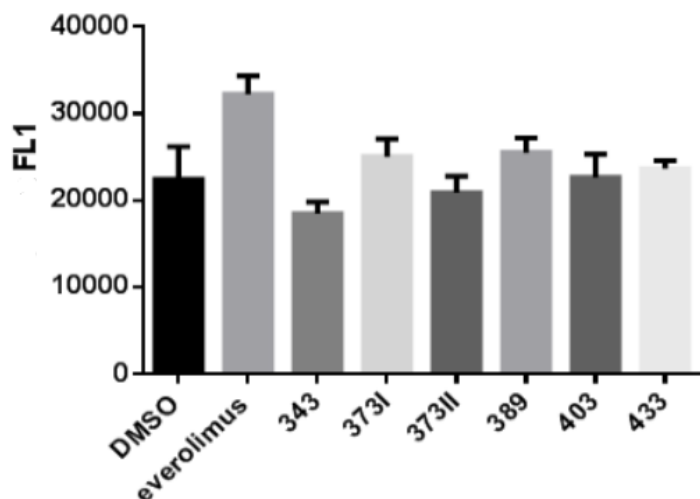
In the first Cyto-ID experiment the cells were treated with polymethoxylated flavonoids (10  $\mu$ M final concentration) isolated from *Citrus* species (see Chapter 3), including 4',5,6,7-tetramethoxyflavone, sinensetin, tangeretin, 5-demethylnobiletin, nobiletin and heptamethoxyflavone.

In the second Cyto-ID experiment the cells were treated with a selected group of compounds (10  $\mu$ M final concentration): previously isolated ones (see Chapter 3), including 4',5,6,7-tetramethoxy flavone, heptamethoxyflavone, tangeretin, sinensetin, 5-demethylnobiletin, vasicine, ginkgetin / isoginkgetin mixture; and commercially available standards: quercetin, (-)-epicatechin, rutin, apigenin, curcumin, amentoflavone, (+)-catechin, bilobetin, ginkgolide A and silybin. The choice for the latter was made based on information in literature.<sup>89,152,153,260</sup>

## *3. Results and discussion*

The selected group of polymethoxylated flavonoids was firstly screened with a Cyto-ID detection kit. The **Jurkat T cells** were incubated with 50  $\mu$ l of test solution (10  $\mu$ M final concentration of test compound) for **18 h**. Everolimus (10  $\mu$ M final concentration) was used as a positive control. The Cyto-ID dye selectively labels autophagosomes, so the increase in fluorescence is indicative of an autophagy induction. Unfortunately, none of

the compounds was able to induce autophagy since no increase of the fluorescence was detected compared to the control sample (Figure 7.3).



**Legend:**

343 – 4',5,6,7-tetramethoxyflavone; 373/I – sinensetin; 373/II – tangeretin; 389 - 5-demethylnobiletin;  
403 – nobiletin; 433 - heptamethoxyflavone

*Figure 7.3. Results for selected polymethoxylated flavonoids (10  $\mu$ M final concentration) tested with the Cyto-ID autophagy detection kit and everolimus as a positive control (10  $\mu$ M final concentration). The experiment was performed two times.*

In the figure, FL1 is the fluorescence channel and the signal was measured between 499 and 548 nm. This first experiment was performed two times. The results from the second experiment, which was performed again only twice, are presented in Figure 7.4.



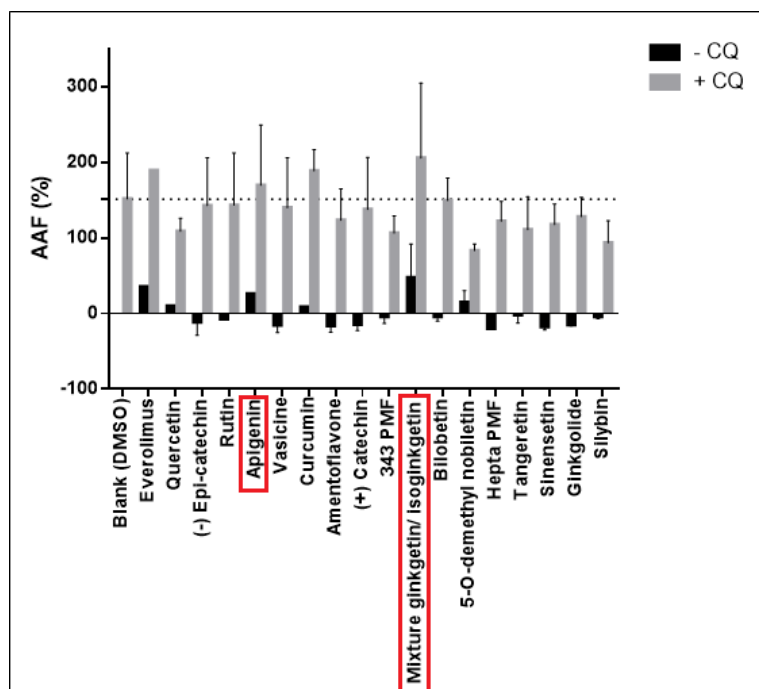


Figure 7.4. Autophagy activity factor (AAF) values from the two Cyto-ID experiments testing isolated and commercially obtained natural products in two sets of samples: with chloroquine (+CQ) and without chloroquine (-CQ), for autophagy modulation properties. The experiment was performed two times.

The majority of the compounds did not show autophagy induction but exhibited even slight inhibition. Only apigenin and the ginkgetin / isoginkgetin mixture showed significant induction of autophagy. To confirm the result more experiments need to be carried out.

The further investigation continued with western blot analysis performed with **L 929 cells** for monitoring the level of GFP-LC3, an assay, generally considered as highly specific.<sup>261</sup>

The data set included samples where the cells were incubated in medium with FBS and the incubation time was **18 h** (Figure 7.5).

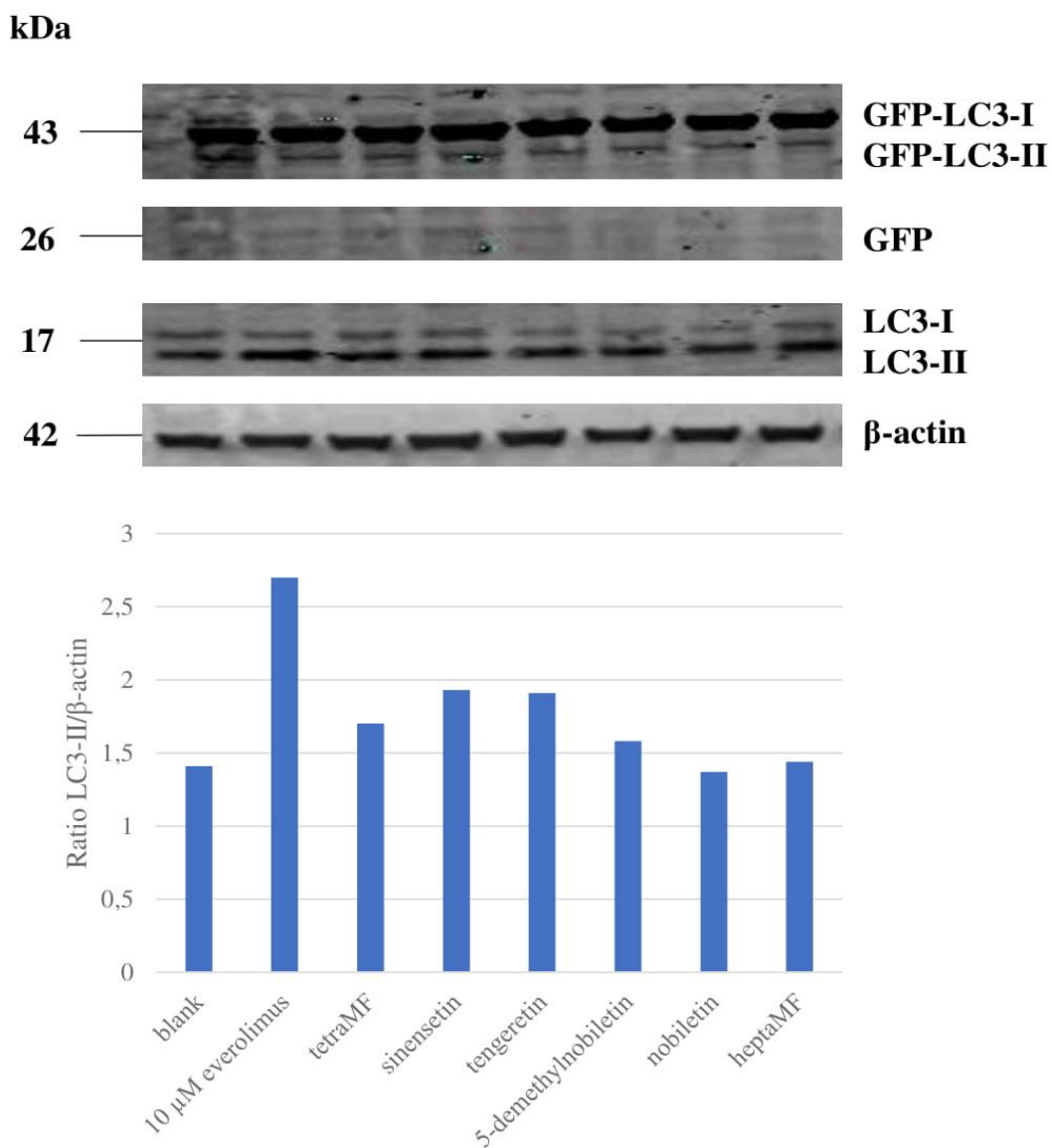


Figure 7.5. GFP-LC3 western blot analysis for several polymethoxylated flavonoids (final concentration 10 μM) and everolimus (final concentration 10 μL) as a positive control. The interpretation of the results was based on the ratio between LC3-II and β-actin. The experiment was performed only once.

The free GFP, however, was not detected, therefore the calculations were based on the ratio between the level of LC3-II and β-actin for each concentration of test compounds. None of them showed higher activity than the positive control. Nevertheless, considering the relatively higher ratio from the first Cyto-ID detection kit assay and the result of the

western blot analysis, three of the compounds, which were available in sufficient amount, were submitted for further investigation by increasing their concentration. Since in the first measurement free GFP failed to be detected, it was decided to use another cell type. Consequently, the western blot was performed using **HEK 293 T cells** for testing nobiletin, sinensetin and heptamethoxyflavone in final concentrations of 10  $\mu\text{M}$  and 30  $\mu\text{M}$  for each compound (Figure 7.6).<sup>117</sup> The incubation time was **24 h**. Based on the information from the *in vitro* tests (see Chapter 5) where it was speculated that the polymethoxylated flavonoids show a tendency to attach to proteins in the reaction mixture, which interferes with the accuracy of the results, the cells were incubated in a medium without FBS. The batch was treated with bafilomycin to stop the process.

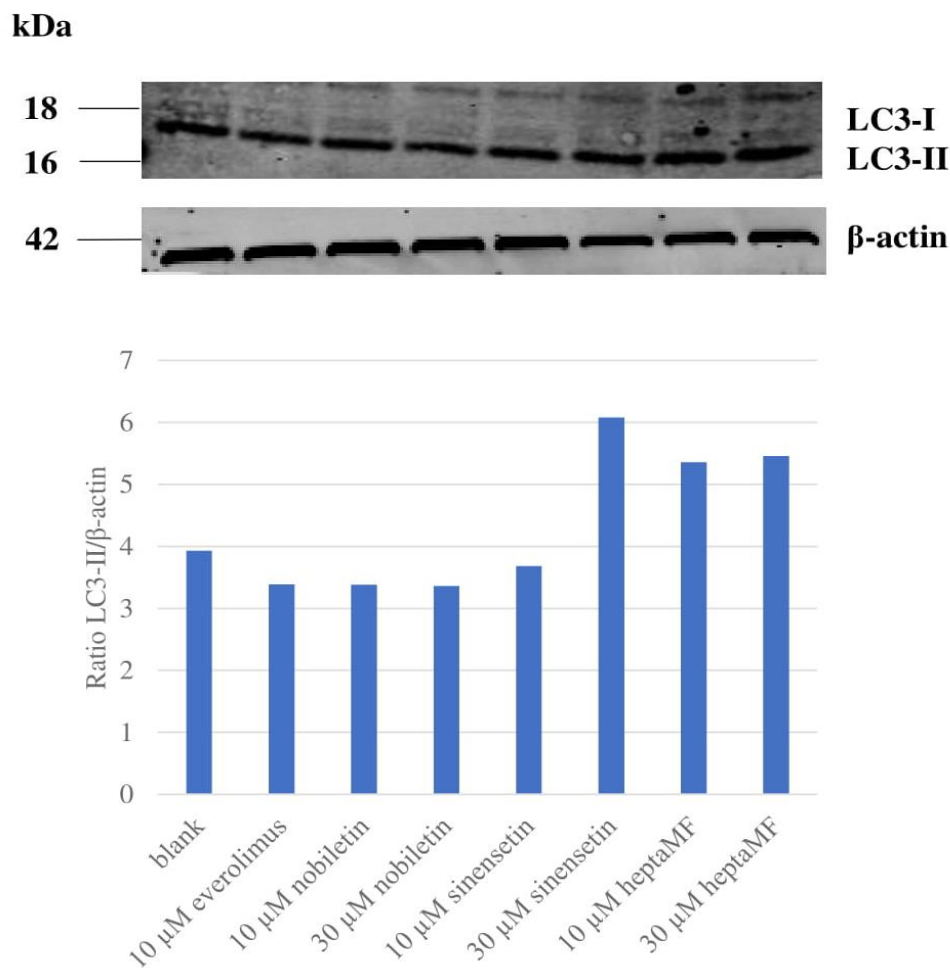


Figure 7.6. Western blot analysis for several polymethoxylated flavonoids (final concentration 10 and 30  $\mu\text{M}$ ) and everolimus (final concentration 10  $\mu\text{L}$ ) as a positive control. The interpretation of the results was based on the ratio between LC3-II and  $\beta$ -actin. The experiment was performed only once.

The blank sample contained only DMSO. From this single experiment it was difficult to draw conclusions because the positive control value of everolimus did not differ much from the blank sample. Nevertheless, based on the visual observation of the blot and the previous results from the Cyto-ID, it was decided to continue the experiments with other groups of compounds. In summary, the polymethoxylated flavonoids showed no activity as autophagy modulators in the current experimental conditions. However, it is worth to mention that for western blot analysis the number of performed experiments is crucial for obtaining statistically significant result on autophagy modulation properties of the test

compounds. Therefore, the number of experiments in the current research can be also seen as quite limited in order to make conclusions.

In the next section, the **HEK 293 T** cell line was used to investigate the activity of biflavonoids, in particular, amentoflavone, as autophagy modulator using the western blot assay. Different dilutions of amentoflavone were prepared in DMSO with a final concentration of 10  $\mu\text{M}$ , 20  $\mu\text{M}$ , 25  $\mu\text{M}$ , 50  $\mu\text{M}$  and 100  $\mu\text{M}$ . Everolimus (10  $\mu\text{M}$  final concentration) was used as positive control. The blank sample contained only the medium and DMSO. The incubation time of the experiment was **16 h** and two sets of samples were examined: without and with the addition of bafilomycin A (100 nM final concentration). The LC3-II was normalized relative to the housekeeping protein ( $\beta$ -actin) and quantified relative to the samples without bafilomycin A. The results from the first set are presented on Figure 7.7.

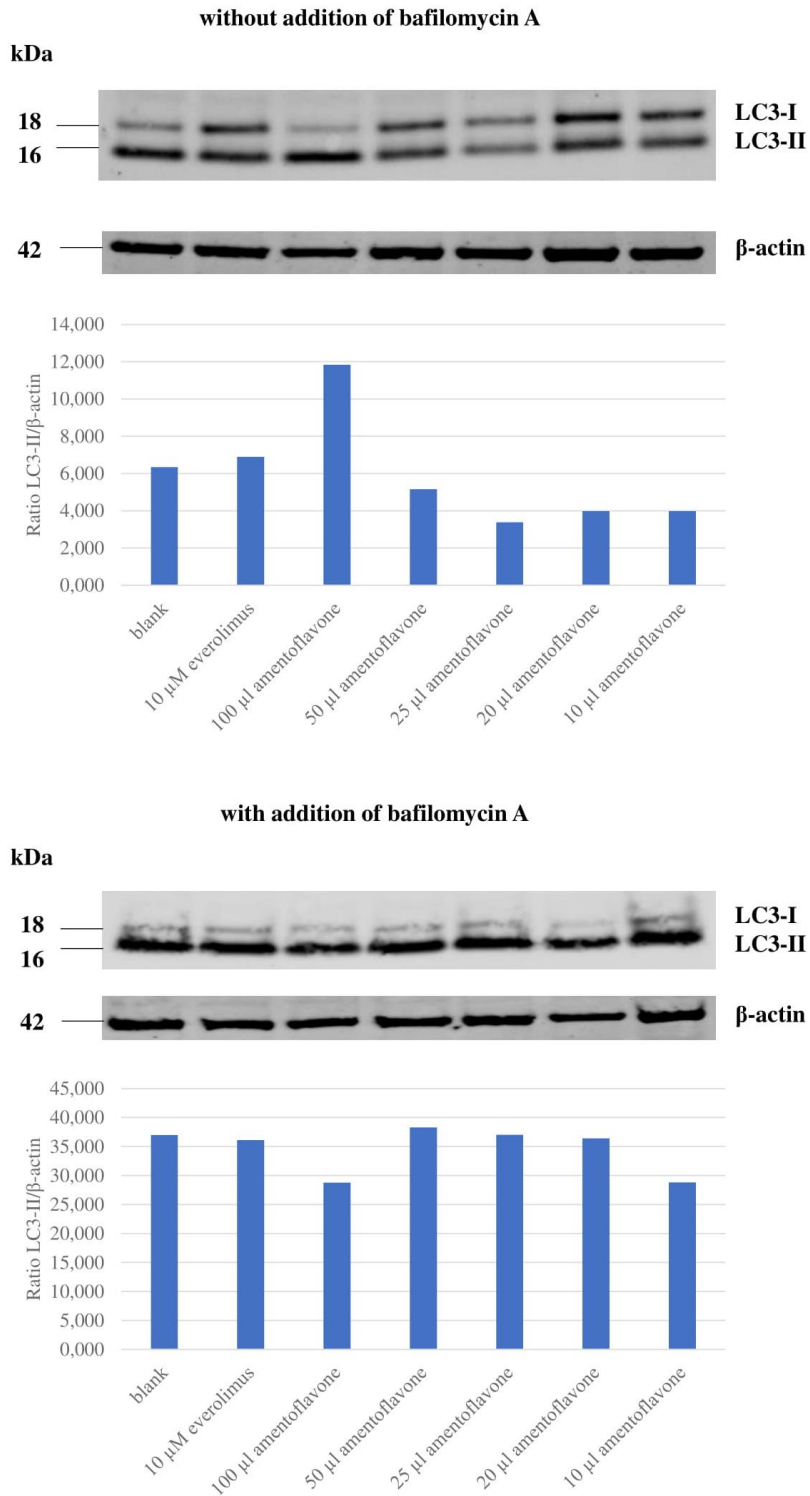


Figure 7.7. Western blot analysis for different concentrations amentoflavone and 10 μl everolimus as a positive control, samples were prepared without and with addition of bafilomycin A. The interpretation of the blot was based on the ratio between LC3-II and β-actin. The experiment was performed only once.

Based on the ratio between the LC3-II and  $\beta$ -actin, the data suggested that in the highest concentration amentoflavone might induce autophagy due to the fact that its value was nearly doubled compared to the positive control. The next set of samples were prepared with the addition of bafilomycin (Figure 7.7).

Subsequently, an extra concentration was added to the test range, namely 75  $\mu$ M amentoflavone (final concentration) and the experiment was performed several times in order to obtain statistically significant data. Results from the blot without/ with addition of bafilomycin are presented in Figure 7.8.

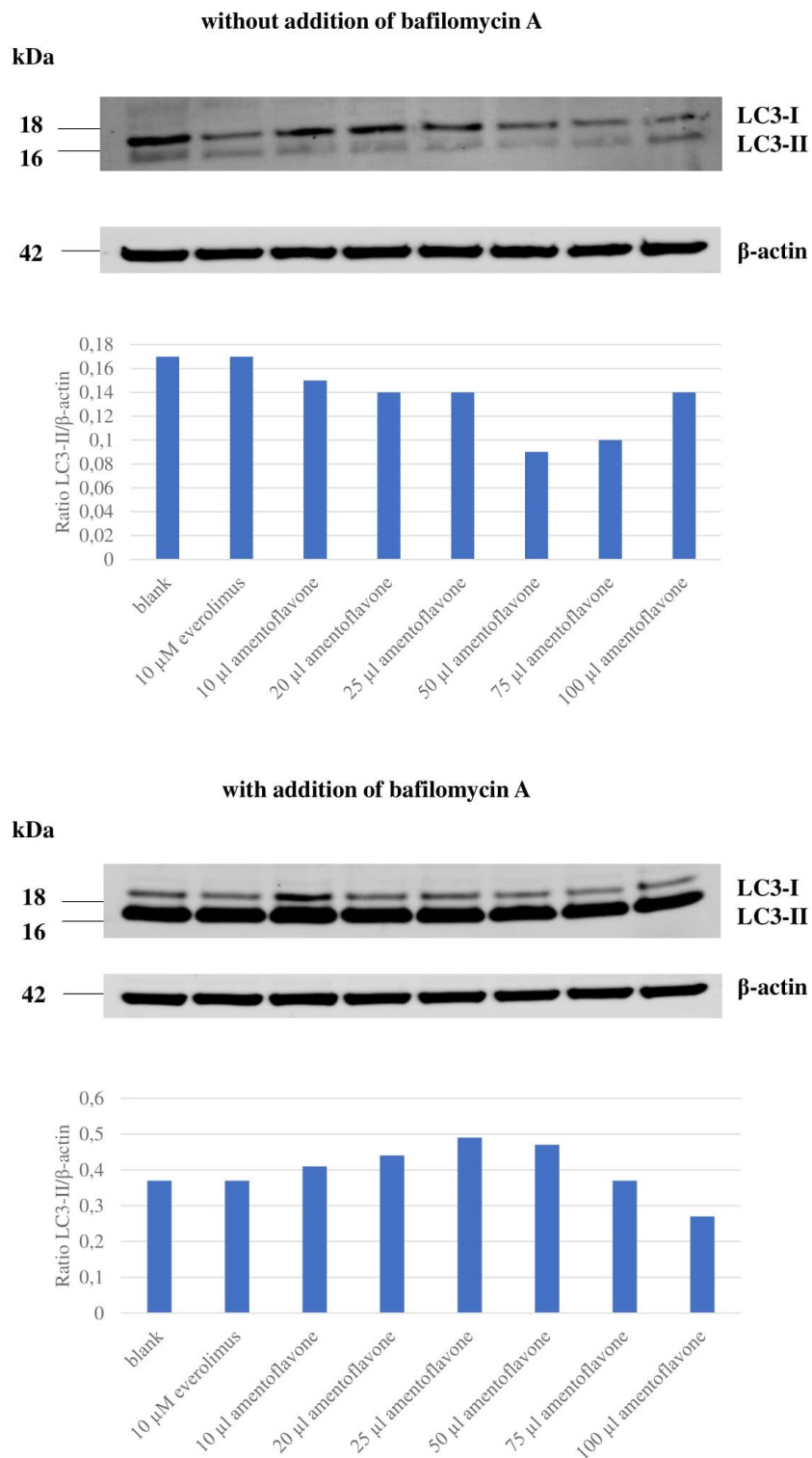


Figure 7.8. Western blot analysis for different concentrations amentoflavone and 10  $\mu$ l everolimus as a positive control, samples were prepared without and with addition of bafilomycin A. The interpretation of the blot was based on the ratio between LC3-II and  $\beta$ -actin. The experiment was performed only once.



However, careful observations in the medium of the cells after incubation with the test compounds revealed small precipitates with the highest concentration of amentoflavone. As long as the presence of precipitates can affect the reliability of the autophagy experiment, the preliminary results were accepted as false positive. In summary, amentoflavone was considered as having no activity as autophagy modulator in the present experimental conditions.

#### 4. Conclusion

A number of data from *in vitro* and *in vivo* models indicated that natural products from medicinal plants and extracts hold great potential for the treatment of human diseases including neurodegenerative diseases and cancer. Modulation of autophagy, as a novel drug target involved in wide range of pathological conditions, can be an important mechanism for treating diseases.<sup>5</sup> In the current project several classes of natural products – polymethoxylated flavonoids (PMFs) (4',5,6,7-tetramethoxyflavone; sinensetin; tangeretin; 5-demethylnobiletin; nobiletin; heptamethoxyflavone, isolated during the research), biflavonoids (ginkgetin/isoginkgetin mixture, isolated during the research and amentoflavone, commercial standard), quinazoline alkaloids (vasicine, isolated during the research), and several commercially obtained standards (quercetin, (-)-epicatechin, rutin, apigenin, curcumin, amentoflavone, (+)-catechin, bilobetin, ginkgolide A, silybin) were tested as candidates for autophagy modulation using western blot analysis and the Cyto-ID autophagy detection kit. Apigenin and the ginkgetin /isoginkgetin mixture were the only compounds which demonstrated autophagy induction in the Cyto-ID assay. However, in order to statistically confirm the result, more repetitions of the measurement ought to be performed.

In general, since the number of experiments for western blot analysis and Cyto-ID detection kit was considerably less, this could hinder the precise determination of autophagy modulation properties of the test compounds. Sufficient repetitions of the experiments are needed in the future so to develop a vision about the potential effect of those compounds on the process of autophagy.

# Chapter 8

**General discussion and future perspectives**

*(Quo Vadis?)*



## 1. General discussion

This research project aimed to investigate a broad range of quite diverse topics, starting with phytochemical isolation of selected pure compounds from four medicinal plants; covering analytical method development and validation for testing their AGEs inhibiting properties, together with several commercial products; and finally, conducting *in vitro* bioanalytical work to test the autophagy modulating properties of some isolated compounds and commercial standards. The far-sighted goal of the current study was to discover novel AGEs inhibitors and autophagy modulators among a small library of natural products. Last but not least, as part of the analytical workflow, method validation was performed on one of the plant species which may have further application in product quality control studies.

A chemistry-based phytochemical approach has been considered for four medicinal plant species: *Citrus sinensis*, *Citrus depressa*, *Ginkgo biloba* and *Adhatoda vasica*, focused on obtaining three classes of compounds: polymethoxylated flavonoids (PMFs), biflavonoids and quinazoline alkaloids. After detailed investigation (Chapter 3) the following pure compounds were successfully isolated and identified: eight PMFs from *C. sinensis* and *C. depressa* – sinensetin, 5,6,7,4'-tetramethoxyflavone, nobiletin, heptamethoxyflavone, tangeretin, 5,7,8,3',4'-pentamethoxyflavone, 5,7,8,4'-tetramethoxyflavone and 5-hydroxy-6,7,8,3',4'-pentamethoxyflavone; two biflavonoids and one mixture of two isomers from *G. biloba* – bilobetin, sciadopitysin and a ginkgetin / isoginkgetin mixture; and two quinazoline alkaloids from *A. vasica* – vasicine and 7-methoxyvasicine. In order to prevent any methylated artefacts formed during the isolation of PMFs, methanol was excluded as extracting solvent during the process. Precautions were taken for the isolation of quinazoline alkaloids as well. Due to the risk for autooxidation of vasicine (the main quinazoline alkaloid) to vasicinone that can take place in bright daylight or sunlight, all steps in the experimental procedure were performed protected from light. This consideration was necessary because of their completely different pharmacological activity.

After generating a small library of natural products, the next step was to investigate their anti-AGEs activity or autophagy modulating properties in an established set of

experimental methods. In preliminary tests, inhibition of glycation of bovine serum albumin (BSA), fructosamine adducts formation and dicarbonyl compounds formation was measured (Chapter 5). The standard BSA / glucose assay was hindered by chemical properties of the test compounds like autofluorescence, or by interactions between the test compounds and some of the constituents in the incubation mixture, which led to quenching of the fluorescence signal. These two scenarios were observed when testing different concentrations of vasicine, and as a consequence the activity of this compound could not be accurately assessed in this assay. However, the results for aminoguanidine, which was used as a positive control, followed the findings reported in literature. Different concentrations of nobiletin were also tested in the BSA/glucose assay. The accurate evaluation of its potential activity was hampered by the poor solubility of nobiletin in the reaction mixture. Concerning the fructosamine experiment, the issue of establishing a reliable positive control and its active concentration range was addressed. Pyridoxamine, thiamine and mangiferin were introduced as candidates for a positive control and after preliminary tests, 5 mM mangiferin and 20 mM thiamine gave some promising results. Then, 5 mM mangiferin and vasicine were analyzed in the assay, but unfortunately, vasicine showed no activity on inhibiting the fructosamine formation. The dicarbonyl entrapment assay was performed for 1 mM vasicine and 0.5 mM nobiletin, while 1 mM aminoguanidine was used as a positive control. The results confirmed the expected mechanism of action for aminoguanidine, which is entrapping glyoxal over time. However, the two test compounds did not show activity in the assay. In conclusion, based on the results obtained with these general fluorimetric / colorimetric methods, the investigated pure compounds showed no inhibition of AGEs formation.

Due to the limitations of these general anti-AGEs assays, further investigation was required to establish a reliable and universal method for unambiguous discovery of novel anti-AGEs agents. Therefore, the development of an analytical procedure (Chapter 6) was undertaken to address the demand for reliable quantification of AGEs in *in vitro* samples. By implementation of mass spectrometry, analysis of CML was performed. In the method development section, a lot of aspects were carefully studied and tested, for instance: the choice of the AGE of interest; different steps in the sample preparation: incubation conditions, hydrolysis, sample clean-up, sample dilution solvent, test vials;

choice of detection system; chromatographic conditions; the internal standard. One of the most significant findings during the method development was the effect of the types of vials and the solvent of the analytical samples on the quantification of the results. The use of polypropylene vials was proved advantageous compared to the common glass vials; and the application of a dissolution mixture containing isopropanol : acetonitrile : water in a proportion 45 : 45 : 10 influenced to a great extent the peak shape and the intensity of the signal. Notwithstanding the numerous attempts to finalise the method, further work is needed to understand the peculiar results with the, though generally applied, deuterated internal standard  $d_4$ -CML. However, despite its exploratory nature, this study offers insight into some underestimated aspects like the vials for analysis, and speculates about the critical role of matrix effects or probable interactions in the reaction mixture on the internal standard response. The next challenge was to test the analytical procedure for investigating the AGEs inhibition of some isolated pure compounds and several commercially available standards. However, the solubility of the natural products again turned out to be an important issue in the application of the method. Similar to the BSA / glucose assay, a factor that limited the concentration range for the tested pure compounds (and extracts in the future), was their solubility in the *in vitro* model conditions. However, despite this issue, the method could detect AGEs inhibition for a set of commercial standards in a rather low concentration range such as: quercetin, rutin, (+)-catechin, (-)-epi-catechin, cyanidin and curcumin. From the isolated compounds the mixture ginkgetin / isoginkgetin and 5-demethylnobiletin demonstrated moderate activity in the method, and extra tests are necessary to obtain the  $IC_{50}$ .

Apart from AGEs inhibition, some isolated compounds were investigated as autophagy modulators by performing cell culture experiments using western blot analysis, and the Cyto-ID Autophagy Detection Kit (Chapter 7). The compounds tested in the western blot experiment were: several isolated PMFs like 4',5,6,7-tetramethoxyflavone, sinensetin, tangeretin, 5-demethylnobiletin, nobiletin and heptamethoxyflavone; and the commercially obtained biflavonoid amentoflavone. The PMFs did not show higher activity than the positive control everolimus, and they were considered as not active in the applied experimental conditions. The western blot analysis was performed using different concentrations of amentoflavone, and the highest concentration gave a positive result.

However, after performing several repetitions of the experiment and careful observation, the finding was declared as false positive due to precipitation of the compound in the culture medium. Finally, also amentoflavone was considered as not active in the current experiment. The Cyto-ID Autophagy Detection Kit was applied for several commercial standards and for some isolated pure compounds: 4',5,6,7-tetramethoxy flavone, heptamethoxyflavone, tangeretin, sinensetin, 5-demethylnobiletin, vasicine, the ginkgetin / isoginkgetin mixture; and commercially available standards: quercetin, rutin, apigenin, (+)-catechin, (-)-epi-catechin, curcumin, silybin, amentoflavone, bilobetin and ginkgolide A. In the end, only apigenin and the ginkgetin / isoginkgetin mixture demonstrated autophagy induction in the Cyto-ID assay. However, more repetitions of the measurement ought to be performed. In conclusion, the results from the western blot analysis and Cyto-ID detection kits, in order to be representative, require a sufficient number of successful repetitions, and only then statistical analysis can be performed. The conclusions for the autophagy modulatory activity of the tested compounds drawn in the current thesis should not be considered as final, because of the rather limited number of experiment repetitions. The second analytical aim of the project was to develop and to validate a reliable method for quantifying vasicine, the main quinazoline alkaloid in *Adhatoda vasica* leaves powder, and subsequently, to apply the same method for commercial products (Chapter 4). The calibration model was found to be linear in the concentration range of 5.125 to 205 µg/ml. The average vasicine content at different concentration levels was 0.99 g/100 g with an RSD% of 0.05%. The average recovery was found to be 102.3% with a RSD of 4.3%. Additionally, it was confirmed that the validated method was still precise and accurate for quantifying vasicine in other matrices like the tested preparations. The experimental conditions were proved to ensure good baseline separation between vasicine and vasicinone, and no co-elution of other compounds in both chromatograms for leaves powder samples and dosage forms products occurred. Therefore, the validated method was suitable for determination of vasicine in leaves of *Adhatoda vasica*, as well as for investigating the quality and the recommended daily intake of several commercial products.



## 2. Future perspectives

Concerning the future perspectives in the phytochemical part of the project, as an alternative to the performed chemistry-based isolation approach, bioassay-guided fractionation of selected plant species could be applied in evaluating their anti-AGEs properties. Most commonly, the plant selection is based on the follow-up of the ethnomedical or traditional use of plants in the treatment of, for instance, diabetic complications or neurodegenerative diseases. There are many examples of potent activity, based not only on a single pure compound but on the presence of several active constituents in an extract (e.g. EGb 761, standardised extract from *Ginkgo biloba*). An interesting outcome might be observed if the fractionation of the total extracts from the plants is directed based on evaluating their activity on AGEs formation in established experimental procedures. Once again, validation and selection of primary screening assays are pivotal to guarantee a sound selection of extracts and molecules with the relevant pharmacological action.

Interesting and challenging pharmacological targets that deserve further investigation are the polymethoxylated flavonoids (PMFs) and hydroxylated PMFs. Due to the presence of multiple methoxy groups, which define their high hydrophobicity, PMFs have superb permeability through the membrane and consequently possess excellent bioavailability. The biological properties of PMFs have been extensively studied in the past years, but the knowledge of their metabolic profile is insufficient due to the lack of biotransformation studies. However, there is evidence that PMFs (e.g. nobiletin) after biotransformation *in vivo* produce metabolites with different bioactivities and pharmacological properties.<sup>121,262</sup> For example, the metabolites of nobiletin - 3'-demethylnobiletin, 4'-demethylnobiletin, 3',4'-didemethylnobiletin have been reported to moderately attenuate COX-2 gene expression in *in vitro* cell model, and to suppress the activation of NF- $\kappa$ B.<sup>262</sup> In order to investigate these biotransformation processes for the isolated PMFs (Chapter 3), a gastro-intestinal dialysis model (GIDM), developed in the research NatuRA lab, can be applied in the future. This model contains a gastric, an intestinal, and a colon compartment (including microbial fermentation), simulating the human GI tract. It is much faster, easier, and cheaper than the investigation of the same processes *in vivo*.<sup>263</sup> To

simulate further conversions in the liver, part of each dialysate will be subjected to biotransformation by microsomal S9 fractions. All isolated PMFs can be subjected to metabolism studies in the model. In this way, small libraries of target compounds and their metabolites can be established. All resulting samples should be profiled by LC-MS and NMR, targeting metabolites of the compound class prior to investigation, which can subsequently be isolated. Then, some of the metabolites (positive hits) will be pharmacologically evaluated for inhibiting AGEs formation through, again, established and validated methods.

In the UPLC/MS analytical method, minor changes of the protocol might be further investigated, for example, the application of enzyme hydrolysis instead of acid hydrolysis. The process is labour intensive and involves several enzymes and antibiotics over 4 days. However, it can be fully automated and performed in control conditions through a robotic processor (e.g. CTC PAL sample autoprocessor with sterile reagent addition of argon). This protocol can avoid oxidative degradation of protein adduct residues and subsequently, overestimation of oxidation adducts. Moreover, additional possibilities can be investigated in the context of the sample clean up step like, for example, 3 KD filters (Millipore Amicon Ultra Centrifugal Filters) suggested by other researchers. After the experimental work in the thesis had been completed, recent anti-adhesive vials were released by Waters. According to the preliminary data, this type of vials possess certain advantages over similar products in their portfolio, and despite the exhaustive testing of vials performed in the thesis, any new possibility deserves attention.

Finalising the development and the validation of the UPLC/MS method can be a starting point for finding further application for *in vivo* samples. Several studies have been using models of diabetic rats in order to investigate the effects of compounds on prevention of diabetic complications (like nephropathy) through inhibiting AGEs formation – MG-H<sub>1</sub>, CML, CEL.<sup>58</sup> The procedure should be adapted to measure the glycation products in plasma samples which inevitably will require additional sample preparation steps. However, the *in vivo* models can offer a better tool for the discovery of promising compounds / extracts acting on glycation.

For a comprehensive analysis of the autophagy pathway multiple approaches are required; therefore in addition to monitoring LC3 levels, the autophagy modulating activity

of the tested compounds can be further improved or confirmed by several other techniques: a fluorescent microscopy-based assay, and transmission electron microscopy.

For instance, a HeLa cell line transfected with mRFP-GFP-LC3 can be used to measure the effect of the test compounds on the autophagic flux through a fluorescent-labelled LC3 protein. The human LC3 protein is fused to two fluorescent proteins: RFP (acid-stable) and GFP (acid-sensitive). The monitoring of autophagy activity relies on microscopy visualisation of fluorescent puncta, progressive degradation of the GFP, and concurrent increase of RFP signal in autolysosomes. The number of fluorescent punctates per cell, the percentages of RFP-GFP positive, and RFP positive cells can be used to assess the autophagic flux. Moreover, a robust method based on monoclonal antibody can be used to detect phospho-ATG16L1 endogenously in mammalian cells. The pATG16L1 is selectively present on newly forming autophagosomes, therefore is tightly tied to autophagy induction. In the absence of lysosomal inhibitor, the level of pARG16L1 is more reliable than LC3-II due to the closer relationship between pARG16L1 and autophagy induction. For the confirmation of eventual positive results obtained in other assays, transmission electron microscopy can be applied. The degradation of the cytoplasmic compartments sequestered by the phagophore, later on, matures to autophagosome, is a morphological characteristic of autophagy. Transmission electron microscopy is used for both qualitative and quantitative analysis of changes in various autophagic structures. It is performed to avoid bias and to ensure correct identification and quantification of autophagic compartments. Despite the alternative pathways, which can be chosen to study the effect of compounds and/or extracts on the process of autophagy, the sufficient successful repetitions of each experiment are utterly important. In my final words, I hope that the work performed and described in the thesis can have the slightest contribution in the context of new research methodologies, which can lead to the discovery of novel bioactive constituents for the treatment of medical conditions with economic and social impact.



# Chapter 9

## Bibliography



1. Zaynab M, Fatima M, Abbas S, et al. Role of secondary metabolites in plant defense against pathogens. *Microb Pathog.* 2018;124(July):198-202.
2. Dias D, Urban S, Roessner U. A Historical overview of natural products in drug discovery. *Metabolites.* 2012;2(2):303-336.
3. Atanasov A, Waltenberger B, Stuppner H. Discovery and resupply of pharmacologically active plant-derived natural products: A review. *Biotechnol Adv.* 2015;33(8):1582-1614.
4. Patwardhan B, Warude D, Pushpangadan P, Bhatt N. Ayurveda and traditional Chinese medicine: A comparative overview. *Evidence-based Complement Altern Med.* 2005;2(4):465-473.
5. Wang S, Wu M, Cai C, Li M, Lu J. Autophagy modulators from traditional Chinese medicine: Mechanisms and therapeutic potentials for cancer and neurodegenerative diseases. *J Ethnopharmacol.* 2016;194(October):861-876.
6. Thornalley P, Yurek-George A, Argirov O. Kinetics and mechanism of the reaction of aminoguanidine with the  $\alpha$ -oxoaldehydes glyoxal, methylglyoxal, and 3-deoxyglucosone under physiological conditions. *Biochem Pharmacol.* 2000;60(1):55-65.
7. Ferrucci L, Fabbri E. Inflammageing: chronic inflammation in ageing, cardiovascular disease, and frailty. *Nat Rev Cardiol.* 2018;15(9):505-522.
8. Levine B, Kroemer G. Autophagy in the Pathogenesis of Disease. *Cell.* 2008;132(1):27-42.
9. Thornalley P. The clinical significance of glycation. *Clin Lab.* 1999;45(5-6):263-273.
10. Rabbani N, Thornalley P. Glycation research in amino acids: A place to call home. *Amino Acids.* 2012;42(4):1087-1096.
11. Scheijen J, van de Waarenburg M, Stehouwer C, Schalkwijk C. Measurement of pentosidine in human plasma protein by a single-column high-performance liquid chromatography method with fluorescence detection. *J Chromatogr B Anal Technol Biomed Life Sci.* 2009;877(7):610-614.
12. Rahbar S, Figarola J. Inhibitors and Breakers of Advanced Glycation Endproducts (AGEs): A Review. *Curr Med Chem Endocr Metab Agents.* 2002;2(2):135-161.
13. Iannuzzi C, Irace G, Sirangelo I, Williams T. Differential effects of glycation on protein

- aggregation and amyloid formation. 2014;1(September):1-8.
14. Lund M, Ray C. Control of Maillard Reactions in Foods: Strategies and Chemical Mechanisms. *J Agric Food Chem*. 2017;65(23):4537-4552.
  15. Ulrike B, Rabhani N, Mullineaux P. Quantitative measurement of specific biomarkers for protein oxidation, nitration and glycation in *Arabidopsis* leaves. *Plant J*. 2009;59:661-671.
  16. [www.urbanmonique.net](http://www.urbanmonique.net). La Réaction de Maillard.
  17. Tessier F. La réaction de Maillard dans le corps humain. Découvertes majeures et facteurs qui affectent la glycation. *Pathol Biol*. 2010;58(3):214-219.
  18. Hodge J. Chemistry of Browning Reactions in Model Systems. 1953:928-943.
  19. Rahbari S, Blumenfeld O, Ranney H, Einstein A. Studies of an unusual hemoglobin in patients with diabetes mellitus. 1969;36(5):1-6.
  20. Allen D, Schroeder W, Balog J. Observations on the Chromatographic Heterogeneity of Normal Adult and Fetal Human Hemoglobin: A Study of the Effects of Crystallization and Chromatography on the Heterogeneity and Isoleucine Content. *J Am Chem Soc*. 1958;80(7):1628-1634.
  21. Ahmed N. Advanced glycation endproducts - Role in pathology of diabetic complications. *Diabetes Res Clin Pract*. 2005;67(1):3-21.
  22. Nguyen H, van der Fels-Klerx H, van Boekel M. N-ε-(carboxymethyl)lysine: A Review on Analytical Methods, Formation, and Occurrence in Processed Food, and Health Impact. *Food Rev Int*. 2014;30(1):36-52.
  23. Ahmed N, Mirshekar-Syahkal B, Kennish L, Karachalias N, Babaei-Jadidi R, Thornalley P. Assay of advanced glycation endproducts in selected beverages and food by liquid chromatography with tandem mass spectrometric detection. *Mol Nutr Food Res*. 2005;49(7):691-699.
  24. Starowicz M, Zieliński H. How Maillard Reaction Influences Sensorial Properties (Color, Flavor and Texture) of Food Products? *Food Rev Int*. 2019;35(8):707-725.
  25. Tessier F. The Maillard reaction in the human body. The main discoveries and factors that affect glycation. *Pathol Biol*. 2010;58(3):214-219.
  26. Wu C, Huang S, Lin J, Yen G. Inhibition of advanced glycation endproduct formation by



- foodstuffs. *Food Funct.* 2011;2(5):224-234.
27. Machiels D, Istasse L. La réaction de Maillard: Importance et applications en chimie des aliments. *Ann Med Vet.* 2002;146(6):347-352.
  28. Troise A, Fiore A, Wiltafsky M, Fogliano V. Quantification of N $\epsilon$ -(2-Furoylmethyl)-l-lysine (furosine), N $\epsilon$ -(Carboxymethyl)-l-lysine (CML), N $\epsilon$ -(Carboxyethyl)-l-lysine (CEL) and total lysine through stable isotope dilution assay and tandem mass spectrometry. *Food Chem.* 2015;188:357-364.
  29. Thornalley P, Langborg A, Minhas H. Formation of glyoxal, methylglyoxal and 3-deoxyglucosone in the glycation of proteins by glucose. *Biochem J.* 2015;344(1):109-116.
  30. Monnier V. Intervention against the Maillard reaction in vivo. *Arch Biochem Biophys.* 2003;419(1):1-15.
  31. Namiki M, Hayashu T. New Mechanism of the Maillard Reaction Free Radical Involving Sugar Fragmentation and Formation. *Mail React Foods Nutr.* 1983;(4):26.
  32. Peyroux J, Sternberg M. Advanced glycation endproducts (AGEs): pharmacological inhibition in diabetes. *Pathol Biol.* 2006;54(7):405-419.
  33. Wolff S, Dean R. Glucose autoxidation and protein modification. The potential role of 'autoxidative glycosylation' in diabetes. *Biochem J.* 1987;245(1):243-250.
  34. Wolff S, Jiang Z, Hunt J. Protein glycation and oxidative stress in diabetes mellitus and ageing. *Free Radic Biol Med.* 1991;10(5):339-352.
  35. Peng X, Ma J, Chen F, Wang M. Naturally occurring inhibitors against the formation of advanced glycation end-products. *Food Funct.* 2011;2(6):289-301.
  36. Tang Y, Hu C, Sang S. Characterization of Reaction Products and Mechanisms between Serotonin and Methylglyoxal in Model Reactions and Mice. *J Agric Food Chem.* 2020;68(8):2437-2444.
  37. Rabbani N, Shaheen F, Anwar A, Masania J, Thornalley P. Assay of methylglyoxal-derived protein and nucleotide AGEs. *Biochem Soc Trans.* 2014;42(2):511-517.
  38. Rahbar S, Natarajan R, Yerneni K, Scott S, Gonzales N, Nadler J. Evidence that pioglitazone, metformin and pentoxifylline are inhibitors of glycation. *Clin Chim Acta.* 2000;301(1-2):65-77.

39. Miura J, Yamagishi S, Uchigata Y, et al. Serum levels of non-carboxymethyllysine advanced glycation endproducts are correlated to severity of microvascular complications in patients with Type 1 diabetes. *J Diabetes Complications*. 2003;17(1):16-21.
40. Ames J. Determination of N $\epsilon$ -(carboxymethyl)lysine in foods and related systems. *New York Acad Sci*. 2008;1126:20-24.
41. Gkogkolou P, Böhm M. Advanced glycation end products: Keyplayers in skin aging? *Dermatoendocrinol*. 2012;4(3):259-270. doi:10.4161/derm.22028
42. Frye E, Degenhardt T, Thorpe S, Baynes J. Role of the Maillard reaction in aging of tissue proteins: Advanced glycation end product-dependent increase in imidazolium cross-links in human lens proteins. *J Biol Chem*. 1998;273(30):18714-18719.
43. Sell D, Monnier V. End-stage renal disease and diabetes catalyze the formation of a pentose-derived crosslink from aging human collagen. *J Clin Invest*. 1990;85(2):380-384.
44. Nakamura K, Nakazawa Y, Ienaga K. Acid-stable fluorescent advanced glycation end products: Vesperlysines A, B, and C are formed as crosslinked products in the maillard reaction between lysine or proteins with glucose. *Biochem Biophys Res Commun*. 1997;232(1):227-230.
45. Munanairi A, O'Banion S, Gamble R, Breuer E, Harris A, Sandwick R. The multiple Maillard reactions of ribose and deoxyribose sugars and sugar phosphates. *Carbohydr Res*. 2007;342(17):2575-2592.
46. Thilavech T, Ngamukote S, Abeywardena M, Adisakwattana S. Protective effects of cyanidin-3-rutinoside against monosaccharides-induced protein glycation and oxidation. *Int J Biol Macromol*. 2015;75:515-520.
47. Ansari N, Dash D. Amadori Glycated Proteins : Role in Production of Autoantibodies in Diabetes Mellitus and Effect of Inhibitors on Non-Enzymatic Glycation. *Age Dis*. 2013;4(1):50-56.
48. Sadowska-Bartosz I, Bartosz G. Prevention of protein glycation by natural compounds. *Molecules*. 2015;20(2):3309-3334.
49. Dyer D, Dunn J, Thorpe S, et al. Accumulation of Maillard reaction products in skin collagen in diabetes and aging. 1993;91(June):2463-2469.

50. Engelen L, Stehouwer C, Schalkwijk C. Current therapeutic interventions in the glycation pathway: Evidence from clinical studies. *Diabetes, Obes Metab.* 2013;15(8):677-689.
51. Khangholi S, Majid F, Berwary N, Ahmad F, Aziz R. The Mechanisms of Inhibition of Advanced Glycation End Products Formation through Polyphenols in Hyperglycemic Condition. *Planta Med.* 2015;82(1-2):32-45.
52. Ferchichi L, Derbré S, Mahmood K, et al. Bioguided fractionation and isolation of natural inhibitors of advanced glycation end-products (AGEs) from *Calophyllum flavoramulum*. *Phytochemistry.* 2012;78:98-106.
53. Rahbar S. Novel inhibitors of glycation and AGE formation. *Cell Biochem Biophys.* 2007;48(2-3):147-157.
54. Barbezier N, Tessier F, Chango A. Le récepteur des produits de glycation avancée RAGE/AGER: une vue intégrative pour des applications en clinique. *Ann Biol Clin (Paris).* 2014;72(6):669-680.
55. Rabbani N, Thornalley P. Dicarbonyl stress in cell and tissue dysfunction contributing to ageing and disease. *Biochem Biophys Res Commun.* 2015;458(2):221-226.
56. Ahmed N, Babaei-Jadidi R, Howell S, Beisswenger P, Thornalley P. Degradation products of proteins damaged by glycation, oxidation and nitration in clinical type 1 diabetes. *Diabetologia.* 2005;48(8):1590-1603.
57. Horiuchi S, Imai N, Ueno M, et al. Histological Localization of Advanced Glycosylation End Products in the Progression of Diabetic Nephropathy. *Nephron.* 2008;76(2):153-160.
58. Babaei-Jadidi R, Karachalias N, Ahmed N, Battah S, Thornalley P. Prevention of incipient diabetic nephropathy by high-dose thiamine and benfotiamine. *Diabetes.* 2003;52(8):2110-2120.
59. Li H, Nakamura S, Miyazaki S, et al. N2-carboxyethyl-2'-deoxyguanosine, a DNA glycation marker, in kidneys and aortas of diabetic and uremic patients. *Kidney Int.* 2006;69(2):388-392.
60. Upadhyay A, Tuenter E, Exarchou V, Apers S, Pieters L. Kavalactones, A Novel Class of Protein Glycation and Lipid Peroxidation Inhibitors. *Planta Med.* 2014:1001-1008.
61. Wu C-H, Yen G-C. Inhibitory Effect of Naturally Occurring Flavonoids on the Formation of

- Advanced Glycation Endproducts. *J Agric Food Chem*. 2005;53:3167-3173.
62. Poitevin P, Levy B, Wolffenbuttel B, et al. Breakers of advanced glycation end products restore large artery properties in experimental diabetes. *Proc Natl Acad Sci*. 1998;95(8):4630-4634.
  63. Odjakova M, Popova E, Sharif M, Mironova R. Plant-Derived Agents with Anti-Glycation Activity.; 2011.
  64. Younus H, Anwar S. Prevention of Non-Enzymatic Glycosylation (Glycation) : Implication in the Treatment of Diabetic Complication. *Int J Health Sci (Qassim)*. 2016;10(2):247-263.
  65. Touchette A, Szwegold B, Lal S, Beisswenger P, Howell S. Metformin reduces systemic methylglyoxal levels in type 2 diabetes. *Diabetes*. 1999;48(1):198-202.
  66. Brownlee M, Vlassara H. Aminoguanidine prevents diabetes-induced arterial wall protein cross-linking. *Sci New Ser*. 1986;232:1629-1632.
  67. Borg D, Forbes J. Targeting advanced glycation with pharmaceutical agents: where are we now? *Glycoconj J*. 2016;33(4):653-670.
  68. Nagai R, Murray D, Metz T, Baynes J. Chelation: A fundamental mechanism of action of AGE inhibitors, AGE breakers, and other inhibitors of diabetes complications. *Diabetes*. 2012;61(3):549-559.
  69. Khalifah R, Voziyan P, Serianni A, et al. Modification of Proteins *in vitro* by Physiological Levels of Glucose. *J Biol Chem*. 2003;278(47):46616-46624.
  70. Nagaraj R, Sarkar P, Mally A, Biemel K, Lederer M, Padayatti P. Effect of pyridoxamine on chemical modification of proteins by carbonyls in diabetic rats: Characterization of a major product from the reaction of pyridoxamine and methylglyoxal. *Arch Biochem Biophys*. 2002;402(1):110-119.
  71. Pagnozzi F, Bena E, Beltramo E, et al. Thiamine corrects delayed replication and decreases production of lactate and advanced glycation endproducts in bovine retinal and human umbilical vein endothelial cells cultured under high glucose conditions. *Diabetologia*. 2002;39(11):1263-1268.
  72. Forbes J, Cooper M, Thallas V, et al. Reduction of the Accumulation of Advanced Glycation Endproducts by ACE Inhibition in Experimental Diabetic Nephropathy. *Blood*

- Press.* 2002;51(November).
73. Ohno R-I, Moroishi N, Nagai M, Nagai R. *Mangosteen* pericarp extract inhibits the formation of pentosidine and ameliorates skin elasticity. *J Clin Biochem Nutr.* 2015;57(1):27-32.
  74. Matsuda H, Wang T, Managi H, Yoshikawa M. Structural requirements of flavonoids for inhibition of protein glycation and radical scavenging activities. *Bioorganic Med Chem.* 2003;11(24):5317-5323.
  75. Derbré S, Gatto J, Pelleray A, Coulon L, Séraphin D, Richomme P. Automating a 96-well microtiter plate assay for identification of AGEs inhibitors or inducers: Application to the screening of a small natural compounds library. *Anal Bioanal Chem.* 2010;398(4):1747-1758.
  76. Mizutani K, Ikeda K, Yamori Y. Resveratrol inhibits AGEs-induced proliferation and collagen synthesis activity in vascular smooth muscle cells from stroke-prone spontaneously hypertensive rats. *Biochem Biophys Res Commun.* 2000;274(1):61-67.
  77. Sajithlal G, Chithra P, Chandrakasan G. Effect of curcumin on the advanced glycation and cross-linking of collagen in diabetic rats. *Biochem Pharmacol.* 1998;56(12):1607-1614.
  78. Hu T, Liu C, Chyau C, Hu M. Trapping of methylglyoxal by curcumin in cell-free systems and in human umbilical vein endothelial cells. *J Agric Food Chem.* 2012;60:8190-8196.
  79. Hou X, Hu Z, Xu H, et al. Advanced glycation endproducts trigger autophagy in cardiomyocyte via RAGE/PI3K/AKT/mTOR pathway. *Cardiovasc Diabetol.* 2014;13(1):1-8.
  80. Enzo Life Sciences. Does autophagy play a role in diseases?
  81. Novus Biologicals. *Autophagy Handbook.*; 2017.
  82. Martinet W, De Meyer I, Verheye S, Schrijvers D, Timmermans JP, De Meyer G. Drug-induced macrophage autophagy in atherosclerosis: For better or worse? *Basic Res Cardiol.* 2013;108(1).
  83. Kang R, Tang D, Lotze M, Zeh H. Apoptosis to autophagy switch triggered by the MHC class III-encoded receptor for advanced glycation endproducts (RAGE). *Autophagy.* 2011;7(1):91-93.

84. Novus Biologicals. Inducing Autophagy : Tat-D11, a Highly Potent and Specific Autophagy-Inducing Peptide.
85. Klionsky D, et al. Guidelines for the use and interpretation of assays for monitoring autophagy (3rd edition). *Autophagy*. 2016;12(1):1-222.
86. Glick D, Barth S, Macleod K. Autophagy: cellular and molecular mechanisms. *J Pathol*. 2010;221(1):6.
87. Mizushima N, Komatsu M. Autophagy: Renovation of cells and tissues. *Cell*. 2011;147(4):728-741.
88. Wang L, Ye X, Zhao T. The physiological roles of autophagy in the mammalian life cycle. *Biol Rev*. 2019;94(2):503-516.
89. Ha J, Kim J. Novel pharmacological modulators of autophagy: an updated patent review (2012-2015). *Expert Opin Ther Pat*. 2016;26(11):1273-1289.
90. van Eupen M, Schram M, Colhoun H, Scheijen J, Stehouwer C, Schalkwijk C. Plasma levels of advanced glycation endproducts are associated with type 1 diabetes and coronary artery calcification. *Cardiovasc Diabetol*. 2013;12(1):1.
91. Xu D, Lao Y, Xu N, et al. Identification and characterization of anticancer compounds targeting apoptosis and autophagy from Chinese native *Garcinia* species. *Planta Med*. 2014;81(1):79-89.
92. Trocoli A, Djavaheri-Mergny M. The complex interplay between autophagy and NF- $\kappa$ B signaling pathways in cancer cells. *Am J Cancer Res*. 2011;1(5):629-649.
93. Kang R, Loux T, Tang D, et al. The expression of the receptor for advanced glycation endproducts (RAGE) is permissive for early pancreatic neoplasia. *Proc Natl Acad Sci*. 2012;109(18):7031-7036.
94. Yang J-S, Lu C-C, Kuo S-C, et al. Autophagy and its link to type II diabetes mellitus. *BioMedicine*. 2017;7(2):8.
95. Wu A, Wong V, Xu S, et al. Onjisaponin b derived from Radix Polygalae enhances autophagy and accelerates the degradation of mutant  $\alpha$ -synuclein and huntingtin in PC-12 cells. *Int J Mol Sci*. 2013;14(11):22618-22641.
96. Knuppertz L, Osiewacz H. Orchestrating the network of molecular pathways affecting

- aging: Role of nonselective autophagy and mitophagy. *Mech Ageing Dev.* 2016;153:30-40.
97. Lao Y, Wan G, Liu Z, et al. The natural compound oblongifolin C inhibits autophagic flux and enhances antitumor efficacy of nutrient deprivation. *Autophagy.* 2014;10(5):736-749.
  98. Zhou J, Hu S, Tan S, et al. Andrographolide sensitizes cisplatin-induced apoptosis via suppression of autophagosome-lysosome fusion in human cancer cells. *Autophagy.* 2012;8(3):338-349.
  99. Upadhyay A, Tuentner E, Amin A, et al. 5- O -Demethylnobiletin , a polymethoxylated flavonoid, from *Citrus depressa* Hayata peel prevents protein glycation. *J Funct Foods.* 2014;11:243-249.
  100. Das C, Poi R, Chowdhury A. HPTLC determination of vasicine and vasicinone in *Adhatoda vasica*. *Phytochem Anal.* 2005;16(2):90-92.
  101. Harborne J. *Phytochemical Methods: A Guide to Modern Techniques of Plant Analysis.* Second edi.; 1984.
  102. Cannell R. *Natural Products Isolation.*; 1998.
  103. Wagner H, Bladt S, Zgainski EM. *Plant Drug Analysis.*; 1984.
  104. Churchwell M, Twaddle N, Meeker L, Doerge D. Improving LC – MS sensitivity through increases in chromatographic performance : Comparisons of UPLC – ES/MS/MS to HPLC – ES/MS/MS. *J Chromatogr B.* 2005;825:134-143.
  105. Favela-Hernández JM, González-Santiago O, Ramírez-Cabrera M, Esquivel-Ferriño P, Camacho-Corona M. Chemistry and Pharmacology of *Citrus sinensis*. *Molecules.* 2016;6.
  106. Yamamoto M, Takakura A, Tanabe A. Diversity of *Citrus depressa* Hayata ( Shiikuwasha ) revealed by DNA analysis. *Genet Resour Crop Evol.* 2017;64(4):805-814.
  107. Li S, Yu H, Ho C. Nobiletin: efficient and large quantity isolation from orange peel extract. 2006;138:133-138.
  108. Okinawa Botanical Garden.
  109. Asikin Y, Taira I, Inafuku-teramoto S, et al. The Composition of Volatile Aroma Components, Flavanones, and Polymethoxylated Flavones in Shiikuwasha ( *Citrus depressa* Hayata) Peels of Different Cultivation Lines. 2012.

110. Liu Y, Heying E, Tanumihardjo S. History, Global Distribution, and Nutritional Importance of *Citrus* Fruits. *Compr Rev Food Sci Food Saf.* 2012;11(6):530-545.
111. Khan M, Abert-Vian M, Dangles O, Chemat F. Ultrasound-assisted extraction of polyphenols (flavanone glycosides) from orange (*Citrus sinensis* L.) peel. *Food Chem.* 2010;119(2):851-858.
112. Chen J, Montanari A, Widmer W. Two New Polymethoxylated Flavones, a Class of Compounds with Potential Anticancer Activity, Isolated from Cold Pressed Dancy Tangerine Peel Oil Solids. *J Agric Food Chem.* 1997:364-368.
113. Yi L, Ma S, Ren D. Phytochemistry and Bioactivity of *Citrus* Flavonoids: A Focus on Antioxidant, Anti-Inflammatory, Anticancer and Cardiovascular Protection Activities. Vol 16. Springer Netherlands; 2017.
114. Wang Z, Goodnow R, Ho C-T. Validated reversed phase LC method for quantitative analysis of polymethoxyflavones in *Citrus* peel extracts. *J Sep Sci.* 2008:30-37.
115. Nogata Y, Ohta H, Sekiya K. Effect of Extraction Method on the Concentrations of Selected Bioactive Compounds in Mandarin Juice. *J Agric Food Chem.* 2003:7346-7351.
116. Li S, Pan M, Lai C, Lo C. Isolation and syntheses of polymethoxyflavones and hydroxylated polymethoxyflavones as inhibitors of HL-60 cell lines. 2007;15:3381-3389.
117. Lee A, Hsiao W, Wright D, et al. Induction of GADD 45 $\alpha$  expression contributes to the anti-proliferative effects of polymethoxyflavones on colorectal cancer cells. *J Funct Foods.* 2013;5(2):616-624.
118. Lam I, Alex D, Wang Y, et al. *In vitro* and *in vivo* structure and activity relationship analysis of polymethoxylated flavonoids: Identifying sinensetin as a novel antiangiogenesis agent. *Mol Nutr Food Res.* 2012;56(6):945-956.
119. Lam KH, Alex D, Lam IK, Tsui SKW, Yang ZF, Lee SMY. Nobiletin, a polymethoxylated flavonoid from citrus, shows anti-angiogenic activity in a zebrafish *in vivo* model and HUVEC *in vitro* model. *J Cell Biochem.* 2011;112(11):3313-3321.
120. Zhang J, Lu J, Zhang Q, et al. Simultaneous screening and identifying four categories of particular flavonoids in the leaves of *Murraya exotica* L. by HPLC-DAD-ESI-MS-MS. *J Chromatogr Sci.* 2014;52(2):103-114.



121. Li S, Pan M, Lo C, et al. Chemistry and health effects of polymethoxyflavones and hydroxylated polymethoxyflavones. *J Funct Foods*. 2009;1(1):2-12.
122. Inafuku-Teramoto S, Suwa R, Fukuzawa Y, Kawamitsu Y. Polymethoxyflavones, Synephrine and Volatile Constitution of Peels of *Citrus* Fruit Grown in Okinawa. 2011;80(2):214-224.
123. Ko H, Jang M, Kang C, et al. Preparation of a polymethoxyflavone-rich fraction (PRF) of *Citrus sunki* Hort.ex Tanaka and its antiproliferative effects. *Food Chem*. 2010;123(2):484-488.
124. Kawaii S, Tomono Y, Katase E, Ogawa K, Yano M. Quantitation of Flavonoid Constituents in *Citrus* Fruits. *J Agric Food Chem*. 1999.
125. Tanaka T, Walker E. Progress in the development of economic botany and knowledge of food plants. *Econ Bot*. 1967;21(4):383-387.
126. Garcia-Castello E, Rodriguez-Lopez A. Optimization of conventional and ultrasound assisted extraction of flavonoids from grapefruit (*Citrus paradisi* L.) solid wastes. *LWT - Food Sci Technol*. 2015;64(2):1114-1122.
127. Baldi A, Rosen RT, Fukuda EK, Ho C. Identification of nonvolatile components in lemon peel by high-performance liquid chromatography with confirmation by mass spectrometry and diode-array detection. 1995;718:89-97.
128. He X, Lian L, Lin L, Bernart M. High-performance liquid chromatography – electrospray mass spectrometry in phytochemical analysis of sour orange (*Citrus aurantium* L.). 1997;791:127-134.
129. Yamamoto K, Ohta H. Chemical Markers of Shiikuwasha Juice Adulterated with Calamondin Juice. *J Agric Food Chem*. 2012.
130. Krasteva I. Phenolic Compounds in Four *Astragalus* Species. *European J Med Plants*. 2014;3(4):616-623.
131. Rojas-Garbanzo C, Zimmermann B, Schulze-Kaysers N, Schieber A. Characterization of phenolic and other polar compounds in peel and flesh of pink guava (*Psidium guajava* L.cv.‘ Criolla’) by ultra-high performance liquid chromatography with diode array and mass spectrometric detection. *Food Res Int*. 2017;100:445-453.

132. Mouly P, Gaydou E, Auffray A. Simultaneous separation of flavanone glycosides and polymethoxylated flavones in citrus juices using liquid chromatography. *J Chromatogr A*. 1998;800(2):171-179.
133. Han S, Kim H, Lee J, Mok S, Lee S. Isolation and identification of polymethoxyflavones from the Hybrid *Citrus*, Hallabong. *J Agric Food Chem*. 2010;58(17):9488-9491.
134. Uckoo R, Jayaprakasha G, Patil B. Chromatographic techniques for the separation of polymethoxyflavones from Citrus. *ACS Symp Ser*. 2012;1093:3-15.
135. Ye X, Cao D, Zhao X, et al. Chemical fingerprint and metabolic profile analysis of *Citrus reticulata* "Chachi" decoction by HPLC-PDA-IT-MSn and HPLC-Quadrupole-Orbitrap-MS method. *J Chromatogr B Anal Technol Biomed Life Sci*. 2014;970:108-120.
136. Guccione C, Bergonzi M, Piazzini V, Bilia A. A Simple and Rapid HPLC-PDA MS Method for the Profiling of Citrus Peels and Traditional Italian Liquors. *Planta Med*. 2016;82(11-12):1039-1045.
137. Encyclopaedia Britannica. *Ginkgo* tree.
138. Montes P, Ruiz-Sanchez E, Rojas C, Rojas P. *Ginkgo biloba* Extract 761: A Review of Basic Studies and Potential Clinical Use in Psychiatric Disorders. *CNS Neurol Disord - Drug Targets*. 2015;14(1):132-149.
139. Van Beek TA. Chemical analysis of *Ginkgo biloba* leaves and extracts. *J Chromatogr A*. 2002;967(1):21-55.
140. Drieu K. Preparation and definition of *Ginkgo biloba* extract. *Press medicale*. 1986;15(31):1455-1457.
141. Krauze-Baranowska M, Baczek T, Kaliszan R, Wollenweber E. HPLC Separation of O-Acylated Flavonoids and Biflavones from Some Species of Gymnospermae. *Chromatographia*. 2004;60(1-2):9-15.
142. 10.0 EP. *Ginkgo* Dry Extract, Refined and Quantified *Ginkgonis extractum siccum raffinatum et quantificatum*. *Eur Pharmacopoeia 70*.:1136-1138.
143. Yao X, Zhou G-S, Duan J-A. Simultaneous quantification of flavonol glycosides, terpene lactones, biflavones, proanthocyanidins, and ginkgolic acids in *Ginkgo biloba* leaves from fruit cultivars by ultrahigh-performance liquid chromatography coupled with triple

- quadrupole mass. *Biomed Res Int.* 2012;2013:11.
144. Rainer M, Mucke H, Schlaefke S. EGb 761: *Ginkgo biloba* extract, Ginkor. *Drugs R D.* 2003;4(3):188-193.
  145. American Botanical Council. Scientific Review of *Ginkgo* Finds Promising Evidence in Improving Memory in Older Patients with Dementia.
  146. Kwak W, Han C, Son K, et al. Effects of ginkgetin from *Ginkgo biloba* leaves on cyclooxygenases and *in vivo* skin inflammation. *Planta Med.* 2002;68(4):316-321.
  147. van Beek T, Montoro P. Chemical analysis and quality control of *Ginkgo biloba* leaves, extracts, and phytopharmaceuticals. *J Chromatogr A.* 2009;1216(11):2002-2032.
  148. Hasler A, Sticher O, Meier B. Identification and determination of the flavonoids from *Ginkgo biloba* by high-performance liquid chromatography. *J Chromatogr A.* 1992;605(1):41-48.
  149. Williams C, Harborne J. Biflavonoids. Vol 1.; 1989.
  150. Ravishankara M, Pillai A, Padh H, Rajani M. A sensitive HPTLC method for estimation of amentoflavone, a bioactive principle from *Biophytum sensitivum* (Linn.) DC and *Putranjiva roxburghii* wall. *J Planar Chromatogr – Mod TLC.* 2007;16(3):201-205.
  151. Gobbato S, Griffini A, Lolla E, Peterlomgo F. HPLC quantitative analysis of biflavones in *Ginkgo biloba* leaf extracts and their identification by thermospray liquid chromatography-mass spectrometry. *Fitoterapia.* 1996;67(2):152-158.
  152. Zhang J, Liu Z, Cao W, et al. Amentoflavone inhibits angiogenesis of endothelial cells and stimulates apoptosis in hypertrophic scar fibroblasts. *Burns.* 2014;40(5):922-929.
  153. Hwang C, Lin Y, Liu Y, et al. 7,7"-Dimethoxyagastisflavone-induced apoptotic or autophagic cell death in different cancer cells. *Phyther Res.* 2012;26(4):528-534.
  154. Yamaguchi L, Vassão D, Kato M, Di Mascio P. Biflavonoids from Brazilian pine *Araucaria angustifolia* as potentials protective agents against DNA damage and lipoperoxidation. *Phytochemistry.* 2005;66(18 SPEC. ISS.):2238-2247.
  155. Baron-Ruppert G, Luepke N. Evidence for toxic effects of alkylphenols from *Ginkgo biloba* in the hen's egg test (HET). *Phytomedicine.* 2001;8(2):133-138.
  156. Natarajan S, Murti V, Seshadri T. Biflavones of some Cupressaceae plants.

- Phytochemistry*. 1970;9(3):575-579.
157. Ritter SD, et al. EP1813280A1 New extracts of *Ginkgo biloba* and their methods of preparation. *Eur Pat Off*. 1990:1-6.
  158. Pietta P, Mauri P, A.Rava. Reversed-phase high-performance liquid chromatographic methods for the analysis of biflavones in *Ginkgo biloba* L. extracts. *J Chromatogr*. 1988;437:453-456.
  159. Kakigi Y, Hakamatsuka T, Icho T, Goda Y, Mochizuki N. Comprehensive Analysis of Flavonols in *Ginkgo biloba* Products by Ultra-High-Performance Liquid Chromatography Coupled with Ultra-Violet Detection and Time-of-Flight Mass Spectrometry. *Biosci Biotechnol Biochem*. 2012;76(5):1003-1007.
  160. D'Arc Felicio J, Rossi M, Braggio M, et al. Chemical constituents from *Ouratea parviflora*. *Biochem Syst Ecol*. 2004;32(1):79-81.
  161. Thuy T, Tam N, Sung T. Taxoids and biflavonoid from *Taxus chinensis*. 2005;43(4):503-507.
  162. Claeson U, Malmfors T, Wikman G, Bruhn J. *Adhatoda vasica*: A critical review of ethnopharmacological and toxicological data. *J Ethnopharmacol*. 2000;72(1-2):1-20.
  163. Sujata B, Mamta P, Priyanka K, Sonam S. Review & Future Perspectives of Using Vasicine, and Related Compounds. *Indo-Global J Pharm Sci*. 2011;1(1):85-98.
  164. Roja G, Vikrant B, Sandur S, Sharma A, Pushpa K. Accumulation of vasicine and vasicinone in tissue cultures of *Adhatoda vasica* and evaluation of the free radical-scavenging activities of the various crude extracts. *Food Chem*. 2011;126(3):1033-1038.
  165. Singh B, Sharma R. Anti-inflammatory and antimicrobial properties of pyrroloquinazoline alkaloids from *Adhatoda vasica* Nees. *Phytomedicine*. 2013;20(5):441-445.
  166. Duraipandiyan V, Al-Dhabi N, Balachandran C, Ignacimuthu S, Sankar C, Balakrishna K. Antimicrobial, Antioxidant, and Cytotoxic Properties of Vasicine Acetate Synthesized from Vasicine Isolated from *Adhatoda vasica* L. *Biomed Res Int*. 2015;2015:1-7.
  167. Gibbs B. Differential modulation of IgE-dependent activation of human basophils by ambroxol and related secretolytic analogues. *Int J Immunopathol Pharmacol*. 2009;22(4):919-927.

168. Huang Y-N, Kawabata J, Inagaki C, Li P, Gao B, Gao H. Inhibitory effect on  $\alpha$ -glucosidase by *Adhatoda vasica* Nees. *Food Chem.* 2006;108(3):965-972.
169. Singh A, Kumar S, Reddy J, Rameshkumar K, Kumar B. Screening of tricyclic quinazoline alkaloids in the alkaloidal fraction of *Adhatoda beddomei* and *Adhatoda vasica* leaves by high-performance liquid chromatography/electrospray ionization quadrupole time-of-flight tandem mass spectrometry. *Rapid Commun Mass Spectrom.* 2015;29(6):485-496.
170. Srivastava S, Verma R, Gupta M, Singh S, Kumar S. HPLC determination of vasicine and vasicinone in *Adhatoda vasica* with photo diode array detection. *J Liq Chromatogr Relat Technol.* 2001;24(2):153-159.
171. Joshi B, Bai Y, Puar M, Dubose K, Pelletier S. <sup>1</sup>H- and <sup>13</sup>C-NMR assignments for some pyrrolo[2,1b]-quinazoline alkaloids of *Adhatoda vasica*. *J Nat Prod.* 1994;57(7):953-962.
172. Chowdhury B, Hirani S, Ngur D. High-performance liquid chromatographic study of the photochemical oxidation of vasicine and its analogues. *J Chromatogr A.* 1987;390(2):439-443.
173. Kuffner F, Lenneis G, Bauer H. Über die Konstitution eines Nebenalkaloides aus *Adhatoda vasica* Nees. In: *Organisch-Chemischen Institut Der Universitet Wien.* ; 1960:1153-1161.
174. Singh TP, Singh OM, Singh HB, Rea G, Giardi MT. *Adhatoda vasica* Nees: Phytochemical and Pharmacological Profile. *Nat Prod J.* 2011;1(1):29-39.
175. Dhankhar S, Kaur R, Ruhil S, Balhara M, Dhankhar S, Chhillar K. A review on *Justicia adhatoda*: A potential source of natural medicine. *African J Plant Sci.* 2011;5(11):620-627.
176. Council of Europe. European Pharmacopoeia 9th edition, Monograph 2.9.5. In: *European Pharmacopoeia.* ; 2017.
177. Dhooghe L, Mesia K, Kohtala E, et al. Development and validation of an HPLC-method for the determination of alkaloids in the stem bark extract of *Nauclea pobeguini*. *Talanta.* 2008;76(2):462-468.
178. Joosen K, Apers S. Elaboration of a monograph for *Adhatoda vasica* Nees in the European Pharmacopoeia : Development and validation of an assay for the determination

- of vasicine. 2016.
179. ICH Expert Working Group. *ICH Harmonised Tripartite Guideline: Note for Guidance on Toxicokinetics.*; 1994.
  180. ICH Harmonised Tripartite Guideline. ICH Guideline for good clinical practice E6(R1). *ICH Harmon Tripart Guidel.* 1996;1996(June).
  181. ICH Expert Working Group. ICH Guideline Q1D Bracketing and Matrixing Designs for Stability Testing of New Drug Substances and Products. *Int Conf Harmon.* 2003;68(11):2339-2340.
  182. Soboleva A, Vikhnina M, Grishina T, Frolov A. Probing protein glycation by chromatography and mass spectrometry: Analysis of glycation adducts. *Int J Mol Sci.* 2017;18(12).
  183. Lin H, Lan J, Guan M, Sheng F, Zhang H. Spectroscopic investigation of interaction between mangiferin and bovine serum albumin. 2009;73:936-941.
  184. Glomb M, Tschirnich R. Detection of  $\alpha$ -Dicarbonyl compounds in Maillard reaction systems and *in vivo*. *J Agric Food Chem.* 2001;49(11):5543-5550.
  185. Mitchel R, Birnboim H. The use of Girard-T reagent in a rapid and sensitive method for measuring glyoxal and certain other  $\alpha$ -dicarbonyl compounds. *Anal Biochem.* 1977;81(1):47-56.
  186. Hirsch J, Mossine V, Feather M. The detection of some dicarbonyl intermediates arising from the degradation of Amadori compounds (the Maillard reaction). *Carbohydr Res.* 1995;273(2):171-177.
  187. Ahmed N, Thornalley P. Chromatographic assay of glycation adducts in human serum albumin glycated *in vitro* by derivatization with 6-aminoquinolyl-N-hydroxysuccinimidyl-carbamate and intrinsic fluorescence. *Biochem J.* 2002;364(1):15-24.
  188. Séro L, Sanguinet L, Blanchard P, et al. Tuning a 96-well microtiter plate fluorescence-based assay to identify AGE inhibitors in crude plant extracts. *Molecules.* 2013;18(11):14320-14339.
  189. Liu E, Qi L, Li P. Structural Relationship and Binding Mechanisms of Five Flavonoids with Bovine Serum Albumin. 2010:9092-9103.

190. Baker J, Zyzak D, Thoroe S, Baynes J. Chemistry of the fructosamine assay: D-glucosone is the product of oxidation of Amadori compounds. *Clin Chem*. 1994;40(10):1950-1955.
191. Johnson R, Metcalf P, Baker J. Fructosamine: A new approach to the estimation of serum glycosyl-protein. An index of diabetic control. *Clin Chim Acta*. 1983;127(1982):87–95.
192. Chompoo J, Upadhyay A, Kishimoto W, Makise T, Tawata S. Advanced glycation end products inhibitors from *Alpinia zerumbet* rhizomes. *Food Chem*. 2011;129(3):709-715.
193. Ahmad S, Shahab U, Baig H, et al. Inhibitory Effect of Metformin and Pyridoxamine in the Formation of Early, Intermediate and Advanced Glycation End-Products. *PLoS One*. 2013;8(9):1-7.
194. Lin H, Chen R, Liu X, Sheng F, Zhang H. Study on interaction of mangiferin to insulin and glucagon in ternary system. *Spectrochim Acta - Part A Mol Biomol Spectrosc*. 2010;75(5):1584-1591.
195. Papadopoulou ATP, Green RJG, Frazier RAF. Interaction of Flavonoids with Bovine Serum Albumin : A Fluorescence Quenching Study. 2005:158-163.
196. Matsuura N, Aradate T, Kurosaka C, et al. Potent Protein Glycation Inhibition of Plantagoside in *Plantago major* Seeds. 2014;2014:1-5.
197. Sasaki C, Aradate T, Ubukata M, et al. Screening System for the Maillard Reaction Inhibitor from Natural Product Extracts. *J Heal Sci*. 2002;48(6):520-526.
198. Assar S, Moloney C, Lima M, Magee R, Ames J. Determination of N $\epsilon$ -(carboxymethyl)lysine in food systems by ultra performance liquid chromatography-mass spectrometry. *Amino Acids*. 2009;36(2):317-326.
199. Nomi Y, Annaka H, Sato S, et al. Simultaneous Quantitation of Advanced Glycation End Products in Soy Sauce and Beer by Liquid Chromatography-Tandem Mass Spectrometry without Ion-Pair Reagents and Derivatization. *J Agric Food Chem*. 2016;64(44):8397-8405.
200. Thornalley P, Battah S, Ahmed N, et al. Quantitative screening of advanced glycation endproducts in cellular and extracellular proteins by tandem mass spectrometry. *Biochem J*. 2003;375(3):581-592.

201. Koito W, Araki T, Horiuchi S, Nagai R. Conventional antibody against N $\epsilon$ -(carboxymethyl)lysine (CML) shows cross-reaction to N $\epsilon$ -(carboxyethyl)lysine (CEL): Immunochemical quantification of CML with a specific antibody. *J Biochem.* 2004;136(6):831-837.
202. Singh VP, Bali A, Singh N, Jaggi AS. Advanced Glycation End Products and Diabetic Complications. *Korean J Physiol Pharmacol.* 2014;18:1-14.
203. Hwang J, Shin C, Yang S. Clinical implications of N-(carboxymethyl)lysine, advanced glycation end product, in children and adolescents with type 1 diabetes. *Diabetes, Obes Metab.* 2005;7(3):263-267.
204. Nerlich A, Schleicher E. N( $\epsilon$ )-(carboxymethyl)lysine in atherosclerotic vascular lesions as a marker for local oxidative stress. *Atherosclerosis.* 1999;144(1):41-47.
205. Rabbani N, Thornalley P. Hidden complexities in the measurement of fructosyl-lysine and advanced glycation end products for risk prediction of vascular complications of diabetes. *Diabetes.* 2015;64(1):9-11.
206. Daykin C, Foxall P, Connor S, Lindon J, Nicholson J. The comparison of plasma deproteinization methods for the detection of low-molecular-weight metabolites by <sup>1</sup>H nuclear magnetic resonance spectroscopy. *Anal Biochem.* 2002;304(2):220-230.
207. Ahmed N, Thornalley P. Assay of early and advanced glycation adducts by enzymatic hydrolysis of proteins and HPLC of 6-aminoquinolylcarbonyl adducts. *Int Congr Ser.* 2002;1245(C):279-283.
208. Delatour T, Hegele J, Parisod V, et al. Analysis of advanced glycation endproducts in dairy products by isotope dilution liquid chromatography-electrospray tandem mass spectrometry. The particular case of carboxymethyllysine. *J Chromatogr A.* 2009;1216(12):2371-2381.
209. Changl J, Ulrich P, Bucala R, Cerami A. Detection of an Advanced Glycosylation Product Bound to Protein in Situ. *J Biol Chem.* 1985;260(13):797-7974.
210. Ouyang Zheng MF. Pellet digestion: a simple and efficient sample preparation technique for LC-MS/MS quantification of large therapeutic proteins in plasma. *Bioanalysis.* 2012;4(1):17-28.
211. Niquet-Léridon C, Tessier F. Quantification of N $\epsilon$ -carboxymethyl-lysine in selected



- chocolate-flavoured drink mixes using high-performance liquid chromatography-linear ion trap tandem mass spectrometry. *Food Chem.* 2011;126(2):655-663.
212. Bayliss M, Venn R, Edgington A, Webster R, Walker D. Determination of a potent urokinase-type plasminogen activator, UK-356,202, in plasma at pg/mL levels using column-switching HPLC and fluorescence detection. *J Chromatogr B Anal Technol Biomed Life Sci.* 2009;877(3):121-126.
  213. Schettgen T, Tings A, Brodowsky C, Müller-Lux A, Musiol A, Kraus T. Simultaneous determination of the advanced glycation endproduct N $\epsilon$ -carboxymethyllysine and its precursor, lysine, in exhaled breath condensate using isotope-dilution-hydrophilic-interaction liquid chromatography coupled to tandem mass spectrometry. *Anal Bioanal Chem.* 2007;387(8):2783-2791.
  214. Xiaolei Xie MK. Comparison of Non-Derivatization and Derivatization Tandem Mass Spectrometry Methods for Analysis of Amino Acids, Acylcarnitines, and Succinylacetone in Dried Blood Spots.; 2016.
  215. Salazar C, Armenta J, Shulaev V. An UPLC-ESI-MS/MS assay using 6-aminoquinolyl-N-hydroxysuccinimidyl carbamate derivatization for targeted amino acid analysis: Application to screening of arabidopsis thaliana mutants. *Metabolites.* 2012;2(3):398-428.
  216. White S, Adcock N, Elbast W, et al. European Bioanalysis Forum: Recommendation for dealing with internal standard variability. *Bioanalysis.* 2014;6(20):2767-2774.
  217. Chambers E, Wagrowski-Diehl D, Lu Z, Mazzeo J. Systematic and comprehensive strategy for reducing matrix effects in LC/MS/MS analyses. *J Chromatogr B Anal Technol Biomed Life Sci.* 2007;852(1-2):22-34.
  218. Bronsema K, Bischoff R, Van de Merbel N. Internal standards in the quantitative determination of protein biopharmaceuticals using liquid chromatography coupled to mass spectrometry. *J Chromatogr B Anal Technol Biomed Life Sci.* 2012;893-894:1-14.
  219. Ni J, Yuan X, Gu J, et al. Plasma Protein Pentosidine and Carboxymethyllysine , Biomarkers for Age-related Macular Degeneration. 2009:1921-1933.
  220. Porvair. Biological Sample Preparation Using Solid Phase Extraction and Protein Crash Techniques in 96 Well Plates The Problem Ex-Vivo Samples Such as Blood , Semen , Serum , Urine and Spinal Fluid in Order to Allow Quantitative Analysis of Small Molecul.

221. Waters Corporation. Xevo G2-XS QToF Quadrupole Time-of-Flight Mass Spectrometer.
222. Waters Corporation. Waters Xevo G2-XS QToF Overview and Maintenance Guide 715004496/Revision B. 2015.
223. He J, Zeng M, Zheng Z, He Z, Chen J. Simultaneous determination of N $\epsilon$ -(carboxymethyl) lysine and N $\epsilon$ -(carboxyethyl) lysine in cereal foods by LC-MS/MS. *Eur Food Res Technol*. 2014;238(3):367-374.
224. Ahmed M, Thorpe S, Baynes J. Identification of N( $\epsilon$ )-carboxymethyllysine as a degradation product of fructoselysine in glycated protein. *J Biol Chem*. 1986;261(11):4889-4894.
225. Hanssen N, Engelen L, Ferreira I, et al. Plasma levels of advanced glycation endproducts N $\epsilon$ -(carboxymethyl) lysine, N $\epsilon$ -(carboxyethyl)lysine, and pentosidine are not independently associated with cardiovascular disease in individuals with or without type 2 diabetes: The hoorn and CODAM studies. *J Clin Endocrinol Metab*. 2013;98(8):1369-1373.
226. Dell'mour M, Jaitz L, Oburger E, Puschenreiter M, Koellensperger G, Hann S. Hydrophilic interaction LC combined with electrospray MS for highly sensitive analysis of underivatized amino acids in rhizosphere research. *J Sep Sci*. 2010;33(6-7):911-922.
227. Scheijen J, Clevers E, Engelen L, et al. Analysis of advanced glycation endproducts in selected food items by ultra-performance liquid chromatography tandem mass spectrometry: Presentation of a dietary AGE database. *Food Chem*. 2016;190:1145-1150.
228. Danaceau J, Chambers E, Fountain K. Hydrophilic interaction chromatography (HILIC) for LC-MS/MS analysis of monoamine neurotransmitters. *Bioanalysis*. 2012;4(7):783-794.
229. Ruta J, Rudaz S, McCalley D, Veuthey JL, Guillarme D. A systematic investigation of the effect of sample diluent on peak shape in hydrophilic interaction liquid chromatography. *J Chromatogr A*. 2010;1217(52):8230-8240.
230. Grumbach E, Fountain K. Comprehensive Guide to HILIC : Hydrophilic Interaction Chromatography. Waters Corporation; 2010.
231. Kalasin S, Santore M. Non-specific adhesion on biomaterial surfaces driven by small amounts of protein adsorption. *Colloids Surfaces B Biointerfaces*. 2009;73(2):229-236.

232. Goebel-Stengel M, Stengel A, Taché Y, Reeve J. The importance of using the optimal plasticware and glassware in studies involving peptides. *Anal Biochem.* 2011;414(1):38-46.
233. Smith J, Hurrell J, Leach S. Elimination of nonspecific adsorption of serum proteins by Sepharose-bound antigens. *Anal Biochem.* 1978;87(2):299-305.
234. Suelter C, Deluca M. How to Prevent Losses of Protein by Adsorption to Glass and Plastic. *Anal Biochem.* 1983;135(1):112-119.
235. Schriewer A, Heilen KJ, Hayen H, Jiang W. Direct analysis of amino acids by HILIC-ESI-MS. *LC GC Eur.* 2017;30(7):386-387.
236. Porvair Science. Protein Crash Plates.
237. Stokvis E, Rosing H, Beijnen J. Stable isotopically labeled internal standards in quantitative bioanalysis using liquid chromatography/mass spectrometry: Necessity or not? *Rapid Commun Mass Spectrom.* 2005;19(3):401-407.
238. U.S. Department of Health and Human Services. Food and Drug Administration (FDA), Guidance for Industry: Bioanalytical Method Validation. 2018;(May).
239. Tan A, Hussain S, Musuku A, Massé R. Internal standard response variations during incurred sample analysis by LC-MS/MS: Case by case trouble-shooting. *J Chromatogr B Anal Technol Biomed Life Sci.* 2009;877(27):3201-3209.
240. Feng Y, He D, Yao Z, Klionsky D. The machinery of macroautophagy. *Cell Res.* 2014;24(1):24-41.
241. Ni H, Bockus A, Wozniak A, et al. Dissecting the dynamic turnover of GFP-LC3 in the autolysosome. *Autophagy.* 2011;7(2):188-204.
242. Tanida I, Waguri S. Measurement of Autophagy in Cells and Tissues. Vol 648.; 2010.
243. Barth S, Glick D, Macleod K. Autophagy assays and artifacts. *Pathol Soc Gt Britain Irel.* 2011;221(2):117-124.
244. GE Healthcare. Western Blotting Principles and Methods. Vol 362.; 2007.
245. Yoshii S, Mizushima N. Monitoring and measuring autophagy. *Int J Mol Sci.* 2017;18(9):1-13.

246. Mizushima N, Yoshimori T. How to interpret LC3 immunoblotting. *Autophagy*. 2007;3(6):542-545.
247. Kurdi A, De Doncker M, Leloup A, et al. Continuous administration of the mTORC1 inhibitor everolimus induces tolerance and decreases autophagy in mice. *Br J Pharmacol*. 2016;173(23):3359-3371.
248. Mahmood T, Yang P. Western blot: Technique, theory, and trouble shooting. *N Am J Med Sci*. 2012;4(9):429-434.
249. Enzo Life Sciences. Cyto-ID Autophagy Detektion Kit 2.0 Product Manual. In: ; 2000:1-5.
250. Guo S, Liang Y, Murphy SF, et al. A rapid and high content assay that measures cyto-ID-stained autophagic compartments and estimates autophagy flux with potential clinical application. 2015;11(3):560-572.
251. ATCC. Jurkat cell line - product file. ATCC.
252. Gibco, Invitrogen. Cell Culture Basics Handbook.
253. ATCC. HEK 293T cell line - product file. ATCC.
254. [www.hek293.com](http://www.hek293.com).
255. ATCC. L 929 cell line - product file. ATCC.
256. Musiwaro P, Smith M, Manifava M, Walker S, Ktistakis N. Characteristics and requirements of basal autophagy in HEK 293 cells. *Autophagy*. 2013;9(9):1407-1417.
257. Novus Biologicals. Western Blot Handbook.; 2011.
258. Milipore M. Protein Blotting Handbook Tips and Tricks.; 2012.
259. Cell Signaling Technology. Guide to Successful Western Blotting. Vol 362.; 2007.
260. Lou J, Bi W, Chan G, et al. Ginkgetin induces autophagic cell death through p62/SQSTM1- mediated autolysosome formation and redox setting in nonsmall cell lung cancer. *Oncotarget*. 2017;8(54):93131-93148.
261. Mizushima N. Methods for Monitoring Autophagy Using GFP-LC3 Transgenic Mice. Vol 451. 1st ed. Elsevier Inc.; 2009.
262. Li S, Wang H, Guo L, Zhao H, Ho CT. Chemistry and bioactivity of nobiletin and its

metabolites. *J Funct Foods*. 2014;6(1):2-10. doi:10.1016/j.jff.2013.12.011

263. Breynaert A, Bosscher D, Kahnt A, et al. Development and Validation of an in vitro Experimental Gastrointestinal Dialysis Model with Colon Phase to Study the Availability and Colonic Metabolisation of Polyphenolic Compounds. *Planta Med*. 2015;81(12-13):1075-1083. doi:10.1055/s-0035-1546154
264. Albert&Brown. *Citrus sinensis*.
265. Palmaverde. *Ginkgo biloba* Japanese notenboom.
266. Prachinayurvedkutir. *Adhatoda vasica*.



# Summary

## (Dutch)





Het doel van dit doctoraatsproject was het isoleren en identificeren van verschillende geselecteerde klassen van natuurproducten (polymethoxyflavonoïden (PMFs), biflavonoïden, chinazoline-alkaloïden) uit vier verschillende planten: *Citrus sinensis*, *Citrus depressa*, *Ginkgo biloba* en *Adhatoda vasica*. De doelverbindingen werden geëvalueerd als remmers van Advanced Glycation Endproducts (AGEs) en autofagie-modulatoren, voor het opstellen van structuur-activiteitsrelaties. AGEs zijn betrokken bij diabetische complicaties, atherosclerose, neurodegeneratieve ziekten, kanker en normale verouderingsprocessen. Net als bij AGEs is autofagie - een subcellulair proces voor bulkvernietiging - geassocieerd met een overvloed aan verschillende pathologische aandoeningen, waaronder hartziekten, kanker, neurodegeneratie en infectieziekten. Daarom zijn AGEs en autofagie nieuwe therapeutische doelwitten in het onderzoek van natuurproducten.

Het eerste werkpakket van het project bestond uit het fytochemisch onderzoek van de specifieke productklassen van de eerder genoemde plantensoorten. Met betrekking tot de isolatie werden de volgende procedures toegepast: De ruwe plantenextracten werden bereid met oplosmiddelen van verschillende polariteit. Vervolgens werden de totale extracten verder gezuiverd en gescheiden in subfracties door middel van open kolom chromatografie, en/of door middel van flash-chromatografie. Op basis van de informatie van de UV- en ELS-detectie werden de veelbelovende fracties verder gescheiden op een semi-preparatief vloeistofchromatografiesysteem voor de isolatie van zuivere verbindingen. Verder werd hun structuur opgehelderd en bevestigd door middel van 1D- en 2D- kernspinresonantie (NMR) spectroscopie en massaspectrometrie (MS).

Het tweede werkpakket richtte zich op het testen van de AGEs remmende eigenschappen van de verkregen zuivere verbindingen, met behulp van bestaande methoden, namelijk het meten van de glycatie van runder-serumalbumine (bovine serum albumine, BSA), de vorming van fructosamine-adducten en de vorming van alfa-dicarbonylverbindingen. De resultaten toonden echter aan dat het standaardexperiment met BSA/glucose niet nauwkeurig kon worden uitgevoerd als gevolg van complexvorming tussen de testverbindingen en het eiwit, wat leidde tot het onderdrukken van het initiële signaal en een verkeerde interpretatie van de gegevens. Als gevolg daarvan werd de BSA-test voor glycatie vervangen door een nieuwe HILIC Ultra-performance liquid chromatography

(UPLC) methode gekoppeld aan massaspectrometrische detectie met behulp van een Xevo G2-XS QToF-massaspectrometer. De methode, die moest worden ontwikkeld en gevalideerd, berustte op de nauwkeurige kwantificering van N- $\epsilon$ -carboxymethyl-L-lysine (CML), één van de meest voorkomende AGEs zowel *in vivo* als *in vitro*, met behulp van d<sub>4</sub>-CML als interne standaard. CML werd gegenereerd door incubatie van Gk-peptide en ribose bij 37 °C gedurende 14 uur. De monstervoorbereiding omvatte een hydrolysestap met zoutzuur en een reinigingsstap met P3 (protein precipitation plate) cartridges. Er werden stappen ondernomen om de methode te valideren volgens de FDA-richtlijnen voor Bioanalytische Methode Validatie met betrekking tot lineariteit, LLOQ, precisie en kwaliteitscontrole. Daarna werd deze methode gebruikt om de AGEs remmende eigenschappen van de verkregen zuivere verbindingen te onderzoeken en werden commercieel beschikbare standaarden geselecteerd.

Tenslotte werden de “dicarbonyl entrapment” test en fructosamine bepaling uitgevoerd, maar om representatieve resultaten te verkrijgen was verdere optimalisatie van de experimentele omstandigheden nodig (bijvoorbeeld het vinden van een betrouwbare positieve controle voor de fructosamine test).

Het derde werkpakket van het doctoraatsproject was het evalueren van de autofagie modulatie door enkele zuivere geïsoleerde verbindingen en commerciële standaarden met verschillende testen zoals: detectie van autofagie op cellulair niveau met behulp van een commercieel beschikbare autofagie detectiekit, en LC3 detectie en kwantificering door middel van western blot analyse.

Het laatste werkpakket van het onderzoek richtte zich op de optimalisatie van een analytische methode voor het kwantificeren van vasicine – een chinazoline alkaloïde in de bladeren van *Adhatoda vasica*. Daarnaast werd de ontwikkelde methode toegepast voor de kwaliteitscontrole van in de handel verkrijgbare kruidenproducten die *Adhatoda*-poeder of -extract bevatten.

Over het algemeen zijn geavanceerde glycatie en verstoorde autofagie belangrijke oorzaken voor de progressie en pathogenese van vele chronische ziekten (bv. diabetes mellitus) in het menselijk organisme en als gevolg daarvan kan het gebruik van gevalideerde methoden en bewezen technieken bijdragen tot de ondubbelzinnige ontdekking van nieuwe krachtige anti-AGEs en autofagie modulerende middelen.

**Scientific**  
**Curriculum Vitae**



## Personal information

Name	Stefaniya Velichkova
Date of birth	September 10 <sup>th</sup> , 1990
Place of birth	Sofia, Bulgaria
e-mail	stefaniyavelichkova1@gmail.com

## Education

October 2015 – September 2020	<b>PhD researcher (FWO aspirant)</b> Laboratory of Natural Products and Food Research and Analysis (NatuRA) University of Antwerpen, Belgium
September 2009 – December 2014	<b>Master of Pharmacy (cum laude)</b> Medical University, Sofia, Bulgaria Main modules: Physiology, Biochemistry, Pharmaceutical Technology; Pharmacognosy and Pharmaceutical Botany; Pharmaceutical Chemistry; Pharmacology and Toxicology; Social Pharmacy

## Scientific experience

October 2015 – September 2020

### PhD thesis

Laboratory of Natural Products and Food  
Research and Analysis (NatuRA)

Research topic:

“Natural products as potential inhibitors of  
advanced glycation endproducts (AGEs) and  
modulators of autophagy”.

Supervisors: Dr. Kenn Foubert and Prof. Luc  
Pieters

University of Antwerpen, Belgium

March 2014–June 2014

### Erasmus project

Laboratory of Natural Products and Food  
Research and Analysis (NatuRA)

Research topic:

„Isolation and structural elucidation of saponins  
in *Herniaria hirsuta*, Caryophyllaceae”

Supervisors: Dr. Ines van Dooren and Prof.  
Sandra Apers

University of Antwerpen, Belgium

October 2012–December 2013

### Research project

Department of Pharmacognosy and  
Pharmaceutical Botany, Faculty of Pharmacy

Research topic:

“Isolation and identification of flavonoids and  
saponins from *Astragalus monspessulanus*”

Medical University Sofia, Bulgaria

## Scientific publications

“Saponins and Flavonoids of *Herniaria hirsuta*”,  
van Dooren Ines, Foubert Kenn, Velichkova  
Stefaniya, Theunis Mart, Claeys Magda, Pieters  
Luc, Exarchou Vassiliki, Apers Sandra, *Planta  
medica: natural products and medicinal plants  
research* – ISSN 0032-0943-82:18(2016), p.  
1576-1583

*Manuscript submitted for a peer review* Velichkova S, Theunis M, Naessens T, Pieters L,  
Foubert K. Development and validation of an  
HPLC-DAD method for rapid quantification of  
vasicine in *Adhatoda vasica* leaves and  
commercial products  
(Submitted to *Journal of Herbal Medicine*)

*Manuscript submitted for a peer review* Velichkova S, Theunis M, Pieters L, Foubert K.  
Method development and validation for  
quantifying AGEs inhibition through a HILIC  
UPLC/ QTOF MS system: a trouble shooting paper  
(Submitted to *Glycoconjugates Journal*)

*Manuscript in preparation* Velichkova S, Pieters L, Foubert K. Natural  
products as potential inhibitors of Advances  
Glycation Endproducts (AGEs): a review  
(In preparation for *Planta Medica*)

## Oral presentation

May 2019

UPLC/QToF MS method development and validation for quantification of Advanced Glycation Endproducts (AGEs) in *in vitro* samples.

BSPS – 20th Forum of Pharmaceutical Sciences, Brussels

## Poster presentation

September 2019

AGEs (Advanced Glycation Endproducts): An Advanced Method for an Advanced Problem. 67<sup>th</sup> International Congress and Annual Meeting of the Society for Medicinal Plant and Natural Product Research (GA)

September 2018

Investigation on selected natural product classes as inhibitors of Advanced Glycation Endproducts (AGEs).

Drug Analysis Congress, Leuven

## Teaching experience

February – May 2018; February – May 2019

Supervision of Master students in the host laboratory.

November 2018, November 2019

Supervision of practical courses with third Bachelor pharmacy students.